AEROSOL SIZE DISTRIBUTION AND SIZE RESOLVED COMPOSITION IN URBAN AREAS OF COLOMBIA

Lady Mateus Fontecha

Universidad Nacional de Colombia

School of Engineering, Chemical and Environmental Engineering Department.

Bogotá, Colombia

2023

AEROSOL SIZE DISTRIBUTION AND SIZE RESOLVED COMPOSITION IN URBAN AREAS OF COLOMBIA.

DISTRIBUCIÓN DE TAMAÑO Y COMPOSICIÓN QUÍMICA DE LOS AEROSOLES PRESENTES EN ÁREAS URBANAS EN COLOMBIA.

Lady Mateus Fontecha

Dissertation submitted as partial requirement to obtain the degree of:

Doctor in Engineering – Chemical Engineering

Advisor:
Ph.D. Néstor Y. Rojas R.
Co-advisor:
Ph.D. Rodrigo Jiménez Pizarro

Research area:
Environmental Process

Research group:
Air Quality Research Group - GICA

Universidad Nacional de Colombia

School of Engineering, Chemical and Environmental Engineering Department.

Bogotá, Colombia

2023

Acknowledgments

I want to express my gratefulness and gratitude to many people who have supported and contributed to completing my doctoral thesis. I am truly grateful because this research would not have been possible without the scientific and personal encouragement and guidance of people and institutions.

First, I am sincerely thankful to the advisers of this doctoral thesis Ph.D. Nestor Y. Rojas R. and Ph.D. Rodrigo Jimenez P., professors of the Chemical Engineering Department of the National University of Colombia. I express gratitude to them for their ongoing support, guidance, and encouragement throughout the entire research process.

I would also like to extend my appreciation to the members of my doctoral committee assessment, Ph.D. Fatima Andrade, Ph.D. Kento Magara and Ph.D. Luis Carlos Belalcazar, for their valuable comment, constructive suggestions, and insights about the results getting in this research that enhanced the quality of this dissertation.

I'm grateful that Colciencias and Margaret Mc Namara funding my doctoral studies. Thank you to the Aerosol and Atmospheric Chemistry Groups of the Leibniz Institute for Tropospheric Research (TROPOS) and the German Academic Exchange Service (DAAD) to welcome me into your groups. Thanks to Professor German Rueda Saa to welcome me the National University of Colombia in Palmira and all your support in the develop of this research. Also, thanks to the Environmental Authority in Bogota (SDA) to facilitate the stations to conduct measurements and to PAPILA program to promote scientist mobility and contributed to building a network between South American and European institutions to evaluate the effects of air pollution in Latin American cities.

I am grateful to the master and doctoral students of the of Air Quality Research Group of the National University of Colombia, Angela Vargas, Karen Blanco and Johana Burbano, Jenniffer

Resumen

La Estrategia Nacional de Calidad del Aire de Colombia ha establecido que las acciones de prevención, reducción y control de emisiones deben estar enfocadas principalmente a las emisiones de material particulado, PM_{10} y $PM_{2.5}$, debido a las excedencias con respecto a los lineamientos de calidad del aire sugeridos por la Organización Mundial de la Salud y la Norma Nacional de Calidad del Aire. Además de los efectos nocivos en la salud pública de la población expuesta a partículas dispersas en el aire. De allí que, uno de los objetivos de la Estrategia es fomentar el conocimiento científico para mejorar la gestión de la calidad del aire a nivel nacional.

El objetivo de esta tesis es contribuir en el conocimiento de la distribución del tamaño de partículas (PSD) de los aerosoles en áreas urbanas de Colombia, vinculando las fuentes locales y regionales de contaminantes del aire y las condiciones meteorológicas locales. Este estudio se realizó en dos lugares de Colombia: Bogotá y Palmira (Valle del Cauca). Los aerosoles en el aire se investigaron utilizando impactadores en cascada para medir el tamaño de las partículas inhaladas. La concentración del número de partículas y la distribución del tamaño del número de partículas se midieron en el rango de tamaño de 17 nm y 10 μm usando un Impactador Eléctrico de Baja Presión (ELPI$^+$). Adicionalmente, se utilizó un impactador en cascada Non-Viable Andersen para determinar la distribución de tamaño en masa y recolectar muestras segregadas en nueve etapas entre 0.1 y 9 μm, para determinar el contenido de carbono orgánico, carbono elemental e iones solubles en agua de las partículas inhalables.

Los hallazgos de este estudio revelaron que el área de fondo urbano de Bogotá tenía una concentración promedio de partículas más alta (3,8 x10^3 #/cm^3) que el área más afectada por las emisiones de los automóviles (2,8 x10^3 #/cm^3). La distribución del tamaño de partículas en número fue unimodal en la estación de calidad del aire "Las Ferias", principalmente afectada por emisiones de tráfico vehicular, con un diámetro centrado en 120 nm, lo que evidenció que las partículas se forman y crecen a través de procesos atmosféricos del entorno. Por otro lado, el área de fondo urbano exhibió una distribución bimodal, con un diámetro modal de 120 nm y un segundo modo centrada en 30 nm de diámetro, la cual es más relevante en las horas pico de la mañana.

El Área de superficie de deposición pulmonar (LDSA) se estimó a partir de la interacción entre la distribución del tamaño de las partículas y el modelo de deposición de partículas en el sistema respiratorio publicado por la Comisión de Protección Radiológica (IRCP) (ICRP, 1994). En este estudio, el área de fondo urbano mostro concentraciones más altas que el área afectada por las emisiones de tráfico en Bogotá, y otros ambientes similares reportados en la literatura científica.

Las partículas submicrométricas PM_1, que pueden ingresar a la región alveolar del sistema respiratorio humano, fue de 20,8 $\mu g/m^3$ en Bogotá y 13,8 $\mu g/m^3$ en Palmira. La distribución de tamaño de masa exhibe una distribución bimodal que está igualmente centrada entre 0.43 y 1.1 μm, y 4.7 y 9.0 μm. De acuerdo con la composición química separada por tamaño, el carbono elemental se acumuló en la fracción fina de $PM_{2.1}$ en Bogotá a una tasa del 72%, frente al 57% en Palmira. Por otro lado, el carbono orgánico se distribuyó más uniformemente en la fracción fina y gruesa. El ion sulfato fue uno de los iones solubles en agua más abundantes en dos sitios, pero la distribución de tamaños fue diferente, mientras que en Palmira se acumuló principalmente en modo fino, en Bogotá se dispersó en la fracción de dos tamaños.

Palabras clave: **Concentración de nanopartículas; Distribución de tamaño de partícula; Composición Química de material Particulado; fracción de deposición pulmonar de partículas**

Abstract

The Colombian Air Quality National Strategy have established that prevention actions, reduction, and control emissions should be focused mainly on particulate matter, PM_{10} and $PM_{2.5}$, due to the consistent exceedances related to the air quality guidelines suggest by the World Health Organization and the Air Quality National Standard in urban areas. In addition, the harmful effects in public health of population exposed to airborne particles. Therefore, one of the aims of the Strategy is encouraging the scientific knowledge to improve the national air quality management.

Therefore, the aim of this dissertation's is to further knowledge of particle size distribution (PSD) of aerosols in urban areas in Colombian, linking the local and regional sources of air pollutants and the local weather patterns. The study was conducted in two places of Colombia: Bogotá and Palmira (Cauca's Valley). The airborne aerosols were investigated utilizing impactors cascades to measure the size of inhale particles. The particle number concentration and particle number size distribution were measured in the size range from 17 nm and 10 mm using an Electrical Low-Pressure Impactor (ELPI[+]). Also, was used an Andersen Non-viable Impactor Cascade to determinate the mass size distribution and collect samples size segregated in nine stages between 0.1 to 9 μm, to determine the contained of organic carbon, elemental carbon, and water-soluble ions in airborne inhalable particles.

The findings of this study revealed that Bogotá's urban background area had a higher average particle number concentration (3.8 x10^3 #/cm^3) than the area that was most adversely affected by automobile emissions (2.8 x10^3 #/cm^3. The number particle size distribution was unimodal in the traffic station of "Las Ferias" with a diameter centered in 120 nm, which evidences the particles are formed and grow through atmospheric process. In other hand, the urban background area exhibited a bimodal distribution, with a larger mode centered in particles of 120 nm of diameter with a second mode centered in 30 nm of diameter, which is more relevant in morning rush traffic hours.

The Lung Deposition Surface Area (LDSA) was estimated from the interaction between particle size distribution and the model of the particle deposition in the respiratory system published by the Commission on Radiological Protection (IRCP) (ICRP, 1994). In this study, the urban background area reveled higher concentrations than the area affected by traffic emissions in Bogota, and other similar environments reported in the scientific literature.

The submicrometric particles PM_1, which can enter the alveolar region of the human respiratory system, was 20.8 μg/m^3 in Bogota and 13.8 μg/m^3 in Palmira. The mass size distribution exhibits a bimodal distribution that is equally centered between 0.43 and 1.1 μm and 4.7 and 9.0 μm. According to the chemical composition size separated, elemental carbon was accumulated in the

fine fraction of PM$_{2.1}$ in Bogotá at a rate of 72%, relative to 57% in Palmira. On the other hand, organic carbon was more evenly distributed in fine and coarse fraction. The sulfate ion was one of the most abundant water-soluble ions in two sites, but the size distribution was different while in Palmira was mainly accumulated in fine mode, in Bogota was dispersed across the two-size fraction.

Palabras claves: Nanoparticles in ambient air, Lung Deposition of Surface Area, Particle Number Size Distribution, Size Distribution of Chemical Components of PM in Colombia.

List of Symbols and Abbreviations

Symbols with latin letters

Símbolo	Término	Unidad SI	Definición
Cu_d	Cunningham slip factor to specific diameter	m²	Equation 0-1
d_{ae}	geometrical midpoint of each ELPI⁺ stage		
d_{me}	geometrical midpoint of mobility diameter equivalent		
#/cm³	Particles number per cubic centimeter		
D50%	Cut diameter		
Di	Diameter geometric mean		
d	diameter	μm	Tabla 3-1
e	1.602 x 10⁻¹⁹ C	C	
I	Currents measured by electrometers in ELPI⁺	fA	
nm	nanometers		
Q	Charge of electron		
P	Product of penetration		

Symbols with greek letters

Símbolo	Término	Unidad SI	Definición
$\alpha = 6.32$			
$\lambda = 1/76$			
$\beta = 2.01$			
$\gamma = 0.2190$			
ρ_p	Particle density	g/cm^3	
ρ_o	unit density	g/cm^3	1 g/cm³
χ	shape factor		Section 1.2.1
μ	micro		

Abbreviations

Abbreviation	Definition
APS	Aerodynamic Particle Sizers
BAM	Beta Attenuation Monitors
DMA	Differential Mobility Analyzers
ELPI$^+$	Electrical Low-Pressure Impactor
PM$_x$	Particulate Matter with aerodynamic diameter less than x μm
PM$_{10}$	Particulate Matter with aerodynamic diameter less than 10 μm
PM$_{2.5}$	Particulate Matter with aerodynamic diameter less than 2.5 μm
PNC	Particle number concentration
PNSD	Particles Number Size Distribution
RMS	Root-Mean-Square
SMPS	Scanning Mobility Particle Sizers
WSI's	Water Soluble Inorganic ions

Contenido

List of Tables

List of Figures

Introduction

Seven million people die every year because of the negative's effects on health of be exposed to air pollution; more than 90% of these deaths happen in developing countries (World Health Organization, 2021)(Kumar et al., 2018). That is the reason why clean air is in one of the main environmental challenges of humankind, and governments and multinational entities around the world, especially in places with high population density – megacities, promote strategies to achieve the reduction of contaminants from industrial, domestic and transportation activities. In urban areas, air pollution is frequently caused by high concentrations of ozone, nitrogen dioxide and sulfur dioxide, besides particulate matter (PM) suspended in the air, from combustion of fuels.

In Colombia, PM is the atmospheric pollutant that exceeds frequently (Ministerio de Ambiente y Desarrollo Sostenible, 2017) the concentration limit established by National Regulation – Resolution 2254 of 2017 (Res. No 2254, 2017), exceeding the Recommendations of World Health Organization (World Health Organization, 2005). Therefore, many studies have been developed to establish the association between atmospheric concentrations of PM_{10} (particles with diameter less to 10 μm) and $PM_{2.5}$ (particles with diameter less to 2.5 μm) and the rate of diseases on population health. One of the recent studies was made by Rodriguez et al. (Rodriguez et al., 2018), who reported an increase of the percentage of visits to emergency rooms of health institutions due to cardiovascular diseases (5.61 %), cerebrovascular diseases (7.17%) in adults over 60 year and by respiratory diseases (8.23%) in children less than 9 years of age. This behavior was associated to the increase of 5 μg/m^3 of $PM_{2.5}$. Similar increase percentages were observed for 10 μg/m^3 of PM_{10}. In the country, epidemiological studies associating concentrations of ultrafine particles (particles with diameter less to 100 nm) with the rate of diseases on the population have not been reported.

Despite the reduction of PM_{10} and $PM_{2.5}$ concentrations in the monitoring stations of Local Environmental Authorities in Colombia, efforts are still needed to achieve the goals for 2030, which are, 30 μg/m^3 for of PM_{10} and 15 μg/m^3 for $PM_{2.5}$ for an annual period (Res. No 2254, 2017). To improve the air quality should recognize the local emissions factors of the major

sources, the impact of daily cycles and weather patterns of pollutants concentration and implement urban air quality prediction models to apply successful contingent plans on critical periods of air pollution (Kumar et al., 2018). Hence, it is important to make high-quality measurements on the ground and get full understanding of physical and chemical properties of pollutants and atmospheric processes.

The particles size and it's chemical composition are important properties to identify the source, their dynamics behavior on the atmosphere and fate (Kulkarni et al., 2004). The particles could have a wide range of size, from a few nanometers to several micrometers (since 1×10^{-9} to 1×10^{-4} meter). Knowing the size of particles, size distribution and their temporal variability is of great importance to identify the source of particles, the ability to penetrate deeply into the lung and effects on the climate (Vu et al., 2015).

The chemical composition of particulate matter depends on the sources as well as the atmospheric process more relevant in each site. The chemical substances predominantly found in $PM_{2.5}$ include a carbonaceous fraction (organic matter and elemental carbon) and inorganic ions (sulfate, ammonium, nitrates mainly). The crustal species (calcium, magnesium, aluminum and iron) are usually into PM_{10} (Seinfeld & Pandis, 2006). There are more than 40 tracer elementals that could arise from different sources including combustion of coal, diesel, petrol, biomass burning, road dust, soil or pavement erosion and brake wear. The chemical composition of PM have been used widely to link receptors and sources using statistical tools and receptor models, like show Hopke in his review (Hopke, 2016).

Studies to understand the temporal and spatial variations of PM10 and PM2.5 in Colombia were conducted using mass concentration monitoring (Ministerio de Ambiente y Desarrollo Sostenible, 2017). A few studies based on the chemical composition of PM_{10} and $PM_{2.5}$ have been developed to identify the main sources of emissions of PM (Vargas et al., 2012)(Ramírez et al., 2018)(Universidad de los Andes; Alcaldia de Bogota, 2009)(Pachon et al., 2014). The most of this research used short-term sample campaigns, which prevents taking into account regional weather trends. Also, it took months or even years to finish the chemical analysis of the samples, so the results were published significantly later. Therefore, the remote sensing has being applied since 2015 through Aeronet (AErosol RObotic NETwork), but the consistent cloudy disrupt the daily data time series (Hernandez, 2016)(Llorente Valbuena, 2017) and the size distribution obtained from Aeronet have been scarce. Up to now, there are not scientific literature or reports about the size distribution of atmospheric particle matter in urban areas in Colombia.

This study aims to understand the Particle Size Distribution (PSD) of aerosols in urban areas in Colombian, linking the local and regional sources of air pollutants and the local weather patterns. The PSD of airborne aerosols was studied in two locations in Colombia: one was Bogotá City, an urban area mainly influenced by traffic emissions, where were chosen three zones; the first corresponded to an urban background station in west of the city, the second was a traffic station, located in the center of the city and third was located at the west of the city, heavily influenced by traffic emissions of cars and trucks as well as industrial emissions. The second location is in the municipality of Palmira, in the Cauca River Valley Department, an agro-industrial area with a significant number of activities related to the harvest and industrial processing of sugar cane, including the production of alcohol, sugar, and electricity through cogeneration from sugarcane bagasse. In Palmira, there is also a significant amount of road transportation associated with agro-industrial activities, serving as a vital vehicle crossing point between the country west and other rural areas.

In the urban background and the central traffic station in Bogota was studied the Particle Number Concentration (PNC), Number Particle Size Distribution (PNSD), and Lung Deposited Surface Area (LDSA). On other hand, in the place located in the western of Bogotá and the site located in Palmira was understood the Mass Particle Size distribution (MPSD) and their chemical composition using two approaches: one was to recognize the main chemical components, such as water-soluble ions (WSI's), organic carbon (OC) and elemental carbon (EC), size segregated in nine stages in the range from 30 to 0.1 μm. The second method involved analyzing the chemical speciation of bulk $PM_{2.5}$ samples, which also included WSI's, OC, and EC species as well as organic species such carbohydrates, PAHs, and n-alkanes. These findings were analyzed to determine the number of particles, mass concentration, and chemical composition of airborne aerosol that can reach and deposit in the human respiratory system.

Hence, the aim of this research was measurement, analyze and compare the size distribution and chemical composition of airborne aerosols in various urban environments throughout Colombia, in order to determine the potential of the PM to accumulate in the respiratory systems of those exposed to each urban site.

Consequently, the following are the study's specific goals:

- To evaluate the temporal and spatial variability of the particle number concentration and particle number size distribution at two urban areas with different characteristics.

- To determinate the chemical composition of inhaling particles based on their size distribution.
- To assess the potential of airborne particle matter deposition into the various parts of the human respiratory system.
- To evaluate the chemical compositions of fine particulate matter from integrated bulk $PM_{2.5}$ samples.
- To infer the air pollutants sources from the particles size distribution and chemical composition of ambient inhaling particulate matter.

This dissertation has four chapters that present the study findings. The first chapter shows the results of the instrumental intercomparison of the Electric Low-Pressure Impactor ELPI$^+$ with a reference instrument to measure number particle concentrations and size distribution, created at the World Center Calibration for Aerosols Physics (WCCAP) in the Institute for Tropospheric Research – TROPOS's. The aim of this chapter is provided accuracy of the data set collected from the ELPI$^+$, which was used to measure Particle Number Concentrations and Particle Size Distribution in the two urban areas of Bogotá. This chapter displays the sequence to convert the raw current signal recorded by the ELPI's electrometers into number of airborne particles in size range of 17 nm to 10 μm.

The second chapter shows the spatial and temporal variability of the particles number concentration and the number and volume size distribution in two stations of air quality network of Bogotá located in the east and center of the city. The number particle size distribution was linked to the model of the particle deposition in the respiratory system published by the Commission on Radiological Protection (IRCP) (ICRP, 1994) to assess the Lung Deposition Surface Area LDSA in both stations.

The third chapter is focused on the mass size distribution of particles and their size segregated chemical composition. This chapter reveals the mass size distribution in one location in Bogotá with high traffic vehicular impact and surrounds of small and medium industrial activities. Additionally, was studied a location in Palmira, Cauca River Valley Department, where there is combination of the typical urban sources, such as, vehicular traffic emissions, with agro industrial emissions, specially derived from a sugarcane harvest. The mass size distribution is segregated into nine stages, allowing simulate the human respiratory tract and recognize the characteristics of particles that could penetrate the upper respiratory airways parts, bronchi and alveoli of people exposed to these.

The results of an extensive chemical characterization of $PM_{2.5}$ samples obtained in Palmira are detailed in the research article published and reproduced, as part of the fourth chapter of a study article. The sampling place, located in Cauca River valley region, is characterized by the harvest of sugarcane and the agroindustry produced from this crop. In this chapter reveals the concentration of water-soluble ions, trace metals, and organic and elemental carbon. Additionally, are included organic species like n-alkanes, polycycle aromatic hydrocarbons (HAPs), and carbohydrates. This chapter contributes to our understanding of the relative abundance of each chemical species and reveals the estimated $PM_{2.5}$ toxicity level based on HAP and tracer metal concentrations.

The outcomes of this study will contribute to understanding the effects of long-term exposure to aerosols on human health at both locations, inferring the major sources of aerosol emissions, and establishing effective methods to lessen the impact on population.

References

Hernandez, L. A. (2016). *Caracterización de la Contaminación por Material Particulado en Bogotá mediante Fotometría Solar Caracterización de la Contaminación por Material Particulado en Bogotá mediante Fotometría Solar*.

Hopke, P. K. (2016). Review of receptor modeling methods for source apportionment. *Journal of the Air & Waste Management Association*, *66*(3), 237–259. https://doi.org/10.1080/10962247.2016.1140693

ICRP. (1994). Human Respiratory Tract Model for Radiological Protection. In *Annals of the ICRP* (Vol. 57). https://doi.org/10.1097/00004032-198907001-00032

Kulkarni, P., Baron, P., & Willleke, K. (2004). *Aerosol Measurements. Principles, Techiniques and Applications* (P. Kulkarni, P. Baron, & K. Willleke (eds.); Third Edit). Wiley.

Kumar, R., Peuch, V., Crawford, J., & Brasseur, G. (2018). Five steps to improve air-quality forecasts. *Nature*, *651*, 27.

Llorente Valbuena, A. M. (2017). *Evaluación de la variabilidad espaciotemporal de la profundidad óptica de aerosoles en la zona carbonífera del Cesar a partir de observaciones satelitales* [Universidad Nacional de Colombia]. http://www.bdigital.unal.edu.co/62133/1/Tesis Versión Final Dic17.pdf

Res. No 2254, 11 (2017). http://www.minambiente.gov.co/images/normativa/app/resoluciones/96-res 2254 de 2017.pdf

Ministerio de Ambiente y Desarrollo Sostenible. (2017). *Informe del estado de la calidad del aire en Colombia 2017*. http://documentacion.ideam.gov.co/openbiblio/bvirtual/023844/Informe_ECalidadl_Aire_2017.pdf

Pachon, J. E., Sarmiento, H., & Hoshiko, T. (2014). Temporal and spatial variability of particle-bound polycyclic aromatic hydrocabons in Bogota, Colombia. *Air Quality, Atmosphere and Health*, *7*(4). https://doi.org/10.1007/s11869-014-0259-6

Ramírez, O., A.M, S. de la C., Amato, F., Catacolí, R. A., Rojas, N. Y., & de la Rosa, J. (2018). *Chemical composition and source apportionment of PM 10 at an urban*

background site in a high e altitude Latin American megacity. *233*, 142–155. https://doi.org/10.1016/j.envpol.2017.10.045

Rodriguez, L., Rojas, N., Blanco, L., Herrera, V., & Fernandez, J. (2018). Short-Term Effects of Air Pollution on Respiratory and Circulatory Morbidity in Colombia 2011 – 2014 : A Multi-City , Time-Series Analysis. *International Journal of Enviromental Research and Public Health*, *15*, 1610. https://doi.org/10.3390/ijerph15081610

Seinfeld, J. H., & Pandis, S. N. (2006). *Atmospheric From Air Pollution to Climate Change* (2 nd).

Universidad de los Andes; Alcaldia de Bogota. (2009). *Elementos tecnicos plan decenal de descontaminación de Bogotá*. http://oab2.ambientebogota.gov.co/es/documentacion-e-investigaciones/resultado-busqueda/elementos-tecnicos-del-plan-decenal-de-descontaminacion-de-bogota-parte-1

Vargas, F. A., Rojas, N. Y., Pachon, J. E., & Russell, A. G. (2012). PM10 characterization and source apportionment at two residential areas in Bogota. *Atmospheric Pollution Research*, *3*(1), 72–80. https://doi.org/10.5094/APR.2012.006

Vu, T. V, Delgado-saborit, J. M., & Harrison, R. M. (2015). *Review : Particle number size distributions from seven major sources and implications for source apportionment studies*. *122*, 114–132.

World Health Organization. (2005). Air quality guidelines for particles matter, ozone, nitrogen dioxide and sulfur dioxide. In *Air Quality Guidelines* (Issue 1). https://doi.org/10.1016/j.atmosenv.2

World Health Organization. (2021). *Air pollution*. https://www.who.int/airpollution/en/

1. Electrical Low-Pressure Impactor (ELPI⁺) performance assessment.

1.1. Introduction

The atmospheric particle size is a crucial factor to recognize the impact of aerosols on respiratory health hazards, visibility reduction, deposition velocity into surfaces, transport process modeling of and impact on regional and global climate. Therefore, measuring and interpretation of the atmosphere's particle size distributions are necessary for a holistic comprehension of the origin and impacts of atmospheric particles. Atmospheric particle size depends on several factors, including location, meteorological conditions, photochemical activity of the atmosphere, which modify the particle size from the originally emitted. In addition, to know the size of particles is helpful to infer the chemical composition and origin of ambient aerosol.

Airborne particles range in size from a few nanometers to several micrometers. The size ranges covered nuclei, Aitken, accumulation, and coarse modes. The nuclei mode is in the size range 5 – 20 nm, Aitken mode from 20 – 100 nm, accumulation mode from 0.1 to 2 μm, and a coarse mode greater than 2 μm (Walter, 2011). Different techniques can be used to measure particle size and understand aerosol dynamics in a wide size range. Some of them are based on the particle optical properties, others on their aerodynamic behavior, or their electrical mobility.

The appropriate particle size definition depends primarily on principle used to classified by size. Hence, for example, the aerodynamic diameter would be used to analyze the data from a cyclone, a cascade impactor, or an Aerodynamic Particle Sizer (APS). The diffusive diameter would be used for a diffusion battery measurement, the mobility

diameter for a differential mobility analyzer and the optical diameter with an optical particle counter (Walter, 2011).

According to the measured property, the particle diameter can be reported as optical diameter, stokes diameter, mobility diameter or aerodynamic diameter. Optical sizes are determined by measuring the amount of light scattered by individual particles, which depends on the particles reflective index, shape, and size. The aerodynamic size is a function of the time of flight in the nozzles of a cascade impactor and is estimated from a balance between drag and gravitational forces to find specific terminal settling velocity. It reports the particle diameter as that of a spherical water droplet (density of ρ = 1 g/cm^3). The Stokes diameter is equivalent to the diameter of the spherical particle with the same terminal settling velocity and density that the measured particles . Finally, the electrical mobility diameter, or simply mobility diameter, is based on the behavior of charged particles in an electric field, which depend on the particles cross section which is proportional to the surface area (Khlystov et al., 2004). The conversion from one measure of size to another typically involves uncertainties that may be significant (Mcmurry, 2000).

Larger particles, with a size larger than 0.5 μm, can follow the flow stream with noticeable inertia, therefore they are better described using the aerodynamic diameter. When a particle is smaller than 0.5 μm, it moves in a Brownian motion and is identified by its diffusive diameter, which is the diameter of a particle with the same diffusion coefficient as the one in question.

The instruments that use the inertial classification of particles principle are based upon the fact that particles move in a gas streamline and are captured by a surface when the inertial of the particles is smaller than the gas where they are flowing. Typically, the instruments that use impactors cascade could classify the particles up to downsize of 0.05 μm, and to cover small sizes are used techniques known as low pressure impactors or micro-orifice impactors. However, when particles are subjected to low pressures, such as 0.03 atm (30 mbar), they undergo size reduction due to the evaporation process. This is more likely to happen if the particles' components are volatile, such as VOCs, are volatile. Consequently, a cascade impactor that operates at low pressures can be employed instead of a large size range, from 50 μm to 5 nm (Kulkarni et al., 2004). The main drawbacks of inertial impactors include interstage

losses, overloading of collect particles deposited on the impaction plates, and particle bounce from the collection surface.

Aerodynamic Particle Sizers (APS), Differential Mobility Analyzers (DMA), and Scanning Mobility Particle Sizers (SMPS) (Holubčík et al., 2021; Shen et al., 2002). These instruments use two different sizing principles to measure particle size: electrical mobility and aerodynamic mobility.

1.1.1 The Electrical Low-Pressure Impactor (ELPI⁺)

The Electrical Low-Pressure Impactor (ELPI⁺) determines an aerosol size distribution in real-time, by combining of 13 cascade impactor stages in the range of 17 nm - 10 μm, and a filter stage. Each impactor stage is connected to an electrometer that detect the currents induced by charged particles. The ELPI⁺ operates in a wide range of size particles and number particle concentrations, as shown in .
Table 1-1, which indicates the diameters geometric mean of each channel (Di), the cut-off diameters (D50%) correspond to the size of particles collected with a 50% efficiency in each stage, and the minimum and maximum number of particles detected according to currents limit detection in each stage by the electrometers.

Table 1-1. Data sheet of cascade impactor in ELPI⁺ for each stage.

Stage	Di (μm)	D 50% [μm]	Number min [1/cm³]	Number max [1/cm³]
15		10		
14	8.25	6.8	0.1	2.4×10^4
13	5.47	4.4	0.1	2.4×10^4
12	3.32	2.5	0.15	5.4×10^4
11	2.00	1.6	0.3	1.1×10^5
10	1.26	1	0.5	1.9×10^5
9	0.80	0.64	1	3.5×10^5
8	0.51	0.4	2	6.4×10^5
7	0.32	0.26	3	1.2×10^6
6	0.21	0.17	5	2.1×10^6

Stage	Di (μm)	D 50% [μm]	Number min [1/cm^3]	Number max [1/cm^3]
5	0.14	0.108	10	3.7×10^6
4	0.08	0.06	20	7.3×10^6
3	0.042	0.03	50	1.7×10^7
2	0.022	0.017	100	3.5×10^7
1	0.010	0.006	250	8.3×10^7

The ELPI$^+$ consists of three parts: a unipolar diffusion chamber, 13-stage cascade impactor and the filter stage, and a set of electrometers connected to each impaction stage, as show in Figure 1-1a. The unipolar diffusion chamber has a corona charger (a needle) that produces a positive high voltage (3.5 kV), constant discharge of 1 μA towards the aerosol particles flowing through it. The released flow of ions produces particles with a known positive charge that is stable under different operation conditions and is high enough to ensure detection by electrometers. The aerosol then flows through a voltage trap, formed by two concentric cones with a potential difference of 20 V $\pm$ 2V, which produces a static direct current (DC) field, removing the charged particles that have a smaller size than the measuring range of the instrument before they enter the impactor (Marjama et al., 2000). It is essential to highlight that the unipolar charging of ELPI$^+$ is related to the active surface area for smaller particles, thus the primary signal of electrometers corresponding to the size distribution of the particle's surface area (Pagels et al., 2007). Figure 1-1b displays a photo of the ELPI$^+$ instrument utilized in this study, which was shot during the intercomparison conducted at Leibniz Institute for Tropospheric Research. The operational parameter that guarantees the proper operation of ELPI$^+$ is summarized in Table 1-4, showing the respective reference values.

The cascade impactor of ELPI$^+$ is used to classify and collect the particles according to the aerodynamic diameter in the 6 nm - 10 μm range. Thus, stage 15 has a cut-off diameter of 10 μm and subsequent stages have smaller cut diameters, down to stage 2, with a cut-off diameter of 17 nm, as shown in .
Table 1-1. Stage 1 or filter stage, consists of multiple layers of fine mesh that traps particles smaller than 17 nm, for a cut-off diameter of 6 nm.

a)   b)
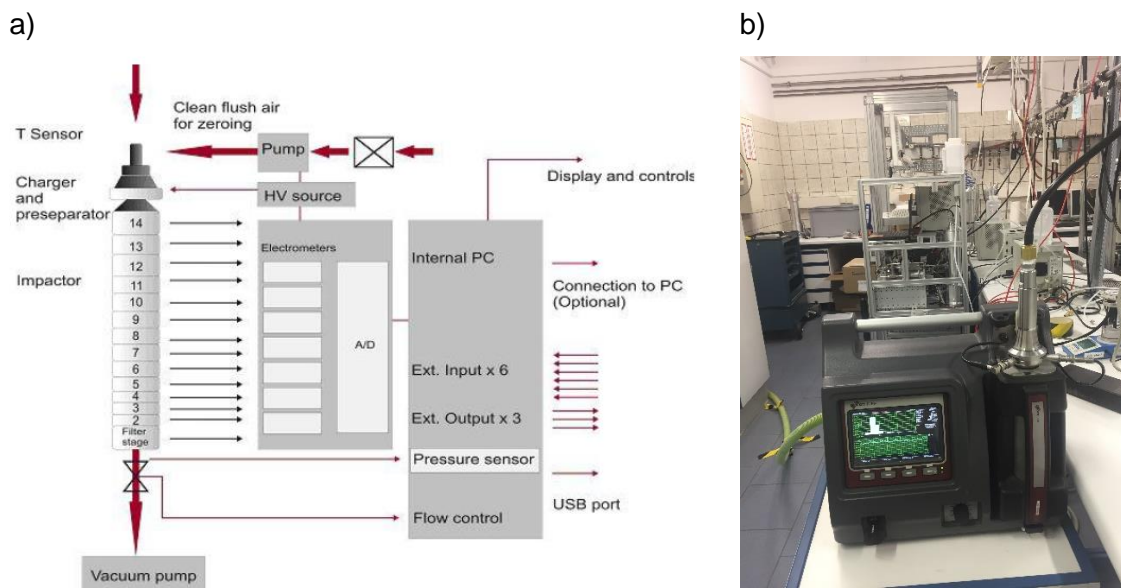
Figure 1-1. a). Schematic of the components and operating principle of the Electrical Low-Pressure Impactor (ELPI⁺). Source: (DEKATI, 2016). b) Photo of ELPI⁺ during the intercomparison with SMPS in Leibniz Institute for tropospheric research.

The electrical current that the particles release as they collide with the impactor surfaces is measured by electrometers. Each electrometer can measure current signals with a resolution of fA between 0 and 500 pA (DEKATI, 2012). Through correlations between the currents detected, particle properties, such as shape (on under assumption of spherical particles), the bulk density (ρ_p), and operational conditions, such as flow rate, these currents are converted to particle surface area, number, volume, and mass size distributions.

The accuracy of ELPI⁺'s measuring is determined by the charger efficiency function, the bulk density, the interstage losses and the particles bounced.

➢ Regarding to the charger efficiency function, it depends on the operational conditions, such as the air flow rate and the pressure under the first stage, in addition to the sizes of the nozzles that affect the cut-off diameter values.

➢ The particle's charge in ELPI⁺ is based on the mobility diameter and then are separated, by inertia, according to the aerodynamic diameter. When the

electrically charged particles is deposited on the impaction stage in the ELPI[+], an electrical current is generated, and the particles are accounted for. Therefore, the particle number concentration detected in each stage uses the two particle diameters concepts, and the conversion between these requires the knowledge of density to convert on into the other, as shown in $d_{me} = d_{ae}\sqrt{\chi\left(\frac{Cu_{d_{ae}}}{Cu_{d_{me}}}\right)\left(\frac{\rho_o}{\rho_p}\right)}$ Equation 1-2 (Charvet et al., 2015). Thus, the aerodynamic diameter is proportional to the particle density and for this reason, also depends on particle chemical composition.

➤ The diffusion in the impactor causes that are smaller particles than the cut-off diameter of an impaction surface to be collected to some extent. This phenomenon has little impact on the outcome in gravimetric impactors since the smaller particles' mass is frequently tiny in comparison to the coarser particles. However, the effect can be large when the particles are detected by electrical charge because the electrometers are more sensitive to it (DEKATI, 2012).

➤ At cascade impactors a fraction of particles could bounce over the impactor collection plate and cause an overestimation of electrical charge measured, and therefore of the number of particles. To reduce the particle's bounce, the collection substrate of each impactor needs to be greased to the particle's stuck once is impacted and sensed. Nevertheless, the filter stage of the cascade impactor in ELPI[+] does not have a substrate to be greased, therefore it can cause particle bounce and overestimation of the particles in the range of 17 to 6 nm.

The collection efficiency curves are used to offset the bounce and diffusion phenomena and to determine accurately the aerodynamic diameter of each stage , which have an s-shaped function. This allows to compensate for the lower and upper tails of the particle size sensed in each stage. The collection efficiency curves are describe by Marjama et al., (2000).

1.1.2 The scanning mobility particle sizer

Figure 1-2 shows the two main components of a SMPS, which consists of an electrostatic size classification (Differential Mobility Analyzer or DMA), typically followed by a condensation nuclei counter (CNC), or condensation particle counter (CPC). Entering particles are charged by a Krypton 85 radioactive device before entering the region between two coaxial cylinders held at different electric potential. Charged particles migrate toward one cylinder. Depending on the voltage, particles of a certain size enter a gap in the cylinder and directed into a CPC, where they grow by the humidification with butanol and then are counted optically. By varying the voltage, particles of different sizes will pass through the gap and be counted (Wallace, 2009).

a)   b)

C)
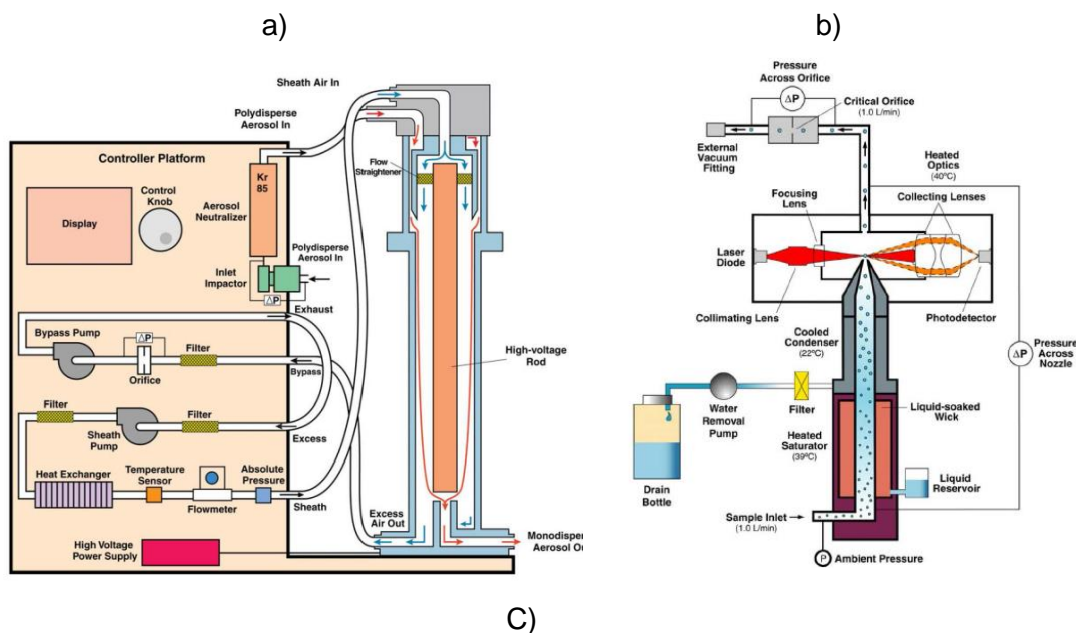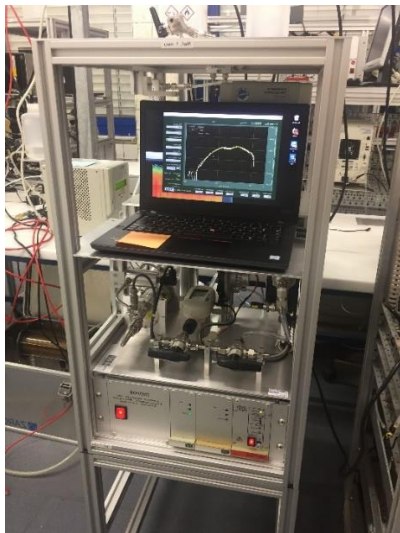
Figure 1-2. Schematic of the of the components and operating principle of the SMPS. a) corresponding to schema of DMA, b) CPC taken from Kuang, (2016) and c) is a photo of SMPS used during the intercomparison with ELPI[+.]

1.1.3 Comparisons of ELPI[+] with other instruments

Due to the air quality current legislation in most countries requiring mass concentration of PM_{10} and $PM_{2.5}$ size fraction and not particle number concentration and size distribution, the instruments with emphasis on the measurement of an ambient number of particles does not have calibration standards available to ensure the accuracy of the measurement in the submicrometric size range. Therefore, the common method to calibrate the instruments such as ELPI[+], has been the intercomparison with electrical mobility analyzers (Charvet et al., 2015; Held et al., 2008; Järvinen et al., 2014a; Yli-ojanper, 2012).

In the first version of ELPI, the instrument measured particles in range from 30 nm to 10 μm, and then was extended the electrically measured size range down to 7 nm by adding a new impactor stage and a filter stage, in the flow direction of the device. The new version of the instrument is recognized as ELPI[+] (Marjama et al., 2000). Thus, the measurements of nanoparticles in range of 10 – 20 nm improves in the ELPI[+], showing a collection efficiency of 97% for particles of these size range and better response of

the inversion algorithms to estimate the nanoparticles concentrations (Järvinen et al., 2014b; Yli-ojanperä et al., 2010).

Several air quality monitoring studies (Charvet et al., 2015; Gouriou et al., 2004; Held et al., 2008; Li et al., 2018; Lingard et al., 2006) compare measurement performed by instruments with different measurement principles. Thus, it is important to know the uncertainty and precision of measurements in different size ranges to compere results obtained from different instruments. For instance, Price, *et al.* (Price et al., 2014) compared Aerodynamic Particle Sizers (APS), Fast Mobility Particle Sizers (FMPS), SMPS and ELPI, using particles generated with different size, morphology and chemical composition. They found good agreement among all instruments in the 50 – 300 nm range, independently if the instrument sensed aerodynamic diameter (APS, ELPI) or electrical mobility diameter (FMPS and SMPS). Particularly, ELPI showed better agreement with SMPS and FMPS for particles of soot in range of 7 to 28 nm and overestimation of particles of TiO_2, NaCl and fumed silica in the same size range. This discrepancy has been attributed to a high impaction velocity on lower ranking range of the ELPI, which caused particle's bounce and therefore, increasing the electrometers signal produced by the corresponding size bin (Kulmala et al., 2010; Leskinen et al., 2012). Otherwise, for particles larger than 1 μm, the ELPI can just be compared with the APS, and higher concentrations were measured with the ELPI. In summary, ELPI generally measures higher particle numbers than other instruments in the upper and lower size limits (stages 15 and 1, respectively). The intercomparison carried out with ambient particles by Held, *et al.* (Held et al., 2008) shows a good agreement with other instruments, such as SMPS (rank correlation coefficient of r = 0.7 – 0.95).

To compare particle number concentrations (PNC) measured by an instrument based on impaction with those measured by an instrument based on electrical mobility, the bulk particle density must be taken into consideration. Charvet et al., (2015) demonstrated that assuming a standard density of 1 g/cm^3 in the conversion could overestimate the PCN by a factor of 1.5. Therefore, choosing density appropriately is relevant.

Table 1-2. Comparison of sampling instruments used in this study

Instrument	Particle size range	Advantages	Disadvantages	References of the use to air quality studies.
ELPI+	7 nm – 10 μm	Wide size range Good time resolution (ca. 1 second) Measures PNC, PNSD, PM_1, $PM_{2.5}$, PM_{10} Long time operation	PSD at low resolution Inability to measure very small particles	(Held et al., 2008)(Klejnowski et al., 2013)(Lingard et al., 2006)
SMPS	14 nm – 800 nm	PSD at high resolution Ability to measure very small particles Long time operation	Low time resolution (minutes)	(Zhang et al., 2005)
BAM	PM_1, $PM_{2.5}$, PM_{10}	Wide size range Long time operation	Limited Size Range Unsuitable for submicrometric particles	(Duc et al., 2020)(Instituto de Salud Carlos III et al., 2013)

This chapter shows the results of the performance assessment of the ELPI+ by intercomparing it to other instruments that measure particle number concentration, particle size distribution, and mass concentration of ambient aerosols. The Particle Number Concentration (PNC) and Particle Number and Volume Size Distributions (PNSD and PVSD) measured with ELPI+ were compared with an SMPS, whereas ELPI+ mass concentrations (PM_{10} and $PM_{2.5}$) were compared with those performed by a Beta Attenuation Monitor (BAM).

1.2 Methodology

1.2.1 Particle number concentration and size distribution assessment

The intercomparison of the ELPI$^+$ used in this doctoral research and a reference SMPS was conducted at the World Calibration Center for Aerosol Physics at the Leibniz Institute for Tropospheric Research in Leipzig, Germany. Both instruments were connected to a single line sampling ambient aerosol, and the metrics for comparison were Particle Number Concentration (PNC) and Particle Number Size Distribution (PNSD). The intercomparison was performed for one week, 7th – 15th March 2019. Electrometers were zeroed and data were download each 24 hours. In total, 2254 data from the ELPI$^+$ and 2483 data from the SMPS were collected, segmented in short term periods, as indicated in Table S1.
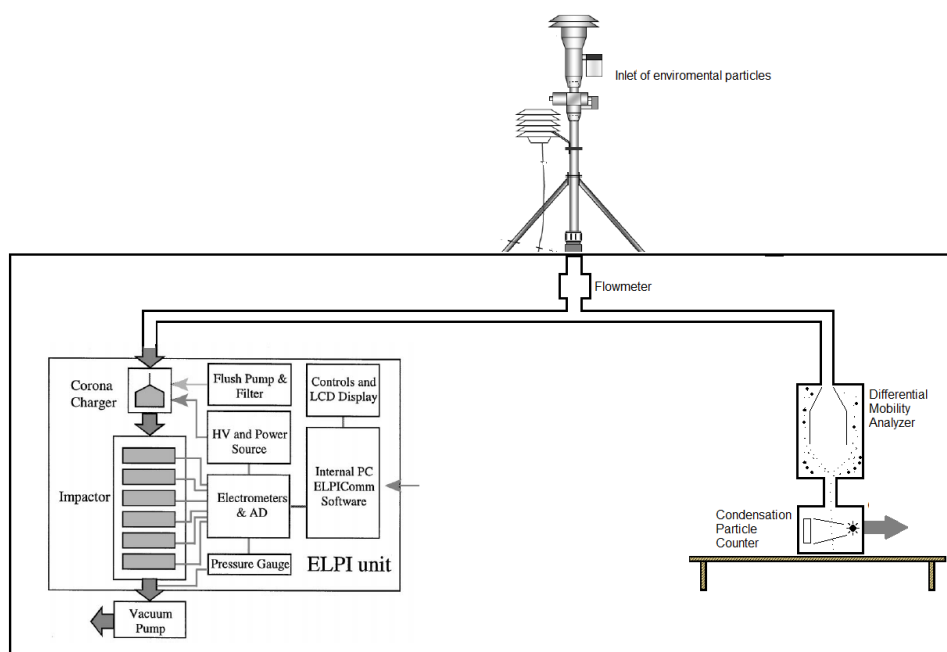
Figure 1-3. Diagram of the experimental setup to compare Particle Number Concentration (PNC) and Particle Number Size Distribution (PNSD).

The ELPI$^+$ sampled ambient air at a nominal flowrate of 9.85 liters per minute. Greased aluminum foils, provided by Dekati®, were used as collection substrates, to minimize particle bounce. The sample was conditioned to 40% relative humidity and 22 ºC of temperature. The

pressure under the filter stage was maintained at 38.3 mbar. The charger voltage (U) was 3500 kV ± 36.7 kV and the charger current (I) was consistent at 1 μA ± 0.004 kV. The trap voltage was kept at 20 V ± 0.00 V. The time resolution of data saving was 1 minute.

Ambient aerosol flow through the SMPS was 4.0 L/min. The instrument time resolution was 5 minutes and its size interval covered from 8.7 nm to 835 nm, which overlaps with ELPI+ stages 1 to 10, with aerodynamic diameters ranging from 6 nm to 1000 nm.

The conversion of aerodynamic to mobility diameter was based on used by Khlystov et al., (2004); & Shen et al., (2002) in the comparison of a coupled system of SMPS and APS with TEOM, MOUDI and Partisol. In this equation d_{ae} is the geometrical midpoint of each ELPI stage, ρ_p is the density assumed for sampled particles, ρ_o is the unit density (1 g/cm³), Cu_d is the Cunningham slip correction factor, which represents the modification to drag in the transition and free molecular regimes, and χ is the shape factor, which is function of the diameter and the particle's morphology (Decarlo et al., 2004). Given there was no available information about morphological properties, such as mass and volume of ambient aerosol; particles were assumed to be perfect spheres ($\chi = 1$) with an effective density of $\rho_p = 1.6 \ g/cm^3$.

Previous studies, based on the chemical composition of urban ambient particles, have found density values in the 1.5 – 1.6 g/cm³ range (Held et al., 2008; Hu et al., 2012; Khlystov et al., 2004; Zhang et al., 2005), as well as χ values in the 1 - 2.5 range, based on the morphology and type of aggregation of components. Spherical and compact (with minimum internal space) particles can be modeled with a value of $\chi \approx 1$, limiting the equivalence between d_{ae} and d_{me} to the factor $\left(\frac{\rho_o}{\rho_p}\right)$= 0.8 for this study. Irregular particles, even more with internal voids, have $\chi > 1$ and therefore $d_{me} \gg d_{ae}$ (Decarlo et al., 2004).

The Cunningham slip factor was calculated using $Cu_d = 1 + \frac{2\lambda}{d}\left[\alpha + \beta exp\left(-\frac{\gamma}{2\lambda/d}\right)\right]$ Equation 1-1, where the parameters were $\lambda = 1/76$, $\alpha = 6.32$, $\beta = 2.01$ and $\gamma = 0.2190$ for d taken as the cut diameter, D50%, of each stage (DEKATI, 2012).

$$Cu_d = 1 + \frac{2\lambda}{d}\left[\alpha + \beta exp\left(-\frac{\gamma}{2\lambda/d}\right)\right] \quad \text{Equation 1-1}$$

$$d_{me} = d_{ae}\sqrt{\chi\left(\frac{Cu_{d_{ae}}}{Cu_{d_{me}}}\right)\left(\frac{\rho_o}{\rho_p}\right)} \quad \text{Equation 1-2}$$

The equivalent mobility diameters calculated by the and $d_{me} = d_{ae}\sqrt{\chi\left(\frac{Cu_{d_{ae}}}{Cu_{d_{me}}}\right)\left(\frac{\rho_o}{\rho_p}\right)}$

Equation 1-2 resulted in a range from 4 nm to 775 nm, as shown Figure 1-4.

Figure 1-4. Equivalence between aerodynamic diameters by stage of ELPI⁺ and mobility diameters assuming a ρ = 1.6 g/cm^3 and spherical ambient particles.
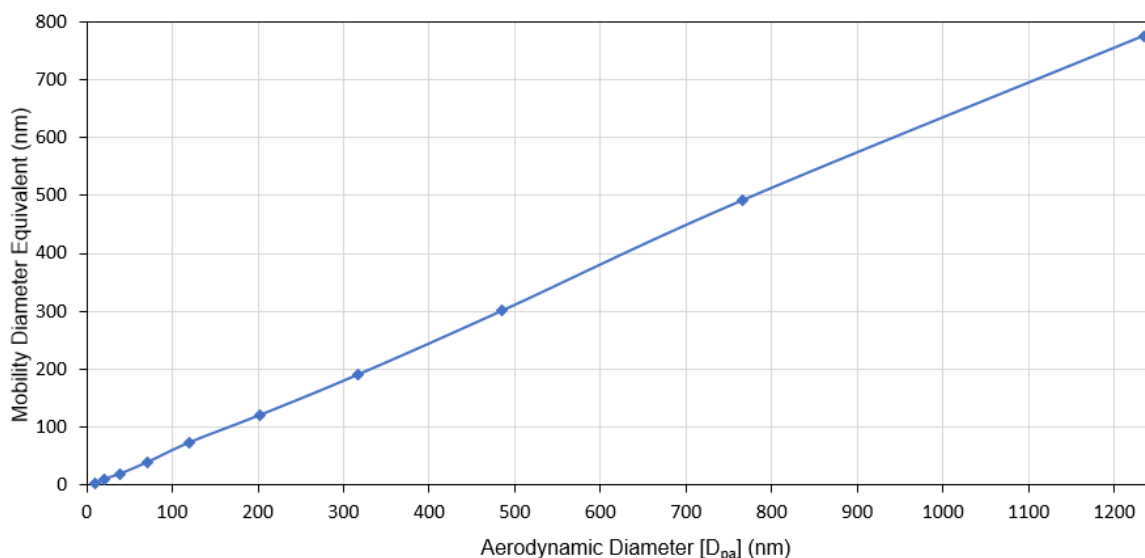
The procedure to compare PNC obtained with SMPS and ELPI⁺ required converting ELPI⁺ raw data, corresponding to electrical currents measured for each stage, into particle number concentrations. This procedure was carried out in four steps. First, raw current values and ELPI⁺ operating parameters were examined to assure that the instrument had operated correctly. Table 1-4 shows the parameters that describe appropriate operation. Second, the aerodynamic diameter was converted to electric mobility diameter for each stage. Third, the ELPI⁺ charge function was evaluated to convert currents in each stage to particle number. Fourth, particles number concentrations and number and volume particle size distribution were compared with those from the SMPS.

To calculate the particle number concentration for each impactor stage, the charging efficiency as a function a particle size must be known. The particle number concentration at a known particle size can be calculated from the currents measured by each electrometer (I) divided by

the product of penetration (*P*), average number of elementary charges per particle (n) multiplied by the charge of an electron *e* (1.602 x 10^{-19} C) and the air flow rate through the charger (*Q*), as indicate the Equation 1-3, *N* corresponding to the particle number concentration (# cm^{-3}) (Järvinen et al., 2014b; Marjama et al., 2000).

$$N= \frac{I}{(Pn)eQ} \qquad \text{Equation 1-3}$$

Then, the current values are multiplied by the conversion factors presented in Table 1-3 to obtain number, diameter, area, volume, and mass for each stage of the cascade impactor.

ELPI$^+$'s performance was assessed in terms of the PNC measured by the ELPI$^+$ in the 6 nm – 1 µm size range and by the SMPS in the 8.7 nm – 835 nm. Additionally, PNSD from both instruments was compared to examine their agreement.

The Deming total least square regression analysis (Therneau, 2018) was performed using the Deming package of the R software, to compare data from both instruments, accounting for the independent variable errors from each instrument. The regression of a variable to other (x ~ y) minimizes the sum of squared horizontal and vertical distances to the predicted values. Slope, intercept, regression coefficient, and root-mean-square difference (RMS) of the correlation were used as tools of comparison between two instruments.

Table 1-3. Conversion vectors used to calculate current, number, diameter, area, volume, and mass from the charge sensed by the electrometer at each stage of ELPI+. Source: (DEKATI, 2012)

Conversion vectors											
ELPI+ stage	1	2	3	4	5	6	7	8	9	10	11
Da (nm)	0.006	0.017	0.028	0.055	0.093	0.155	0.263	0.383	0.615	0.951	1.600
Di (nm)	0.0099	0.0213	0.0389	0.0714	0.1198	0.2019	0.3174	0.4853	0.7648	1.2335	1.9596
dLogDp	0.44	0.22	0.30	0.23	0.22	0.23	0.16	0.21	0.19	0.23	0.18
Current I [fA]	1.000	1.000	1.000	1.000	1.000	1.000	1.000	1.000	1.000	1.000	1.000
Number N [1/cm³]	209.476	76.634	34.557	15.498	7.827	3.928	2.161	1.233	0.676	0.360	0.195
Diameter D [μm/cm³]	2.084	1.632	1.345	1.107	0.938	0.793	0.686	0.598	0.517	0.444	0.382
Area A [μm²/cm³]	0.065	0.109	0.165	0.248	0.353	0.503	0.684	0.912	1.243	1.719	2.354
Volume V [μm³/cm³]	0.000	0.000	0.001	0.003	0.007	0.017	0.036	0.074	0.158	0.353	0.769
Mass M [mg/m³]	0.000	0.000	0.000	0.000	0.000	0.000	0.000	0.000	0.000	0.000	0.001
Current dI/dlogDp [fA]	2.276	4.508	3.313	4.435	4.470	4.355	6.126	4.862	5.282	4.426	5.679
Number dN/dlogDp [1/cm³]	476.805	345.436	114.497	68.739	34.985	17.106	13.238	5.995	3.572	1.592	1.108
Diameter dD/dlogDp [μm/cm³]	4.744	7.358	4.457	4.910	4.191	3.454	4.202	2.910	2.732	1.963	2.171
Area dA/dlogDp [μm²/cm³]	0.148	0.492	0.545	1.102	1.578	2.191	4.189	4.436	6.564	7.609	13.367
Volume dV/dlogDp [μm³/cm³]	0.000	0.002	0.004	0.013	0.031	0.074	0.222	0.359	0.837	1.564	4.366
Mass dM/dlogDp [mg/m³]	0.000	0.000	0.000	0.000	0.000	0.000	0.000	0.000	0.001	0.002	0.004

1.2.2 Particle number concentration assessment

The particle mass concentration assessment was conducted in two sites of Bogota's Air Quality Monitoring Network (Figure 1-5). The first site was "Las Ferias", close to the geographical centroid of the city (Lat: 4º 44'9.12" N; Lon: 74º 4'56.94" W), which is representative of an urban area primarily affected by traffic emissions. The second site was "San Cristobal" (Lat: 4º 34'21.19" N; Lon: 74º 5' 1.73" W), which is a representative of a suburban area in the southeast of the city, upwind from the most significant urban pollutants that have a continuous impact on Bogotá's air quality.

Las Ferias and San Cristobal sites have Beta Attenuation Monitors (BAM) to produce hourly values of PM_{10} and $PM_{2.5}$. Simultaneous measurements with BAM and ELPI+ were conducted for 13 consecutive days in Las Ferias (23 June and 5 July 2017) and 14 days in San Cristobal (30 August – 11 September and 27 September to 10 October 2017). BAM measurements hourly PM_{10} and $PM_{2.5}$ concentrations were compared with hourly PM_{10} and $PM_{2.5}$ estimated from

ELPI⁺, averaged from second-by-second number concentrations. Both instruments' inlets were situated at approximately 4.6 m and 4.0 m, respectively, from the ground (Secretaría Distrital de Ambiente (SDA), 2017).

PM_{10} and $PM_{2.5}$ were calculated using Equation 1-4 and Equation 1-5, respectively. PM_{10} was obtained as the sum of particle mass concentrations between stages 1 to 15, since stage 15 has a cut diameter of 10 µm. Likewise, $PM_{2.5}$ was calculated as the sum of particle mass concentrations between stages 1 to 12, since stage 12 has a cut diameter of 2.5 µm. The mass concentration for each stage was estimated as a function of the density associated with the environmental aerosols (1.6 g/cm³), the number of particles counted in each stage and the cubed aerodynamic diameter.

Equation 1-4
$$PM_{10} = \sum_{i=1}^{15} mass\ concetracion\ in\ stage\ i\ \ = \sum_{1}^{15} \frac{\pi(\rho_{aerosol})(D_{pa})^3}{6}(\#\ particles\ cm^{-3})_i$$

Equation 1-5
$$PM_{2.5} = \sum_{i=1}^{12} mass\ concetracion\ in\ stage\ i\ \ =$$
$$\sum_{1}^{12} \frac{\pi(\rho_{aerosol})(D_{pa})^3}{6}\left(\#\ particles\ cm^{-3}\right)_i$$
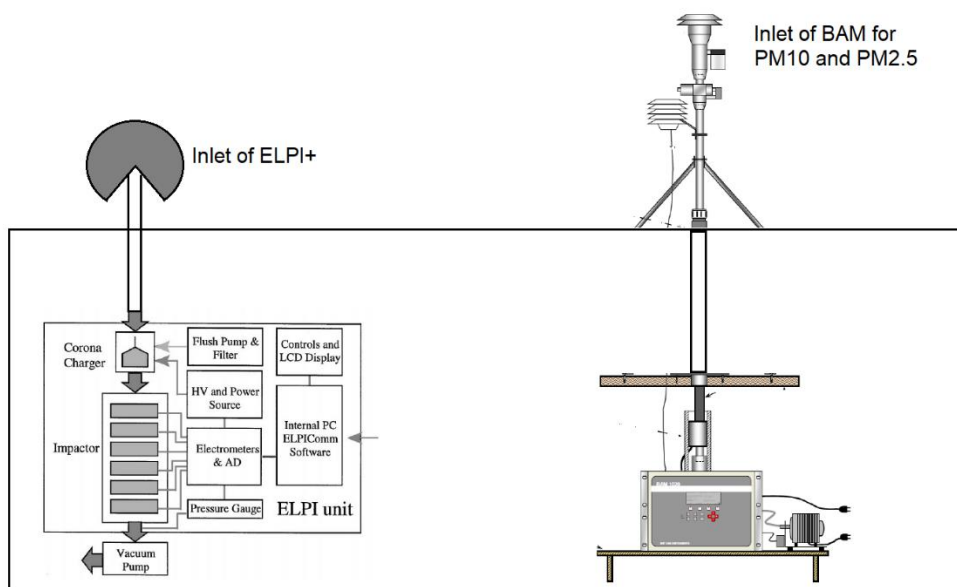
Figure 1-5. Experimental setup scheme to compare PM_{10} and $PM_{2.5}$ estimated by ELPI⁺ and measured with BAM.

As in the case of particle number concentration comparisons, the Deming total least square regression analysis was performed for particle mass concentration comparisons (Therneau, 2018).

1.3 Results

Results from two measurement intercomparison campaigns are presented below. The intercomparison of the particle number concentrations, and particle number size distribution derived from simultaneous measurements of airborne particles carried out with ELPI$^+$ and SMPS in Germany, and the comparison of PM_{10} and $PM_{2.5}$ mass concentrations estimated from ELPI$^+$ measurements and made with BAMs installed in Bogota's Air Quality Monitoring Network. The ELPI$^+$ operation parameters used for the quality assurance of data are included in this chapter.

1.3.1 ELPI$^+$ raw data examination

ELPI$^+$ operating parameters recorded during the intercomparison with the SMPS are summarized in Table 1-4 and plotted in Figure S1, demonstrating that the instrument operated correctly during the intercomparison period. Only stages 1 – 10 of the ELPI$^+$ (range of aerodynamic diameter from 10 nm to 1.2 μm) were considered in this intercomparison because the SMPS diameter range was 8.7 nm – 835 nm (0.835 μm). Over 97% of the current was measured in the first ten stages, which implies that the same percentage of the particles have an aerodynamic diameter between 10 nm and 1.2 μm. Figure 1-6 displays that the electrometer of stages with an aerodynamic diametric larger than 1 μm had currents lower than 2 fA, while stages 2, 3 and 7 measured the maximum current intensities, around 12,5, 9.2 and 9.7 fA.

Table 1-4. Operating parameters of ELPI⁺ during its intercomparison with SMPS

Parameter	Reference value	Average ± sd	Relative sd (%)
Charger U (kV)	3.5 ± 0.5	3.512 ± 0.036	1.1%
Charger I (μA)	1	1 ± 0	0.4
Trap U (V)	20 ± 2	20 ± 0	0.0
Pressure at first stage (mbar)	40 ± 5	38.3 ±0.25	0.7
Air flow (Liters per minute)	10	9.85	
Ambient Pressure (mbar)		1226.61	0.5
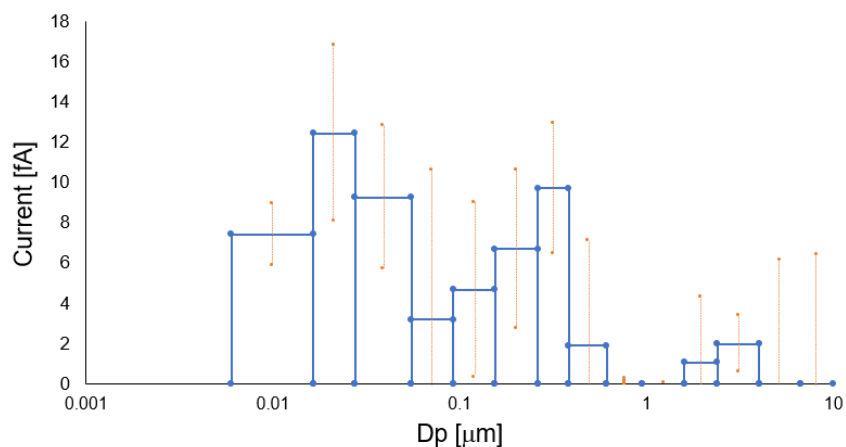
Figure 1-6. Average currents measured by electrometers in ELPI⁺ as a function of aerodynamic diameter.

Once ELPI⁺ operating parameters from all measurement series were examined, the particle number concentrations in the 0.1 nm – 1.2 μm rage were compared with those obtained from SMPS in the 8.7 nm – 835 nm range.

1.3.2 Particle number concentrations

Particle Number Concentrations (PNC) in ambient air measured with ELPI⁺ and SMPS are shown in Figure 1-7a. It is notable that PNC calculated by adding the first ten stages of ELPI⁺ (from 6 nm to 1 μm of aerodynamic diameter) were higher than PNC measured by SMPS (8.7 nm – 835 nm mobility diameter), while ELPI⁺ PNC excluding the first stage shows better agreement with SMPS PNC. The Spearman correlation between PNC measurement with SMPS and ELPI⁺ considering the ten first stages was $r^2 = 0.71$, while the correlation excluding the first stage was $r^2 = 0.82$, as shown in Figure 1-7b. Higher correlations were reported by (Held et al.,

2008), with a correlation coefficient of r^2 = 0.94 between and ELPI[+] and SMPS. In addition, the linear correlation showed a positive bias of 508 particles/cm³ when the first stage was included, which is the average overestimation observed in the PNC time series (Figure 1-7a), whereas omitting the first stage, corresponding to the 17 nm – 1 µm size range in ELPI[+], produced a negative bias of 29 #/cm³.

The PCN overestimation measured with ELPI[+] was mainly attributed to the first stage, in the 6 – 17 nm size range. This stage has a relevant role in PNC because it measured 47.6% ± 16.9% of submicrometric particles. Other relevant stages were stage 2 (17 nm – 30 nm) with 24.7% ± 7.7%, stage 3 (30 – 60 nm) with 13.2 ± 10.0%, and stage 4 (60 nm – 108 nm) with 6.5 ± 5.2% of submicrometric particles. That means that approximately 92% of PNC were estimated in the 6 nm - 100 nm range. Particularly, the higher the PNC, the larger the overestimation produced by the first stage of ELPI[+].

In addition, the 24-h average PNC time series also show the overestimation obtained by the ELPI[+] when stage 1 was included, whereas a better agreement was found excluding it, as observed in Figure 1-7d. At the traffic rush hour (6:00 and 18:00 h), ELPI+ PNC including stage 1 had a larger difference than ELPI+ PMC excluding it. The relative error (rms) between PCN of ELPI[+] excluding the first stage and SMPS was 414.3 #/cm³.
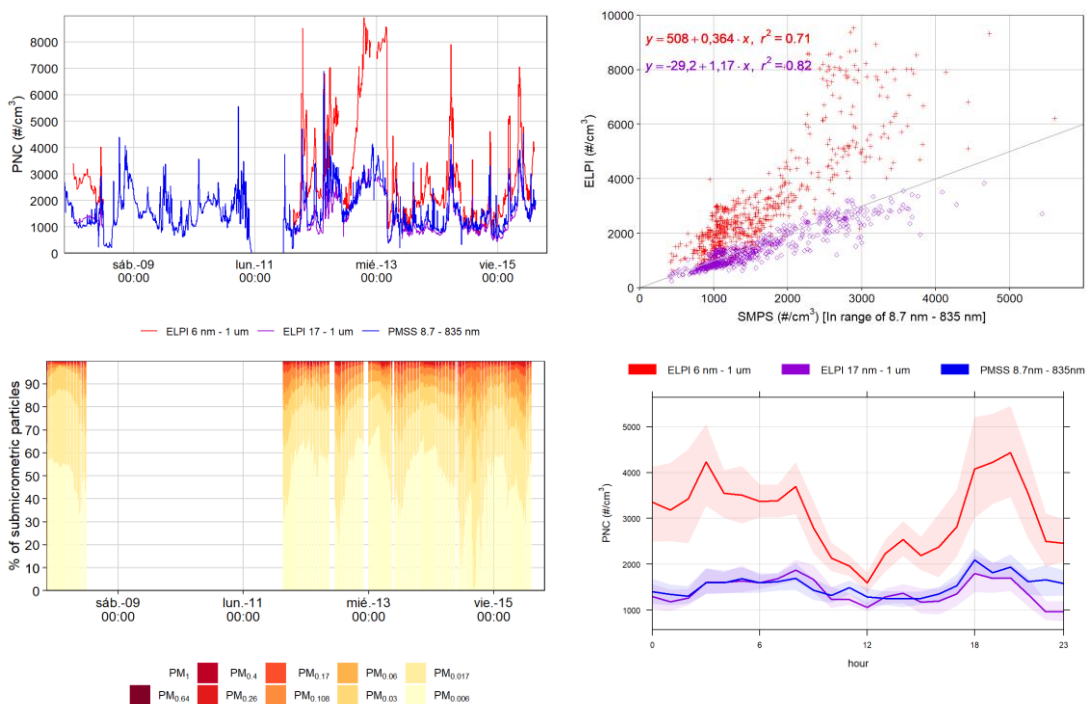
Figure 1-7. Comparison of PNC obtained with ELPI[+] and SMPS (10 min averages) in Leipzig – Germany (N=615 pairs of variables considered). A) Time series of PNC measured with ELPI[+] including stage 1 in red, excluding stage 1 in purple, with SMPS between 8.7 nm and 835 nm in blue. B) Linear fit between PNC measured in SMPS and ELPI+ including stage 1 in red crosses and excluding stage 1 in purple circles. C) Time series of the percentage of PNC determined in stages of ELPI[+]. D) Time variation plot comparing the hourly variation of ELPI[+] PNC including stage 1 in red, and excluding stage 1 in purple, with SMPS (8.7 nm – 835) in blue.

In summary, the first stage of the cascade impactor, associated with particles in the 6 nm – 17 nm aerodynamic diameter range, produces a large bias and should not be taken into consideration when estimating ambient air PNC with ELPI[+]. This has been reported to happen in atmospheric aerosol by (Held et al., 2008). To avoid artificial maxima at the lower end of the size distribution, the number of particles estimated by this stage of ELPI[+] should be excluded.

1.3.3   Particle number size distribution

PNSD measured with ELPI[+] and SMPS were compared on a 24-h average basis. PNC generally decreases with increasing particle diameter. SMPS shows mostly two modes, one from 10 to 100 nm and the other from 100 nm to 1 μm. The first mode reached over $1x10^3$ #/cm^3 and the second was between $1x10^2 - 1x10^3$ #/cm^3. On the other hand, PNSD measured by ELPI[+] was unimodal and centered in the second stage, around 21 nm. Figure 1-8 illustrates the comparison of average PNSD measured with ELPI[+] and SMPS from ambient air in a suburban area of Leipzig, Germany.
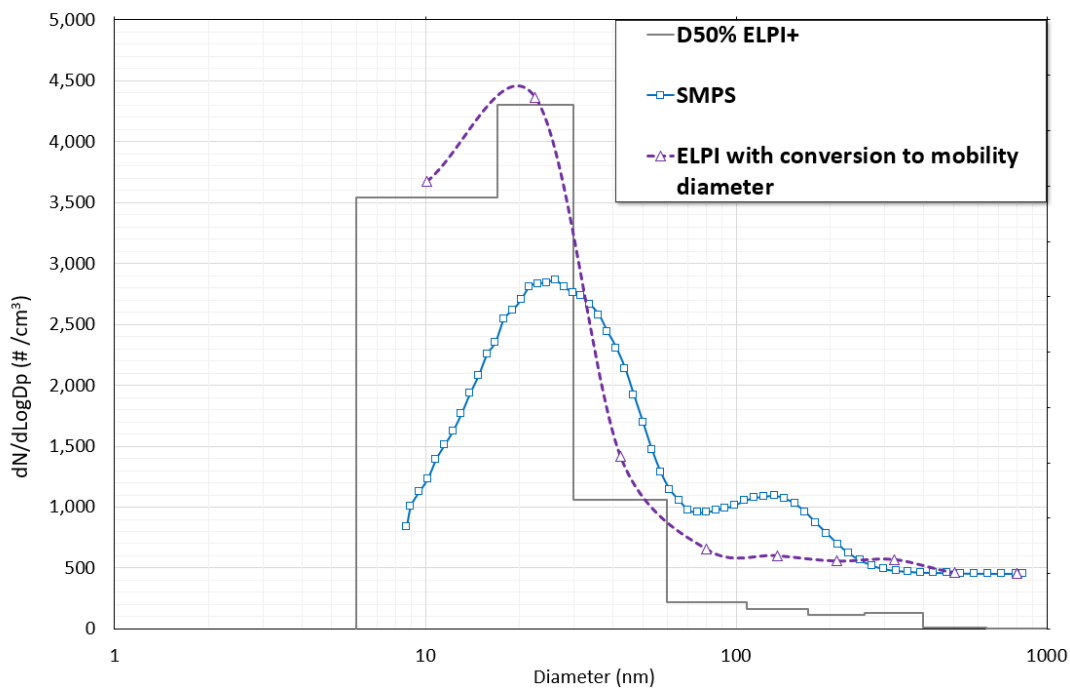
Figure 1-8. Number Particle Size Distribution (PNSD) measured with SMPS and ELPI+ from ambient air in Leipzig. Purple dashed line is the PNSD of ELPI[+], the blue line is the PNSD of SMPS and grey solid line is PNSD by ELPI stages.

The PNC overestimation produced in stage 1 of ELPI[+] generated an artificial maximum for particle diameters below 10 nm. Therefore, PNC estimated in this stage was not considered in this study to assess PNSD. The average maximum number of particles recorded by the SMPS was 2362 ± 619 (CV: 26%) in the range of 27 ± 5 nm, while the average maximum number of particles recorded with ELPI[+] was 4073 ± 1481 (CV = 36%) centered in stage 2 for all measurement series, in the 17 − 23 nm particle size range. A positive finding was that the diameter where the maximum concentrations of particles were identified in ELPI[+] and SMPS were similar. However, the maximum PNC had a significant difference between both instruments (a factor ~2 larger with ELPI[+]).

1.3.4 Volume particle size distribution

The particle volume size distribution from SMPS showed a unimodal distribution, centered around 190 nm, which corresponds to stage 6 of ELPI$^+$ (*D50%* = 170 nm), as shown in Figure 1-9. The PVSD measured by ELPI$^+$ had a higher peak than the one measured by SMPS, specifically noticeable at the diameter where the distribution is centered, but with similar width (or standard deviation) and a lower tail, showing the influence of the little volume of fine particles.
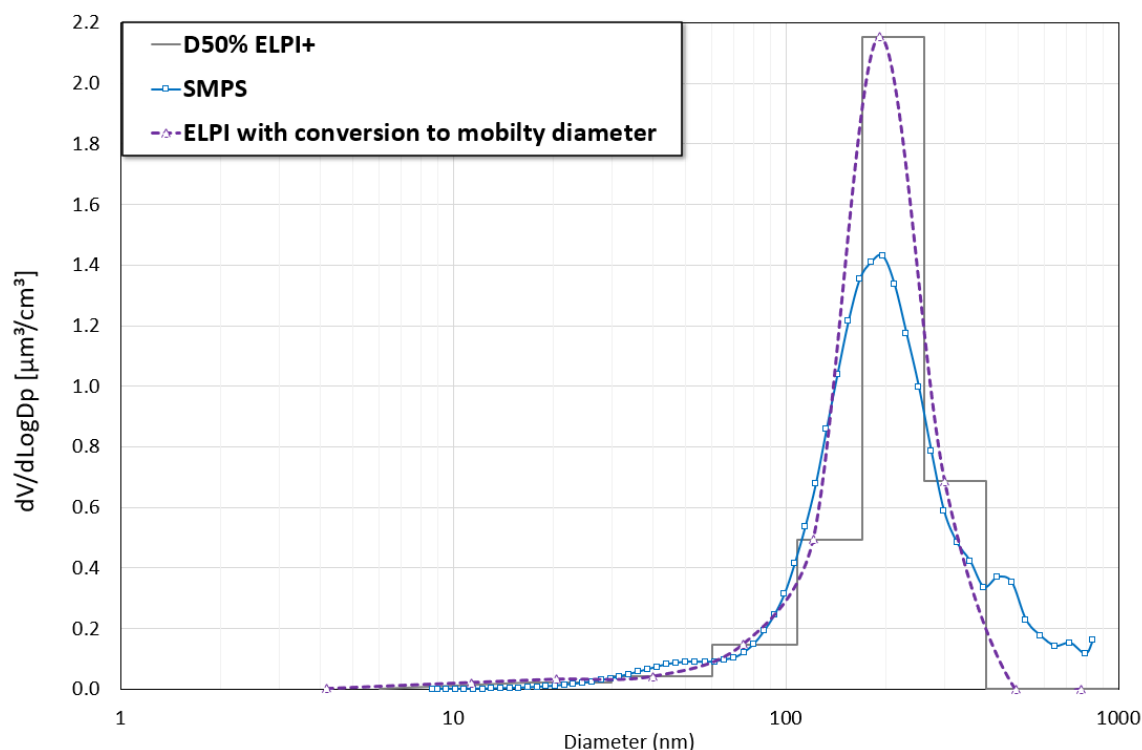
Figure 1-9. Volume Particle Size Distribution (VPSD) measured with SMPS and ELPI$^+$ from ambient air in Leipzig. Purple dashed line is the VPSD of ELPI$^+$, the blue line is the VPSD of SMPS and grey solid line is VNSD by ELPI+ stages.

1.3.5 PM$_{10}$ and PM$_{2.5}$ mass concentration

Figure 1-10 exhibit hourly PM$_{10}$ and PM$_{2.5}$ mass concentrations obtained directly from BAM observations and estimated from the number of particles measured with ELPI$^+$. PM$_{10}$ concentration estimated by ELPI$^+$ in Las Ferias revealed much larger variability and overestimation compared with the PM$_{10}$ concentrations reported by BAM (Figure 1-10a). A better result was obtained in San Cristobal for PM$_{10}$, where the time series estimated from

ELPI[+] followed the BAM reported variations (Figure 1-10b). Additionally, ELPI[+] tended to underestimate PM_{10} at low loads (<25 μg/m^3), and did not show a satisfactory agreement at higher loads, as show in Figure 1-11a.

At both sites, the linear fit between $PM_{2.5}$ BAM concentrations with those estimated by ELPI[+] was better than that for PM_{10}. At Las Ferias, it had a better linear fit (slope ~1), despite having more dispersion (r^2:0.62). At San Cristobal, the dispersion was lower ($r^2 = 0.7$), but a slope of the linear regression of 0.45 revels that ELPI[+] underestimated $PM_{2.5}$ concentrations by a factor of ~2 (Figure 1-11b).
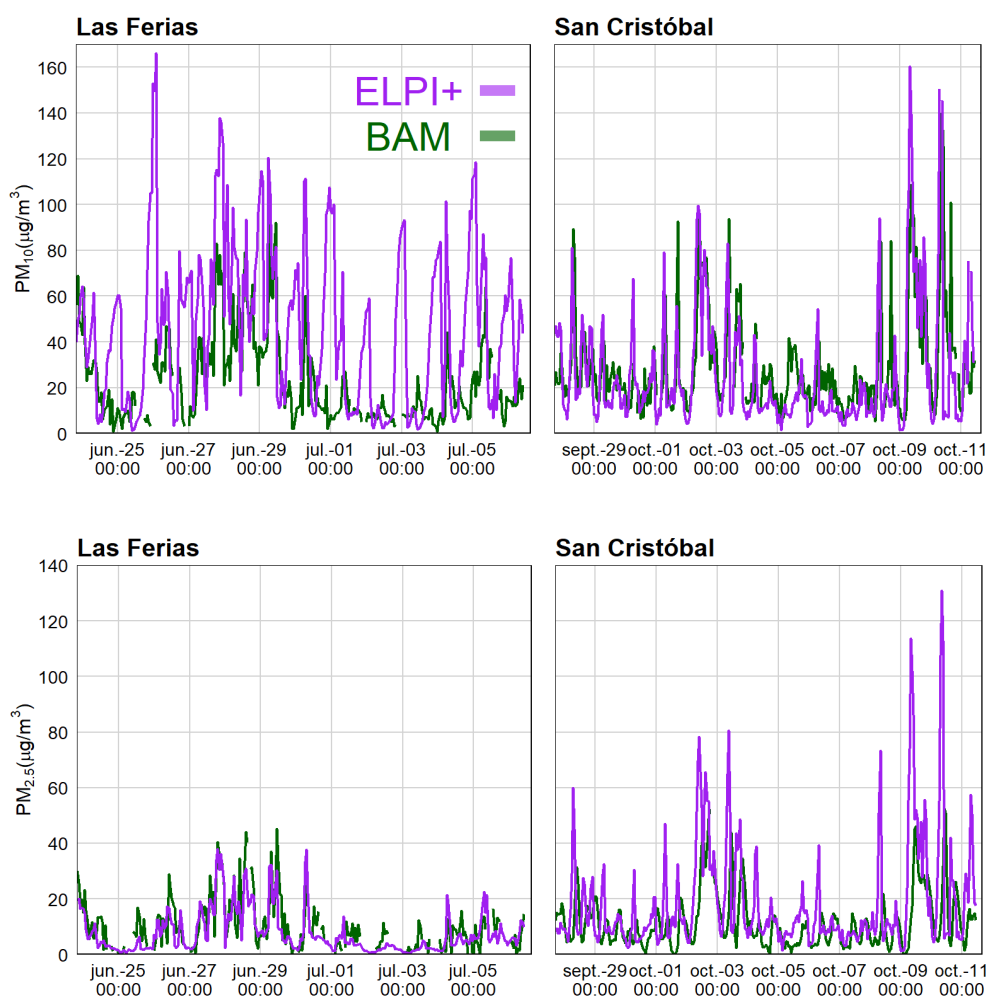
Figure 1-10. PM_{10} (μg/m^3) and $PM_{2.5}$ (μg/m^3) hourly mass concentrations measured with BAM (green line) and with ELPI[+] (purple line) in Las Ferias and San Cristobal sites of Bogotá's Air Quality Monitoring Network.
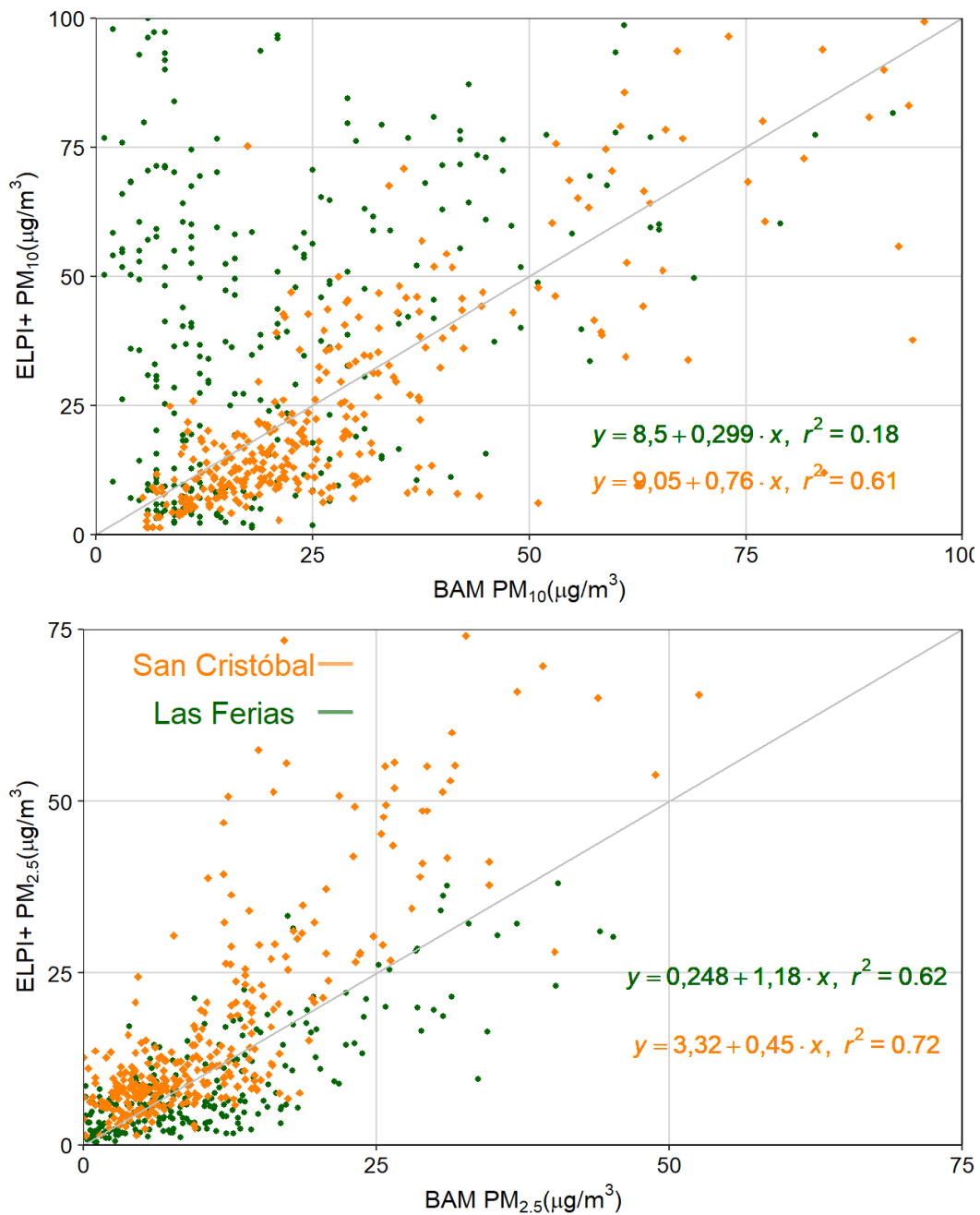
Figure 1-11. Correlation of hourly concentrations of a) PM_{10} (µg/m³) and b) $PM_{2.5}$ (µg/m³) measured with BAM and ELPI+ in Las Ferias (circle green) and in San Cristobal (orange diamonds).

1.4 Conclusions

The comparison between ELPI[+] and the other two instruments used as references in the measurements of PM_{10} and $PM_{2.5}$ mass concentrations, particle number concentration (PNC),

and particle number size distribution (PNSD), was reported in this chapter. A mobility particles size spectrometer (SMPS) and a beta monitor attenuation (BAM), both employing ambient air, were used as the reference instruments.

As a result, when considering the fourteen stages of ELPI$^+$ in the range of 6 nm to 1 μm was counted on average 508 #/cm^3 more than in the SMPS. The better fit of PNC measured with ELPI+ was obtained by neglecting the filter stage and just considering the stages two up to ten of this instrument. Therefore, the size range of PNC measured with ELPI$^+$ in this study was between 17 nm up to 1 μm, assuming an underestimation of 29 #/cm^3. The PNC overestimation obtained on the filter stage could happened by the bounce of particle.

PNSD was assessed in the 17 nm – 1 μm size range. ELPI$^+$ showed a unimodal distribution centered an aerodynamic diameter size of 21 nm, while the reference instrument had a bimodal distribution, centered at 25 nm and 130 nm. ELPI$^+$ did not show the second mode detected by the reference instrument. The variability of PNSD was 1811 ± 1160 #/cm^3 in average (min: 525 #/cm^3 - max:4453 #/cm^3) around the same mode diameter. An advantage of this intercomparison was that the diameter in the highest mode of NPSD reported by ELPI$^+$ was similar to that reported by SMPS, but the drawback was that the maximum number of particles in the center diameter of ELPI$^+$ was a factor 2 of the observed by the SMPS.

PVSD of an ambient aerosol measured with the ELPI$^+$ and the reference instrument had similar distribution modes: 291 nm ± 31 nm with the SMPS and 260 nm with the ELPI$^+$. The modal geometric standard deviation was around 1.5 for both instruments. However, the maximum particle volume concentration estimated from ELPI$^+$ was twice as high as that measured by SMPS.

The results of this intercomparison highlight the importance of assessing the ELPI$^+$ performance and cross-validating data from ELPI$^+$ with those obtained from other instruments. The uncertainty of data obtained from ELPI$^+$ in this study could be attributed to the use of ambient air, which has particles in a wide range of sizes, with different morphology, and variable chemical composition, which affects the bulk particle density; besides differences associated with each instrument's measurement principle.

As part of future work, it is recommended to determine the bulk particle density through simultaneous measurements of PVSD and particle mass size distribution. In addition, assessing the impact of ambient particle's morphology and shape factor (χ) on the equivalence of aerodynamic and mobility diameter would be a significant contribution.

1.5 References

Charvet, A., Bau, S., Bémer, D., Thomas, D., Charvet, A., Bau, S., Bémer, D., Thomas, D., Charvet, A. and Denis, B.: On the Importance of Density in ELPI Data Post- Treatment On the Importance of Density in ELPI Data Post-Treatment, , 6826, https://doi.org/10.1080/02786826.2015.1117568, 2015.

Decarlo, P. F., Slowik, J. G., Worsnop, D. R., Davidovits, P. and Jimenez, J. L.: Particle Morphology and Density Characterization by Combined Mobility and Aerodynamic Diameter Measurements . Part 1 : Theory, Aerosol Sci. Technol., 38, 1185–1205, https://doi.org/10.1080/027868290903907, 2004.

DEKATI: User manual ELPI+, Tampere., 2012.

DEKATI: ELPI+, http://www.dekati.com/products/Fine Particle Measurement/ELPI®%2B, last access: 18 October 2016, 2016.

Duc, H. N., Shingles, K., White, S., Salter, D., Chang, L. T. C., Gunashanhar, G., Riley, M., Trieu, T., Dutt, U., Azzi, M., Beyer, K., Hynes, R. and Kirkwood, J.: Spatial-temporal pattern of black carbon (BC) emission from biomass burning and anthropogenic sources in New South Wales and the greater metropolitan region of Sydney, Australia, Atmosphere (Basel)., 11(6), https://doi.org/10.3390/atmos11060570, 2020.

Gouriou, F., Morin, J. and Weill, M.: On-road measurements of particle number concentrations and size distributions in urban and tunnel environments, , 38(2), 2831–2840, https://doi.org/10.1016/j.atmosenv.2004.02.039, 2004.

Held, A., Zerrath, A., McKeon, U., Fehrenbach, T., Niessner, R., Plass-D??lmer, C., Kaminski, U., Berresheim, H. and Poschl, U.: Aerosol size distributions measured in urban, rural and high-alpine air with an electrical low pressure impactor (ELPI), Atmos. Environ., 42(36), 8502–8512, https://doi.org/10.1016/j.atmosenv.2008.06.015, 2008.

Holubčík, M., Jandačka, J., Ďurčanský, P. and Čaja, A.: Particulate matter measurement by using the particle sizers APS and SMPS., 2021.

Hu, M., Peng, J., Sun, K., Yue, D., Guo, S., Wiedensohler, A. and Wu, Z.: Estimation of Size-Resolved Ambient Particle Density Based on the Measurement of Aerosol Number, Mass, and Chemical Size Distributions in the Winter in Beijing, 2012.

Instituto de Salud Carlos III, Instituto de Diagnostico Ambiental y Esudios del agua and Ministerio de Agricultura, A. y M. A.: COMPOSICIÓN Y FUENTES DE PM 10 y PM 2 . 5 EN ESPAÑA : Aragón , Asturias , Castilla La Mancha , y Madrid, Madrid. http://www.magrama.gob.es/es/calidad-y-evaluacion-ambiental/temas/atmosfera-y-calidad-

del-aire/Informe+niveles+y+quimica_entregado2013[1]_tcm7-289194.pdf, 2013.

Järvinen, A., Aitomaa, M., Rostedt, A. and Keskinen, J.: Calibration of the new electrical low pressure impactor (ELPI þ), , 69, 150–159, 2014a.

Järvinen, A., Aitomaa, M., Rostedt, A., Keskinen, J. and Yli-Ojanperä, J.: Calibration of the new electrical low pressure impactor (ELPI+), J. Aerosol Sci., 69, 150–159, https://doi.org/10.1016/j.jaerosci.2013.12.006, 2014b.

Khlystov, A., Stanier, C. and Pandis, S. N.: An algorithm for combining electrical mobility and aerodynamic size distributions data when measuring ambient aerosol, Aerosol Sci. Technol., 38(SUPPL. 1), 229–238, https://doi.org/10.1080/02786820390229543, 2004.

Klejnowski, K., Krasa, A., Rogula-Kozłowska, W. and Błaszczak, B.: Number size distribution of ambient particles in a typical urban site: The first polish assessment based on long-term (9 months) measurements, Sci. World J., 2013, https://doi.org/10.1155/2013/539568, 2013.

Kuang, C.: Scanning Mobility Particle Spectrometer Instrument Handbook., 2016.

Kulkarni, P., Baron, P. and Willleke, K.: Aerosol Measurements. Principles, Techiniques and Applications, Third Edit., edited by P. Kulkarni, P. Baron, and K. Willleke, Wiley., 2004.

Kulmala, M., Worsnop, D. R., Laaksonen, A., Holopainen, J. K. and Po, U.: An amorphous solid state of biogenic secondary organic aerosol particles, Nature, 467, 824–827, https://doi.org/10.1038/nature09455, 2010.

Leskinen, J., Joutsensaari, J., Lyyra, J., Koivisto, J., Ruusunen, J., Ja, M., Auvinen, A., Jokiniemi, J., Tuomi, T. and Ha, K.: Comparison of nanoparticle measurement instruments for occupational health applications, , https://doi.org/10.1007/s11051-012-0718-7, 2012.

Li, Z., Wei, Y. and Zhang, Y.: Retrieval of Atmospheric Fine Particulate Density Based on Merging Particle Size Distribution Measurements : Multi-instrument Observation and Quality Control at Shouxian, J. Geophys. Res. Atmos., 123(12), 474–488, https://doi.org/10.1029/2018JD028956, 2018.

Lingard, J. J. N., Agus, E. L., Young, D. T., Andrews, E. and Tomlin, A. S.: Observations of urban airborne particle number concentrations during rush-hour conditions : analysis of the number based size distributions and modal parameters, , 1203–1218, https://doi.org/10.1039/b611479b, 2006.

Marjama, M., Keskinen, R. J., Chen, S. A. D. and Pui, D. Y. H.: Performance evaluation of the electrical low pressure impactor (ELPI), J. Aerosol Sci., 31(2), 249–261, 2000.

Mcmurry, P. H.: A review of atmospheric aerosol measurements ɤ, , 34, 2000.

Pagels, J., Gudmundsson, A., Gustavsson, E., Asking, L., Bohgard, M., Pagels, J., Gudmundsson, A., Gustavsson, E., Asking, L. and Bohgard, M.: Evaluation of Aerodynamic Particle Sizer and Electrical Low-Pressure Impactor for Unimodal and Bimodal Mass-Weighted Size Distributions Evaluation of Aerodynamic Particle Sizer and Electrical Low-Pressure Impactor for Unimodal and Bimodal Mass-Weighted Si, , 6826, https://doi.org/10.1080/02786820500295677, 2007.

Price, H. D., Stahlmecke, B., Arthur, R., Kaminski, H., Lindermann, J., Däuber, E., Asbach, C.,

Kuhlbusch, T. A. J., Bérubé, K. A. and Jones, T. P.: Comparison of instruments for particle number size distribution measurements in air quality monitoring, J. Aerosol Sci., 76, 48–55, 2014.

Secretaría Distrital de Ambiente (SDA): Informe anual de calidad del aire en Bogotá 2017, Bogotá D.C. http://rmcab.ambientebogota.gov.co/Pagesfiles/180601_Informe Anual 2017_V6.pdf, 2017.

Seinfeld, J. H. and Pandis, S. N.: Atmospheric From Air Pollution to Climate Change, 2 nd., 2006.

Shen, S., Jaques, P. A., Zhu, Y., Geller, M. D. and Sioutas, C.: Evaluation of the SMPS-APS system as a continuous monitor for measuring PM2.5, PM10 and coarse (PM2.5-10) concentrations, Atmos. Environ., 36(24), 3939–3950, https://doi.org/10.1016/S1352-2310(02)00330-8, 2002.

Therneau, T.: Total Least Squares : Deming , Theil-Sen , and Passing-Bablock Regression Generalized Deming regression., 2018.

Wallace, L.: Ultrafine Particles : A Review., 2009.

Walter, J.: Size Distribution Characteristics of Aerosols, in Aerosol Measurement: Principles, Techniques, and Applications: Third Edition, pp. 41–54, https://doi.org/10.1002/9781118001684.ch4, , 2011.

Yli-ojanper, J.: Calibration of Aerosol Instruments in a Wide Particle Size Range, Tampere University of Technology, 2012.

Yli-ojanperä, J., Kannosto, J., Marjamäki, M. and Keskinen, J.: Improving the Nanoparticle Resolution of the ELPI, , 360–366, https://doi.org/10.4209/aaqr.2009.10.0060, 2010.

Zhang, Q., Canagaratna, M. R., Jayne, J. T. and Worsnop, D. R.: Time- and size-resolved chemical composition of submicron particles in Pittsburgh : Implications for aerosol sources and processes, , 110, 1–19, https://doi.org/10.1029/2004JD004649, 2005.

1.6 Supplementary information

Table S1. Time periods during the intercomparison between ELPI⁺ and SMPS.

PERIODS OF INTERCOMPARISON					
# Item	Start date	End date	No rows ELPI	No rows SMPS	Diameter
1	07/03/2019 21:00	07/03/2019 23:00	148	36	Aerodynamic
2	08/03/2019 0:01	08/03/2019 8:00	536	108	Aerodynamic
3	11/03/2019 16:00	11/03/2019 23:00	472	96	Stockes
4	12/03/2019 0:01	12/03/2019 8:00	535	108	Stockes
5	12/03/2019 11:00	12/03/2019 21:00	654	131	Stockes
6	13/03/2019 0:01	13/03/2019 8:00	535	108	Stockes
7	13/03/2019 10:00	13/03/2019 23:00	833	168	Stockes
8	14/03/2019 0:01	14/03/2019 8:00	535	108	Stockes
9	14/03/2019 10:00	14/03/2019 23:00	833	168	Aerodynamic
10	15/03/2019 0:01	14/03/2019 14:00	860	179	Aerodynamic
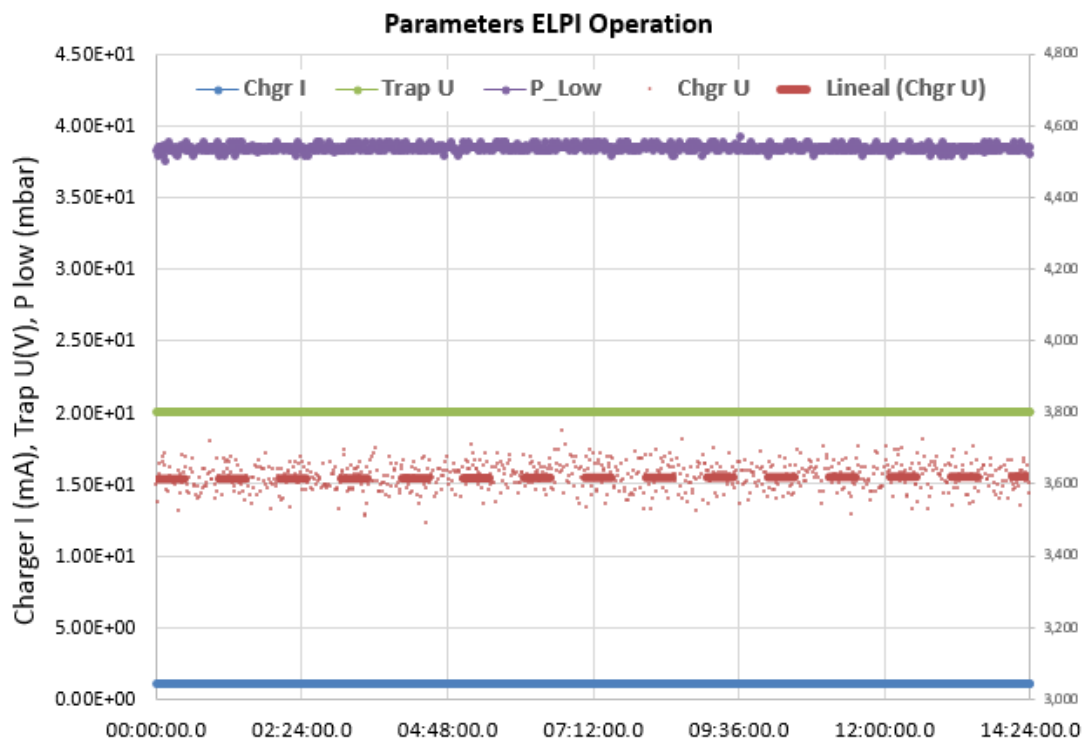
Figure S1. ELPI⁺ operating parameter

2. Number Concentration, Size Distribution and Lung-Deposited Surface Area of Ambient Particles in Urban Areas of Bogotá - Colombia

2.1. Introduction

Analyzing the chemical composition and size distribution of aerosols is important for understanding their effects on both human health and the environment. Depending on its size and composition, particulate matter may impact human health through changes in 1) the autonomic nervous system's functions, 2) pulmonary function, 3) the tissues and structure of the lungs, and 4) the respiratory system's defense mechanisms may have an impact on population health in the form of premature mortality and the exacerbation of respiratory and cardiovascular diseases.

A large number of studies have focused on relating the concentration of fine (aerodynamic diameter less than 2.5 μm) and ultrafine (aerodynamic diameter less than 100 nm) particles with mortality and morbidity rates of the population, demonstrating that fine particles have short term health effects and ultrafine particles have long-term effects Morawska et al., 2004; Pekkanen et al., 2000). Part of the short-term impacts are death and respiratory diseases, while long-term effects include respiratory and cardiovascular diseases.

Airborne aerosols can be categorized into four modes: nuclei, Aitken, accumulation, and coarse modes, based in the aerodynamic diameter size, as illustrated in Figure 2-1. Sources, topography, and atmospheric conditions influence the size distribution of airborne particles. Some of the factors affecting the size distribution of airborne aerosols are: high temperature vapor, coagulation and condensation processes, aggregate formation, mechanical processes, precipitation washout and sedimentation (Seinfeld and Pandis, 2006).
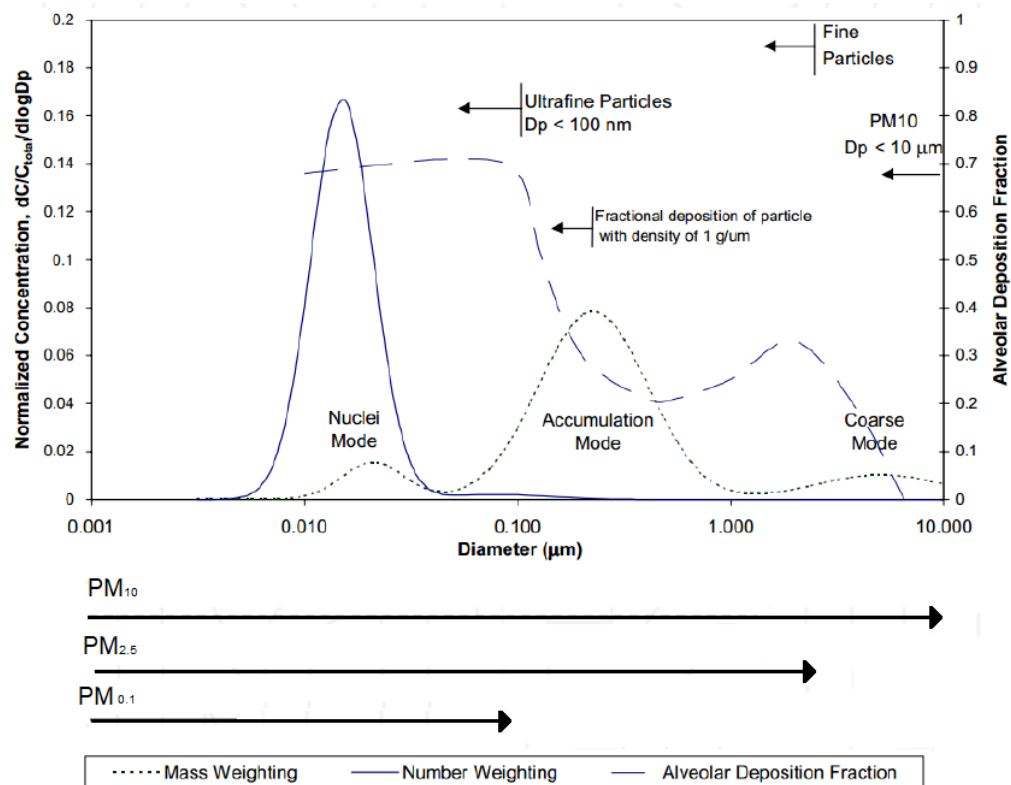
Figure 2-1. Multimodal distribution of aerosols in ambient air weighted by number, surface area and particle mass size distribution. Source (Lefol et al., 2015).

The size distribution of ambient aerosol based on particle number is different from that based on surface area, volume or mass. Particles smaller than 0.1 μm highly affect particle number but its effect on volume and mass size distributions is negligible, as indicated with the solid blue line (number size distribution) and black dotted line (mass distribution). The nuclei mode (particles range in diameter from 5 to 20 nm), and the Aitken mode (particles range in diameter of 20 to 100 nm) dominate the number size distribution, whereas accumulation and coarse modes govern volume and mass size distributions.

Nuclei mode particles are usually fresh aerosols created in situ from the gas phase by nucleation, and their presence depends on atmospheric conditions. The Aitken mode starts as primary particles and secondary material condensed onto existing particles. Larger Aitken particles are susceptible to grow and form part of the accumulation mode of the mass size distribution. The main mechanisms of particle growth are coagulation and condensation of vapors. Coagulation is a slow process and does not represent the main method to transfer Aitken-mode particles to the accumulation mode (Seinfeld and Pandis, 2006).

The accumulation mode ranges in size from roughly 100 to 1000 nm (1 μm). These particles are derived from Aitken-mode particles that grow by heterogenous chemical reactions. The residence time of accumulation particles is larger than Nuclei and Aitken particles, therefore, the chemical compounds existing in these particles can be used as tracers of specific sources on contamination by atmospheric transboundary. The coarse mode consists of particles larger than about 1 μm. These relatively large particles are formed by soil erosion and marine aerosols. Coarse mode contributes negligible in the number size distribution but noteworthy in volume and mass size distribution. The parameters to describe size distribution are number concentration (Ni), median diameter (Dpi) and standard deviation of the lognormal mode (σ).

shows the size range definitions for atmospheric particles. Thus, particles larger than 2.5 μm are called as coarse particles ($PM_{10\ -2.5}$), and those smaller than this size are classified as fine particles ($PM_{2.5}$). Particles with diameters smaller than 0.1 μm, are classified as ultrafine particles ($PM_{0.1}$). Fine particles include most of the total particle number and surface area.

Coarse particles are mainly produced by mechanical processes and consist of soil dust, sea salt, fly ash, tire and break wear particles. The Aitken and accumulation particles contain primary particles from combustion sources and secondary aerosol materials (sulfate, nitrate, ammonium, secondary organics) formed by chemical reactions resulting from gas to particle conversion (Seinfeld and Pandis, 2006).

Ultrafine particles have a higher surface area per unit volume than larger particles, making them more able to adsorb organic chemicals, some of which may be carcinogenic, and can be easily absorbed and deposited in the deeper parts of the respiratory tracts, i.e., alveoli (Kumar et al., 2010). Due to the health implications of ultrafine particles, the knowledge of their characteristics has improved considerably around the world, as shows (Kulmala et al., 2004). This has led to particle number standards for automotive emissions. However, no guidelines or regulatory limits for particle number concentrations in ambient air have been established. The lack of standard procedures and equipment, as well as uncertainty in the measurement repeatability and reproducibility, and insufficient long term monitoring studies, are some of the major technical limitations to define standards for ultrafine particles in ambient air. Local target values, established by local environmental agencies, might be helpful as a temporary measure for pollutants that are not yet subject to regulation (European Commission, 2021).

The toxicity of chemical constituents and the particle's ability to enter the alveolar region of the lungs determine how harmful the particles are, because this way the toxic constituents can enter the circulatory system and disseminate to organs like the brain. In this regard, the International Commission on Radiology Protection (IRCP) has published the rate deposition fraction of particles for the human respiratory system in the head airways, tracheobronchial, and alveolar area, (Figure S 2-1). The total deposition fraction, which is represented by the blue line in Figure 2-1, is the sum of these three fractions and has a minimum particle size of between 0.2 and 0.3 μm, where approximately 30% of the particles are deposited in the respiratory system. In contrast, the human respiratory system receives more than half of particles with diameters larger than 2 μm and less than 50 nm.

The particle surface area is relevant due to the ability to absorb and transport chemical components (Asbach et al., 2009; Brown et al., 2001; Oberdörster et al., 2005) and interact with the cells to create reactive oxygen species (ROS), which contribute to the oxidative potential (OP) of the particles and are considered central for a mechanistic understanding of many adverse health effects (Zhang et al., 2022). Therefore, have been used the Lung Deposition Surface Area (LDSA) as a sensible metric to combine the lung deposition of particles with the area surface of particles.

Relatively few techniques are available to monitor the aerosol's surface area. One of the instruments is the Nanoparticle Surface Area Monitor (NSAM) of TSI®, which consist of a unipolar charger, that associate the surface area of particles to currents sensed with electrometers (Shin et al., 2007). This instrument is limited to the tracheobronchial and alveolar lung regions (10 - 1000 nm) but has the advantage that can be used in the monitoring of occupational exposure. Other studies have estimated LDSA using handheld devices, such as the miniDisc (Fierz et al., 2011; Mills et al., 2013), the Aerasense Nanotracer (Marra, 2011), and Partector (Fierz et al., 2014). Robust instruments to measure environmental particles number concentration and size distribution, such as ELPI[+] and SMPS, joint to average deposition rates published by the International Commission on Radiological Protection, (2015) also have been used to estimate the LDSA by (Chalvatzaki et al., 2022; Kuuluvainen et al., 2016).

Studies of the number particle concentrations and size distribution based on ground measurements have been conducted for a very long time, primarily in Europe (Hovorka et al., 2018; Klejnowski et al., 2013a; Rivas et al., 2020; Vu et al., 2016), the United States and Canada (Kasumba et al., 2009; Ogulei et al., 2007) and some Asian countries (Gani et al., 2020; Lee et al., 2021; Liang et al., 2020; Wang et al., 2013). Many studies were conducted over relatively short periods of time, which establish a

restriction to recognize the importance of the meteorology changes in the particle size distribution (Lorelei de Jesus et al., 2020). Few and recent studies have been undertaken in Latin America, such as those in Brazil (Agudelo-castañeda et al., 2018; Monteiro Dos Santos et al., 2021), Chile (Fults et al., 2019; Manzano et al., 2021) and aircraft measurements in Mexico (Kleinman et al., 2009). In Colombia, the variations of the ultrafine particle concentrations in transportation microenvironments have been studied by Avila Prada, (2016), who revealed an exposure with a range of 1.7 - 1.0 x 10^5 particles/cm^3 for commuters who utilize bicycles, cars, buses, and walking. Furthermore, the volume particle size distribution (VPSD) was remotely sensed, using the aerosol optical depth as the function of wavelength. A limited number of distributions were obtained in comparison with the long-term observations, due to the cloudy conditions in the sites (Hernandez, 2016; Hernandez Villamizar, 2019). As result, the VPSD in Bogotá was observed at sunrise and sunset, finding the fine a coarse mode centered 0.16 and 3.0 μm, respectively. The lung deposition fraction was assessed by Martins et al., (2010) in Brazil using the particle size distribution and the model multiple path particle dosimetry model (MPPD), showing a significant deposition fraction in pulmonary region during the traffic rush time hours (8:00) of particles with a size of 43 nm. No studies about lung deposition surface area were identified to have been conducted in Colombia, maybe because of the frightened investigations about the ambient number of particle concentrations and their size distribution in this region.

Because of this, the aim of this study is to compare the particle number concentrations and particle number and volume size distribution in two different moderately polluted areas of Bogota - Colombia. The focus is on comparing average concentrations and particle size distribution, but also interested in estimated the pulmonary deposition of particles. The results discussed below come from the first measurements of particle number carried out on ground level in Bogota.

2.2.   Methodology

2.1.1 Monitoring sites

Airborne particle number concentration and particle size distribution were measured in two sites of Bogotá, Colombia. Las Ferias (Lat: 4.699033º; Long: -74.082483º) and San Cristobal (Lat: 4.572553 º; Long: -74.083814 º) sites are part of the Air Quality Network Bogotá (Secretaría Distrital de Ambiente (SDA), 2018), as shown in Figure 2-2. Las Ferias is highly influenced by vehicular emissions located in the geographic center of the city. It is equipped with instruments to register hourly meteorological conditions (ambient temperature, humidity, relative pressure, precipitation, and speed and direction winds), and EPA reference instruments to measure criteria pollutants (NO, NO_2, NO_x, CO, O_3, PM_{10}, and $PM_{2.5}$). Sampling inlets are at a 4.6 m height over ground level.

San Cristobal is an urban background site, located in a park southeast of the city. This station has instruments to register hourly meteorological conditions (ambient temperature, humidity, solar radiation, precipitation and speed, and direction winds) and some criteria pollutants (PM$_{10}$, PM$_{2.5}$ and O$_3$). Sampling inlets are placed at 4 m above ground level.

The instrument used to measure the particle number concentration and size distribution was the Electrical Low-Pressure Impactor (ELPI$^+$), which consistent in a unipolar corona charger, a cascade impactor with 14 stages of size classification with and additional filter stage, and a set of electrometers to sense de current of each particle when impact over each stage. Chapter 1 of this publication provides more information on the operation parameters and calibration status of the instrument employed.

Measurements were conducted between 23 June and 5 July 2017 at Las Ferias, and between 30 August – 11 September and 27 September to 10 October 2017 at San Cristobal (N =37553). The currents recorded at each ELPI$^+$ stages were saved by second (17634 data saved in Las Ferias and 37553 data saved in San Cristobal) and later averaged to 1 hour. PNC was associated with meteorological conditions and criteria pollutants to establish the similitudes or differences with the PM$_{2.5}$ concentrations monitored in each station.
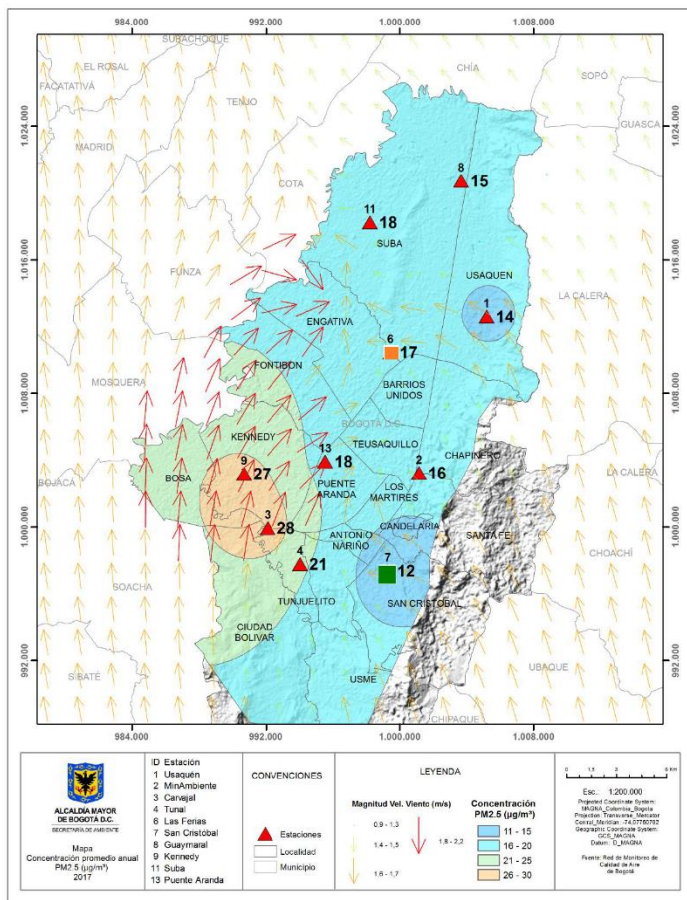
Map of Bogotá Air Quality Network in 2017. The ID station and name of each one is listed below the map. The red triangles on the map correspond to the location of air quality sites. The orange square is the location of Las Ferias site, and the green square corresponds to the location of San Cristobal site. The red and yellow arrows indicate average wind speed and direction. PM$_{2.5}$ annual average concentration in 2017 in each station is shown ins a bold number next to each one.

Figure 2-2. Measurement location of atmospheric number particles and size distribution in Bogotá – Colombia. A) Map of Bogotá Air Quality Network in 2017 (Secretaría Distrital de Ambiente, 2018).

Pictures of Las Ferias station (B1) and San Cristobal (B2). Pictures of representative areas that surrounded Las Ferias station (C1) and San Cristobal (C2).

2.2.1. Particles number concentration and size distribution measurement.

The Electrical Low-Pressure Impactor (ELPI+, DEKATI, Finland) was used to assess the number concentration and number size distribution. ELPI+ is used worldwide in continuous air quality monitoring for assessing PM size distribution and PM concentrations (Held et al., 2008; Klejnowski et al., 2013b). In addition, ELPI+ has been used to estimated LDSA (Kuuluvainen et al., 2016). The description of ELPI+ was detailed in Section 1.1.1.

The statistical operation parameters of ELPI+ recorded during the atmospheric particles sampling period time in Las Ferias and San Cristobal sites are displayed in Table 2-1. The current on the corona charger is one of the most crucial elements to ensure the appropriate operation of the instrument, enabling a fluctuation from 1 KV to the setup value of 3.5 KV, is one of the most crucial elements. The corona charger exhibits the most variation across all parameters in this investigation, as shown in Figure S 2-2, with a tendency to reduce the current in Las Ferias from 3600 up to the lower value of 3050 KV, while in San Cristobal there was a slight drift in the corona charger's currents from 2950 to 3280. During all measurements period, the corona charger was in the range of values acceptable to consider a proper operation of ELPI+. The relative standard deviations given in Table 2-1 show that other parameters exhibited less variation from the setup arrangement.

Table 2-1. Operating parameters of ELPI+ recorded during the sampling period time in Las Ferias and San Cristobal site in Bogotá.

Parameter	Reference value	Las Ferias		San Cristobal	
		Average ± sd	Relative sd (%)	Average ± sd	Relative sd (%)
Charger U (KV)	3.5 ± 0.5	3320 ± 127	3.8	3242± 30.93	0.95
Charger I (μA)	1	1.041± 0.004	0.43	1.054± 0.004	0.45
Trap U (V)	20 ± 2	19.20±0.003	0.001	19.99±0.005	0.02
Pressure at first stage (mbar)	40 ± 5	39.11±0.269	0.67	38.73±12.7	32.7
Air flow (Liters per minute)	10	10		10	
Ambient Pressure (mbar)		742±5.11	0.17	737.6±5.22	0.71

Measurements were performed in Las Ferias between 23 June and 5 July 2017, saving data of each stage of the ELPI+ every second and then averaged hourly to combine and analyze them meteorological conditions and criteria pollutants.

2.2.2.   Lung Deposition Surface Area.

Measuring the Lung Deposition Surface Area (LDSA) requires the measurement of the entire particle size distribution followed by a sum of particles surface in each size stage, weighted by the lung-deposition efficiency, as indicated the Equation 2-1.

Equation 2-1.   LDSA = (surface area) x (alveolar deposition efficiency)

In this study, the alveolar deposition efficiency was estimated by interpolation, using the geometric mean of each stage's cut-off diameter of the ELPI+, and the function of regional lung deposition of particles in alveolar-interstitial (AI) airways presented in ICRP, (1994). Figure 2-3 shows the Alveolar Deposition Efficiency by particle diameter (black line), as shown in ICRP (1994), and the Alveolar Deposition Efficiency calculated by each geometric mean diameter of ELPI+ (blue squares).
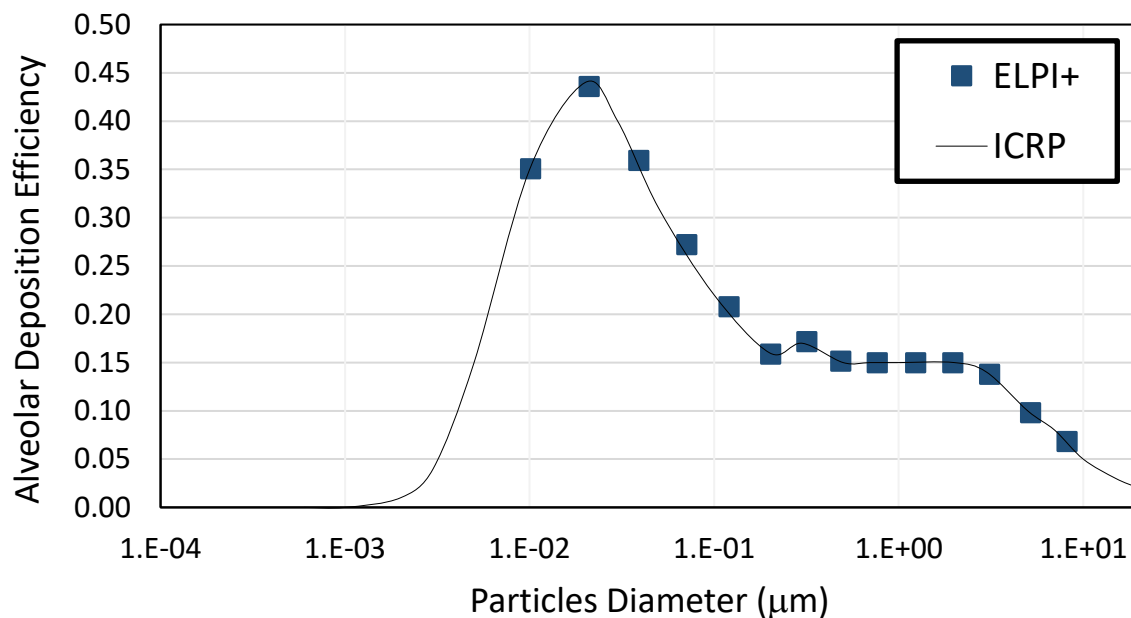
Figure 2-3. Particle deposition efficiency in the human respiratory tract as a function of particle size according to ICRP (black line) and the fraction interpolated for geometric mean aerodynamic diameter of each stage of ELPI+ (blue squares).

Particle surface area was estimated with the assumption that particles are spherical and therefore the surface area could be estimated using de Equation 2-2, where D_{ia} corresponding to geometric mean of each stage n of the ELPI+. The hourly variability of particles surface area was calculated with the Equation 2-3, which indicates the sum of the surface area for the stages 2 to 14 of ELPI+.

Equation 2-2. $\text{surface area}_n = \left[Number\ of\ particles \cdot \left(D_{ia}{}^2 \right) \cdot \pi \right]_n$ ($\mu m^2/cm^3$)

Equation 2-3. $Total\ surface\ area = \sum_{n=2}^{n=14}(surface\ area)_{hourly}$ ($\mu m^2/cm^3$).

2.3. Results

The key results from measurements of particles number concentrations, number and volume particle size distribution and lung deposited surface area, in two urban sites in Bogotá - Colombia, are presented and discussed in this section.

2.3.1. Meteorological conditions at the study sites.

The meteorological conditions registered by the air quality stations Las Ferias and San Cristobal by the RMCAB during the period time of the number of particles measurements are summarized in Table 2-2. The percentage of relative humidity (RH%) in San Cristobal was significantly higher in San Cristobal than in Las Ferias (p value < 0.0001), particularly during the first hours of the day (between 0:00 to 6:00 H), when San Cristobal registered RH% above 70%, while in Las Ferias this range values was observed only between 4:00 to 6:00. At midday was observed a decreased of RH% reporting values less than 55% at 13:00 in San Cristobal and between 12:00 H and 17:00H in Las Ferias (see Figure S 2-3a).

Pertaining to wind speed, was not significantly different in the two sites, with an hourly average of 1.9 m/s in Las Ferias and 1.7 m/s in San Cristobal. Winds come mainly from the East in San Cristobal, while there were winds from the southeast during the daylight in Las Ferias, which indicates the influence of the emissions of a road with high vehicular traffic (see Figure S 2-3c). The hourly variation of wind speed (Figure S 2-3b) shows a maximum between 12:00 and 17:00 H in both sites (2.0 – 2.5 m s^{-1}) and a minimum at 8:00 H (0.7 m s^{-1}) in San Cristobal, possibly associated to the minimum boundary layer height (Ortiz Duran, 2016). The minimum wind speed in Las Ferias was registered at 4:00 H (0.9 m s^{-1}).

No precipitation events were registered in Las Ferias, while San Cristobal registered precipitations below 5 mm per day on August 30 and 31, and September 8, 10, and 18 (Figure S 2-3d). Atmospheric pressure was measured just in Las Ferias (Figure S 2-3e), while solar radiation was measured only in San Cristobal, with a maximum at 11:00 H, an average of 782 W/m^2 and minimum at 17:00 H of 37 W/m^2 (Figure S 2-3f.)

Table 2-2 shows hourly average concentrations of criteria gases and particles (PM$_{10}$ and PM$_{2.5}$). There were no significant differences in hourly PM$_{10}$ and PM$_{2.5}$ between these two sites. Figure 2-4 displays the diurnal variation of PM$_{2.5}$ and PM$_{10}$, with higher concentrations in the evening rush hour (16 μg/m at 18:00 H) than in the morning rush hour (12 μg/m at 8:00 H) in San Cristobal. Both PM$_{2.5}$ peaks were

similar in Las Ferias (13 μg/m^3). PM$_{10}$ concentrations were higher in the morning (40 and 34 μg/m^3 at 8:00 H in San Cristobal and Las Ferias, respectively) than in the evening (24 and 31 μg/m^3 at 19:00 H in San Cristobal and Las Ferias, respectively).

Table 2-2. Data registered during the measurements period of the number particles in Las Ferias and San Cristobal sites. The measurement of particles number in Las Ferias was 23 June – 5 July 2017, while in San Cristobal was carried out in two periods August 30 - September 11, and Sept 27 - October 11, 2017.

Variable	Las Ferias	San Cristobal
Relative Humidity (%)	59.5 ± 9.36	64.1 ± 10.9
Wind speed (m s^{-1})	1.9 ± 0.8	1.7 ± 0.9
Daylight Solar radiation (W m^{-2})		373
Pressure (mm Hg)	565 ± 0.7	
PM$_{10}$ (μg m^{-3})	22.6 ± 18.6	24.4 ± 17.2
PM$_{2.5}$ (μg m^{-3})	10.7 ± 9.1	10.3 ± 8.0
NO$_x$ (ppb)	28.26 ± 20.1	
CO (ppm)	0.41 ± 0.2	
O$_3$ (ppb)	13.5 ± 3.3	17.3 ±7.6
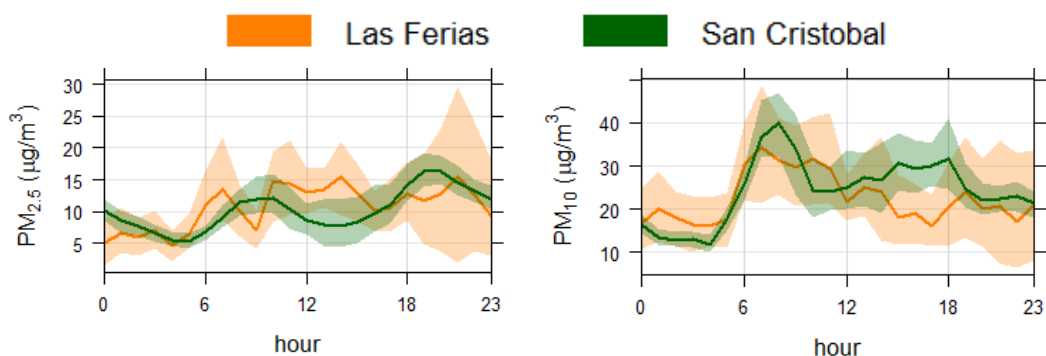
Figure 2-4. PM$_{2.5}$ and PM$_{10}$ concentrations registered in Las Ferias and San Cristobal site during the measurement campaign.

2.3.2. Particle Number Concentration

The number of particles measured with ELPI$^+$ were measured in Las Ferias and San Cristobal sites, every second and then averaged to 1 hour. The basic descriptive statistics for hourly particle number concentrations for both sites are summarized in Figure 2-5, which displays a significant difference between particle number concentration in San Cristobal and Las Ferias (p value: 0.001). San Cristobal exhibited a higher number of particles with an hourly average of 3.8 x 10^3 ± 3.3 x 10^3 #/cm^3 (min: 3.3x10^2 #/cm^3 and max: 2.2x10^5 #/cm^3), while in Las Ferias had an hourly average of 2.8x10^3 ± 2.7x10^3 #/cm^3 (min: 1.7 x10^2 #/cm^3 and max: 1.3 x10^5 #/cm^3). 83.4% of particles in Las Ferias and 79.8% of particles in San Cristobal were in size range of the nanoparticles (D$_a$ < 104 nm). Therefore, the hourly

average nanoparticle number in San Cristobal and Las Ferias were $3.0 \times 10^3 \pm 2.6 \times 10^3$ and $2.3 \times 10^3 \pm 2.2 \times 10^3$, respectively. The circumstances that can influence the difference in PNC for both sites are that measurements were not conducted synchronously; therefore, local, and regional events, as well meteorological conditions can affect the results.

The PNC obtained in this study were compared with other studies in Colombia, Latin America, and around the world. Díaz Fonseca (2021) found a higher concentration of nanoparticles ($\sim$ 40 times as high) in a sidewalk located next to a road highway than in this study.

The PNC found in Bogota was similar to those found in Atlanta (USA), Brisbane (Australia), London (UK), Zurich (Switzerland), Stockholm (Sweden), Barcelona (Spain), Rome and Milan (Italy), which reported concentrations between 1×10^4 and 9.7×10^4 # particles/cm^3 (Klejnowski et al., 2013a), while Zabrze (Poland), Vienna (Austria), Prague (Czech Republic) and HohenpeiBenberg (Germany) reported concentrations of 1.1×10^3 to 8.0×10^3 # particles/cm^3.
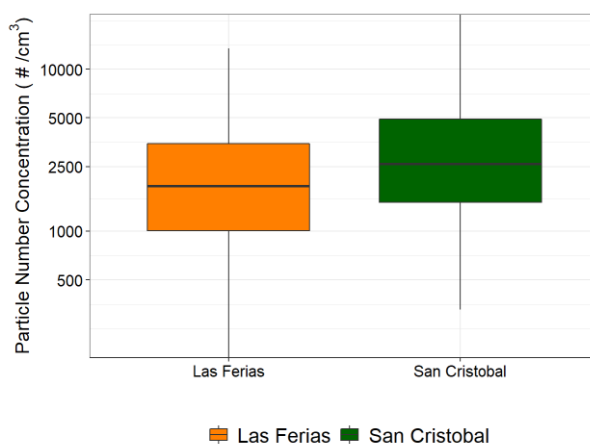
Figure 2-5. Box plot of hourly particle number concentration estimated in the sites Las Ferias (N=295) and San Cristobal (N=631) in Bogota. The aerodynamic diameter range of particles counted were counted in the range of 10 nm to 10 μm.

2.3.3. Hourly variation of Particles Number Concentration

The PNC measurements conducted in both sites in Bogota revealed a daily profile of the number of particles. A peak of the number particles concentrations was observed in the morning, between 5:00 to 9:00 hour. This peak is associated with rush hour emissions (Secretaría Distrital de Ambiente (SDA), 2022) intensified by meteorological conditions that influence the boundary layer height (mixing layer). Typically, the minimal height of mixing layer is registered at 6:00 -7:00 H (Manuel Rincón-Riveros et al., 2020), which results in the stagnation of the atmosphere that prevents particle dispersion in the air.

After 8:30 - 9:00 H, the mixing layer expands over the height of the eastern mountain range, facilitating the dispersion and, hence, reducing particle number concentration.

The maximum PNCs were observed at 6:00H − 7:00H in both sites, with 8.2×10^3 #/cm^3 and 5.8×10^3 #/cm^3 in San Cristobal and Las Ferias, respectively. In contrast, the minimum concentration was observed at midnight 0:00 H − 1:00 H, with 2.0×10^3 and 1.6×10^3 #/cm^3 , respectively. Figure 2-6a displays the daily profile of the particle number concentrations.

The PNC had a weekly profile with higher values on weekdays than on weekends. Weekdays had a greater impact on Las Ferias (p value: $<2 \times 10^{-16}$) than San Cristobal (p value 4.23×10^{-7}). The PNC daily pattern in Las Ferias exhibited significantly (p value: 1×10^{-16}) higher concentrations on weekdays (3.6×10^3 #/cm^3 on average) than on weekends (1.2×10^3 #/cm^3). In San Cristobal, the weekend reduction was smaller (2.7×10^3 #/cm^3 on weekends and 4.2×10^3 #/cm^3 on weekdays). Sunday's PNC was just one third of weekdays' PNC in in Las Ferias, and half in San Cristobal.
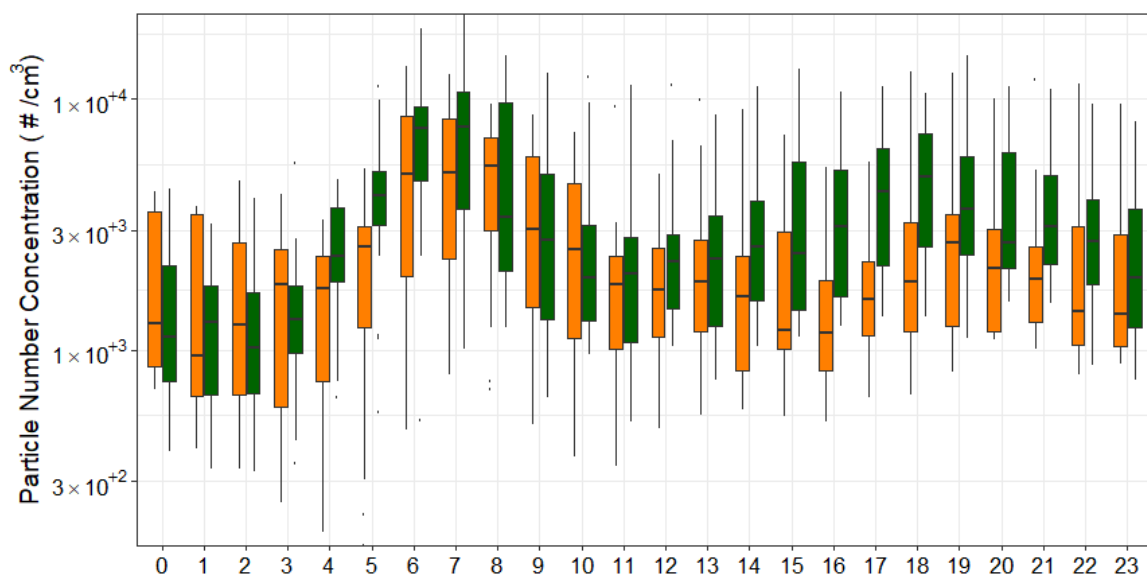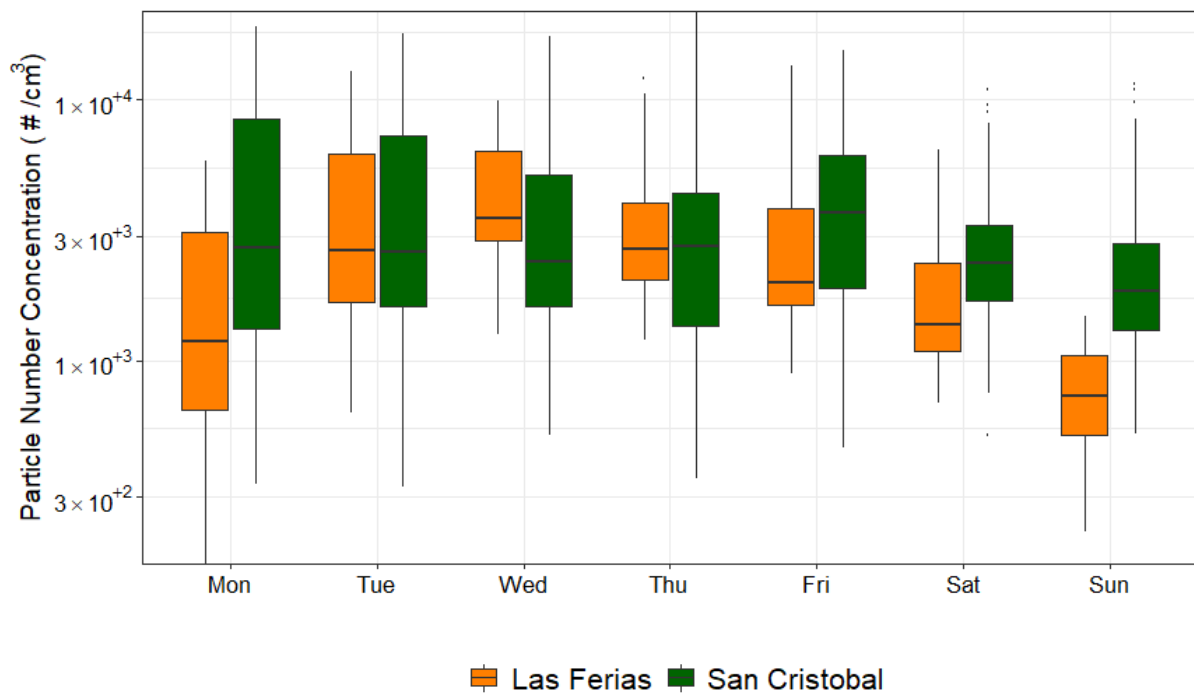
Figure 2-6. Seasonal variation of particles number concentration in ambient air of two sites in Bogotá. a) daily variation, b) weekly profile had a differences

2.3.4. Number Particle Size Distribution

The comparison of hourly average particle number size distribution (PNSD) for both sites is presented in Figure 2-7. The PNSD was unimodal in Las Ferias and can be infer a bimodal distribution in San Cristobal. The maximum of number size distribution occurred for the 120 nm of aerodynamic diameter.

The PNSD in Las Ferias was remarkably unimodal, with a maximum of 5.12 x 10^3 #/cm^3 in the diameter range of 60 to 108 nm. While, San Cristobal shows a bimodal shape, with a mode completely defined in the same diameter range and a maximum of 4.8 x 10^3 #/cm^3. The instrument used in this study shows a tendency to overestimate the number of particles counted in the range of 6 to 17 nm (see conclusions of this document's first chapter). As a result, the finest mode observable in the PNSD of San Cristobal cannot be completely trustworthy due to instrumental limitations in the minimum diameter of cut off.

The PNSD of both sites showed that the maximum number falls into the accumulation mode , with an aerodynamic diameter between 100 to 1000 nm). The PNSD is dynamic throughout the day, as shown in Figure 2-8, reflecting the influence of emission sources, as well as meteorological conditions, particle formation, transformation, and transport in the atmosphere (Boogaard et al., 2010; Dal Maso et al., 2005; Klejnowski et al., 2013a).
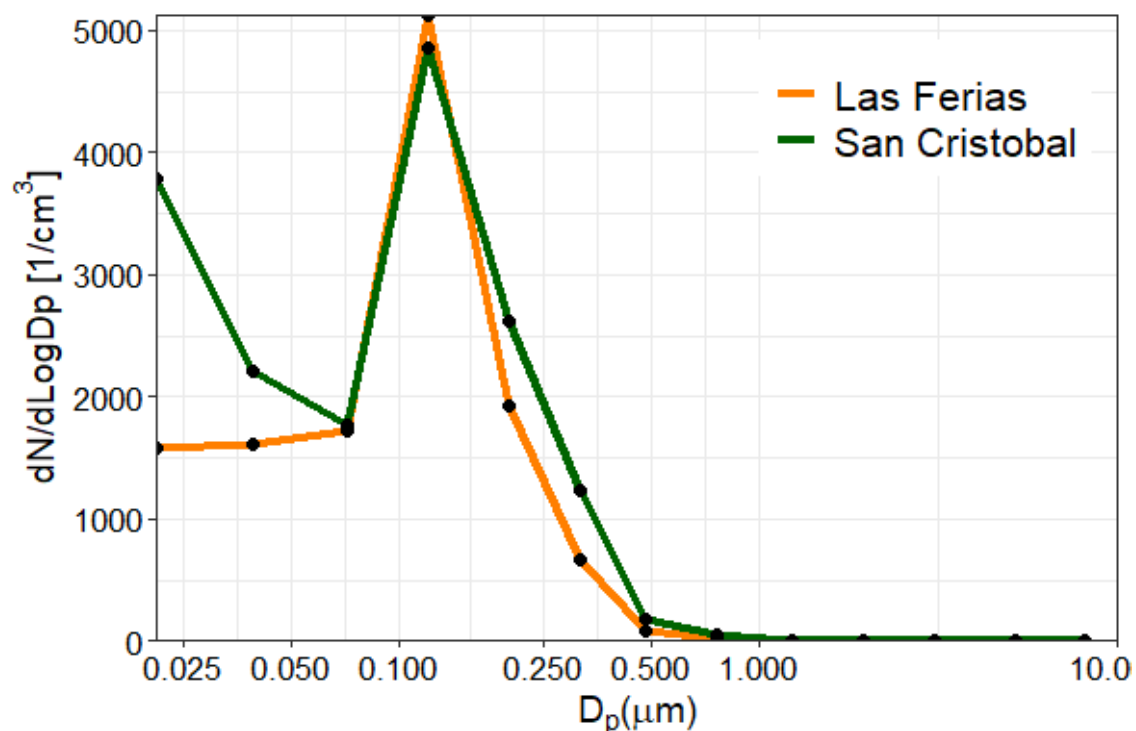
Figure 2-7. Particle number size distribution in Las Ferias (June 23 –July 5, 2017) and San Cristobal (August 30 –September 11 and September 27 - October 11, 2017).

A maximum of nucleation mode particles (with an aerodynamic diameter smaller than 100 nm) was observable only in San Cristobal, reaching 8.4×10^3 particles in the $17 - 30$ nm range, while it was not over 2.9×10^3 particles in the same range in Las Ferias. The results presented in this study show that San Cristobal can reach three times more ultrafine particles at rush traffic hours (6:00 to 9:00 H) than Las Ferias. The increase of nucleation particles in San Cristobal suggests the presence of precursors that suffer chemical and physical processes, such as, nucleation and condensation of supersaturated vapors. Thus, nucleation-mode particles in San Cristobal might have resulted from vapors derived from the combustion process, intensified during the rush traffic hours as well as meteorological conditions that affect the boundary level height.

The maxima number size distributions (5.12×10^3 #/cm³ in Las Ferias and 5.12×10^3 #/cm³ San Cristobal) were lower than the reported in the urban area of Beijing during the Olympics (1.3×10^4 #/cm³), when were applied the majors control measures to avoid high levels of air pollutants and was centered in particle size larger than in Beijing ($70 - 100$ nm) (Wang et al., 2013). On other hand, the mode particles size observed in the urban areas in Poland were unimodal and was centered into the accumulation mode particles ($157 - 263$ nm) (Klejnowski et al., 2013a) than the found in this study.

Previous studies have showed that NPSD measurement proximity to the roadways affected to high level of traffic rate exhibit a distribution center in an Aitken mode centered ~ 75 nm (Rose et al., 2006; Virtanen et al., 2006). Particularly, the NPSD of diesel exhaust emissions have revealed a unimodal distribution centered in 88 nm during the transient cycles, while in the idling operation exhibited two modes, a dominant accumulation mode centered in 16 nm and a second mode centered in ~ 75 nm. It can suggest that the diesel exhaust emissions are dominated by an accumulation of mode composed of agglomerated soot particles formed by at higher temperatures during the incomplete combustion process (Rissler et al., 2012). Hence, it is possible to hypothesize that the accumulation particles observed in Las Ferias and in San Cristobal could be derived from the vehicular emissions and that later shifted to bigger size due to the agglomeration process in the atmosphere. On the other hand, the Aitken mode observed in the morning traffic rush hour San Cristobal reveled the production of fresh particles from the combustion emissions and from particle growth process (Hama et al., 2017).
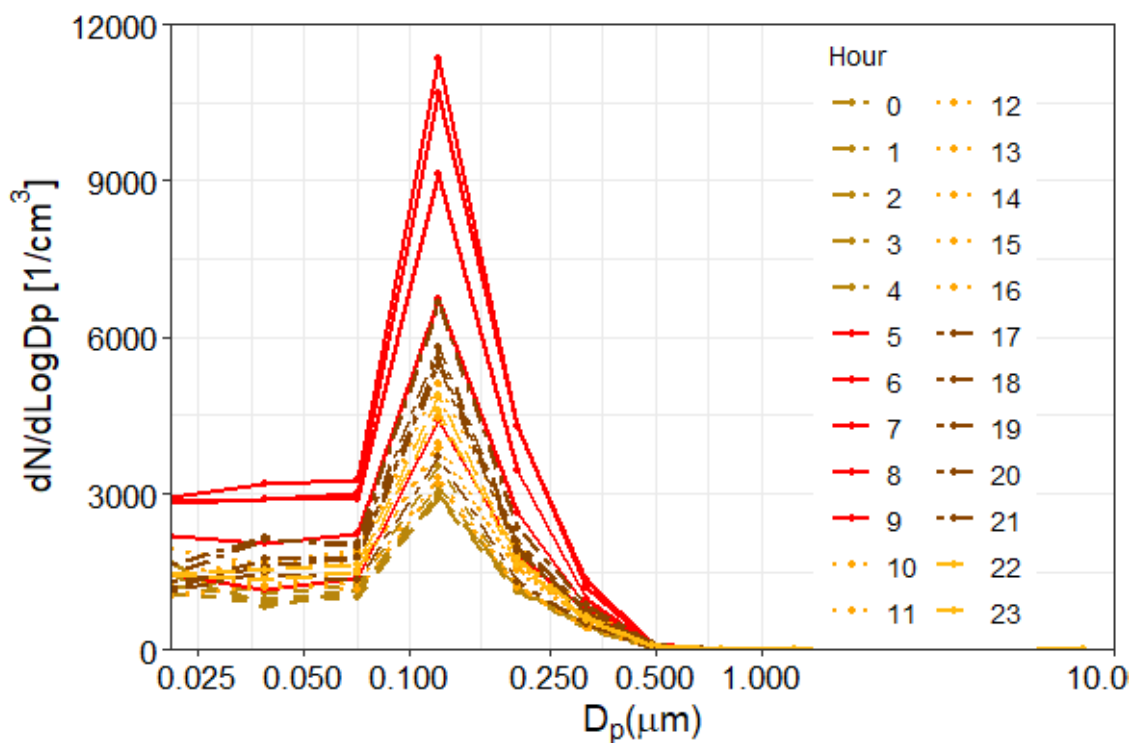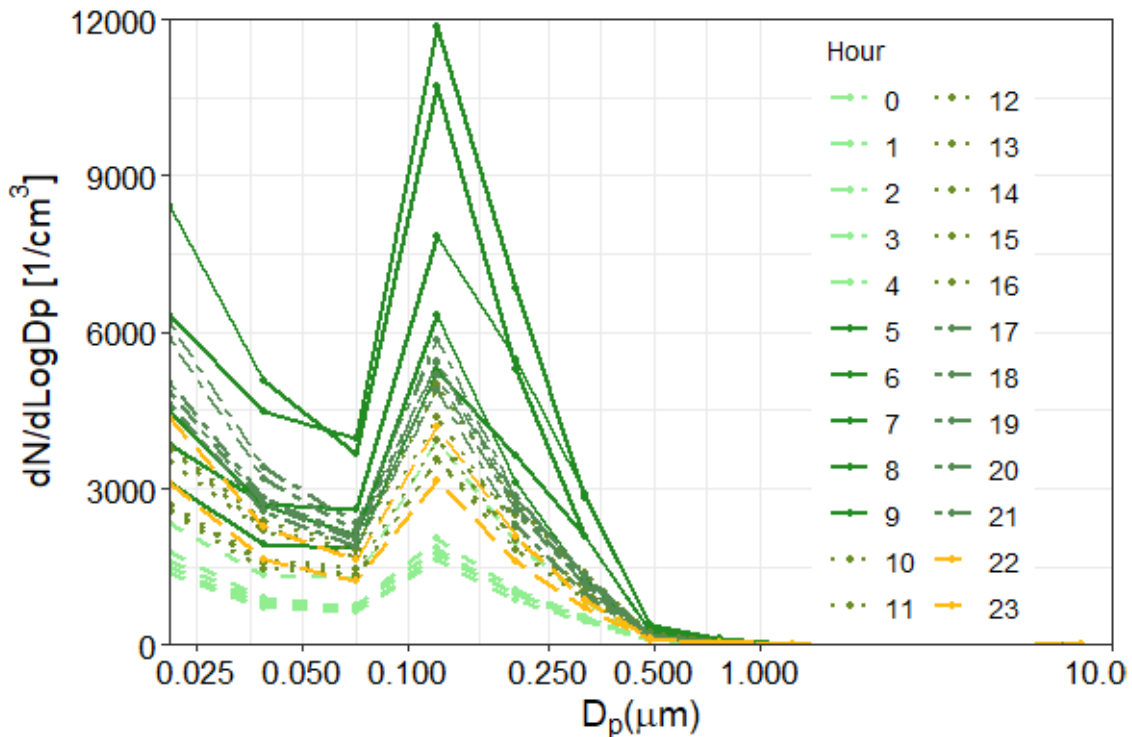
Figure 2-8. 1-hour average Number Particle Size Distribution in a) Las Ferias and b) San Cristobal sites.

2.3.5. Lung Deposited Area Surface

The average LDSA was higher in the San Cristobal site than in Las Ferias, with LDSA concentrations of 48.1 and 34.2 $\mu m^2/cm^3$, respectively. The LDSA estimated in this study were notably higher than that found in other places. In the Helsinki Metropolitan area, the average LDSA was 27.2 $\mu m^2/cm^3$ in a street canyon, 13.6 $\mu m^2/cm^3$ in a highway and 20.3 $\mu m^2/cm^3$ in a harbor (Lepistö et al., 2022). In the same city, was registered a LDSA of 19.7 $\mu m^2/cm^3$ in a street canyon and 11.2 $\mu m^2/cm^3$ in an urban background (Fung et al., 2021). In other urban background areas, the LDSA concentration was between 37 ± 26 $\mu m^2/cm^3$ in Barcelona (Spain) (Reche et al., 2015), 12 $\mu m^2/cm^3$ in an area park, 16 - 31 $\mu m^2/cm^3$ in residential areas, 15 $\mu m^2/cm^3$ in a suburban residential area, 23 $\mu m^2/cm^3$ in a residential area near to traffic sources, and 94 $\mu m^2/cm^3$ in a traffic site inner city, (Kuuluvainen et al., 2016). Thus, the LDSA resulting in this study was significantly higher to reported in other urban background areas.

The LDSA showed a diurnal variation with the highest concentrations during the morning rush hours from 4:00 to 10:00, with a peak at 7:00 H, as show in Figure 2-9. The maximum LDSA concentrations were on average 109.89 and 66.46 $\mu m^2/cm^3$ in San Cristobal and Las Ferias, correspondingly. In addition, during the afternoon, LDSA concentrations were observed with maximum concentrations of 54.72 and 42.16 $\mu m^2/cm^3$ for each site between 18:00 -19:00 H. The hourly pattern of LDSA

concentrations was similar to that of PM$_{2.5}$ concentrations (Figure 2-4a) for both sites, which suggests a link with combustion emissions derived from traffic rush hours. The maximum LDSA concentrations observed in the morning hours can be explained by high concentrations of particles caused by the minimum mixing layer height in these hours.

The LDSA concentrations were higher in San Cristobal than in Las Ferias most of the time, except for midnight (23:00 H – 3:00 H), when LDSA concentrations were higher in Las Ferias.
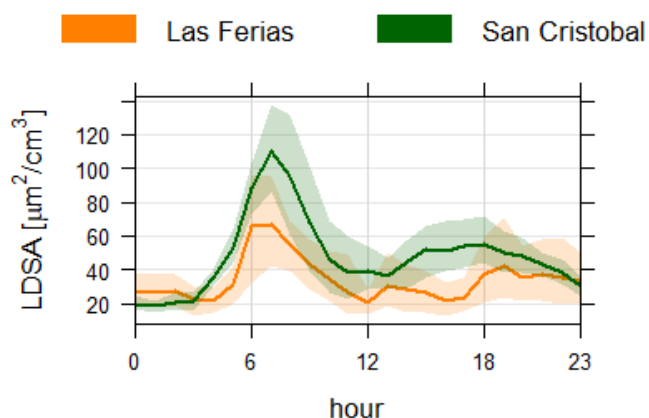
Figure 2-9. The average LDSA concentrations in the Las Ferias and San Cristobal sites and during different times of the day.

The LDSA size distribution average over the measurement periods for each site is shown in Figure 2-10. Even though the distributions at both sites were unimodal centered in the accumulation mode, different modal diameters between sites were observed. It was centered between 120 and 202 nm, with a tail over bigger diameters at Las Ferias, and around a larger diameter (317 to 485 nm) at San Cristobal. This suggests that emissions from combustion sources, such as traffic, affect Las Ferias more strongly than San Cristobal, which seems to have slightly more aged combustion aerosols. The Aitken mode (Dp < 100 nm) was not meaningful for LDSA, and coarse particles were more important in San Cristobal than in Las Ferias, with a minor mode at 2.5 μm. The difference in LDSA size distribution between San Cristobal and Las Ferias is partly explained by the differences in the sources and environments surrounding each site. Thus, while San Cristobal is an urban background site located in a park, Las Ferias is a traffic site located close to a crossing of two busy roads in the inner city. Coarse particles were more relevant in San Cristobal than in Las Ferias, with a slight mode at 2.5 μm.

LDSA size distributions showed the same modal diameters throughout the day. The highest concentrations were observed around the morning rush hour, reaching a value of 106.57 μm^2/cm^3 in las Ferias and 156.54 μm^2/cm^3 in San Cristobal at 7:00 H, as shown in Figure 2-11. The minimum LDSA concentration in San Cristobal (~22 μm^2/cm^3) was lower than observed in Las Ferias (~27 μm^2/cm^3), between 23:00 and 4:00 H.
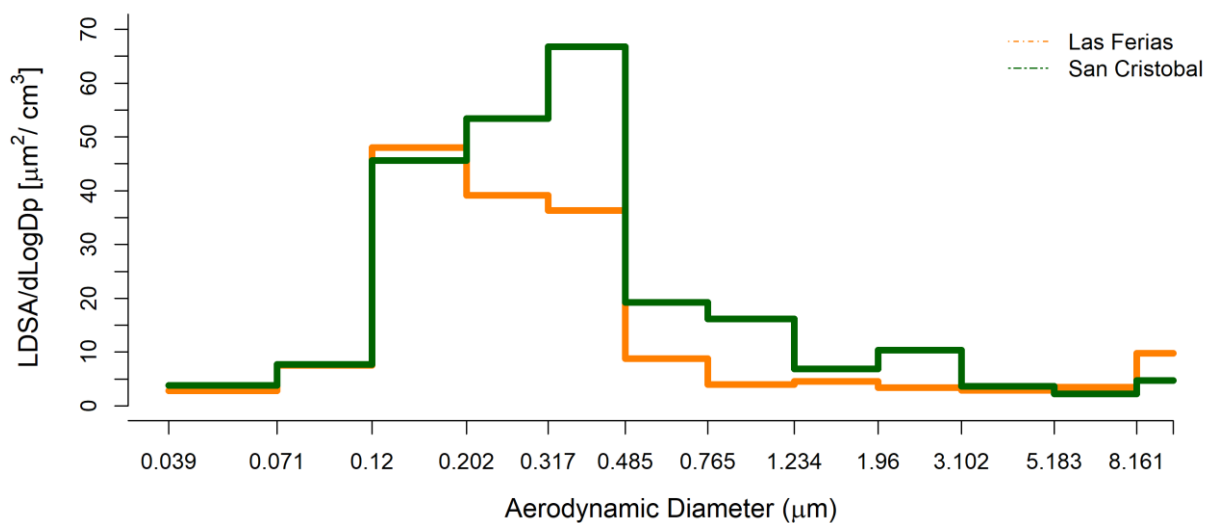
Figure 2-10. The average LDSA concentrations in the Las Ferias and San Cristobal sites and during different times of the day.
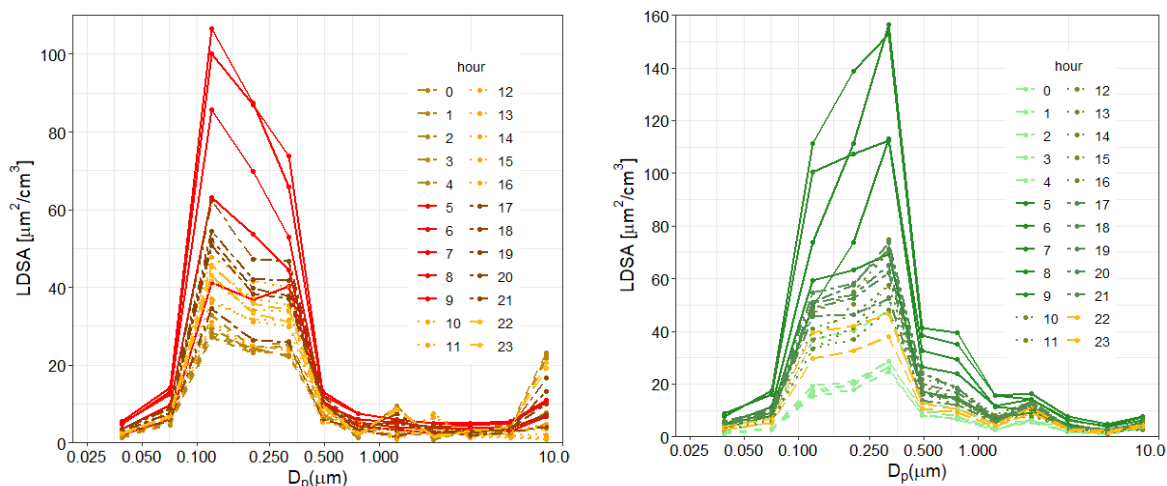
Figure 2-11. Average LDSA size distribution in Las Ferias and San Cristobal sites during the different times of the day.

2.3.6. Relationship between meteorological conditions and PNC

To differentiate whether particles are formed by the nucleation process or derived from the vehicular sources, polar plots segregated by particle size are generated by Nuclei and Aitken or nanoparticle modes and TPC. Figure 2-12a shows that nanoparticles determine the TPC present in the ambient air at Las Ferias station, because the correlation between nanoparticles and TPC is the unit ($r_{pearson} = 1$). On other hand, the correlation between Nuclei and nanoparticles modes was not the unit during the whole day. In the southeast direction and especially during the night was find a lower correlation between Nuclei and nanoparticles ($r_{pearson}$ ~0.5) (Figure 2-12b). The polar plots for nuclei and nanoparticles show that the higher nanoparticles concentration comes from the west and south direction at lower wind speeds, particularly during daylight (Figure 2-12d). In this direction is the highway closer to the Ferias

station. Also, some part of the nuclei particles come from the West, which means that some Nuclei particles could be derived from the traffic emission. However, a significant particles concentration arrives from the East at higher wind speeds, at any time of day. These particles could be transported from the easter highways and mountains that boundary the city or even far away (Figure 2-12c).
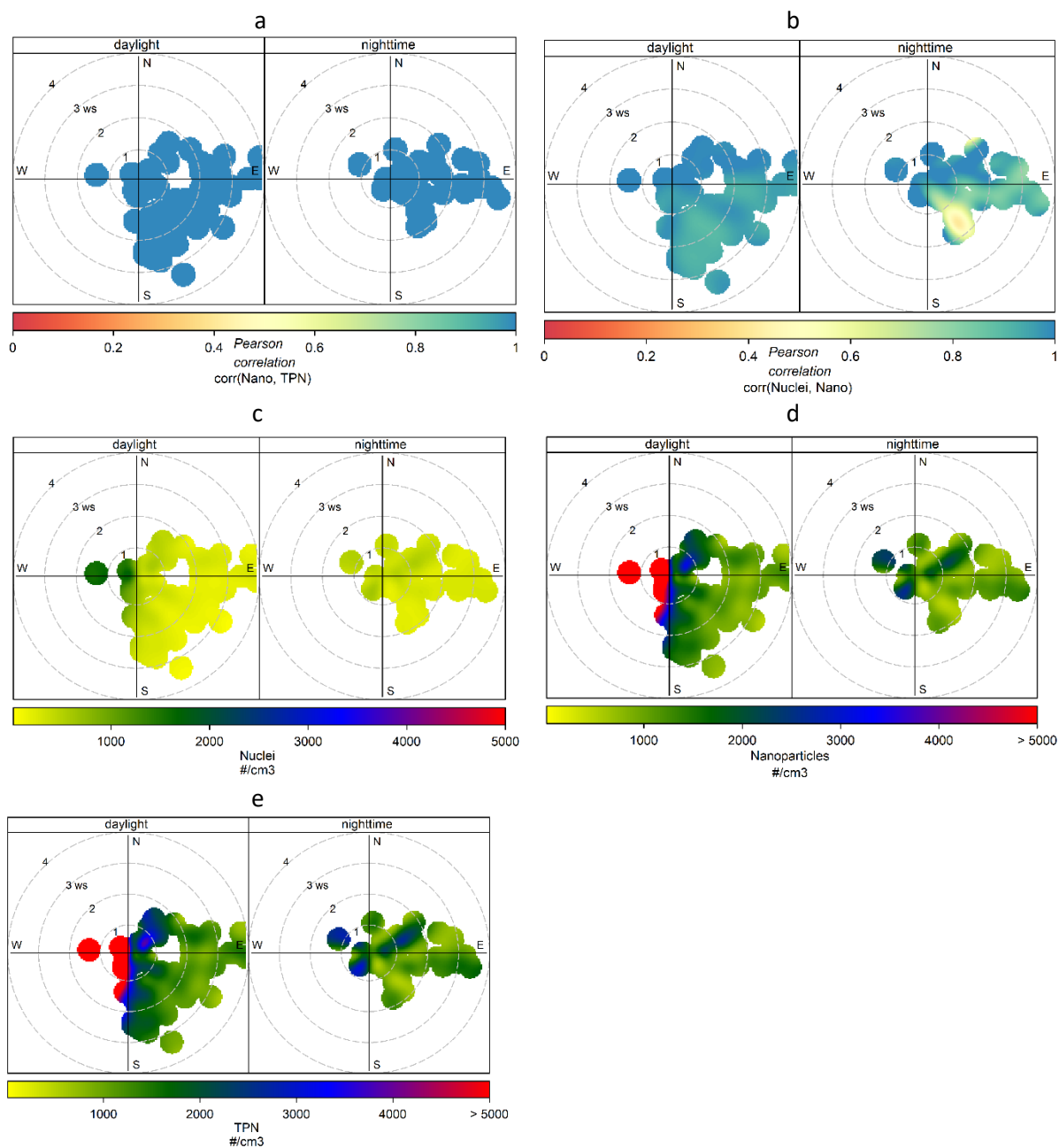
Figure 2-12. Polar plot of Nuclei, nanoparticles and TPC at Las Ferias station in Bogotá D.C. for 23 June to 5 July 2017 (c, d and e) and polar plot of the correlation between Nuclei and nanoparticles and nanoparticles and TPC (a and b).

In the San Cristobal station was find correlation coefficients between nanoparticles and TPC were closer to the unit. Except in the second measurement campaign, when the coefficient correlation decreases until 0.7 for particles that arrives from the Northwest direction, when TPC was significantly higher than

nanoparticles. The higher concentrations of nanoparticles and TPC arrive from the West, North and East during daylight. The long-range sourced particulate for all sizes comes from the east and southeast, even during the nighttime.
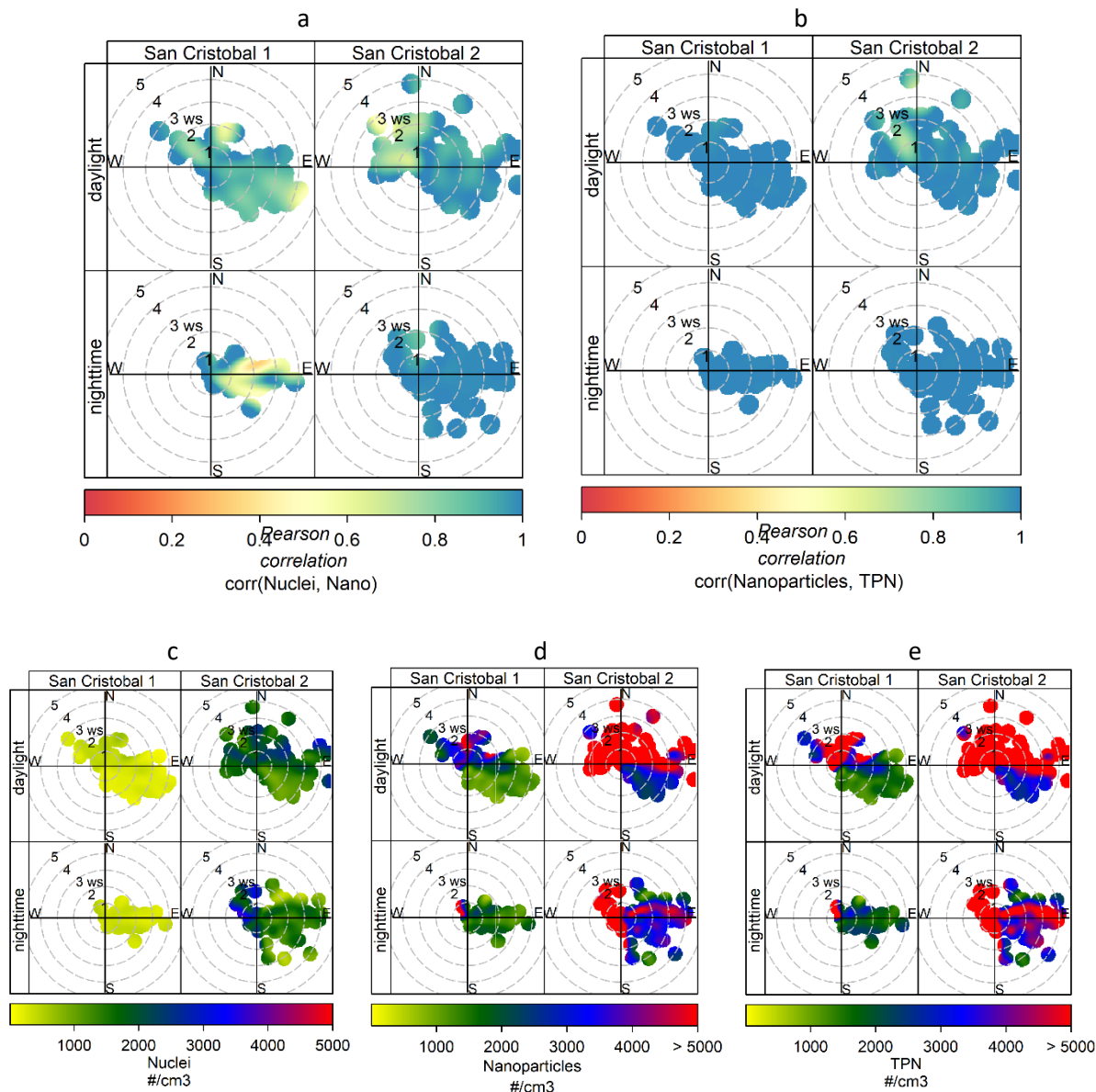
Figure 2-13. Polar plot of the correlation between Nuclei (c) , nanoparticles (d) and TPC (e) at San Cristobal station in Bogotá D.C. for 30 August 2023 to 11 September 2017 (San Cristobal 1) and from 27 September to 10 October 2017 (San Cristobal 2) and polar plot of the correlation between Nuclei and nanoparticles and nanoparticles and TPC for both periods (a and b).

Although the relative humidity (%RH) was significantly different in San Cristobal than in las Ferias Station, this meteorological parameter did not show a statistical correlation with the number of particles in the nuclei mode, nanoparticles and TPC. The Spearman correlation between Nuclei mode,

nanoparticles and TPC and %HR was not significantly different from zero (r^2 = 0.01 - 0.15), for the two stations and the three measurement periods.

Due to the %RH change during the day was explored the statistical association of nuclei mode, nanoparticles and TPC by time of day for each station and measurement period. Table 2-3 shows the square Spearman correlation segregated by hour, size of particles and station. A higher correlation was found during the first period of measurement conducted in the San Cristobal station between the %RH with nanoparticles and TPC in the afternoon (13:00H – 15:00H). At this time was no rush-hour traffic and the %RH decreased to 50%. The stronger correlation coefficient was observed at 10:00 H in Las Ferias for the three sizes of particles, although there was no discernible pattern seen around this time. Overall, this study could not demonstrate that differences in nuclei mode, nanoparticles, and PNC seen during the two observation periods in the San Cristobal station were caused by variations in the ambient air's relative humidity (%RH). Similar results were found by Wehner and Wiedensohler, (2003) with no relevant correlation between humidity and the process of particles formation.

Table 2-3. Correlation coefficient of Spearman (R^2) between Relative Humidity and number of particles segregate by aerodynamic diameter for the Nuclei mode (21 – 38 nm), nanoparticles (21 – 119 nm) and TPC (21 nm – 10 µm) and time of day.

Hour/Station	0:00	1:00	2:00	3:00	4:00	5:00	6:00	7:00	8:00	9:00	10:00	11:00	12:00	13:00	14:00	15:00	16:00	17:00	18:00	19:00	20:00	21:00	22:00	23:00	Size of particles
Las Ferias		0.80				0.95	0.39	0.51			0.86				0.39		0.43					0.46		0.47	Nuclei (21 - 38 nm)
San Cristobal 1										0.47	0.64	0.43		0.71	0.82	0.61			0.38						
San Cristobal 2					0.37			0.32									0.39			0.57					
Las Ferias		0.50			0.30	0.79		0.46			0.91						0.31					0.39			Nanoparticles (21 - 119 nm)
San Cristobal 1			0.40							0.46	0.34			0.74	0.74	0.73	0.75	0.43	0.54	0.32					
San Cristobal 2				0.32													0.46		0.49	0.59	0.32				
Las Ferias		0.43			0.32	0.79		0.46			0.92											0.37			TPC (21 nm - 10 µm)
San Cristobal 1			0.38	0.50						0.42				0.72	0.74	0.72	0.76	0.52	0.56	0.36					
San Cristobal 2					0.30												0.53	0.41	0.61	0.61	0.38				

2.4. Conclusions

The findings of a pioneering study in Colombia that measured the number particle concentration, number particle size distribution, and lung deposited surface area were presented in this chapter. This investigation was conducted in two urban sites of Bogotá, Colombia: the first in a location affected by traffic pollution (Las Ferias), and the second in a location designated as an urban background site (San Cristobal). Measurements were not performed simultaneously, but under similar meteorological conditions They were made with a high time resolution (1 second), and then averaged hourly and daily. Weather-related factors, PM_{10}, $PM_{2.5}$, and other criteria gases, like O_3 and NO_x, were monitored in the same sites of the Air Quality Network of Bogota.

The Particle Number Concentration (PNC) observed in PNC in San Cristobal (3.8×10^3 #/cm^3) was higher than in Las Ferias (2.8×10^3 #/cm^3), despite the average PM$_{2.5}$ concentration being similar in the two places. 80% of these particles are nanoparticles. The PNC found in this study has similar magnitude orders to report in other to those studies conducted in Europe and US cities. In terms of the hourly variations, during morning rush hour traffic was observed around the double PNC in comparison to the daily average of PNC, while the minimum concentrations were registered at midnight with half of the average daily concentration. As was expected, during on the weekdays the PNC was higher than on the weekends and these differences were most notable in Las Ferias than in San Cristobal.

The Particles Number Size Distribution (PNSD) was unimodal, centered in the aerodynamic diameter of 120 nm in Las Ferias site and the hourly variation was not affected in the PNSD, while the San Cristobal site exhibited a different shape in the morning rush traffic hour, showing the formation of an ultrafine mode during these hours. A larger mode was found in San Cristobal centered in 120 nm and the finest mode was observed in the range between 17 and 30 nm.

Regarding the Lung Deposited Area Surface (LDSA), this study revealed that particles with the most significant potential to lodge in the lungs had a smaller aerodynamic diameter in Las Ferias than in the San Cristobal site, attributed to the proximity to the vehicular emissions. Hence, in Las Ferias the particles with an aerodynamic diameter between 120 and 202 nm have a large lung deposition potential, while in San Cristobal are the particles with an aerodynamic diameter between 317 and 485 nm.

The average LDSA concentration was much lower in Las Ferias than in San Cristobal, with an average of 48.1 and 34.2 μm^2/cm^3, for each site, despite the PM$_{2.5}$ and PM$_{10}$ concentrations were not statistically different between the two sites. In comparison to other studies conducted in urban backgrounds, San Cristobal showed higher levels of LDSA. The hourly LDSA concentrations have a different pattern than PM$_{2.5}$ concentrations because LDSA was noticeably greater during the morning traffic rush hours while PM$_{2.5}$ concentrations were much higher during the evening rush hours, especially in the San Cristobal site. The hourly LDSA average in both sites was impacted by peak traffic hours.

The variations in the primary particle sources that are present surrounding each site can be seen on the LDSA. As a result, in Las Ferias there was a greater effect on vehicle emissions than San Cristobal, which is visible in the size of particles that are more likely to lodge in the lungs. Particles from biogenic emissions, both local and distant, are present in the San Cristobal site, which promotes the formation of new particles by condensation over existing particles as well as they are its subsequent growth.

2.5. References

Agudelo-castañeda, D. M., Teixeira, E. C., Braga, M., Rolim, S. B. A., Silva, L. F. O., Beddows, D. C. S., Harrison, R. M. and Querol, X.: Cluster analysis of urban ultra fi ne particles size distributions, Atmos. Pollut. Res., (June), 0–1, https://doi.org/10.1016/j.apr.2018.06.006, 2018.

Asbach, C., Fissan, H., Stahlmecke, B., Kuhlbusch, T. A. J. and Pui, D. Y. H.: Conceptual limitations and extensions of lung-deposited Nanoparticle Surface Area Monitor (NSAM), J. Nanoparticle Res., 11(1), 101–109, https://doi.org/10.1007/s11051-008-9479-8, 2009.

Avila Prada, L. T.: Determinación del Nivel de Exposición de Viajeros Pendulares a Partículas Ultrafinas Según el Modo de Transporte en la ciudad de Bogotá, Universidad Nacional de Colombia https://repositorio.unal.edu.co/handle/unal/59281, 2016.

Boogaard, H., Montagne, D. R., Brandenburg, A. P., Meliefste, K. and Hoek, G.: Comparison of short-term exposure to particle number, PM10 and soot concentrations on three (sub) urban locations, Sci. Total Environ., 408(20), 4403–4411, https://doi.org/10.1016/j.scitotenv.2010.06.022, 2010.

Brown, D. M., Wilson, M. R., MacNee, W., Stone, V. and Donaldson, K.: Size-dependent proinflammatory effects of ultrafine polystyrene particles: A role for surface area and oxidative stress in the enhanced activity of ultrafines, Toxicol. Appl. Pharmacol., 175(3), 191–199, https://doi.org/10.1006/taap.2001.9240, 2001.

Chalvatzaki, E., Chatoutsidou, S. E. and Lazaridis, M.: Regional deposited dose in the human respiratory tract using different particulate metrics, J. Environ. Expo. Assess., 1(3), 18, https://doi.org/10.20517/jeea.2022.16, 2022.

Dal Maso, M., Kulmala, M., Riipinen, I., Wagner, R., Hussein, T., Aalto, P. P. and Lehtinen, K. E. J.: Formation and growth of fresh atmospheric aerosols: Eight years of aerosol size distribution data from SMEAR II, Hyytiälä, Finland, Boreal Environ. Res., 10(5), 323–336, 2005.

Díaz Fonseca, Ó. D.: Impacto de la contaminación producto del tráfico vehicular sobre los niveles de carboxihemoglobina y la respuesta respiratoria en ciclistas urbanos de la universidad nacional de colombia–sede Bogotá, Universidad Nacional de Colombia, 2021.

European Commission: FIT FOR FUTURE Platform Opinion. https://ec.europa.eu/info/law/law-making-process/evaluating-and-improving-existing-laws/refit-making-eu-law-simpler-less-costly-and-future-proof/fit-future-platform-f4f/annual-work-programme_en, 2021.

Fierz, M., Houle, C., Steigmeier, P. and Burtscher, H.: Design, calibration, and field performance of a miniature diffusion size classifier, Aerosol Sci. Technol., 45(1), 1–10, https://doi.org/10.1080/02786826.2010.516283, 2011.

Fierz, M., Meier, D., Steigmeier, P. and Burtscher, H.: Aerosol measurement by induced currents, Aerosol Sci. Technol., 48(4), 350–357, https://doi.org/10.1080/02786826.2013.875981, 2014.

Fults, S. L., Massmann, A. K., Montecinos, A., Andrews, E., Kingsmill, D. E., Minder, J. R., Garreaud, R. D. and Snider, J. R.: Wintertime aerosol measurements during the Chilean Coastal Orographic Precipitation Experiment, Atmos. Chem. Phys., 19(19), 12377–12396, https://doi.org/10.5194/acp-19-12377-2019, 2019.

Fung, P. L., Zaidan, M. A., Niemi, J. V, Saukko, E., Timonen, H. and Kousa, A.: Input-adaptive linear mixed-effects model for estimating alveolar Lung Deposited Surface Area (LDSA) using multipollutant datasets, , (July), 1–33, 2021.

Gani, S., Bhandari, S., Patel, K., Seraj, S., Soni, P., Arub, Z., Habib, G., Hildebrandt Ruiz, L. and Apte, J. S.: Particle number concentrations and size distribution in a polluted megacity: The Delhi Aerosol

Supersite study, Atmos. Chem. Phys., 20(14), 8533–8549, https://doi.org/10.5194/acp-20-8533-2020, 2020.

Hama, S. M. L., Ma, N., Cordell, R. L., Kos, G. P. A., Wiedensohler, A. and Monks, P. S.: Lung deposited surface area in Leicester urban background site/UK: Sources and contribution of new particle formation, Atmos. Environ., https://doi.org/10.1016/j.atmosenv.2016.12.002, 2017.

Held, A., Zerrath, A., McKeon, U., Fehrenbach, T., Niessner, R., Plass-D??lmer, C., Kaminski, U., Berresheim, H. and Poschl, U.: Aerosol size distributions measured in urban, rural and high-alpine air with an electrical low pressure impactor (ELPI), Atmos. Environ., 42(36), 8502–8512, https://doi.org/10.1016/j.atmosenv.2008.06.015, 2008.

Hernandez, L. A.: Caracterización de la Contaminación por Material Particulado en Bogotá mediante Fotometría Solar Caracterización de la Contaminación por Material Particulado en Bogotá mediante Fotometría Solar, 2016.

Hernandez Villamizar, A. J.: Assessment of the impact of biomass burning on air quality in the Colombian Orinoco River Basin, Universidad Nacional de Colombia https://repositorio.unal.edu.co/handle/unal/76979?show=full, 2019.

Hovorka, J., Masiol, M., Topinka, J., Leoni, C., Pokorn, P., Cliff, S., Miku, P., Zhao, Y. and Kamil, K.: Source apportionment of aerosol particles at a European air pollution hot spot using particle number size distributions and chemical composition, Environ. Pollut., 234, 145–154, https://doi.org/10.1016/j.envpol.2017.10.097, 2018.

ICRP: Human Respiratory Tract Model for Radiological Protection., 1994.

International Commission on Radiological Protection: Annals of the ICRP. www.icrp.org, 2015.

Kasumba, J., Hopke, P. K., Chalupa, D. C. and Utell, M. J.: Comparison of sources of submicron particle number concentrations measured at two sites in Rochester, NY, Sci. Total Environ., 407(18), 5071–5084, https://doi.org/10.1016/j.scitotenv.2009.05.040, 2009.

Kleinman, L. I., Springston, S. R., Wang, J., Daum, P. H., Lee, Y., Nunnermacker, L. J. and Senum, G. I.: and Physics The time evolution of aerosol size distribution over the Mexico City plateau, , 4261–4278, 2009.

Klejnowski, K., Krasa, A., B, W. R. and Barbara, B. B.: Number Size Distribution of Ambient Particles in a Typical Urban Site : The First Polish Assessment Based on Long-Term (9 Months) Measurements, , 2013, 2013a.

Klejnowski, K., Krasa, A., Rogula-Kozłowska, W. and Błaszczak, B.: Number size distribution of ambient particles in a typical urban site: The first polish assessment based on long-term (9 months) measurements, Sci. World J., 2013, https://doi.org/10.1155/2013/539568, 2013b.

Kulmala, M., Vehkamäki, H., Petäjä, T., Dal Maso, M., Lauri, A., Kerminen, V. M., Birmili, W. and McMurry, P. H.: Formation and growth rates of ultrafine atmospheric particles: A review of observations, J. Aerosol Sci., 35(2), 143–176, https://doi.org/10.1016/j.jaerosci.2003.10.003, 2004.

Kumar, P., Robins, A., Vardoulakis, S. and Britter, R.: A review of the characteristics of nanoparticles in the urban atmosphere and the prospects for developing regulatory controls, Atmos. Environ., 1–18, https://doi.org/10.1016/j.atmosenv.2010.08.016, 2010.

Kuuluvainen, H., Rönkkö, T., Järvinen, A., Saari, S., Karjalainen, P., Lähde, T., Pirjola, L., Niemi, J. V., Hillamo, R. and Keskinen, J.: Lung deposited surface area size distributions of particulate matter in different urban areas, Atmos. Environ., 136, 105–113, https://doi.org/10.1016/j.atmosenv.2016.04.019, 2016.

Lee, Y., Choi, Y., An, H., Park, J. and Sung, Y.: Cluster analysis of atmospheric particle number size distributions at a rural site downwind of Seoul , Korea, Atmos. Pollut. Res., 12(6), 101086, https://doi.org/10.1016/j.apr.2021.101086, 2021.

Lefol, L., Guarieiro, N., Lefol, A. and Guarieiro, N.: Impact of the Biofuels Burning on Particle Emissions from the Vehicular Exhaust, in Biofuels - Status and Perspective, p. Chapter 11, https://doi.org/10.5772/60110, , 2015.

Lepistö, T., Kuuluvainen, H., Lintusaari, H., Kuittinen, N., Salo, L., Helin, A., Niemi, J. V., Manninen, H. E., Timonen, H., Jalava, P., Saarikoski, S. and Rönkkö, T.: Connection between lung deposited surface area (LDSA) and black carbon (BC) concentrations in road traffic and harbour environments, Atmos. Environ., 272(September 2021), https://doi.org/10.1016/j.atmosenv.2021.118931, 2022.

Liang, C., Wu, H., Li, H., Zhang, Q., Li, Z. and He, K.: Efficient data preprocessing, episode classifi cation , and source apportionment of particle number concentrations, Sci. Total Environ., 744, 1–17, https://doi.org/10.1016/j.scitotenv.2020.140923, 2020.

Lorelei de Jesus, A., Thompson, H., Knibbs, L. D., Kowalski, M., Cyrys, J., Niemi, J. V., Kousa, A., Timonen, H., Luoma, K., Petäjä, T., Beddows, D., Harrison, R. M., Hopke, P. and Morawska, L.: Long-term trends in PM2.5 mass and particle number concentrations in urban air: The impacts of mitigation measures and extreme events due to changing climates, Environ. Pollut., 263, https://doi.org/10.1016/j.envpol.2020.114500, 2020.

Manuel Rincón-Riveros, J., Alejandra Rincón-Caro, M., Sullivan, A. P., Felipe Mendez-Espinosa, J., Carlos Belalcazar, L., Quirama Aguilar, M. and Morales Betancourt, R.: Long-term brown carbon and smoke tracer observations in Bogotá, Colombia: Association with medium-range transport of biomass burning plumes, Atmos. Chem. Phys., 20(12), 7459–7472, https://doi.org/10.5194/acp-20-7459-2020, 2020.

Manzano, C. A., Leiva-guzm, M. A., S, L. F., A, M. C. and Araya, R. T.: Urban atmospheric particle size distribution in Santiago , Chile, , 12(September), https://doi.org/10.1016/j.apr.2021.101201, 2021.

Marra, J.: Using the Aerasense NanoTracer for simultaneously obtaining several ultrafine particle exposure metrics, J. Phys. Conf. Ser., 304(1), https://doi.org/10.1088/1742-6596/304/1/012010, 2011.

Martins, L. D., Martins, J. A., Freitas, E. D., Mazzoli, C. R., Gonçalves, F. L. T., Ynoue, R. Y. and Hallak, R.: Potential health impact of ultrafine particles under clean and polluted urban atmospheric conditions : a model-based study, Air Qual. Atmos. Heal., 3, 29–39, https://doi.org/10.1007/s11869-009-0048-9, 2010.

Mills, J. B., Park, J. H. and and Peters, T. M.: Comparison of the DiSCmini aerosol monitor to a handheld condensation particle counter and a scanning mobility particle sizer for submicrometer sodium chloride and metal aerosols, Occup Env. Hyg, 10(5), 250–258, https://doi.org/10.1080/15459624.2013.769077.Comparison, 2013.

Monteiro Dos Santos, D., Rizzo, L. V., Carbone, S., Schlag, P. and Artaxo, P.: Physical and chemical properties of urban aerosols in São Paulo, Brazil: Links between composition and size distribution of submicron particles, Atmos. Chem. Phys., 21(11), 8761–8773, https://doi.org/10.5194/acp-21-8761-2021, 2021.

Oberdörster, G., Oberdörster, E. and Oberdörster, J.: Nanotoxicology: An emerging discipline evolving from studies of ultrafine particles, Environ. Health Perspect., 113(7), 823–839, https://doi.org/10.1289/ehp.7339, 2005.

Ogulei, D., Hopke, P. K., Ferro, A. R. and Jaques, P. a: Factor analysis of submicron particle size distributions near a major United States-Canada trade bridge., J. Air Waste Manag. Assoc., 57(2), 190–203, https://doi.org/10.1080/10473289.2007.10465316, 2007.

Ortiz Duran, E. Y.: Medición y caracterización de la turbulencia atmosférica en Bogotá y su influencia en la dispersión de contaminantes, Universidad Nacional de Colombia, 2016.

Pekkanen, J., Timonen, K., Tiittanen, P., Vallius, M., Lanki, T., Sinkko, H., Ruuskanen, J., Mirme, A., Kulmala, M., E, V., A, B., Vanninen, E., Bernard, A., Ibald-Mulli, A., Wölke, G., Stadeler, M., Tuch, T., Kreyling, W., Peters, A., Heinrich, J., de Hartog, J., Oldenwening, M., Kos, G., ten Brink, H., Khlystov, A., van Wijnen, J., Brunekreef, B. and and Hoek, G.: Exposure and risk assessment for fine and ultrafine particles in ambient air. Study manual and data book. http://thl32-kk.lib.helsinki.fi/bitstream/handle/10024/78817/ULTRA study_manual.pdf?sequence=1, 2000.

Reche, C., Viana, M., Brines, M., Pérez, N., Beddows, D., Alastuey, A. and Querol, X.: Determinants of aerosol lung-deposited surface area variation in an urban environment, Sci. Total Environ., 517, 38–47, https://doi.org/10.1016/j.scitotenv.2015.02.049, 2015.

Rissler, J., Swietlicki, E., Bengtsson, A., Boman, C., Pagels, J., Sandström, T., Blomberg, A. and Löndahl, J.: Experimental determination of deposition of diesel exhaust particles in the human respiratory tract, J. Aerosol Sci., 48, 18–33, https://doi.org/10.1016/j.jaerosci.2012.01.005, 2012.

Rivas, I., Beddows, D. C. S., Amato, F., Green, D. C., Järvi, L., Hueglin, C., Reche, C., Timonen, H., Fuller, G. W., Niemi, J. V, Pérez, N., Aurela, M., Hopke, P. K., Alastuey, A., Kulmala, M., Harrison, R. M., Querol, X. and Kelly, F. J.: Source apportionment of particle number size distribution in urban background and traffic stations in four European cities, Environ. Int., 135(May 2019), 105345, https://doi.org/10.1016/j.envint.2019.105345, 2020.

Rose, D., Wehner, B., Ketzel, M., Engler, C. and Voigtl, J.: Atmospheric number size distributions of soot particles and estimation of emission factors, Atmosphere (Basel)., 6, 1021–1031, 2006.

Secretaría Distrital de Ambiente: Informe anual de calidad del aire en Bogotá 2017., 2018.

Secretaría Distrital de Ambiente (SDA): Red de Monitoreo de Calidad del Aire de Bogotá, Mapas la Red http://rmcab.ambientebogota.gov.co/home/map, last access: 5 October 2022, 2018.

Secretaría Distrital de Ambiente (SDA): Inventario de emisiones de Bogotá contaminantes atmosféricos 2020, Bogotá D.C., 2022.

Seinfeld, J. H. and Pandis, S. N.: Atmospheric From Air Pollution to Climate Change, 2 nd., 2006.

Shin, W. G., Pui, D. Y. H., Fissan, H., Neumann, S. and Trampe, A.: Calibration and numerical simulation of Nanoparticle Surface Area Monitor (TSI Model 3550 NSAM), J. Nanoparticle Res., 9(1), 61–69, https://doi.org/10.1007/s11051-006-9153-y, 2007.

Virtanen, A., Ronkko¨, T., Kannosto, J., Ristimaki, J., Makela, J. M., Keskinen, J., Pakkanen, T., Hillamo, R., Pirjola, L. and K. Hameri, K.: Winter and summer time size distributions and densities of traffic-related aerosol particles at a busy highway in Helsinki, Atmos. Chem. Phys., 6, 2411–2421, 2006.

Vu, T. V., Beddows, D. C. S., Delgado-Saborit, J. M. and Harrison, R. M.: Source apportionment of the lung dose of ambient submicrometre particulate matter, Aerosol Air Qual. Res., 16(7), 1548–1557, https://doi.org/10.4209/aaqr.2015.09.0553, 2016.

Wang, Z. B., Hu, M., Wu, Z. J., Yue, D. L., He, L. Y., Huang, X. F., Liu, X. G. and Wiedensohler, A.: Long-term measurements of particle number size distributions and the relationships with air mass history and source apportionment in the summer of Beijing, , 10159–10170, https://doi.org/10.5194/acp-13-10159-2013, 2013.

Wehner, B. and Wiedensohler, A.: and Physics Long term measurements of submicrometer urban aerosols : statistical analysis for correlations with meteorological conditions and trace gases, Atmos. Chem. Phys., 3(2001), 867–879, 2003.

Zhang, Z. H., Hartner, E., Utinger, B., Gfeller, B., Paul, A., Sklorz, M., Czech, H., Yang, B. X., Su, X. Y., Jakobi, G., Orasche, J., Schnelle-Kreis, J., Jeong, S., Gröger, T., Pardo, M., Hohaus, T., Adam, T., Kiendler-Scharr, A., Rudich, Y., Zimmermann, R. and Kalberer, M.: Are reactive oxygen species (ROS) a suitable metric to predict toxicity of carbonaceous aerosol particles?, Atmos. Chem. Phys., 22(3), 1793–1809, https://doi.org/10.5194/acp-22-1793-2022, 2022.

2.6. Supplementary information
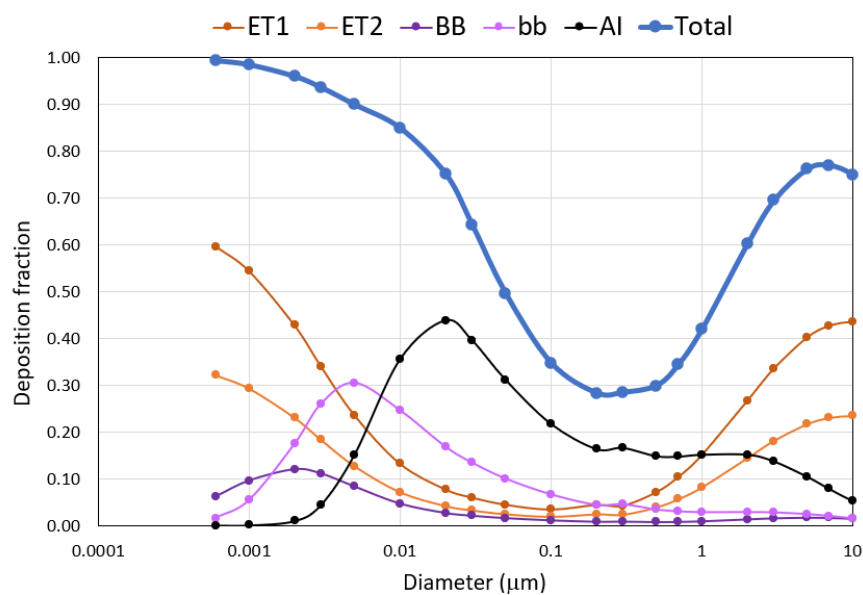
Figure S 2-1. Deposition fraction curves in alveolar, bronchiolar and head airways published by (International Commission on Radiological Protection, 2015). Each curve corresponded to ET1, anterior nasal passage; ET2, posterior nasal passage, pharynx, and larynx; BB, bronchial; bb, bronchiolar; AI, alveolar interstitial for median aerodynamic diameter.
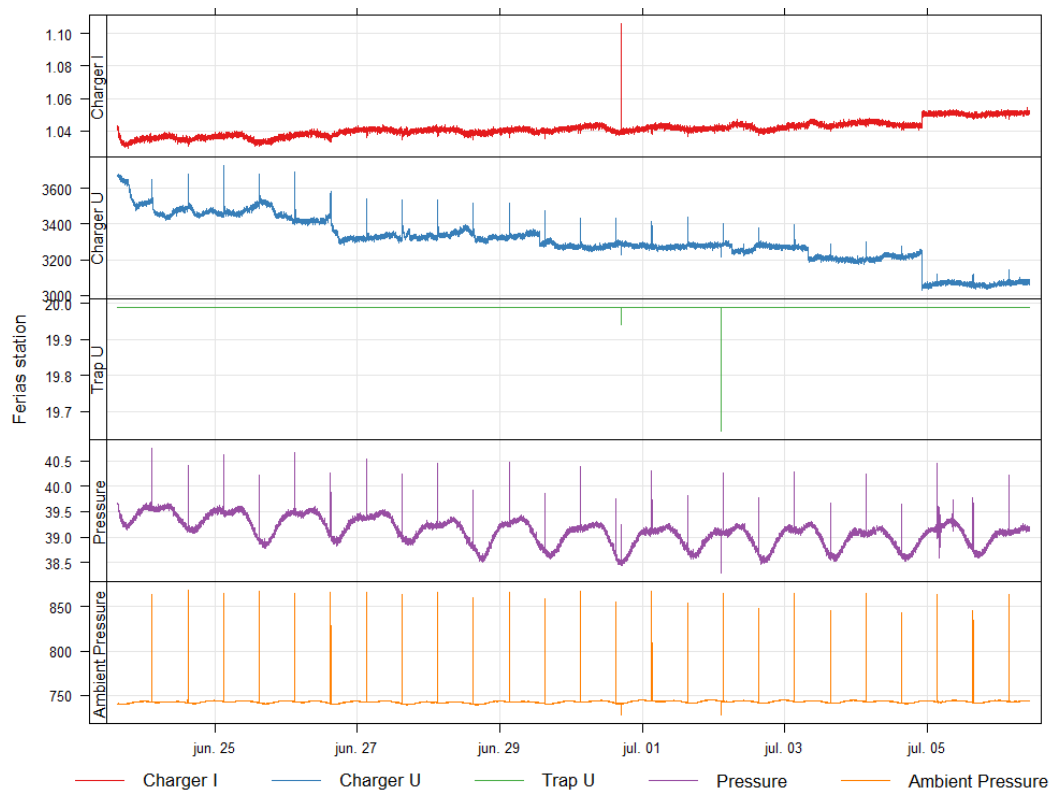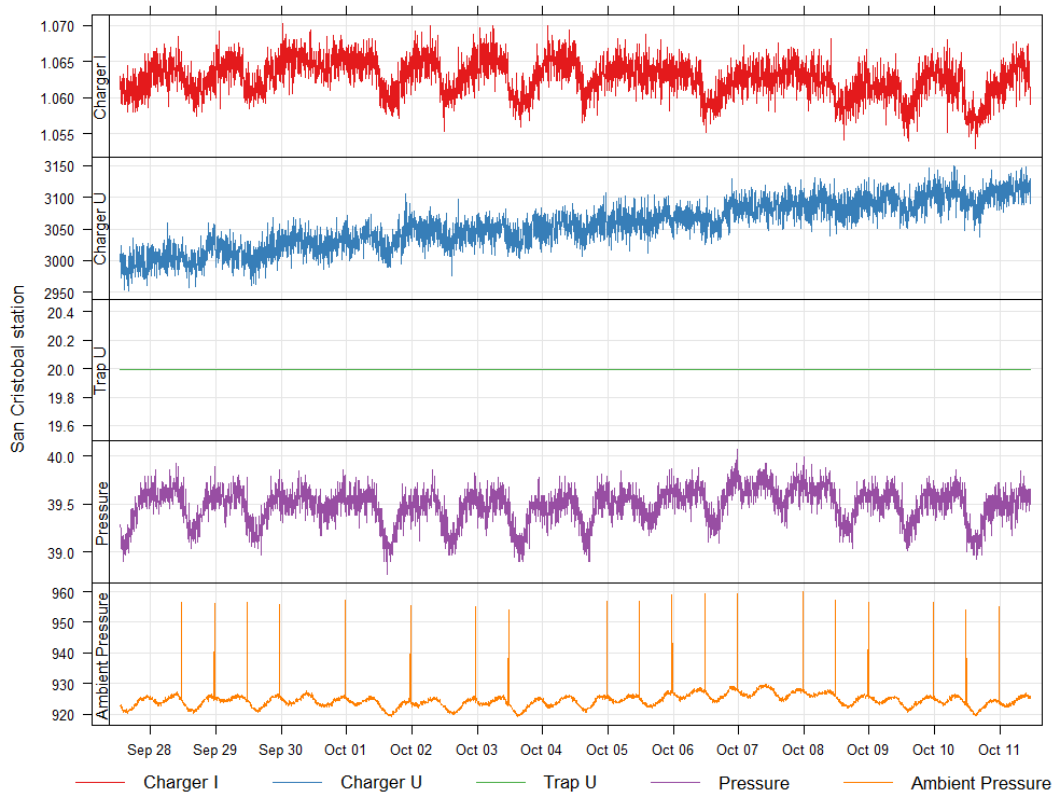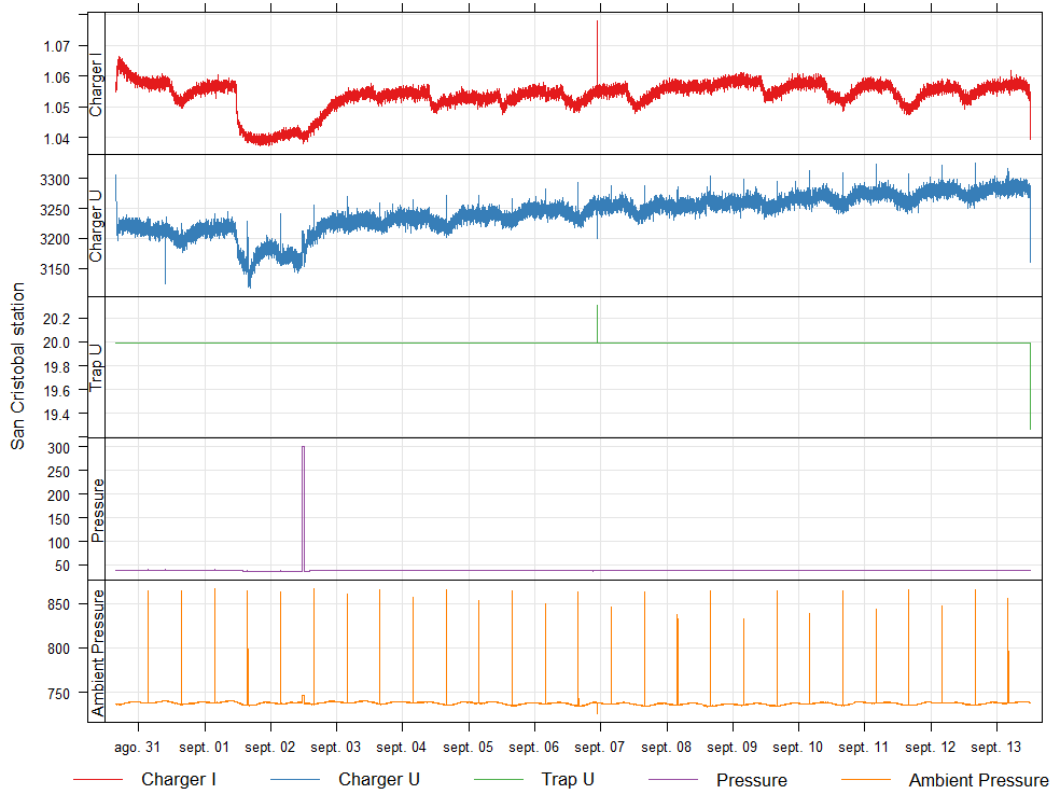
Figure S 2-2. Time series of the operational ELPI⁺ parameters recorded during measurements at Las Ferias and San Cristobal (minute average).

a

b

C

Frequency of counts by wind direction (%)

d

e

f
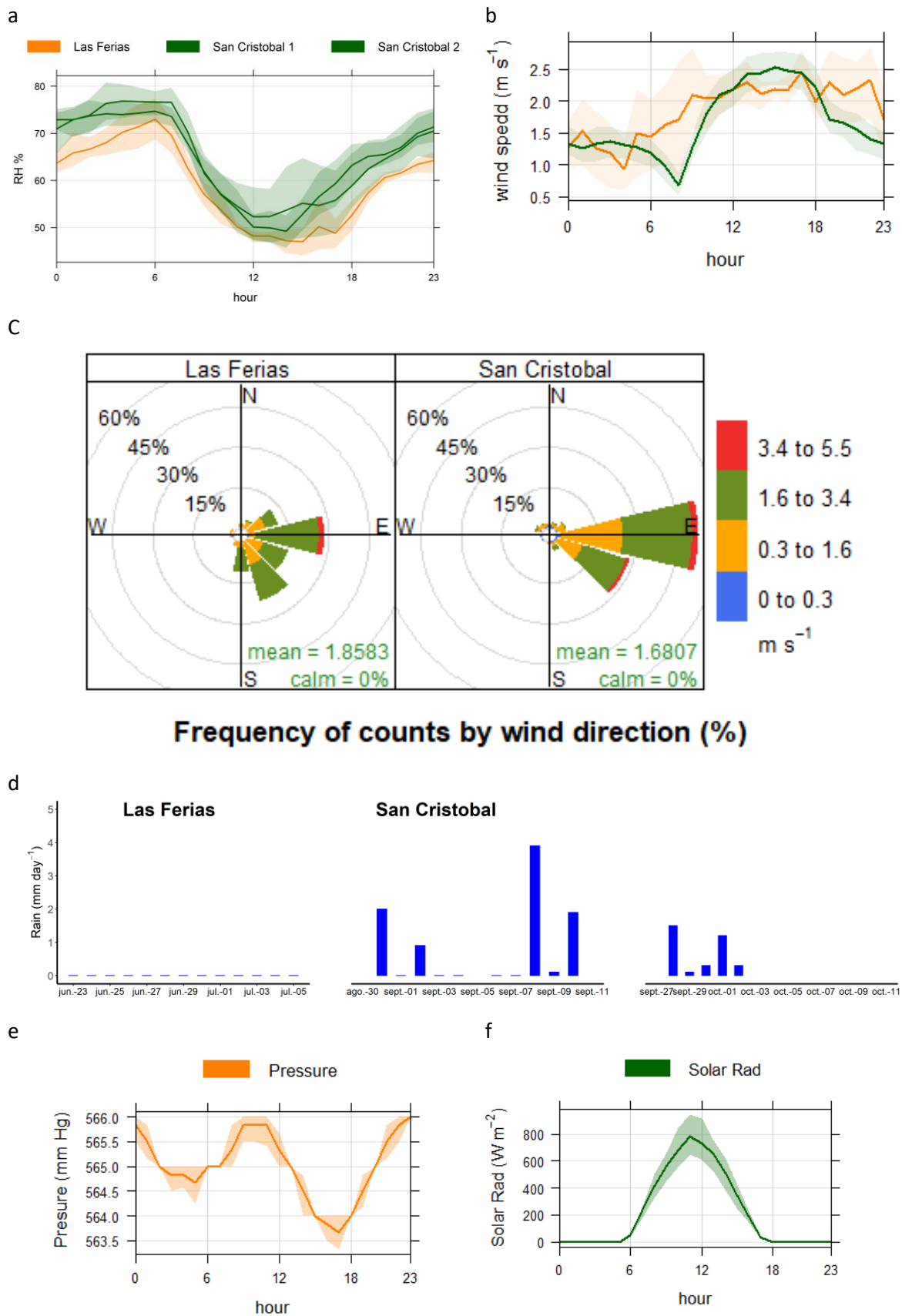
Figure S 2-3. Meteorological conditions registered by the RMCAB in Las Ferias and San Cristobal sites, during the period of the number particles measurements in each site.
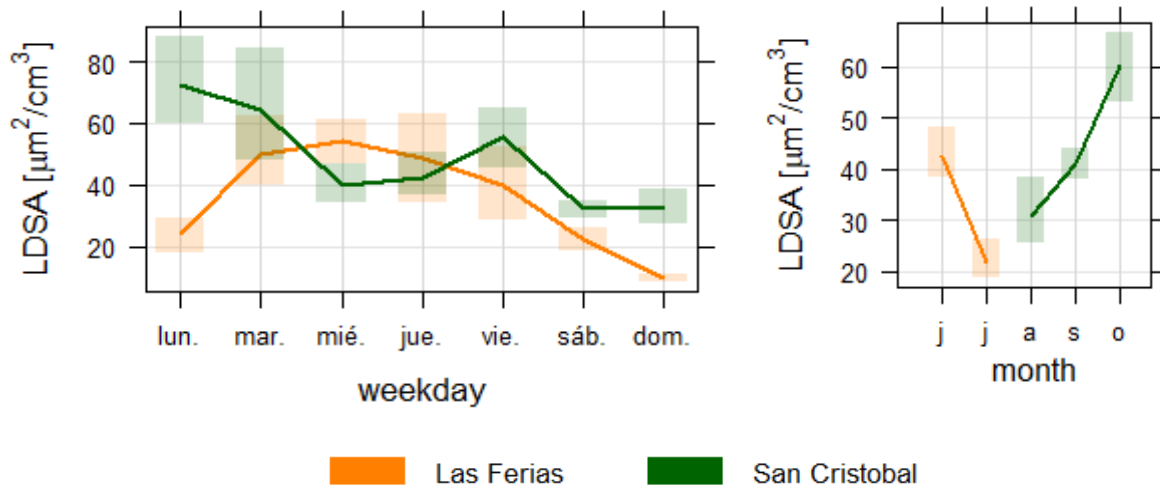
Figure S 2-4. Weekly and monthly variation of LDSA observed in Las Ferias and San Cristobal sites.

3. Comparison of Ambient Particle Mass Size Distribution and Size-Segregated Colombian Urban Areas

3.1.   Introduction

Premature mortality has been related to a variety of factors, including prolonged exposure to air pollutants like ozone and fine particulate matter ($PM_{2.5}$, particles having an aerodynamic diameter smaller than 2.5 μm), in the assessments of the global burden of disease. Ambient $PM_{2.5}$ pollution is responsible for around 3.3 million premature deaths (1.61 - 4.81 million) each year worldwide (World Health Organization, 2019; World Health Organization, 2013; Morawska et al., 2004). Living in areas with polluted air raises the risk of cardiovascular and respiratory system dysfunction, which decreases a person's quality of life. Exposure to air pollutants, even at low concentrations, is linked to respiratory symptoms like airway irritation, coughing, and difficulty breathing as well as non-fatal heart attacks, irregular heartbeats, asthma, decreased lung function, and death in people with heart and lung diseases (HEI, 2013).

Particulate matter (PM) is emitted by a wide range of sources including motor vehicles, industrial activities, dust resuspension, construction, biomass burning, volcano emissions, soil erosion, vegetation, and the oceans, among others. PM can be classified by its size; the aerodynamic diameter being used to describe the aerosol penetrating ability into the respiratory system. Most environmental agencies around the world have regulatory frameworks based on two size categories, namely PM_{10} and $PM_{2.5}$. PM_{10} corresponds to particles with aerodynamic diameters smaller than 10 μm, whereas $PM_{2.5}$ refer to particles smaller than 2.5 μm (fine particles). Particles with sizes between 2.5 and 10 μm ($PM_{10} - PM_{2.5}$) are described as coarse particles. Fine particles are distributed in two size groups: accumulation-mode particles (between 0.1 and 1 μm), and ultrafine particles (UFPs, smaller than 0.1 μm.

The penetration, deposition, and impacts of ambient PM depend on the anatomy of the respiratory tract, the airflow patterns in the lungs, and PM characteristics such as size and chemical composition (Löndahl et al., 2006). The smallest particles will penetrate and deposit on deeper parts of respiratory tract, at an increasing rate (Kim et al., 2015). In nasal breathing,

the cilia, and the mucus act as a filter of particles that exceed 10 μm. Particles between 5 to 10 μm are most likely to be deposited in the tracheobronchial tree, while those between 1 and 5 μm are deposited in the bronchioles. PM_1 has a similar behavior to that of gas molecules and penetrate the alveoli, where gaseous exchange occurs. UFPs can have a larger potential for lung deposition and escape into the blood stream to migrate to the cell tissue and through the circulatory system. They can also arrive to the brain, via the olfactory nerve (Kim et al., 2015). Figure 3-1 outlined the size of the inhale particles retained in each part of the human respiratory tract.
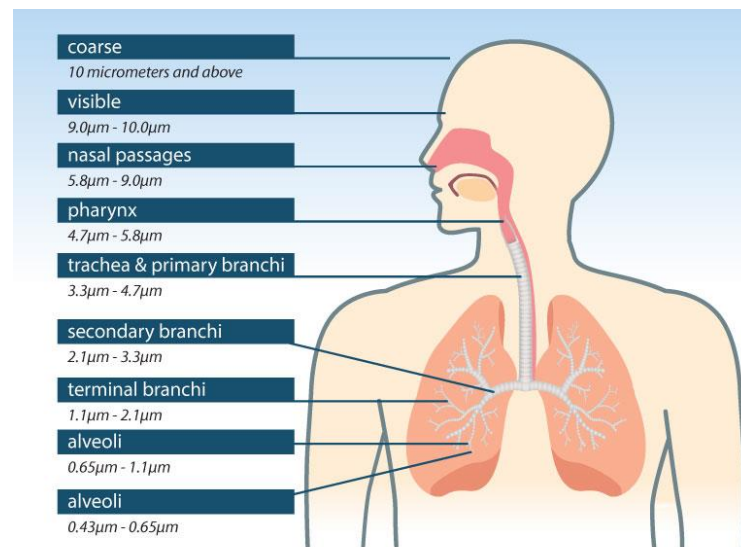
Figure 3-1. Deposition potential for particles of varying sizes by parts of the human respiratory system in accordance with stages of the Andersen Cascade Impactor (Source: https://andersencascading.com/about-andersen-cascade-impactor/)

The chemical composition of particles varies with their size. Overall, urban aerosols are constituted mainly by a carbonaceous fraction (organic material (OM) and elemental carbon (EC)), an ionic fraction (sulfate (SO_4^{-2}), nitrate (NO_3^-), and ammonium (NH_4^+) with a smaller fraction of other inorganic ions (Ca^{+2}, Cl^-, K^+)), and trace elements (Fe, Zn, Pb, Al, Si, Ca and Mg) (Seinfeld and Pandis, 2006). Studies by Li et al. (2012) and Tian, Pan, & Wang (2016) showed that EC concentrations increase as particle size decrease, and the OC/EC ratio, frequently used to determinate the sources of carbonaceous material, can be between 3.0 and 12.2. Saarikoski, Timonen, Saarnio, & Aurela (2008) reported an OC/EC ratio of 0.71 for traffic emissions, 3.3 for

secondary organic carbon, 6.6 for biomass burning and 12 for long-range transport. The ionic fraction dominated the chemical composition of the fine mode, as shown by Li et al. (2012) and Tian et al. (2016). This fraction decreased as particle size increased, whereas crustal material, essentially defined by trace elements, exhibited the opposite trend (Tian et al., 2016).

There are few studies addressing mass size distribution and its chemical composition in Latin America and the Caribbean. Most related studies have focused on PM_{10} or $PM_{2.5}$ bulk chemical composition in megacities. Such is the case of Bogota, the largest city in Northern South America, focusing on a bulk of PM_{10} (Universidad de los Andes; Alcaldia de Bogota, 2009; Vargas, Rojas, Pachon, & Russell 2012; Ramírez et al., 2018). There are also a few studies on $PM_{2.5}$ (Universidad de los Andes; Alcaldia de Bogota, 2009) in areas categorized as residential, industrial and high vehicular traffic zone. These studies revealed that carbonaceous fraction was the main constituent of PM_{10} (~51% for Ramírez et al. (2018) and ~55% for Vargas et al. (2012). The OC concentration was higher than EC and their ratio (OC/EC = 2 - 3) indicated the formation of Secondary Organic Carbon (SOC), suggesting that all carbonaceous species were not emitted by a common source (Ramírez et al., 2018). To date, the information about carbonaceous fraction for $PM_{2.5}$ is not available. For Universidad de los Andes and the Alcaldia de Bogota (2009), the only study that presents the chemical composition of ions and metals in PM_{10} and $PM_{2.5}$ simultaneously found that the ionic fraction contributed between 4.5 to 9% for PM_{10} and 4 to 13.5% for $PM_{2.5}$. The most abundant ions were SO_4^{-2}, NO_3^- and Cl^- for both fractions.

Reducing PM_{10} and $PM_{2.5}$ concentrations has been the main goal of Colombian environmental agencies for more than 2 decades. The most recent emission inventories in the main cities and in the country as a whole report that dust resuspension and motor vehicles are the main emitters of PM_{10} and $PM_{2.5}$. However, the contribution of different source types to particle toxicity, which depends on PM composition and size distribution, is still unclear. Size-dependent toxicity of ambient PM is also uncertain. The aim of this chapter is to address this uncertainty by analyzing the mass size distribution and size-segregated chemical composition of two Colombian sites with different ambient environments. The first site is Bogota, a densely populated city, mostly affected by traffic pollution. The second one is Palmira, a suburban area in the Cauca River Valley, southwest of the country, heavily influenced by several forms of air pollution sources, including agroindustry emissions and motor vehicles. This chapter shows the mass concentration that penetrates different parts of the human respiratory system based on the particle aerodynamic size, as well as the main chemical components that can penetrate

some respiratory organs and be transported by the bloodstream to other body organs. The outcomes of this study will contribute to understanding the effects of long-term exposure to aerosols on human health at both locations, inferring the major sources of aerosol emissions, and establishing effective methods to lessen the impact on population.

3.2.   Experimental

3.2.1. Sampling sites

Size segregated sampling was performed in two places of Colombia, form 14 March to 6 June and 4 October to 6 November 2018, at the urban area of Bogotá D.C; and from 14 August to 16 September 2018 in the Suburban area of Palmira, 27 km northeast from the city of Cali.

Bogotá D.C. is a Tropical Andes megacity with more than 8 million inhabitants (DANE, 2018) and round 2.4 million vehicles (Secretaria Distrital de Ambiente de Bogotá, 2020). The primary sources of air pollutants generated in Bogotá are emitted directly by the combustion processes of fossil or not fossil fuels, also by the soil and vegetation erosion that disperse particles by the wind into the air masses and the leaks or irregular releases of gases or vapors of chemical compounds stored as part of the industrial processes (Secretaria Distrital de Ambiente de Bogotá, 2020). The resuspension of pavements and no pavements highways was the main source of $PM_{2.5}$ (56%), joint to freight vehicles (7%), campers and trucks (3%) and automobiles (3%) and the industry sector with the use of coal in the brinks and pottery factories (5%) for a total 9501 ton of $PM_{2.5}$ reported in the emissions inventory of 2018. There are seasonal peaks of PM_{10} and $PM_{2.5}$ concentrations caused by transboundary pollution and local meteorological conditions (Mendez-Espinosa, Belalcazar, & Betancourt, 2019). Higher concentrations of PM have been typically observed at the southwest of the city, with maximum daily concentrations of 66 $\mu g/m^3$ for PM_{10} and 28 $\mu g/m^3$ for $PM_{2.5}$ in 2017 (Secretaría Distrital de Ambiente, 2018).

Palmira is in the Cauca River Valley (CRV) Region, an inter-Andean valley in southwestern Colombia. Palmira is located at 27 km northeast of Cali and 22 km southeast of Yumbo. The Pacific Ocean coastline stretches at 120 km across the western Cordillera, where one of the busiest international trade seaports in Colombia operates (Larada, 2017). Palmira is 313000 inhabitants. Most of the freight is transported by diesel-powered trucks (Mateus-Fontecha et

al., 2022).. Road traffic is also substantial within the CRV, together with Bogotá, and along the Pan-American highway that connects Colombia with other South American countries (Orozco et al., 2012).

The sampling site in Bogotá D.C. was located at Fontibon District Fire Station (4º40'12.36" N, 74º8'29.58" W; 2591 m.a.s.l), in the west of Bogota (Figure 3-2a). This District has an extension of 33 km^2 and is characterized by the high influence of both industrial and vehicular sources of pollutants. It is one the most important industrial and commercial centers of the city, especially due to the manufacturing industry and in terms of vehicular influence, this zone includes one of the major transportation nuclei of the city. This district also contains the largest international airport of Colombia: El Dorado and the sampling site was 2.72 km distance from the airport. Samples were collected at approximately 9 m above the ground, on the roof of a building.
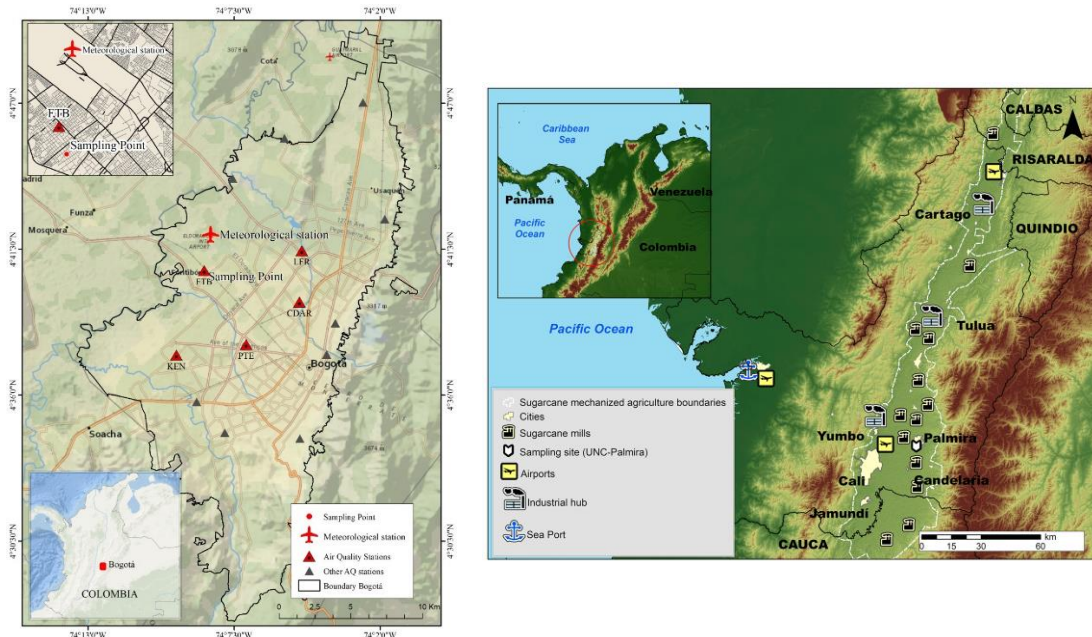
Figure 3-2. Location of the sampling sites in Bogotá D.C. and in Palmira, Colombia.

3.2.2. Meteorology

The local meteorology parameters monitored were ambient temperature, pressure, relative humidity (RH), solar radiation, precipitation, and wind speed (WS) and direction (WD). In Bogotá

was used the data from the airport weather station, reported to 10 m above ground published by the IDEAM with the ID: 21205791 (IDEAM, 2019).The weather station is located to 2.7 km of the sampling site. In Bogotá was used a Davis Vantage Pro weather station collocated with the instruments to collect the samples. The data were collected with a 5 min time resolution during all sampling periods.

3.2.3.Sampling

A non-viable Andersen Cascade Impactor (Tisch Environmental, Cleves, OH, USA) was used to collect particulate matter in nine size fractions, according to the particles' aerodynamic diameter. The inertial impaction cut-off diameters are 9.0, 5.8, 4.7, 3.3, 2.1, 1.1, 0.65, and 0.43 μm. The finest particles (D_p < 0.43 μm) pass through the previous 8 impaction stages and are filtered. The sampled air is drawn through the Cascade Impactor using a vacuum pump with a flow rate of 28 liters per minute – LPM.

Quartz filters (81-mm diameter, TE-QMA-47, Whatman®) were used as collection substrates, with two kinds of filters, one with open centers for stages 0 and 1, and another with solid centers for stages 2 to 7 and the back filter. Filters were pre-baked at 600°C for 8 hours before sampling to eliminate hydrocarbons. They were conditioned at constant humidity and temperature (36%, 24°C) for 24 hours before weighing with a microbalance (Sartorius R200D) with a maximum readability of 0.01 mg, before and after sampling. Filters were transported in sealed Petri dishes to the sampling site and subsequently to the lab.

Nineteen sets of size-segregated ambient particulate matter were collected over two periods: March – June 2018 and October to November 2018. Sampling time for each set was 72 or 96 hours on working days, to ensure enough mass over each collection substrate. The 96-hour sampling time was used for periods with rainy days. Sampling started at 00:00 of the first day and ended at 23:59 on the third or fourth day, accordingly.

3.2.4.Mass size distribution

Mass size distributions were derived by offline analysis of the particle mass concentrations of each sample set. Mass concentration of each quartz filter was calculated from the difference between pre- and post-weighing, the volume flow rate and the total sampling time. Mass

concentrations were then divided into the logarithmic difference of the upper and lower effective cut-off diameters (ECD) of the respective stage to plot the semi-lognormal mass distribution as ECD vs $\left[\frac{dC}{dLogD_p}\right]$. To include the backup and top filters in the size distributions, an artificial lower and upper cut size of 0.1 and 30 μm was used. These sizes were just defined as operational procedure without influence of the discussion of mass size concentrations. The same upper artificial size cut was used for Hitzenberger and Tohno, (2001).

3.2.5. Chemical Analysis

Nineteen sets on Andersen Impactor samplers were used to perform OC/EC and water-soluble ions analysis at the chemistry lab of the Leibniz Institute for Tropospheric Research, TROPOS. A fraction of the filter was used to determine organic and elemental carbon (OC/EC) following the analytical procedure described by Van Pinxteren et al. (2009), which applies the thermogravimetric, or VDI, analysis method (VDI 2465 Blatt 2:2016-11) with a C-mat 5500 carbon analyser (Strohlein, Germany). In the first heating step, OC is volatilized up to 650ºC for 8 minutes under a nitrogen atmosphere and converted to CO_2 with a CuO catalyst at 850ºC. In the second heating step, EC fractions are burnt to CO_2 on oxygen atmosphere at 650ºC for 8 minutes. The CO_2 formed is determined with a NDIR detector. The VDI method may underestimate the fraction of OC and overestimate the fraction of EC due to the charring of a fraction of OC to EC during the first step (Neusüss et al., 2000).

Water-soluble ions were determined from another filter fraction (approximately 30% of the filter), that was cut into small pieces, and extracted in 4 mL of deionized water (18 MΩ) in a shaker for 120 min at 400 rpm in an ultrasonic bath. The extract was filtered through 0.45 μm-pore syringe filters, and then analysed using an ion chromatograph (IC690, Metrohm AG, Herisau, CH) to quantify the content of calcium (Ca^{+2}), magnesium (Mg^{+2}), ammonium (NH_4^+), sodium (Na^+), potassium (K^+), sulphate (SO_4^{-2}), nitrate (NO_3^-), Chloride (Cl^-), oxalate ($C_2O_4^{-2}$), methanesulfonate ($CH_3O_3S^-$), phosphate (PO_4^{-3}), nitrite (NO_2^-), bromide (Br^-), fluoride (F^-), and formate (CHO_2^-).

3.3.   Results and discussion

3.3.1.Meteorology and transport patterns

Figure 3-3 depicts the weather conditions observed during the sampling dates in Bogotá D.C., including ambient temperature, solar radiation, relative humidity, daily cumulative precipitation, wind speed, and direction. Ambient temperature was 14.5ºC ± 3.2 C, with no notable time fluctuation from March to November 2018. The maximum temperature was observed at the middle day (18.7 ºC) and the minimum happens to 6:00 H (10.8ºC) (See Figure S3-1). Solar radiation varied more from month to month, with average daylight solar radiation income being higher in March (327 W), October (372 W), and November (398 W) than in April and June (220 W) (See Figure S3-1b). Cloudiness and wet patterns typical of tropical places over the Andes Mountain range determine solar radiation income. The relative humidity was 76% ± 14.5%, with higher values in the rainy months of April, May, October, and November, when RH exceeded 80% and lower values in March, when RH was proxy to 75%. The behaviour of temperature, solar radiation and relative humidity between March and November of 2018 are show in the panel Figure 3-3a. A major part of samples, twelve in total, were collected during the rainy season between April and May and most of October to November. Four sets were collected during the dry season in March plus one set in May, June and November, respectively. Figure 3-3b shows the daily precipitation as blue lines and the sampling period duration of each set of samples collected in the Andersen cascade impactor by yellow dark bars. The average wind speed over the sampling period was 2.12 ±1.1 m/s, with a slightly lower speed in April (~1.8 m/s) than in March (~2.3 m/s), whereas May, October, and November were within the typical range. Winds from the northeast had a considerable impact on this site, primarily in March and May, with a minor or inconsequential influence from winds from the southeast. Winds from the west were consistently detected throughout the months when samples were collected.

The meteorological conditions in Palmira were stable during the sampling period. The ambient temperature was on average 24.2ºC ± 1.1 ºC and the maximum temperature was observed at 15:00 H of 28ºC and the minimum at 06:00 H of 20ºC (Figure S3-2a). The average daily solar radiation income was 353 W/m^2, with a maximum at middle day of 700 W/m^2. The average relative humidity was 71.6% ± 4.5%. No rain events were registered during the period time sampling, therefore the chemical composition observed was representative only of the dry period in CRV. The average wind speed on the sampling point was 2.3 m/s. The wind often blew

from the northwest and from the west with the highest velocities blowing winds, which suggest an important influence of mill sugar factories emissions, events of open-field sugarcane burnings and the industrial emissions from Yumbo (Fundación Empresarial para el Desarrollo de Yumbo, 2015).
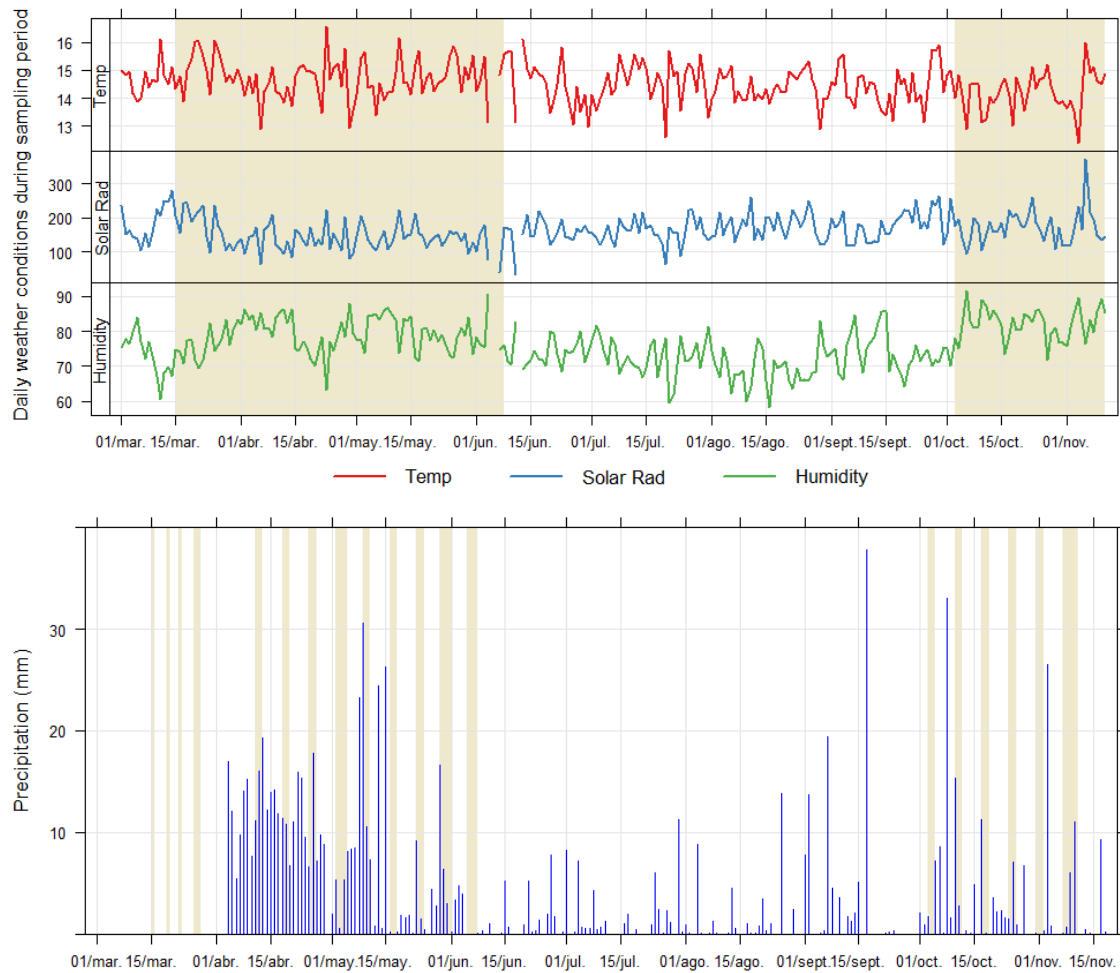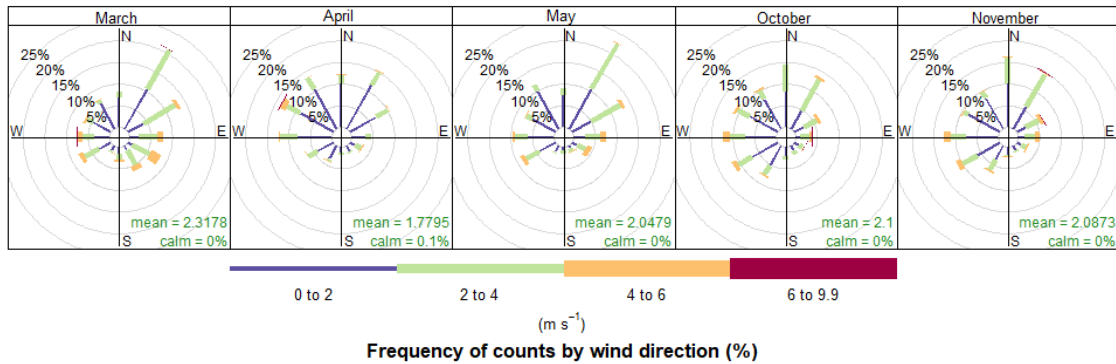
Figure 3-3. Meteorological conditions registered in El Dorado Airport station (ID: 21205791). a) Time series of daily average of ambient temperature, solar radiation and relative humidity, b) daily precipitation accumulated represented in blue lines and period time of sampling of each set of samples collected in Andersen Impactor cascade and c) wind rose observed month to month between March to November in 2018.
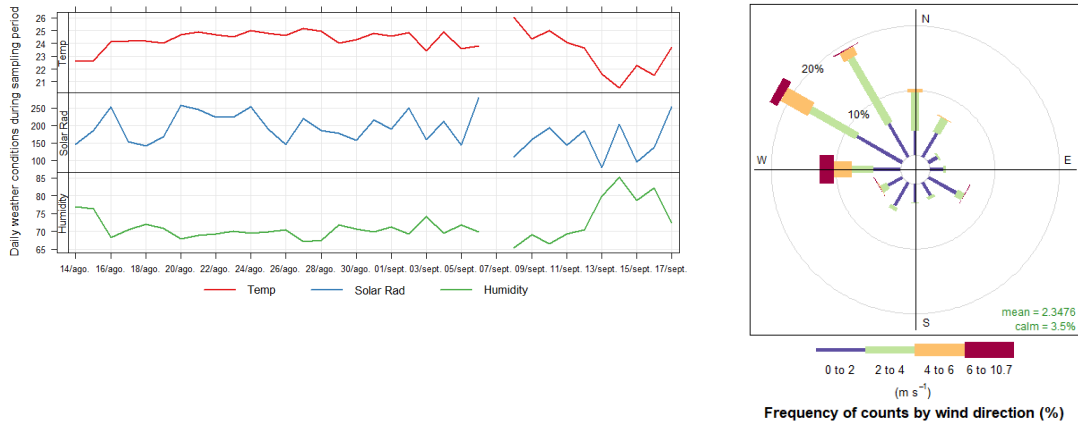
Figure 3-4. Meteorological conditions registered in Palmira with an own weather station colocalized in the sampling. a) Time series of daily average of ambient temperature, solar radiation and relative humidity, b) wind rose observed during August and September 2018.

3.3.2. Coarse and fine mass concentrations: PM_9, $PM_{2.1}$, $PM_{1.1}$ and $PM_{0.43}$

PM_9, $PM_{2.1}$, $PM_{1.1}$ and $PM_{0.43}$ mean concentrations significantly differed between Bogota and Palmira (p value < 0.1), such that each size fraction in Palmira being lower than in Bogota. PM_9 mass concentrations in Bogota and Palmira were 59.8 $\mu g/m^3$ and 46.3 $\mu g/m^3$, respectively. $PM_{2.1}$ mass concentrations were 28.4 $\mu g/m^3$ and 19.2 $\mu g/m^3$, respectively; $PM_{1.1}$ mass concentrations were 20.8 $\mu g/m^3$ and 13.8 $\mu g/m^3$, respectively; and $PM_{0.43}$ mass concentrations were, 6.8 $\mu g/m^3$ and 4.2 $\mu g/m^3$, respectively, as show Figure 3-5b.

PM_9 and $PM_{2.1}$ concentrations found in this study were compared to the PM_{10} and $PM_{2.5}$ concentrations reported by monitoring conducted for the local environmental agencies in each region. In the case of Bogota, the local air quality station[1] closest to the site used in this study is 1 km away, where the annual mean for PM_{10} and $PM_{2.5}$ was 37.1 $\mu g/m^3$ and 18.4 $\mu g/m^3$, respectively in 2019 (Secretaría Distrital de Ambiente, 2020). Hence, the PM_9 and $PM_{2.1}$ concentrations estimated from the sum of the mass accumulated in many stages of the Andersen Impactor were higher than reported by the closest local air quality station. It could be explained by the proximity between the sampling point to the high-flow roads, which were less in this study than for the local air quality station. In the case of Palmira, PM_9 was compared with the PM_{10} concentration of a rural station located 12 km from our sampling point, which reported a 36 $\mu g/m^3$ in 2019 (Corporación Autonoma Regional del Valle del Cauca - C.V.C., 2019). $PM_{2.1}$ concentrations in Palmira could not be compared with data reported by the local environmental authorities because of the lack of stations with simultaneous monitoring of $PM_{2.5}$. Instead, we estimated gravimetric bulk concentrations of PM_{10} and $PM_{2.5}$ synchronized with the Andersen Impactor, resulting in 34.9 $\mu g/m^3$ and 14.4 $\mu g/m^3$ respectively. As a result, the evidence reveals that PM_9 and $PM_{2.1}$ concentrations estimated from the accumulation of Andersen Impactor stages were higher than the measurements of PM_{10} and $PM_{2.5}$ bulk concentrations.

---

[1] This station was installed in October 2018, therefore this concentration corresponding to annual mean concentration to 2019.

The mass concentration of each size fraction in Bogota fluctuated throughout time. PM_9, $PM_{2.1}$, $PM_{1.1}$ and $PM_{0.43}$ had the highest concentration in March, followed by the lowest concentrations in April and May. Figure 3-5a shows that the samples taken in October and November were more consistent, with values similar to the mean campaign concentrations. In Palmira, all PM concentrations remained steady around mean values. Compared to other particle sizes, smaller particles, $PM_{0.43}$, showed more time variability (See Figure S3-3), however, it does not seem associated with the rain pattern (p value: 0.12). Concerning the variability of PM_9, $PM_{2.1}$ and $PM_{1.1}$ in Bogota, larger particles display a high vulnerability to the rain levels, evidenced by the ANOVA test between rain level and PM concentrations showing p values of 0.02, 0.02 and 0.009, respectively. On the other hand, no noticeable meteorological changes were recorded in Palmira during the sampling period, and the PM concentration variance was not higher than in Bogota.
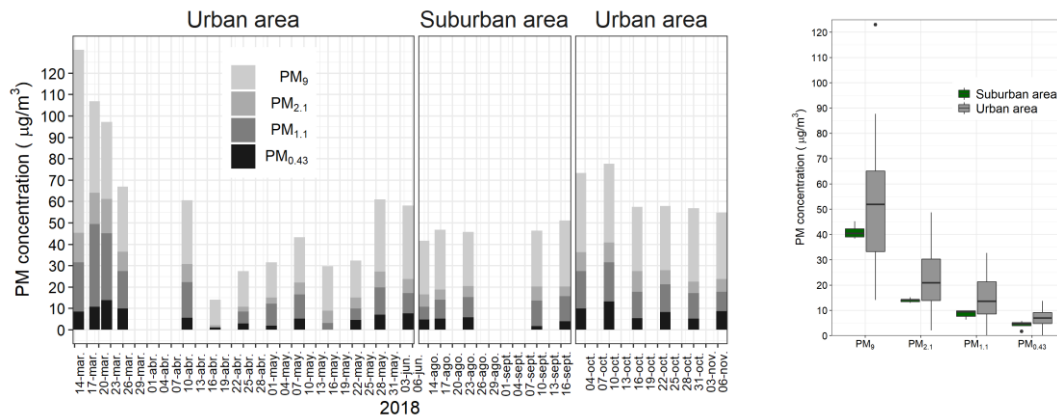
Figure 3-5. PM_9, $PM_{2.1}$, $PM_{1.1}$ and $PM_{0.43}$ concentrations in Bogota (urban area) and Palmira (suburban area): a) Time series of accumulated concentrations and b) Boxplot of mass fractions.

In Bogota, the fractions of $PM_{2.1}$, $PM_{1.1}$ and $PM_{0.43}$ relative to PM_9 were 47.1% ± 7.3%, 35.4% ± 6.1% and 11.8% ± 3.1%, respectively. $PM_{0.43}$ displayed the greatest range, with greater levels in

some months (October, November, and March) and lower values in others (April) (Figure S3-3). These fractions were reliable although the precipitation events (p value > 0.5), therefore they can be obtained from the dynamics of local emissions rather than the rain pattern. In 2019, the RMCAB *Fontibon* air quality station, which is just one kilometer from the study sampling site, recorded that 52.6% ± 10.7% of PM_{10} is $PM_{2.5}$.

In Palmira, these fractions these fractions remained stable at roughly 41.5 ± 2.3%, 29.8 ± 2.7% and 9.2 ± 3.6% respectively for $PM_{2.1}$, $PM_{1.1}$ and $PM_{0.43}$. The air quality station of RMCAB used as reference to validate the mass concentration size segregated have showed that $PM_{2.5}$ is 56.9 ± 12.4%[2] of PM_{10}, despite large variability of this percentage, it is comparable with fraction of $PM_{2.1}$ relative to PM_9 observed in this study. At the day of this report did not have been published PM_{10} and $PM_{2.5}$ concentrations of close to suburban area that can be used as reference to validate the fraction of $PM_{2.1}$ relative to PM_9. These results of the average fraction of $PM_{2.1}$ and $PM_{1.1}$ relative to PM_9 were lower than those found in China by Li et al., (2012) and (Wang et al., 2015) which were in ranging of 55% to 67%.
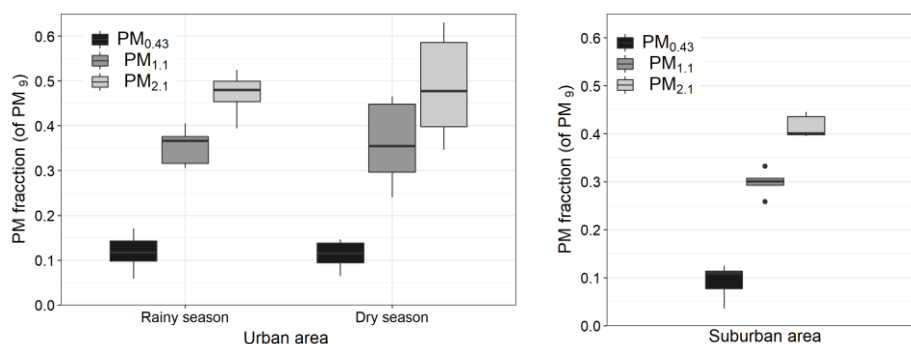
Figure 3-6. Boxplot of $PM_{0.43}$, $PM_{1.1}$ and $PM_{2.1}$ fractions contained in PM_9 in Bogota and Palmira. Precipitation events were registered during sample collection in Bogota. Therefore, fractions were categorized by rainy and dry season. Samples collected during the dry season (n= 6), the rainy season (n = 11), and in Palmira (n = 5) were collected.

In Colombia, as most of other countries, air quality standards do not include PM_1 monitoring. Therefore, information on this fraction is non-existent. In the present study, $PM_{1.1}$ concentration

---

[2] Daily mean between October 2018 – December 2021

was 29.4 µg/m^3 and 17.1µg/m^3 for dry and wet patterns, respectively. The maximum concentrations of PM$_{1.1}$ reach was 49.3 µg/m^3 in dry pattern. The PM$_{1.1}$ concentration observed in Bogotá are lower than reported in Beijing (78.2 µg/m^3) by Zhang et al. (2018) and other Asiatic urban areas (Majewski et al., 2018) and it had similar magnitude order to PM$_1$ observed in European studies in Milan (~30 µg/m^3)(Vecchi et al., 2018), Barcelona (18 – 21 µg/m^3) (N. Perez et al., 2008), Istanbul (7 – 30 µg/m^3) (Onat et al., 2013), Warsaw (14 µg/m^3) among other (Majewski et al., 2018). In Latin America, the studies that explore the PM$_1$ concentrations and its chemical composition are yet very scarce, and just concentrations for Ciudad de Mexico (27.8 µg/m^3) were found (Guerrero et al., 2017). Most of the studies that include the PM$_1$ concentrations have been conducted in Europe and China, where PM$_1$ concentration is affected by seasonal variation, showing higher concentrations in winter, associated with biomass burning to heating, while in this study show high concentrations in dry season. Figure 3-5 shows the time series of PM$_9$, PM$_{2.1}$ and PM$_{1.1}$ concentration observed in the study area. The average concentrations of smaller particles than 0.43 µm was 9.18 µg/m^3 and 5.23 µg/m^3 for dry and wet patters, respectively.

3.3.3. Mass size distribution

Figure 3-6 illustrates the bimodal distribution of mass concentrations in both Bogota and Palmira. The finest mode in Bogota was 0.43–1.1 µm and in Palmira was 0.43–0.65 µm, whereas the coarse mode in both sites was 4.7–5.8 µm. The mass fraction collected at each stage was similar, accounting for 3.0%, 10.0%, 9.6%, 7.5%, 10.2%, 17.0%, 23.4%, 14.9%, and 7.2 % of total mass for particles smaller than 0.43, 0.65, 1.1, 2.1, 3.3, 4.7, 5.8, 9, and 30 µm, respectively. Only the proportion of particles collected with a diameter of 0.65–1.1 µm differed substantially between Bogota and Palmira (p value: 0.04), indicating that in Bogota had a greater percentage than Palmira, with 10 and 7 % for each one. The variability of fraction mass distribution is nearly double in Bogota compared to Palmira, except for particles with diameters between 4.7 and 5.8 µm, in which there is a larger variability in Palmira than in Bogota. The overall mass concentration acquired across the nine stages of the Andersen impactor had no effect on the mass fraction recovery in each stage, as evidence in Figure S3-4.
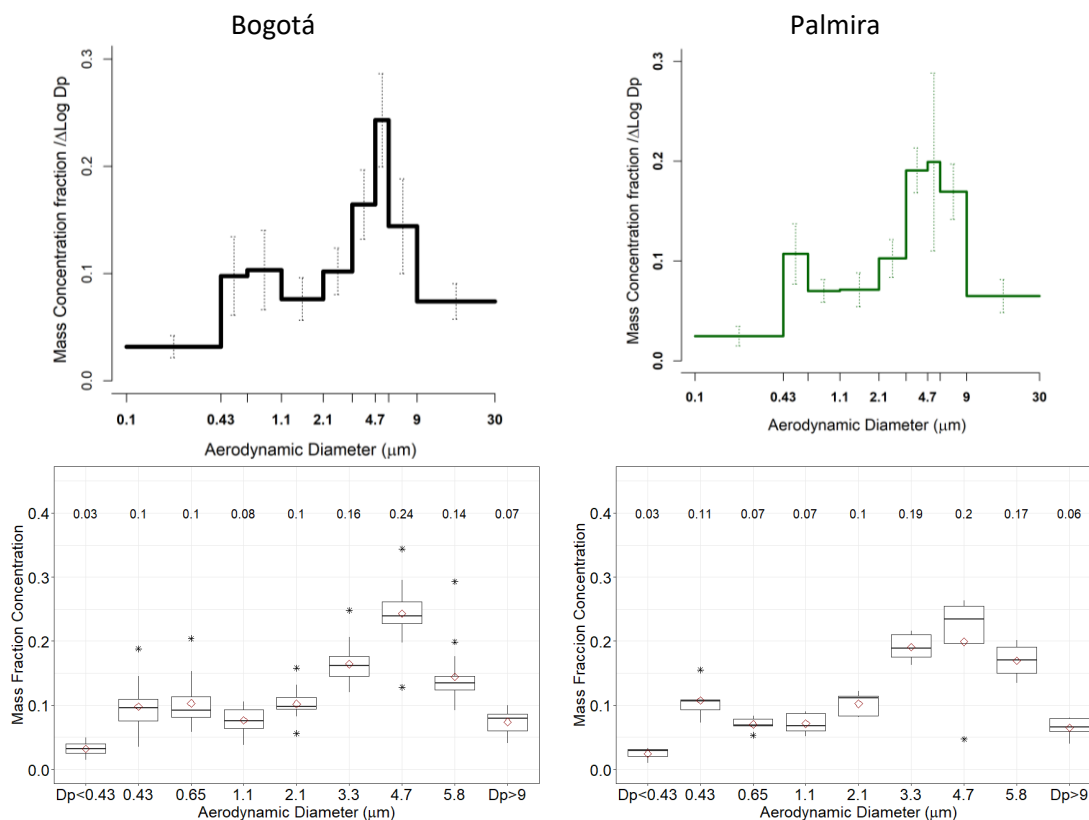
Figure 3-7. Mass-based particle size distribution and boxplots of mass fractions observed in Bogota (Urban area) and Palmira (Suburban area).

3.3.4. Chemical composition in fine and coarse particles

Carbonaceous species (OC and EC) were the most prevalent in particles sizes smaller than 0.43 µm. In the particles PM_1, $PM_{2.1}$ and PM_9, EC was narrowly surpassed by SO_4^{2-} in Palmira. Figure 3-8A displays the OC and EC concentrations for each size of particle. The concentrations of OC and EC are higher for smaller particles (p value = 0.02). In Bogota, OC stand for 22.8±5.7%, 27.3±8.5%, 27.9±9.2%, 33.9±13.0% of PM_9, $PM_{2.1}$, $PM_{1.1}$ and $PM_{0.43}$, while EC accounted for 9.5±3.6%, 19.5±7.7%, 22.9±9.3%, 36.4±15.1%. In comparison, in Palmira PM_9, $PM_{2.1}$, $PM_{1.1}$ and $PM_{0.43}$ had 29.2±7.9%, 39.0±6.1%, 41.7±9.6%, 61.2±41.9% of OC and 3.4±0.4%, 6.1±0.9, 7.7±1.3%, 15.5±10.8% of EC, respectively. The variance in OC and EC contained in the PM concentrations for each size category is not clearly explained by the rainy pattern (p value = 0.2).

Figure 3-8B displays the Total Carbon (TC) concentration for each type of area, which is determined as the sum of the EC and OC concentrations. For each size category, such as PM_9, $PM_{2.1}$, $PM_{1.1}$ and $PM_{0.43}$, TC represents 38.6%±9.6; 46.8%±15.0; 50.8%±17.5% and 70.3%±25.7% in Bogota and 38.8%±7.9%; 45.2%±59%; 49.4%±9.9% and 76.7%±52.7% in Palmira.

The (OC/EC) ratio is a method for identifying primary and secondary OC. This ratio shows lower values in larger cities than in suburban areas, which typically have lower pollution levels. Urban locations are frequently negatively impacted by local emissions combined with long-distance regional transport, whereas suburban areas consistently receive regional contributions of aged aerosols with higher OC secondary content, raising the OC/EC ratios. In this study, the (OC/EC) ratio between urban and suburban areas differs (p value: 0.001). For example, all particle size categories in Palmira had (OC/EC) ratios that were twice as high as those in Bogota (see Figure 3-8C), highlighting the impact of incomplete combustion as a source of aerosols and the nature of fresh emission in Bogota.

The variability of (OC/EC) ratio from fossil fuel combustion in road transport depend on multiple factors like the type of fuel, the driving condition, and the emissions control technology. The photochemical processes in the ambient air result in (OC/EC) ratios between 1 to 2 in urban areas affected by traffic, while this ratio is 1-4 for $PM_{2.5}$, and 5 for PM_{10} in rural areas. In this study, smaller particles had a lower (OC/EC) value in agreement with (Pio et al., 2011). In Bogota, OC/EC ratios in $PM_{0.43}$, $PM_{1.1}$, $PM_{2.1}$, and PM_9 were 1.2±0.9; 1.9±1.2; 2.2±1.2 and 5.6±2.2, respectively, while they were 4.0±0.6; 6.4±2.2; 8.7±2.6 and 10.7±3.1 in Palmira. Pio et al., (2011) showed through direct dynamometric measurements that diesel vehicles had higher EC emissions than gasoline vehicles, with OC/EC ratios lower than 1 for diesel vehicles, and higher than 1 for gasoline vehicles. $PM_{0.43}$ in Bogota were very close to 1, which suggests a similar contribution of diesel and gasoline vehicle emissions to EC/OC ratios of ambient particles. Saarikoski et al., (2008) provided references for (OC/EC) ratios for various sources reporting values of 3.3 for secondary organic aerosol, 6.6 for biomass burning aerosols, and 12 for long-range transport. Comparing OC/EC average ratios from this study to data from Saarikoski et al., (2008), it can be inferred that $PM_{2.1}$ in urban sites indicates the presence of secondary organic carbonaceous compounds, whereas $PM_{2.1}$ in suburban areas is more closely related to emissions from biomass burning. The impact of aerosol long-range transport can be attributed a source of PM_9 in Palmira.

The results of this study show lower values of the fraction of EC found in $PM_{2.1}$ (22.9±9.3%) in urban areas when compared to the RMCAB reports of eBC and $PM_{2.5}$ at the *Fontibon* station, whose measurements indicate that 40.6±8.1% of $PM_{2.5}$ is composed of soot. EC concentrations (5.7 ± 3.2 µg/m³) found in this study for $PM_{2.1}$ were similar to eBC concentrations measured in $PM_{2.5}$ in *Fontibon* (5.9 ± 2.2 µg/m³). Based on this similarity and using the (OC/EC) ratio resulting to $PM_{2.1}$, a proxy of OC concentrations in $PM_{2.5}$ was estimated. Taking the long-term monitoring of eBC and $PM_{2.5}$ measured by the RMCAB in *Fontibon*, OC was roughly 12.6± 4.6 µg/m³ and Total Carbon was 18.3 ±6.7 µg/m³ for this area of the city.
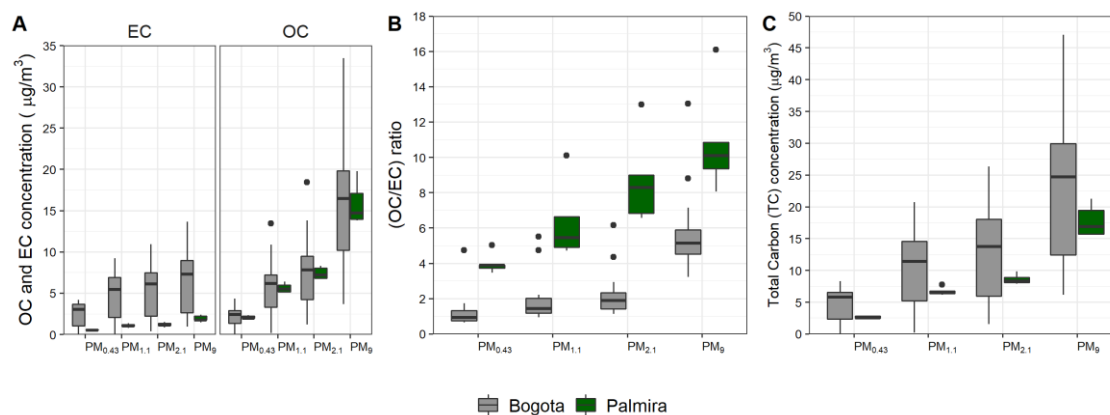
Figure 3-8. Size-segregated boxplots for carbonaceous species in $PM_{0.43}$, $PM_{1.1}$, $PM_{2.1}$, and PM_9 in Bogota and Palmira. A) OC and EC; B) Total carbon (TC); and C) OC/EC ratio.

Water Soluble Ions (WSIs) average concentration in PM_9, $PM_{2.1}$, $PM_{1.1}$ and $PM_{0.43}$ were 7.8±5.0 µg/m³, 4.7±3.7 µg/m³, 3.4±2.8 µg/m³ and 0.8±1 µg/m³. WSIs were 12.5±5.1%, 15.4±7.9%, 14.6±7.5% and 10.7±9.1% of the total PM concentration for corresponding size of particle category, in Bogota. While, in Palmira, the concentration for each size particle category corresponds to 5.9±1.6 µg/m³, 7.3±1.6 µg/m³, 3.0±1.3 µg/m³ and 0.8±0.5 µg/m³, which represent 12.8±3.5%, 19.2±7.1%, 21.9±9.3% and 28.9±35.8% of the total PM concentration. The percentage of WSI contained in the finest particles ($PM_{0.43}$) was higher in Palmira than in Bogota, just the opposite to what was observed for coarse particles.

SO_4^{2-} and NO_3^- were the most abundant ions, which indicates the development of secondary inorganic aerosol (SIA). SO_4^{2-} was the most abundant in Palmira than in Bogota, especially in the $PM_{0.43}$ and $PM_{1.1}$ fractions, in contrast to the observed in coarse particles. In Palmira, SO_4^{2-} played a substantial role in particle composition, notably in smallest fraction ($PM_{0.43}$), where it accounted for $15.7 \pm 18.1\%$ of the overall PM concentration. The fraction of SO_4^{2-} gradually decreases for larger particles, changing from $11.3 \pm 5.1\%$ in $PM_{1.1}$ to 9.7 ± 4.0 in $PM_{2.1}$, and $4.7 \pm 1.7\%$ in PM_9. In Bogota, the fraction of SO_4^{2-} was not negligible and about the same for all sizes of particles. The percentage of SO_4^{2-} was not affected by total PM concentration.

The largest WSI contribution was observed in Palmira's $PM_{0.43}$ particles. Along with SO_4^{2-}; NO_3^- ~NH_4^+>Ca^{2+}>$C_2O_4^{2-}$, accounting for most of 1% of the total PM concentration each one ion. Other ions such, K^+> $CH_3O_3S^-$> Na^+> Cl^- > Mg^{2+} and CHO_2^- were less common and each one contributed between 0.2 and 1% of the total mass concentration. In contrast, the ions Na^+ > PO_4^{3-} > NO^{3-} contributed more than 1% of the total mass concentration in Bogota for particles of the same size, while Ca^{2+}, Cl^-, NH_4^+, $C_2O_4^{2-}$, Mg^{2+}, K^+ and CHO_2^- were the least common ions. While $CH_3O_3S^-$ was a significant component of Palmira's $PM_{0.43}$, it had a less important role in Bogota. In PO_4^{3-} contracting behaviour, which was more prevalent in Bogota than in Palmira. NO_2^-, F^- and Br^- were scarce for all particle sizes in both sites.

Concerning with $CH_3O_3S^-$, this is produced by the aqueous oxidation of dimethyl sulfide (DMS), one of the most prevalent biogenic sulphur compounds in the troposphere, mostly from sea salt (Tang et al., 2019), and also associated with biomass burning (Gondwe, 2004; Meinardi et al., 2003; Sorooshian et al., 2015; Stahl et al., 2020). The nearby of Palmira to the Pacific Ocean and the often of open-field sugarcane burnings could be a reason to explain the higher abundance of $CH_3O_3S^-$ in Palmira's particles than in Bogota.

About $PM_{1.1}$ in Palmira, NH_4^+ was more abundant than NO_3^-. The abundance of Ca^{2+}>$C_2O_4^{2-}$ were at comparable levels in $PM_{0.43}$. PO_4^{3-} had a significant higher proportion in $PM_{1.1}$ (0.7%) than in $PM_{0.43}$ (<0.1%); while Cl^- was more abundant in coarse particles than in $PM_{0.43}$, with an abundance similar (~0.8%) in the larger size particles of $PM_{1.1}$, $PM_{2.1}$ and PM_9. Na^+>K^+>Methansulfonate>Mg^{2+} > CHO_2^- were in the same percentage in $PM_{1.1}$ and $PM_{0.43}$ both. The order of ions abundance in $PM_{2.1}$ in the suburban area were NH_4^+> NO_3^-> Ca^{2+}>$C_2O_4^{2-}$, which were in range of 2.3 – 1%, followed by Cl^-> Na^+ >PO_4^{3-}> K^+ > $CH_3O_3S^-$ > Mg^{2+} and CHO_2^-, in range

of 0.8 – 0.1% of total PM concentration. The prevalence of ions in PM_9 emphasize the importance of $NO_3^- > Ca^{2+}$ with 2 - 1% of the total mass concentration, while NH_4^+ and $C_2O_4^{2-}$ play a smaller role, contributing less than 1%, and being followed by $Na^+ > PO_4^{3-} > Mg^{2+} > K^+ >$ Methanesulfonate > and CHO_2^-.

In Bogota, Na^+, PO_4^{3-}, NO^{3-} and NH_4^+ play a relevant role in particle sizes $PM_{0.43}$, $PM_{1.1}$, $PM_{2.1}$, but not in PM_9, where NH_4^+ was under 1%. Other ions, such as Cl^-, Ca^{2+}, $C_2O_4^{2-}$, Mg^{2+}, K^+ and CHO_2^-, were in range 1 - 0.1% each one, for all size particles.

The abundance of NH_4^+, $C_2O_4^{2-}$ and K^+ were altered by precipitation levels, as shown in Figure S3-5, such that, their concentrations were higher in samples unaffected by precipitation events. $PM_{1.1}$, $PM_{2.1}$ and PM_9 had a significative higher abundance of $C_2O_4^{2-}$ in days without rains (p value < 0.005), while in $PM_{0.43}$ the difference was lower significant (p value < 0.07). $C_2O_4^{2-}$ used to be produced from radicals involved in chemical/photochemical oxidation of volatile organic compounds (VOCs) such as ethene, toluene, isoprene, in PM_1 (Sullivan and Prather, 2007). There was an increase in $C_2O_4^{2-}$ (from 0.4 to 0.7%) in $PM_{1.1}$ in dry days. The organic ions $C_2O_4^{2-}$ together with formate, play a role in solubility, photochemistry and bioavailability of transition metals in aerosols (Deguillaume et al., 2005). Therefore, the increase in $C_2O_4^{2-}$ concentrations favour the solubility and bioavailability of transition metals such as iron (Fe), Copper (Cu) and Manganese (Mg). On the other hand, $PM_{0.43}$ showed a higher increase in the abundance of NH_4^+ and K^+ (p value: 0.01) than larger particles (p value > 0.1), during dry days. The abundance of other chemicals species did not show a change associated to rain patterns.
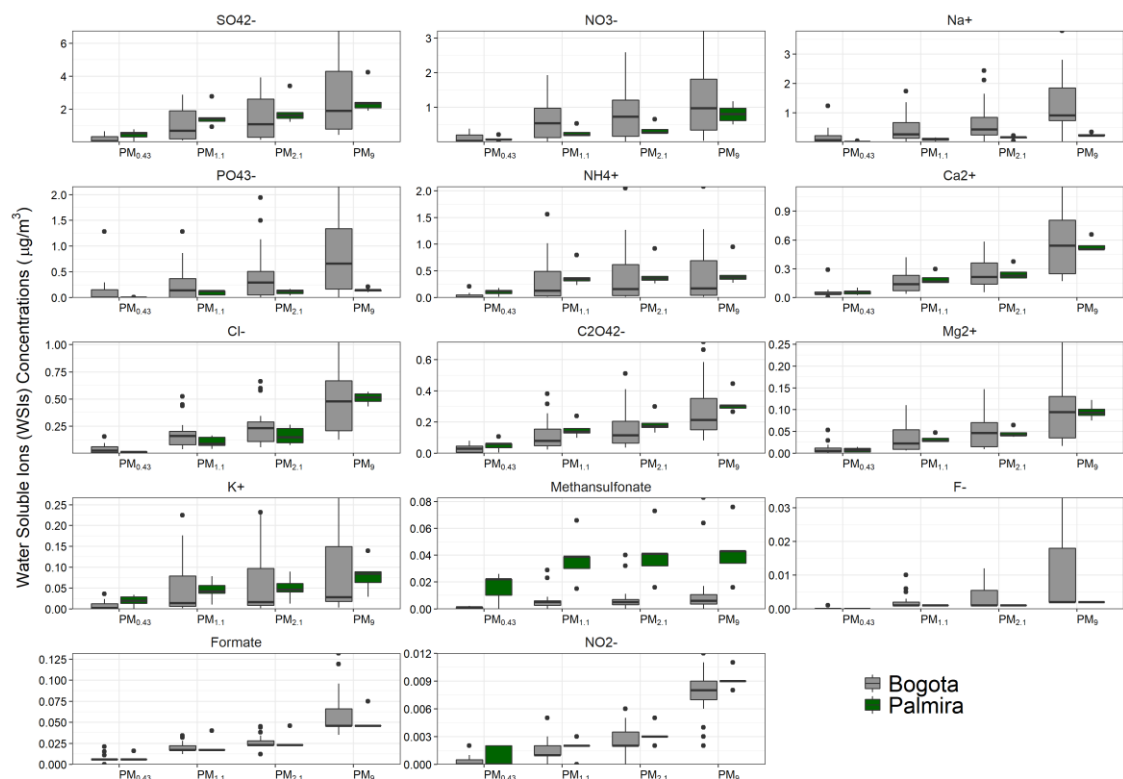
Figure 3-9. Boxplot of size-segregated concentrations of Water-Soluble Ions (WSIs) in $PM_{0.43}$, $PM_{1.1}$, $PM_{2.1}$, and PM_9 in Bogota and Palmira.

3.3.5. Ion balance

There are two commonly proxy methods to estimate aerosol pH, namely the cation/anion equivalent ratio (AE/CE) – or molar ratio – and the charge balance, based upon the principle of solution electroneutrality concept. In both approaches, the amount of H^+ is assumed to balance the exceedance of anions, and the $[H^+]$ concentrations estimated is assumed to scale inversely with the level of the cations relative to anions (Pye et al., 2020). AE/CE ratios higher than 1 suggest that aerosols are acidic. In this study, average values of the AE/CE ratio were found to be higher than 1 for all sizes categories, in both sites. Thus, AE/CE ratios in $PM_{0.43}$, $PM_{1.1}$, $PM_{2.1}$

and PM_9 were 1.1±0.4, 1.1±0.1, 1.2±0.1 and 1.2±0.1, respectively, which suggest an abundance of anion equivalents, considered to be neutralized by the protons [H^+], showing the acidic characteristic of the particles. In Bogota, $PM_{1.1}$, $PM_{2.1}$ and PM_9 exhibited AE/CE ratios of 1.2±0.6, 1.1±0.6, 1.1±0.4, respectively, while $PM_{0.43}$ showed an AE/CE ratio below 1 (0.9±0.6). These results reveal a nature alkaline for $PM_{0.43}$ and acidic for $PM_{1.1}$ and $PM_{2.1}$.
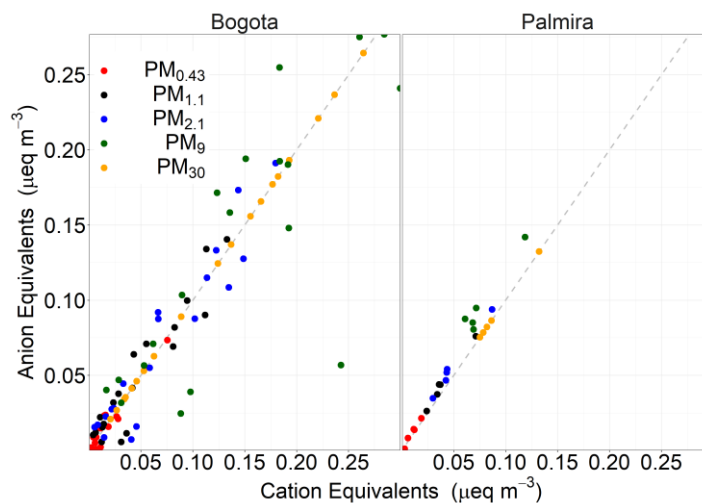
Figure 3-10. Scatterplot of particulate anion and cation equivalents (AE vs CE) in Bogota and Palmira. Different colours represent different PM fractions.

3.3.6. Size distributions of chemical components

The size distribution of chemical components can contribute to elucidate important information about ambient aerosols. It can be used to infer PM emission sources, chemical formation mechanisms (Huang et al., 2016), and the fraction that can deposit on different parts of the human respiratory system. Generally, size distributions of OC, EC, SO_4^{2-}, NO_3^-, K^+, $C_2O_4^{2-}$ and formate exhibited bimodal types in urban and suburban area. Meanwhile, Na^+, NH_4^+, $CH_3O_3S^-$, and Cl- showed unimodal types in this study. Other compounds showed different mass size distributions between Bogota and Palmira, such as Ca^{2+} and Mg^{2+}, which were unimodal in Bogota and bimodal in Palmira. The size distributions of OC, EC and WSI are shown in Figure 3-11, which notably peaked at 0.43–1.1 μm in the fine mode, and at 4.7–9.0 μm in the coarse mode.

OC size distribution was very similar in both sites, with a higher mass in the coarse mode, peaking at 4.7–5.8 µm. This carbonaceous fraction was strongly correlated with the size distribution of total mass distribution ($r^2 > 0.8$). Also, the organic ion $C_2O_4^{2-}$ showed a similar distribution in both areas, the only variation being that Palmira samples had a lower size diameter for the fine mode (0.43 - 0.65 µm) than Bogota samples (0.65 - 1.1 µm). Considering the abundance of vegetation land cover in Palmira and their potential to emit VOCs as part of biogenic emissions, the environmental conditions that favor the hygroscopic growth of condensate particles is expected a higher fraction of $C_2O_4^{2-}$ in fine particles in Palmira than in Bogota. CHO_2^-, other organic water-soluble ion, show similar distribution in both locations, with a higher fine fraction in Palmira. In the case of K^+, the peak size diameters, for both fine and coarse mode, were smaller in Palmira than in Bogota, suggesting freshly emitted particles in Palmira and aged particles in Bogota. The size distribution of PO_4^{3-} was bimodal in Palmira, with a wide range of particle sizes in Bogota (0.43 – 9 µm) and without an identifiable mode.

EC in Bogota was strongly concentrated in the fine mode (0.43–0.65 µm), with a minor fraction in the coarse mode (5.8 – 9 µm). EC in Palmira, in contrast, was both in the coarse and the fine mode in similar fractions. This difference can be attributed to: 1) the proximity of sampling sites to major sources of emissions. For example, traffic and industrial emissions are concentrated around the sampling point within a 2-kilometer radius in Bogota, whereas the sampling site in Palmira was at a higher elevation from the ground and showed higher wind speeds, making it possible for those points to be affected by regional emissions. Additional factors that contribute to the variance in EC size distribution include density, fuel type, and driving dynamics in these locations. For example, in urban settings, EC is less likely to condense and grow because of their proximity to roads. EC contained in larger particles can be associated to resuspended road dust.

Secondary inorganic ions SO_4^{2-} and nitrate NO_3^- showed a bimodal distribution. SO_4^{2-} exhibited a stronger fine mode (0.43 – 0.65 µm) in Palmira than in Bogota. In contrast, NO_3^- displayed a stronger fine mode in Bogota (0.65 – 1.1 µm). NH_4^+ is formed from its gaseous precursor, NH_3, through gas phase and aqueous phase reactions with acidic species, such as H_2SO_4, HNO_3 and HCl (Li et al., 2013a). In this research, NH_4^+ displays an outstanding unimodal distribution in Palmira, biased towards the fine mode (0.43 –

0.65 μm), while there was a minor coarse mode peak (4.7 – 5.8 μm) in Bogota. The size distribution of NH_4^+ agrees with that observed in other sites (Li et al., 2013a).

Cl^- was the only WSI with a unimodal distribution in both sites, with a coarse mode centered in the 4.7 -5.8 μm range. A fraction of Cl^- accumulates in the fine mode but doesn't show a specific diameter range. Also, there was a notably high variability in the Cl^- size distribution. In contrast, $CH_3O_3S^-$ was clearly unimodal in Palmira, centered in the fine mode (0.43 – 0.65 μm), while it shows a bimodal size distribution with a larger size in the fine mode (0.65 – 1.1 μm) and a minor fraction of $CH_3O_3S^-$ in the coarse mode (4.7 – 5.8 μm) in Bogota.

The size distribution of Ca^{2+} and Mg^{2+} were unimodal in Bogota, with a coarse mode centered in the 4.7 -5.8 μm range and a small fine mode in Palmira (0.43 – 0.65 μm). Na^+ size distribution is similar to that of Ca^{2+} and Mg^{2+}; nevertheless, the bimodal distribution observed in Palmira was more evident, with a wide accumulation mode (0.43 – 2.1 μm).

This study provides evidence that $PM_{2.1}$ particles in the urban region contained more than 75% of EC, NH_4^+ and $CH_3O_3S^-$, roughly 50% of NO_3^-, PO_4^{3-}, $C_2O_4^{2-}$, Mg^{2+}, K^+ and 30% of OC, SO_4^{2-} Na^+, Ca^{2+}, Cl^- and CHO_2^-. This is depicted in Figure S3-6. In Palmira, SO_4^{2-}, PO_4^{3-}, NH_4^+ and $CH_3O_3S^-$ accumulated mainly in $PM_{2.1}$. This fraction also contained a significant amount (~30 - 50%) of OC, EC, Na^+, Ca^{2+}, $C_2O_4^{2-}$, Mg^{2+}, K^+. The majority of Cl^- was found in coarse particles. K^+ has multiple-sources, including sea-salt, soil derived particles biomass burning and vegetation (Li et al., 2013b). Some studies have indicates that the abundance of K^+ in submicron particles can serve as a diagnostic tracer for biomass burning sources (Andreae et al., 1998), while sea salt and dust sources dominate the coarse fraction (Shen et al., 2009). In this research, it was revealed that 48% and 39% of K^+ was in submicrometric particles in Palmira and Bogota, respectively. This can be used to infer the role that biomass burning played in the generation of aerosols in each location.
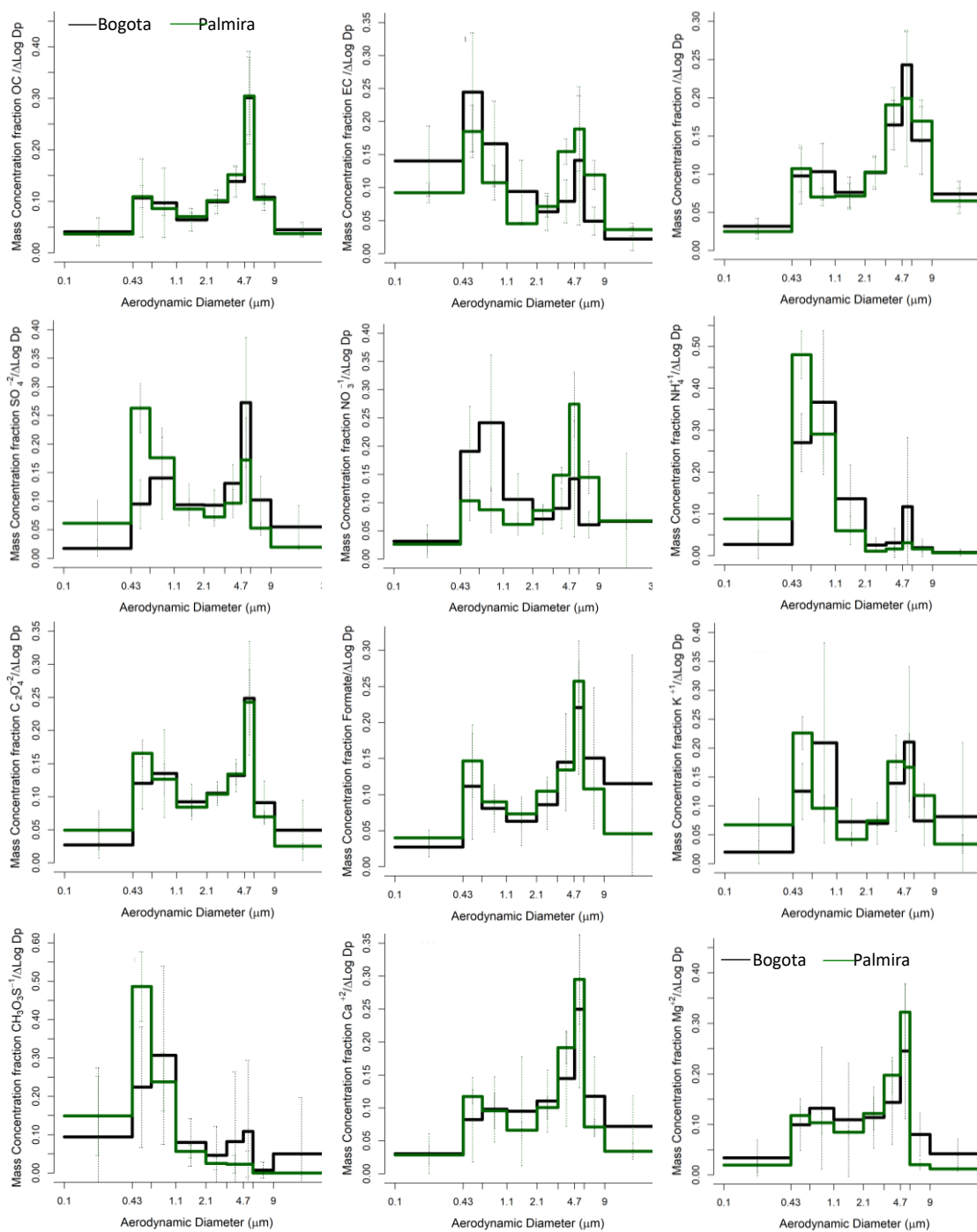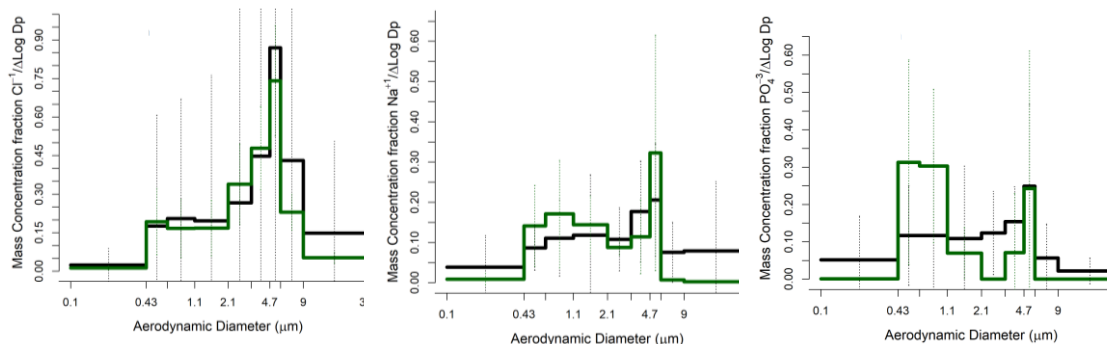
Figure 3-11. Size distribution of OC, EC, main WSIs, and PM mass in Bogota and Palmira.

3.3.7. Correlation matrix of size-segregated chemical species

The correlation between the concentrations of all species analysed can help to understand particle chemical composition and infer their sources. Figure 3-12 shows the correlation coefficient found between carbonaceous fractions (OC and EC) and WSI concentrations in $PM_{0.43}$, $PM_{1.1}$, $PM_{2.1}$ and PM_9. In Bogota, EC concentrations exhibited a strong correlation with OC in all size categories, especially in $PM_{0.43}$ and PM_9 ($r^2 = 0.8$) followed by $PM_{1.1}$ and $PM_{2.1}$ ($r^2 = 0.7$), revelling the association between the organic components and the incomplete combustion process in all size categories. $C_2O_4^{2-}$, usually one of the most abundant water-soluble organic ions, was strongly associated with OC, particularly in coarse particles (from $r^2 = 0.8$ for PM_9 up to $r^2 = 0.45$ for $PM_{0.43}$). Thus, this study indicates that OC in $PM_{0.43}$ and PM_9 were linked to incomplete combustion, and that OC in larger particles are linked to the formation of secondary organic aerosols (SOA).

Agricultural activities are one of the main source of NH_3, precursor to the NH_4^+ (Behera et al., 2013), in addition of the fossil fuel exhaust from selective catalytic reduction (SCR) processes (Cape et al., 2004). In this study, NH_4^+ was mostly associated with $C_2O_4^{2-}$, Mg^{2+}, K^+, and showed moderate correlation with EC. Its correlation with $C_2O_4^{2-}$ was similar in all particle sizes ($r^2 > 0.8$ for $PM_{2.1}$, $PM_{1.1}$ and r^2: 0.7 for PM_9 and $PM_{0.43}$), while it was stronger in larger particles with Mg^{2+} ($r^2 = 0.8$ in PM_9 and $PM_{2.1}$), and stronger in submicrometric particles with K^+ ($r^2 = 0.7$ in $PM_{0.43}$). Its correlation with EC was moderate in upper micrometric particles ($r^2 = 0.4$). All these correlations point to a connection with agricultural processes that include agricultural waste burning and encourage the formation of SOA.

The correlation between two major N-containing aerosols components, NO_3^- and NH_4^+ was approximately the same for $PM_{1.1}$, $PM_{2.1}$ and PM_9 (r^2 = 0.6), slightly smaller to $PM_{0.43}$ (r^2 = 0.5) and the higher correlation was for PM_9 (r^2 = 0.7), indicating that can exist a common source as precursor of both ions. The oxidation of nitrogen oxides (NO_x), emitted from fossil fuel combustion, biomass burning, lightening, and biogenic soil emissions, are the main precursors of NO_3^- (Cape et al., 2004). The formation pathway of NO_3^- depends on the condition to favour the oxidation of the precursors (Seinfeld and Pandis, 2006).

$C_2O_4^{2-}$, as one of the most abundant dicarboxylic acids (DCAs) that can be emitted directly from fossil fuel combustion, biomass burning, and biogenic activity and as well as be formed in the atmosphere via photochemical oxidation of VOC precursors of both anthropogenic and biogenic origin (Kerminen et al., 2000). Therefore, the correlation between $C_2O_4^{2-}$ and EC helps to distinguish if the source is associated with fossil fuel combustion or biomass burning. In Bogota, this study found a significant correlation between $C_2O_4^{2-}$ and EC for all size particles, higher in PM_9 (r^2 = 0.7) than in $PM_{2.1}$ and $PM_{1.1}$ (r^2 = 0.6), and in $PM_{0.43}$ (r^2 = 0.2), revealing the association with incomplete combustion. K^+ has multiple-sources, including sea-salt, soil derived particles biomass burning and vegetation (Li et al., 2013b). Some studies have indicates that the abundance of K^+ in submicron particles can serve as a diagnostic tracer for biomass burning sources (Andreae et al., 1998), while sea salt and dust sources have dominance in coarse fraction (Shen et al., 2009). The correlation between K^+ and $C_2O_4^{2-}$ was higher in the smaller particles $PM_{0.43}$ (r^2 = 0.75) than in larger particles (PM_9). In $PM_{2.1}$ (r^2 = 0.55), it suggests that biomass burning is a source of $C_2O_4^{2-}$ in smaller particles in Bogota, which increased in the dry season.

On the other hand, the formation pathway of SO_4^{2-} in the continental troposphere corresponds to the aqueous oxidation of SO_2 (Seinfeld and Pandis, 2006), in common with $C_2O_4^{2-}$, because it comes from of gas phase oxidation of polycyclic aromatic hydrocarbons, cyclic olefins, and aldehydes in polluted continental areas (Yu et al., 2005). The correlations between these ions were higher in $PM_{0.43}$ (r^2 = 0.8) and decreased in PM_9 (r^2 = 0.6) in Bogota. The correlation between $C_2O_4^{2-}$ and SO_4^{2-} can be taken as an indication of aqueous phase formation of DCAs (Van Pinxteren et al., 2014) in smaller particles. Previous studies have shown a positive correlation of $C_2O_4^{2-}$ and SO_4^2. In Bogota's smallest particles ($PM_{0.43}$), there was a significant correlation between two groups of ions: Ca^{2+}, Mg^{2+}, PO_4^{3-} (r^2 = 0.85) and $C_2O_4^{2-}$, SO_4^{2-}, NO_3^- (r^2 = 0.8).

The correlation between chemical components collected in Palmira showed stronger correlations than in Bogota, which can be explained by a lower concentration variability. For instance, in particles below 0.43 µm, most of WSI (Na_+, PO_4^{3-}, NH_4^+, SO_4^{2-}, Methanesulfonate, K^+, $C_2O_4^{2-}$, NO_3^-, Ca^{2+}, Mg^{2+}) showed a strong association ($r^2 > 0.78$). Specifically, the correlation between K^+ and NH_4^+ with EC ($r^2 = 0.95$ and 0.85, respectively) suggests a strong association between incomplete combustion and agricultural activities, reflecting the simultaneous contribution of both sources.

The most important findings from the comparison of correlation in the two analysed areas were that Ca^{2+} and Mg^{2+} had strong correlations for all particle sizes in both sites ($r^2 > 0.8$), whereas methanesulfonate and OC showed various levels of association in both locations. In all particle sizes, methanesulfonate demonstrated significant correlations ($r^2 > 0.8$) with NH_4^+, $C_2O_4^{2-}$, and K^+. In addition, in $PM_{0.43}$, methanesulfonate also displayed strong correlations with SO_4^{2-} ($r^2 > 0.9$). On another hand, the highest associations of methanesulfonate in Bogota in $PM_{0.43}$ occurred with NO_3^- ($r^2 = 0.7$), SO_4^{2-}, and Cl^- ($r^2 = 0.6$), and a weaker correlation with Mg^{2+}, Ca^{2+}, Na^+ and $C_2O_4^{2-}$ ($r^2 = 0.3$). Other component that differs between the two sites was OC, which was highly correlated with EC and WSI in Bogota, not being the case in Palmira (p values > 0.05). The correlation between $C_2O_4^{2-}$ and SO_4^{2-} was significant only for $PM_{0.43}$ in Palmira.
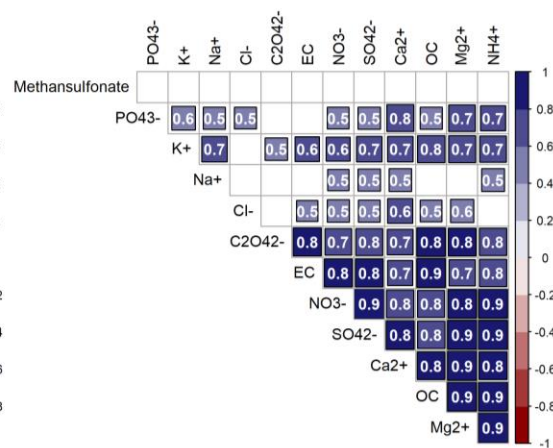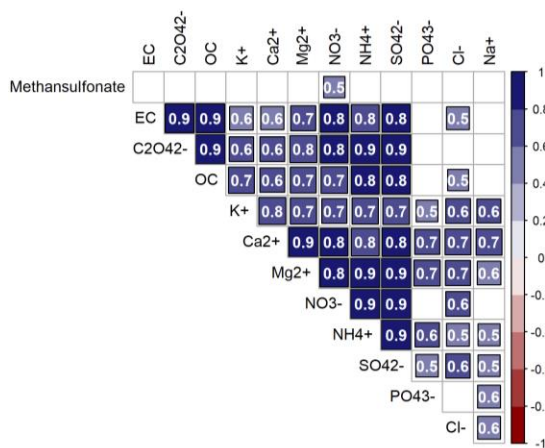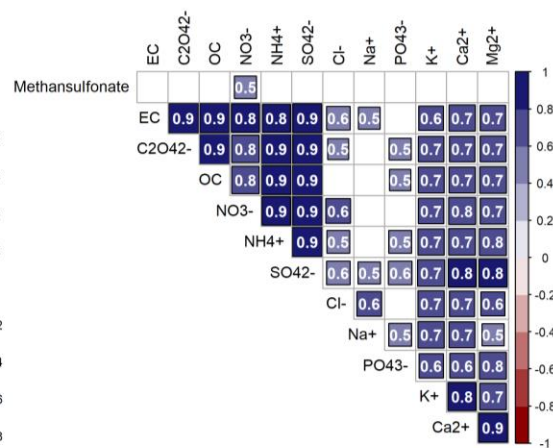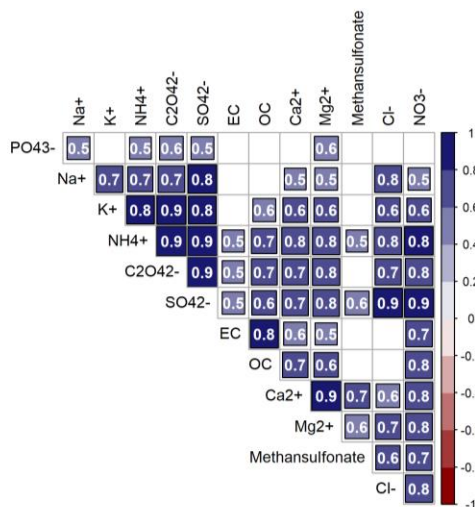
Bogota.
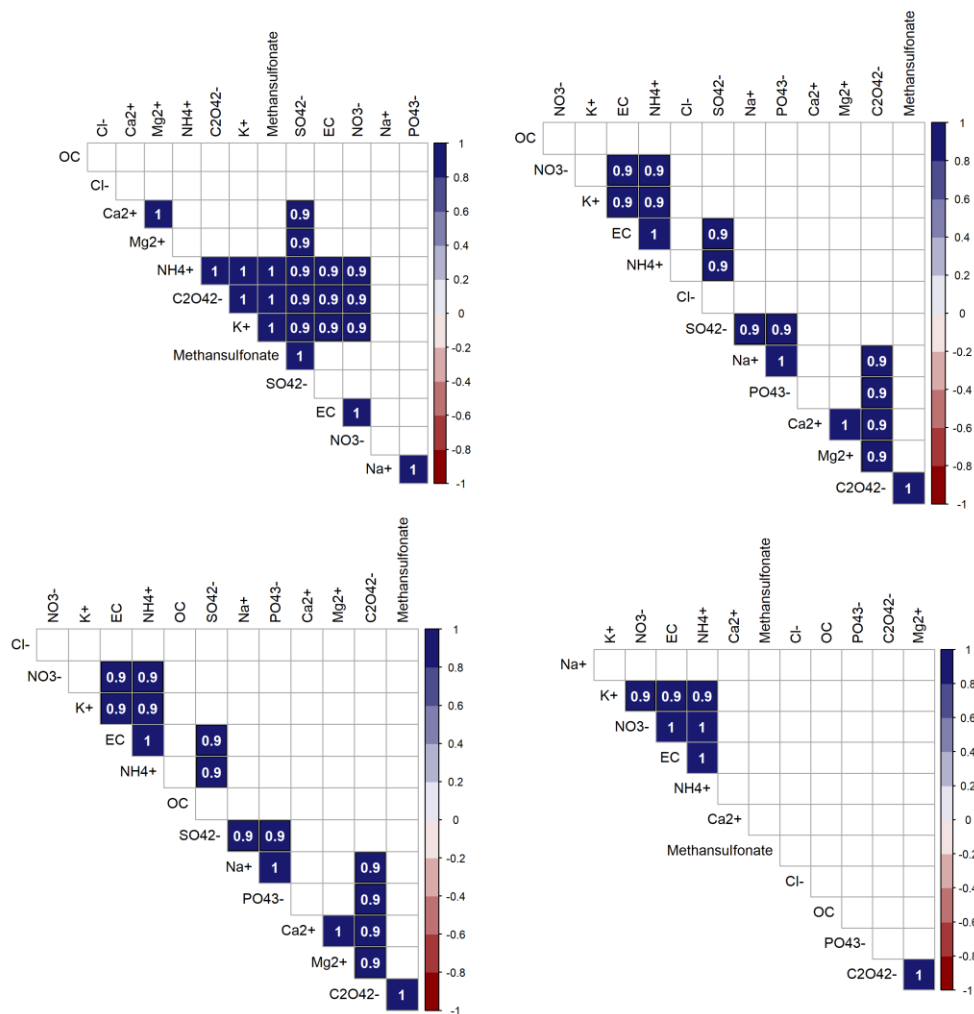
Figure 3-12. Correlation matrix of the carbonaceous fraction (OC and EC) and water-soluble ions (WSIs) concentrations in different size ranges in Bogota and Palmira. Values inside the matrix correspond to the correlation coefficient (r), positive in blue and negative in red. White squares represent no significant correlations (the p value threshold was slower than 0.05), therefore were not considered in the analysis.

3.3.8. Characteristics of PM on the human respiratory system.

PM average concentrations and their chemical species are comprised in Table 3-1, summarised according to particle size deposition onto different parts of the human respiratory system. Thus, particles larger than 9 μm were classified as inhaled particles that can be retained by nasal cilia. Particles between 9 and 4.7 μm (stages of Andersen impactor between 9-5.8 μm and 5.8-4.7 μm) can deposit onto the tracheobronchial tree. Particles between 4.7 and 1.1 μm can deposit onto the bronchioles (Stages of Andersen impactor between 4.7-3.3, 3.3-2.1 and 2.1-1.1 μm), and particles smaller than 1.1 μm (Stages Andersen impactor between 1.1-0.65, 0.65-0.43 and $D_p < 0.43$ μm) will reach the alveoli and, by translocation, cell tissue and the circulatory system.

The findings of this study showed that there was no significant difference between the percentages of PM that can enter, deposit, and be retained in the different parts of the human respiratory system for both sites. Thus, 16.3%± 6.3%, 23.3%±2.3%, 31.7%±4.4% and 28.7% ± 6.5% of PM breathed by persons exposed to outdoor environment can reach and deposit in the nasal cilia, tracheobronchial tree, bronchioles, and alveoli, respectively. This percentage barely changed for the samples taken in the Bogota and Palmira.

This study revealed that in Bogota had average PM concentrations of 11.22 μg/m^3, 16.61 μg/m^3, 22.37 μg/m^3, and 20.83 μg/m^3 that may enter and deposit in the nasal cilia, tracheobronchial tree, bronchioles, and alveoli, respectively. Whereas in Palmira, those concentrations are 11.22 μg/m^3, 16.61 μg/m^3, 22.37 μg/m^3, and 20.83 μg/m^3, respectively, for each segment of the human respiratory tract.

According to those concentrations and percentages, the population in both urban and suburban areas has been continuously exposed to a moderate concentration of PM. The third part of breathable particles in Bogotá (29.9%) can reach and deposit in the alveoli and more than a half (60.1%) in the bronchioles and deeper parts of the human respiratory system, increasing the risk of negative health effects. In Palmira, those percentages were slightly lower, 25% into alveoli and 58.8% into bronchioles and deeper parts, which is not a favorable finding for the public health of those places.

Organic Carbon (OC) is the most abundant species for all particle sizes, which implies that either alveolus, bronchioles, the tracheobronchial tree, and the nasal breathing areas were available to be impacted by OC. However, deeper parts of the respiratory system contain higher amounts. As a result, in both urban and suburban environments, 32% of OC breathable can enter alveoli, 31% can access bronchioles, 25% to the tracheobronchial tree, and 11% is retained in the nasal breathing area. The next species with the highest quantities is elemental carbon, however because of its higher concentration in smaller particles, a greater proportion of EC reaches the alveoli. Consequently, 68% (Bogota) – 58% (Palmira) of EC enter the alveoli, 20% reach the bronchioles, 9% (urban) – 18% (suburban) reach the tracheobronchial tree, and 9% (urban) – 4% (suburban) reach the nasal breathing area. In this instance, a lower amount of EC reaches the alveoli, but more EC builds up in the tracheobronchial tree in Palmira than in Bogota. Additionally, there are variations in the amount of EC in inhaled particles, which can be attribute to the high concentrations of EC in resuspended dust in Bogota.

WISI comprised 12.4 ± 5.0% and 11.4 ± 2.9% of the overall concentration of inhale particles in Bogota and Palmira, respectively. At both sites, similar fractions of WISI will could enter to different parts of the human respiratory system, because there was no noticeable difference between these fractions (p > 0.35). In Bogota, 4.4±2.6%, 4.0±2.2 %, 2.0±0.8 %, and 2.0±2.9 % of total particle mass inhaled can enter alveoli, bronchioles, the tracheobronchial tree and the nasal breathing area. In Palmira, those fractions correspond to 5.4±2.1%, 3.2±0.7%, 2.0±0.8%, and 0.8±0.2%.
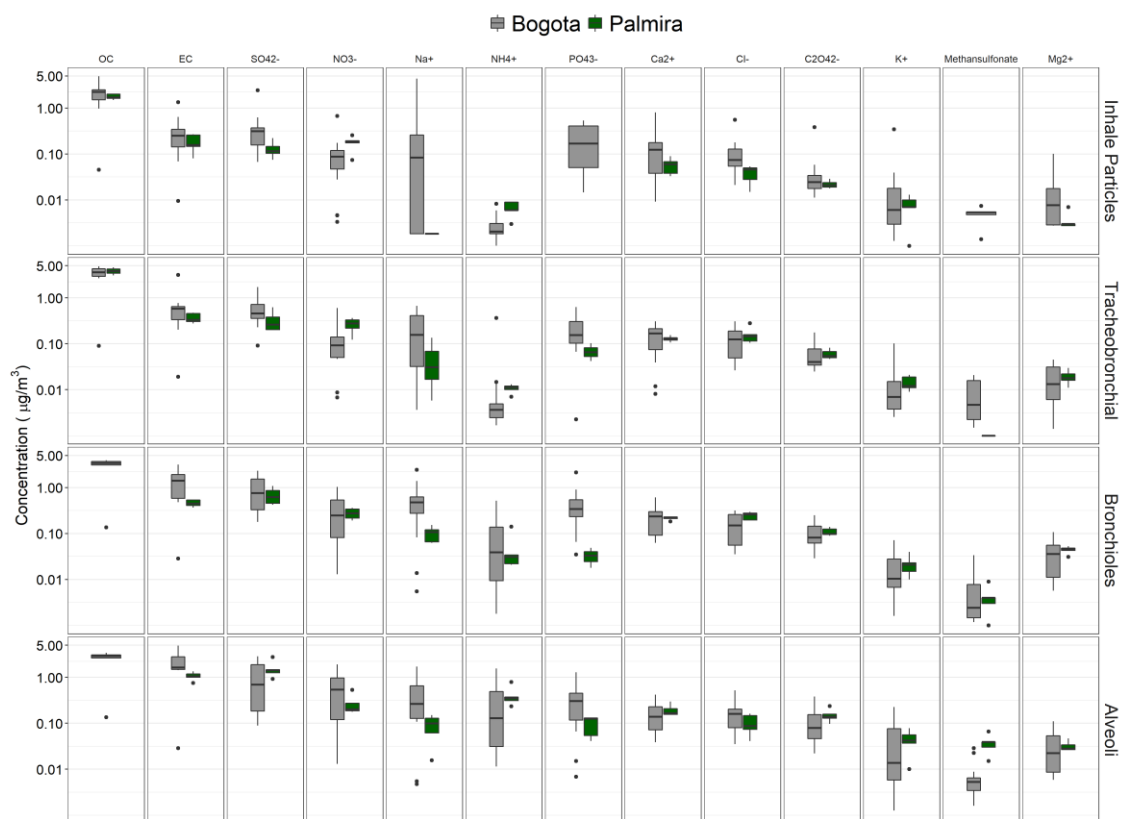
Figure 3-13. Boxplot of the chemical species concentrations in Bogota and Palmira, for different parts of the human respiratory tract.

Table 3-1. Average and standard deviation of OC, EC, and WSI concentrations ($\mu g/m^3$) classified by particle size, according to their deposition along the human respiratory tract.

Location	Species	Alveoli		Bronchioles		Tracheobronchial tree		Inhaled Particles	
		mean	sd	mean	sd	mean	sd	mean	sd
Bogota	OC	6.079	3.256	5.948	2.91	4.68	1.773	2.367	1.277
Palmira	OC	5.632	0.559	5.742	0.619	4.502	1.589	1.782	0.248
Bogota	EC	4.924	2.735	1.43	0.892	0.632	0.646	0.303	0.298
Palmira	EC	1.069	0.219	0.463	0.081	0.369	0.089	0.183	0.08
Bogota	SO_4^{2-}	1.099	1.014	0.98	0.696	0.568	0.364	0.402	0.516
Palmira	SO_4^{2-}	1.567	0.699	0.691	0.284	0.333	0.176	0.132	0.056
Bogota	NO_3^-	0.656	0.608	0.337	0.309	0.117	0.133	0.112	0.145
Palmira	NO_3^-	0.275	0.149	0.277	0.074	0.263	0.096	0.177	0.066
Bogota	Na^+	0.462	0.466	0.574	0.554	0.239	0.216	0.396	1.016
Palmira	Na^+	0.091	0.054	0.102	0.038	0.052	0.053	0.002	0
Palmira	NH_4^+	0.412	0.219	0.05	0.052	0.011	0.002	0.007	0.003
Bogota	NH_4^+	0.301	0.413	0.093	0.128	0.024	0.083	0.002	0.002
Bogota	PO_4^{3-}	0.274	0.349	0.356	0.507	0.129	0.181	0.053	0.146
Palmira	PO_4^{3-}	0.097	0.045	0.02	0.021	0.029	0.045	0	0
Palmira	Ca^{2+}	0.196	0.061	0.215	0.019	0.129	0.018	0.058	0.023
Bogota	Ca^{2+}	0.168	0.114	0.234	0.147	0.159	0.093	0.149	0.176
Bogota	Cl^-	0.183	0.143	0.162	0.103	0.13	0.088	0.11	0.118
Palmira	Cl^-	0.102	0.051	0.244	0.047	0.16	0.07	0.039	0.017
Palmira	$C_2O_4^{2-}$	0.152	0.053	0.11	0.022	0.06	0.015	0.022	0.004
Bogota	$C_2O_4^{2-}$	0.121	0.105	0.106	0.069	0.058	0.036	0.045	0.084
Bogota	K^+	0.05	0.068	0.02	0.022	0.013	0.022	0.026	0.078
Palmira	K^+	0.045	0.025	0.022	0.011	0.014	0.005	0.008	0.004
Bogota	Methansulfonate	0.006	0.007	0.004	0.009	0.002	0.006	0.001	0.002
Palmira	Methansulfonate	0.038	0.019	0.004	0.003	0	0.001	0	0
Bogota	Mg^{2+}	0.035	0.031	0.038	0.03	0.019	0.015	0.014	0.022
Palmira	Mg^{2+}	0.032	0.009	0.044	0.008	0.019	0.007	0.004	0.002
Bogota	CHO_2^-	0.02	0.007	0.021	0.009	0.02	0.014	0.043	0.123
Palmira	CHO_2^-	0.022	0.01	0.017	0	0.013	0.003	0.007	0.003

Bogota	NO$_2^-$	0.002	0.001	0.003	0.002	0.002	0.001	0.004	0.012
Palmira	NO$_2^-$	0.002	0.001	0.005	0	0.003	0	0.002	0
Bogota	F$^-$	0.002	0.002	0.005	0.006	0.003	0.004	0.003	0.009
Palmira	F$^-$	0.001	0	0.001	0	0	0	0	0
Bogota	Br$^-$	0.001	0.004	0	0.002	0	0	0	0
Palmira	Br$^-$	0	0	0	0	0	0	0	0

3.3.9. Chemical composition of breathily particles.

Based on the chemical composition size-segregated was estimated the chemical composition of the particles breathable in Bogota and Palmira, establishing the average concentrations and percentage of organic carbon, elemental carbon and the major water-soluble ions contained in the particles that can reach into the nasal cilia, tracheobronchial tree, bronchioles, and alveoli, respectively. The average concentrations and percentages of each chemical species present in the particles that can enter the various parts of the human respiratory system are shown in Figure 3-14. According to the findings of this study, the carbonaceous fraction of OC and EC and the WSI's can explain about 70% of the average particle mass concentration that reaches alveoli, 44% of particles that enter bronchioles, 42% of particles that reach the tracheobronchial area, and 30% of mass. 40.6% and 29.2% of particle mass concentrations that reach alveoli corresponds to OC in Palmira and Bogota, respectively, while EC represent 7,7% and 23.6% for each site. Despite the percentage of OC was notably higher in Palmira, the average concentration of OC that reach to Alveoli was not much different between both places, 5.6 μg/m^3 and 6.1 μg/m^3 in Bogotá and Palmira, respectively. Whereas the concentration of EC in alveoli was significantly higher in Bogota (4.9 μg/m^3) than Palmira (1.1 μg/m^3) as shown in Table 3-1.
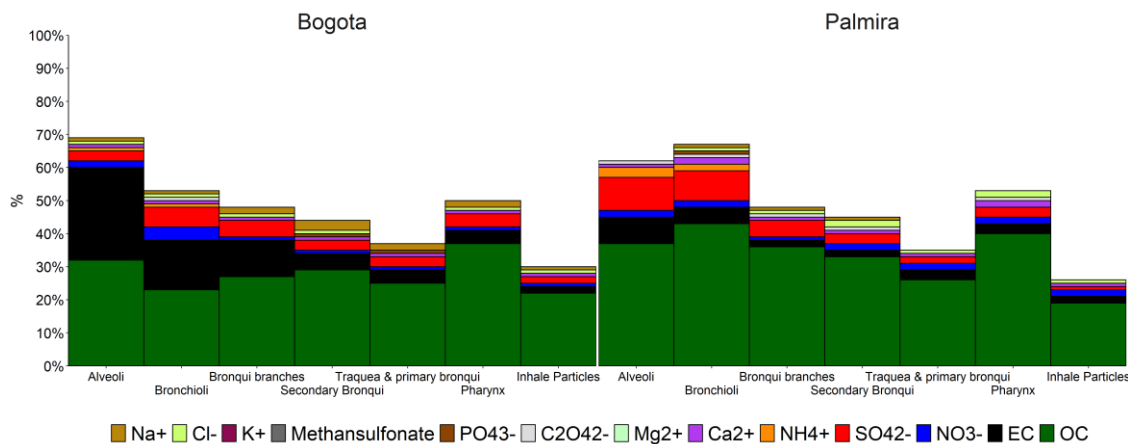
Figure 3-14. Chemical composition of aerosol particles based on their size and their penetration into the human respiratory tract.

The composition of ammonium sulphate ($(NH_4)_2SO_4$), ammonium nitrate (NH_4NO_3), Organic material (OM), Elemental Carbon (EC) and Particle-bound water (PBW) were calculated, according to the size fraction that can penetrate in the different parts of the human respiratory system, as simulated by the Andersen impactor. Figure 3-14 shows pie plots of the chemical composition of particles that can penetrate the alveoli, bronchi, trachea, pharynx and inhalable particles for rainy and dry periods. There was no perceptible influence of seasonal variations in the chemical composition of particles. The best mass closure was obtained for smaller particles that can penetrate the alveoli ($D_p < 1.1$ μm), which contained 22% elemental carbon, 12% inorganic salts (Ammonium nitrate and Ammonium sulfate), 50% organic material, and 3% of particle-bound water (PBW). OM was nearly 50% of PM mass in the size fractions that penetrate bronchi, trachea, and pharynx; and decreased for inhalable particles. EC gradually decreases, being 11% of PM mass concentration that reach the terminal bronchi, 5% in secondary bronchi, 4% in trachea & primary bronchi and 3% in pharynx. Besides, inorganic salts decrease its proportion in the largest particles. Considering that PBW was estimated from concentrations of hygroscopic ions (SO_4^{2-}, NH_4 and NO_3), its percentage also

decreased in larger particles, staying in the range of 1 to 3% of PM mass concentration. Conversely, the unreconstructed fraction was higher in larger particles, which can be attributed to the fraction associated with traces of elemental oxides and crustal material. The unreconstructed fraction of particles that can reach the alveoli was 13%. Previous studies about PM_1 and their chemical composition conducted in urban areas, with similar mass concentrations of PM_1, obtained comparable percentages of OM, EC, and slightly higher percentages of sulphate and nitrate (Aiken et al., 2009). In those studies, components derived from elemental analysis, such as, soil, and trace metals explained 5% and 3% of mass, respectively, which is in the same range of unreconstructed fraction in $PM_{1.1}$ in this study.
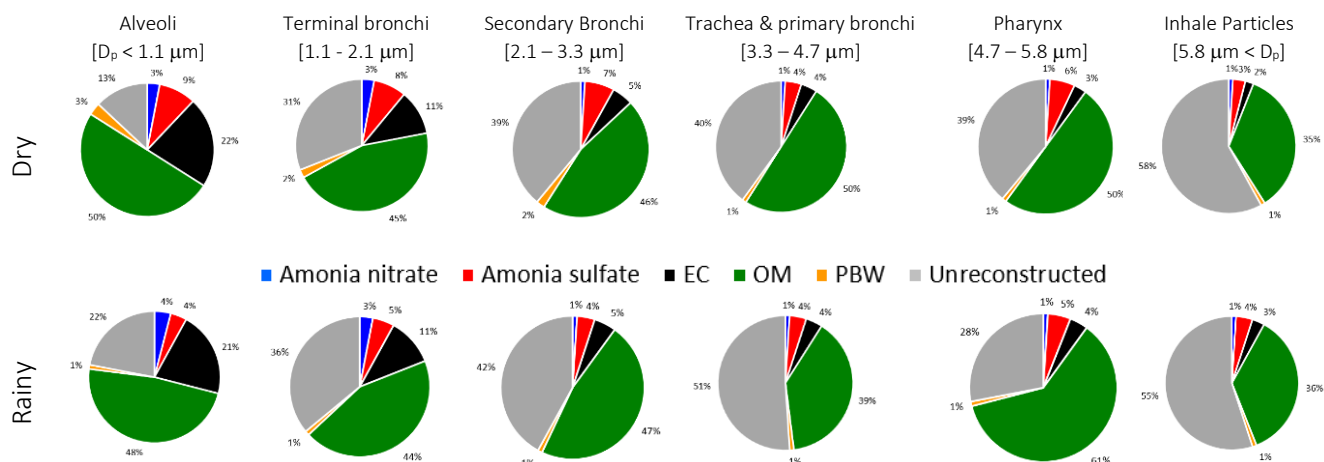
Figure 3-15. Chemical composition of aerosol particles based on their size and their penetration into the human respiratory tract.

3.4. Conclusions

In this study, environmental aerosols from two sites in Colombia were examined for their total mass size distribution, as well as organic and elemental carbon, and water-soluble ion concentrations. The first site, in the megacity of Bogota, was mostly impacted by industrial and traffic emissions, whereas the second site was in Palmira, an agro-industrial town impacted by

a diversity of atmospheric emission sources, including both anthropogenic and biogenic emissions.

This study determined that the mass concentrations were higher in Bogota than in Palmira. In this way average PM_9, $PM_{2.1}$, $PM_{1.1}$ and $PM_{0.43}$ concentrations were 59.8 µg/m^3, 28.4 µg/m^3, 20.8 µg/m^3, 6.8 µg/m^3, respectively, in Bogota; 46.3 µg/m^3, 19.2 µg/m^3, 13.8 µg/m^3, 4.2 µg/m^3, respectively, in Palmira. In Bogota, particularly, larger particles had a wide variability of their concentrations and were more strongly influenced by the rain events in comparison with the smaller particles. On the other hand, $PM_{0.43}/PM_9$, $PM_{1.1}/PM_9$ and $PM_{2.1}/PM_9$ did not show a substantial deviation and were unaffected by the amount of precipitation.

The distribution of total mass size was bimodal in both locations, with peaks in the fine mode at 0.43–1.1µm and the coarse mode at 4.7–9.0 µm. The results of this study settled that 23 ±11.3 % of PM inhalable collected in Bogotá have a size smaller than 1.1 µm, which corresponding to the fraction of PM inhalable that can enter to the alveoli of people exposed of air pollution in the area studied. In case of samples collected in Palmira, this fraction corresponded to 13.8 ±1.9% of PM inhalable.

Most components analyzed in this study, such as OC, EC, SO_4^{2-}, NO_3^-, K^+, $C_2O_4^{2-}$, and formate showed bimodal mass size distributions in Bogota and Palmira, while other water-soluble ions, for instance, Na^+, NH_4^+, $CH_3O_3S^-$, and Cl^- clearly displayed unimodal distributions. The mass size distributions of other chemicals, such as Ca^{2+} and Mg^{2+} were different for each site studied.

Particles in Bogota had a different distribution of EC than Palmira, with 57% of EC in the fine mode ($D_p < 2.1$ µm) in Palmira and 72% in Bogota. In both sites, 42% of OC was in the fine mode. A considerable amount of SO_4^{2-}, one of the most common WSIs in PM, was found in the fine mode, with a notable difference in the proportion depending on the site: 69% in Palmira and 43% in Bogota. NO_3^- showed an opposite distribution for SO_4^{2-}, accumulating 62% in the fine mode in Bogota and 36% in Palmira. More than 75% of $CH_3O_3S^-$ was in the fine mode.

The relative abundance of some chemical components noticed during the no precipitations days in Bogotá, particularly in $PM_{1.1}$ and $PM_{2.1}$, reveled the formation of secondary aerosols during

this weather conditions. The increases of PM1.1 and PM2.1 concentrations during the no precipitation days could be associated to emissions derived from agriculture and open biomass buring, explained by the abundance of $C_2O_4^{2-}$, K^+, and NH_4^+, mainly.

The percentage of PM breathily that can enter, deposit, and be retained in the nasal cilia, tracheobronchial tree, bronchioles, and alveoli was no significant different in Bogota than Palmira, equivalent to 16.3%± 6.3%, 23.3%±2.3%, 31.7%±4.4% and 28.7% ± 6.5%, respectively. The third part of breathable particles in Bogotá (29.9%) can reach and deposit in the alveoli and more than a half (60.1%) in the bronchioles and deeper parts of the human respiratory system. In Palmira, those percentages were slightly lower, 25% into alveoli and 58.8% into bronchioles and deeper parts.

3.5.   References

Aiken, A. C., Salcedo, D., Cubison, M. J., Huffman, J. A., DeCarlo, P. F., Ulbrich, I. M., Docherty, K. S., Sueper, D., Kimmel, J. R., Worsnop, D. R., Trimborn, A., Northway, M., Stone, E. A., Schauer, J. J., Volkamer, R. M., Fortner, E., De Foy, B., Wang, J., Laskin, A., Shutthanandan, V., Zheng, J., Zhang, R., Gaffney, J., Marley, N. A., Paredes-Miranda, G., Arnott, W. P., Molina, L. T., Sosa, G. and Jimenez, J. L.: Mexico City aerosol analysis during MILAGRO using high resolution aerosol mass spectrometry at the urban supersite (T0) - Part 1: Fine particle composition and organic source apportionment, Atmos. Chem. Phys., 9(17), 6633–6653, https://doi.org/10.5194/acp-9-6633-2009, 2009.

Andreae, M. O., Andreae, T. W., Annegarn, H., Beer, J., Cachier, H., Le Canut, P., Elbert, W., Maenhaut, W., Salma, I., Wienhold, F. G. and Zenker, T.: Airborne studies of aerosol emissions from savanna fires in southern Africa: 2. Aerosol chemical composition, J. Geophys. Res. Atmos., 103(D24), 32119–32128, https://doi.org/10.1029/98JD02280, 1998.

Behera, S. N., Sharma, M., Aneja, V. P. and Balasubramanian, R.: Ammonia in the atmosphere: A review on emission sources, atmospheric chemistry and deposition on terrestrial bodies, Environ. Sci. Pollut. Res., 20(11), 8092–8131, https://doi.org/10.1007/s11356-013-2051-9, 2013.

Cape, J. N., Tang, Y. S., Van Dijk, N., Love, L., Sutton, M. A. and Palmer, S. C. F.: Concentrations of ammonia and nitrogen dioxide at roadside verges, and their contribution to nitrogen deposition, Environ. Pollut., 132(3), 469–478, https://doi.org/10.1016/j.envpol.2004.05.009,

2004.

Corporación Autonoma Regional del Valle del Cauca - C.V.C.: Informe de la calidad del aire Año 2018, Santiago de Cali. https://sites.google.com/site/cvccalidadaire/informes-calidad-de-aire/2018, 2019.

DANE: Bogotá. Indicadores demográficos, https://www.dane.gov.co/files/investigaciones/poblacion/ITMoDto2005.../Bogota.xls, last access: 14 May 2018, 2018.

Deguillaume, L., Leriche, M., Desboeufs, K., Mailhot, G., George, C. and Chaumerliac, N.: Transition Metals in Atmospheric Liquid Phases: Sources, Reactivity, and Sensitive Parameters, Chem. Rev., 105(9), 3388–3431, https://doi.org/10.1021/cr040649c, 2005.

Fundación Empresarial para el Desarrollo de Yumbo: Lineamientos para adelantar la revisión ordinaria de contenidos de largo plazo del PBOT de Yumbo., 2015.

Gondwe, M.: Comparison of modeled versus measured MSA : nss SO = 4 ratios : A global analysis, Global Biogeochem. Cycles, 18, 1–18, https://doi.org/10.1029/2003GB002144, 2004.

Guerrero, F., Alvarez-Ospina, H., Retama, A., López-Medina, A., Castro, T. and Salcedo, D.: Seasonal changes in the PM 1 chemical composition north of Mexico City, Atmosfera, 30(3), 243–258, https://doi.org/10.20937/ATM.2017.30.03.05, 2017.

HEI: HEI Perspectives 3: Understanding the Health Effects of Ambient Ultrafine Particles. https://www.healtheffects.org/system/files/Perspectives3.pdf, 2013.

Hitzenberger, R. and Tohno, S.: Comparison of black carbon (BC) aerosols in two urban areas - concentrations and size distributions, Atmos. Environ., 35(12), 2153–2167, https://doi.org/10.1016/S1352-2310(00)00480-5, 2001.

Huang, X., Liu, Z., Zhang, J., Wen, T., Ji, D. and Wang, Y.: Seasonal variation and secondary formation of size-segregated aerosol water-soluble inorganic ions during pollution episodes in Beijing, Atmos. Res., 168, 70–79, https://doi.org/10.1016/j.atmosres.2015.08.021, 2016.

IDEAM: Consulta y Descarga de Datos Hidrometeorológicos, http://dhime.ideam.gov.co/atencionciudadano/, last access: 20 May 2019, 2019.

Kerminen, V. M., Ojanen, C., Pakkanen, T., Hillamo, R., Aurela, M. and Meriläinen, J.: Low-molecular-weight dicarboxylic acids in an urban and rural atmosphere, J. Aerosol Sci., 31(3), 349–362, https://doi.org/10.1016/S0021-8502(99)00063-4, 2000.

Kim, K., Kabir, E. and Kabir, S.: A review on the human health impact of airborne particulate matter, Environ. Int., 74, 136–143, https://doi.org/10.1016/j.envint.2014.10.005, 2015.

Larada, J. L.: Zona portuaria de Buenaventura : y su importancia en Colombia Trabajo de Grado presentado para optar al título de Negociador Internacional Asesor : Nancy Estella Grajales Montoya , Magíster (MSc) en Gestión de las organizaciones . Universidad de San B, Universidad de San Buenaventura Colombia https://bibliotecadigital.usb.edu.co/server/api/core/bitstreams/5406fcb8-799b-43a4-98c5-814d4944baee/content, 2017.

Li, X., Wang, L., Wang, Y., Wen, T., Yang, Y., Zhao, Y. and Wang, Y.: Chemical composition and size distribution of airborne particulate matters in Beijing during the 2008 Olympics, Atmos. Environ., 50, 278–286, https://doi.org/10.1016/j.atmosenv.2011.12.021, 2012.

Li, X., Wang, L., Ji, D., Wen, T., Pan, Y., Sun, Y. and Wang, Y.: Characterization of the size-segregated water-soluble inorganic ions in the Jing-Jin-Ji urban agglomeration: Spatial/temporal variability, size distribution and sources, Atmos. Environ., 77, 250–259, https://doi.org/10.1016/j.atmosenv.2013.03.042, 2013a.

Li, X., Wang, L., Ji, D., Wen, T., Pan, Y., Sun, Y. and Wang, Y.: Characterization of the size-segregated water-soluble inorganic ions in the Jing-Jin-Ji urban agglomeration: Spatial/temporal variability, size distribution and sources, Atmos. Environ., 77, 250–259, https://doi.org/10.1016/j.atmosenv.2013.03.042, 2013b.

Löndahl, J., Pagels, J., Swietlicki, E., Zhou, J., Ketzel, M., Massling, A. and Bohgard, M.: A set-up for field studies of respiratory tract deposition of fine and ultrafine particles in humans, J. Aerosol Sci., 37(9), 1152–1163, https://doi.org/10.1016/j.jaerosci.2005.11.004, 2006.

Majewski, G., Rogula-Kozłowska, W., Rozbicka, K., Rogula-Kopiec, P., Mathews, B. and Brandyk, A.: Concentration, chemical composition and origin of PM1: Results from the first long-term measurement campaign in warsaw (Poland), Aerosol Air Qual. Res., 18(3), 636–654, https://doi.org/10.4209/aaqr.2017.06.0221, 2018.

Mateus-Fontecha, Lady, Vargas-Burbano, A., Jimenez, R., Rojas, N. Y., Rueda-Saa, G., Pinxteren, D. van, Pinxteren, M. van, Fomba, K. W. and Herrmann, H.: Understanding aerosol composition in a tropical inter-Andean valley impacted by agro-industrial and urban emissions, Atmos. Chem. Phys., 22, 8473–8495, 2022.

Meinardi, S., Simpson, I. J., Blake, N. J., Blake, D. R. and Rowland, F. S.: Dimethyl disulfide (DMDS) and dimethyl sulfide (DMS) emissions from biomass burning in Australia., 2003.

Mendez-espinosa, J. F., Belalcazar, L. C. and Betancourt, R. M.: Regional air quality impact of northern South America biomass burning emissions, Atmos. Environ., 203(February), 131–140, https://doi.org/10.1016/j.atmosenv.2019.01.042, 2019.

Morawska, L., Moore, M. R., Ristovski, Z. D. and Review, D. L.: Health Impacts of Ultrafine Particles. http://www.environment.gov.au/atmosphere/airquality/publications/health-impacts/index.html, 2004.

N. Perez, J., Querol, P., Alastuey, A., Lopez, J. . and Viana, M.: Partitioning of major and trace components in PM 10 – PM 2 . 5 – PM 1 at an urban site in Southern Europe, Atmos. Environ., 42, 1677–1691, https://doi.org/10.1016/j.atmosenv.2007.11.034, 2008.

Neusüss, C., Pelzing, M., Plewka, A. and Herrmann, H.: A new analytical approach for size-resolved speciation of organic compounds in atmospheric aerosol particles: Methods and first results, J. Geophys. Res. Atmos., 105(D4), 4513–4527, https://doi.org/10.1029/1999JD901038, 2000.

Onat, B., Sahin, U. A. and Akyuz, T.: Elemental characterization of PM2.5 and PM1 in dense traffic area in Istanbul, Turkey, Atmos. Pollut. Res., 4(1), 101–105, https://doi.org/10.5094/APR.2013.010, 2013.

Orozco, C., Sanandres, E. and Molinares, I.: Colombia, Panamá y la Ruta Panamericana: Encuentros y Desencuentros, Memorias Rev. Digit. Hist. y Arqueol. desde el Caribe, 16(ISSN 1794-8886), 2012.

Van Pinxteren, D., Brüggemann, E., Gnauk, T., Iinuma, Y., Müller, K., Nowak, A., Achtert, P., Wiedensohler, A. and Herrmann, H.: Size- and time-resolved chemical particle characterization during carebeijing-2006: Different pollution regimes and diurnal profiles, J. Geophys. Res. Atmos., 114(9), https://doi.org/10.1029/2008JD010890, 2009.

Van Pinxteren, D., Neusüß, C. and Herrmann, H.: On the abundance and source contributions of dicarboxylic acids in size-resolved aerosol particles at continental sites in central Europe, Atmos. Chem. Phys., 14(8), 3913–3928, https://doi.org/10.5194/acp-14-3913-2014, 2014.

Pio, C., Cerqueira, M., Harrison, R. M., Nunes, T., Mirante, F., Alves, C., Oliveira, C., Sanchez de la Campa, A., Artíñano, B. and Matos, M.: OC/EC ratio observations in Europe: Re-thinking the approach for apportionment between primary and secondary organic carbon, Atmos. Environ., 45(34), 6121–6132, https://doi.org/10.1016/j.atmosenv.2011.08.045, 2011.

Pye, H. O. T., Nenes, A., Alexander, B., Ault, A. P., Barth, M. C., Clegg, S. L., Collett, J. L., Fahey, K. M., Hennigan, C. J., Herrmann, H., Kanakidou, M., Kelly, J. T., Ku, I. T., Faye McNeill, V.,

Riemer, N., Schaefer, T., Shi, G., Tilgner, A., Walker, J. T., Wang, T., Weber, R., Xing, J., Zaveri, R. A. and Zuend, A.: The acidity of atmospheric particles and clouds., 2020.

Ramírez, O., A.M, S. de la C., Amato, F., Catacolí, R. A., Rojas, N. Y. and de la Rosa, J.: Chemical composition and source apportionment of PM 10 at an urban background site in a high e altitude Latin American megacity, , 233, 142–155, https://doi.org/10.1016/j.envpol.2017.10.045, 2018.

Saarikoski, S., Timonen, H., Saarnio, K. and Aurela, M.: Sources of organic carbon in fine particulate matter in northern European urban air, Atmos. Chem. Phys., 6281–6295, 2008.

Secretaría Distrital de Ambiente: Informe anual de calidad del aire en Bogotá 2017., 2018.

Secretaría Distrital de Ambiente: Informe Anual de Calidad del aire de Bogotá - 2019. http://rmcab.ambientebogota.gov.co/Pagesfiles/IA 200531 Informe Anual de Calidad del Aire Año 2019.pdf, 2020.

Secretaria Distrital de Ambiente de Bogotá: Inventario de Emisions de Bogotá 2018, Bogotá D.C. https://www.ambientebogota.gov.co/documents/10184/397082/Inventario+de+Emisiones+de+Bogota+portal+nuevo.pdf/972994eb-7f58-42c2-a801-0f8579937919, 2020.

Seinfeld, J. H. and Pandis, S. N.: Atmospheric From Air Pollution to Climate Change, 2 nd., 2006.

Shen, Z., Cao, J., Arimoto, R., Han, Z., Zhang, R., Han, Y., Liu, S., Okuda, T., Nakao, S. and Tanaka, S.: Ionic composition of TSP and PM2.5 during dust storms and air pollution episodes at Xi'an, China, Atmos. Environ., 43(18), 2911–2918, https://doi.org/10.1016/j.atmosenv.2009.03.005, 2009.

Sorooshian, A., Crosbie, E., Maudlin, L. C., Youn, J., Wang, Z., Shingler, T., Ortega, A. M., Hersey, S. and Woods, R. K.: Surface and airborne measurements of organosulfur and methanesulfonate over the western United States and coastal areas, J. Geophys. Res. Atmos., 8535–8548, https://doi.org/10.1002/2015JD023822.Received, 2015.

Stahl, C., Templonuevo Cruz, M., Angela Banãga, P., Betito, G., Braun, R. A., Azadi Aghdam, M., Obíminda Cambaliza, M., Rose Lorenzo, G., MacDonald, A. B., Hilario, M. R. A., Corazon Pabroa, P., Robin Yee, J., Bernard Simpas, J. and Sorooshian, A.: Sources and characteristics of size-resolved particulate organic acids and methanesulfonate in a coastal megacity: Manila, Philippines, Atmos. Chem. Phys., 20(24), 15907–15935, https://doi.org/10.5194/acp-20-15907-2020, 2020.

Sullivan, R. C. and Prather, K. A.: Investigations of the diurnal cycle and mixing state of oxalic acid in individual particles in Asian aerosol outflow, Environ. Sci. Technol., 41(23), 8062–8069, https://doi.org/10.1021/es071134g, 2007.

Tang, M., Guo, L., Bai, Y., Huang, R., Wu, Z. and Wang, Z.: Impacts of methanesulfonate on the cloud condensation nucleation activity of sea salt aerosol, Atmos. Environ., 201(October 2018), 13–17, https://doi.org/10.1016/j.atmosenv.2018.12.034, 2019.

Tian, S. L., Pan, Y. P. and Wang, Y. S.: Size-resolved source apportionment of particulate matter in urban Beijing during haze and non-haze episodes, Atmos. Chem. Phys., 16(1), 1–19, https://doi.org/10.5194/acp-16-1-2016, 2016.

Universidad de los Andes; Alcaldia de Bogota: Elementos tecnicos plan decenal de descontaminación de Bogotá, http://oab2.ambientebogota.gov.co/es/documentacion-e-investigaciones/resultado-busqueda/elementos-tecnicos-del-plan-decenal-de-descontaminacion-de-bogota-parte-1, 2009.

Vargas, F. A., Rojas, N. Y., Pachon, J. E. and Russell, A. G.: PM10 characterization and source apportionment at two residential areas in Bogota, Atmos. Pollut. Res., 3(1), 72–80, https://doi.org/10.5094/APR.2012.006, 2012a.

Vargas, F. A., Rojas, N. Y., Pachon, J. E. and Armistead G, R.: PM10 characterization and source apportionmentat two residential areas inBogota, Atmos. Pollut. Res., 3, 72–80, 2012b.

Vecchi, R., Bernardoni, V., Valentini, S., Piazzalunga, A., Fermo, P. and Valli, G.: Assessment of light extinction at a European polluted urban area during wintertime : Impact of PM 1 composition and sources *, Environ. Pollut., 233, 679–689, https://doi.org/10.1016/j.envpol.2017.10.059, 2018.

Wang, L., Xin, J., Li, X. and Wang, Y.: The variability of biomass burning and its influence on regional aerosol properties during the wheat harvest season in North China, Atmos. Res., 157, 153–163, https://doi.org/10.1016/j.atmosres.2015.01.009, 2015.

World Health Organization: Review of evidence on health aspects of air pollution – REVIHAAP Project. http://www.euro.who.int/en/health-topics/environment-and-health/air-quality/publications/2013/review-of-evidence-on-health-aspects-of-air-pollution-revihaap-project-final-technical-report, 2013.

World Health Organization: Air pollution, https://www.who.int/airpollution/en/, last access: 9 May 2019, 2021.

Yu, J. Z., Huang, X. F., Xu, J. and Hu, M.: When aerosol sulfate goes up, so does oxalate: Implication for the formation mechanisms of oxalate, Environ. Sci. Technol., 39(1), 128–133, https://doi.org/10.1021/es049559f, 2005.

Zhang, Y., Lang, J., Cheng, S., Li, S., Zhou, Y., Chen, D., Zhang, H. and Wang, H.: Chemical composition and sources of PM1 and PM2.5 in Beijing in autumn, Sci. Total Environ., 630, 72–82, https://doi.org/10.1016/j.scitotenv.2018.02.151, 2018.

3.6. Supplementary material

a   b   c
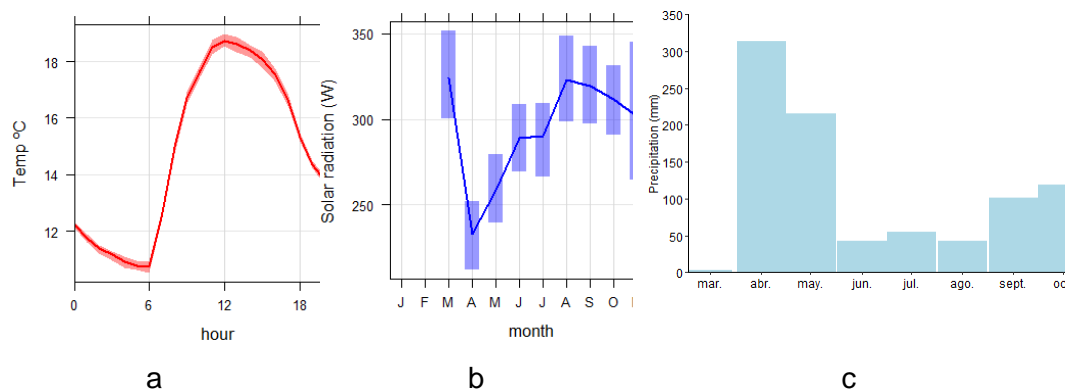
Figure S3-1. Meteorological conditions registered in Bogotá using the "El Dorado Airport" weather station (ID: 21205791). a) Hourly average ambient temperature, b) Monthly average of daylight solar radiation income and c) Monthly accumulated precipitation between March to November of 2018 in Bogotá.

a   b
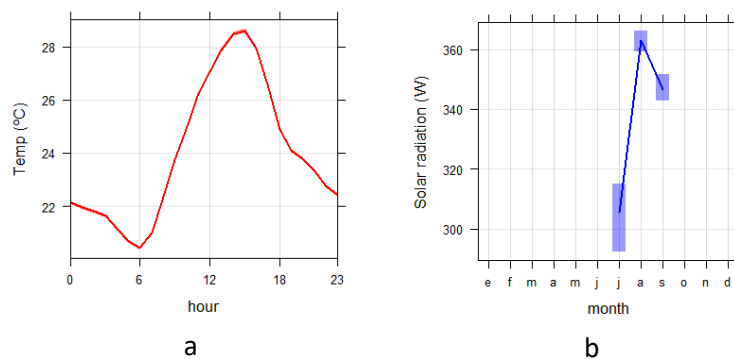
Figure S3-2. Meteorological conditions registered in Palmira weather station. a) Hourly average ambient temperature, b) Monthly average of daylight solar radiation income between July to September 2018.
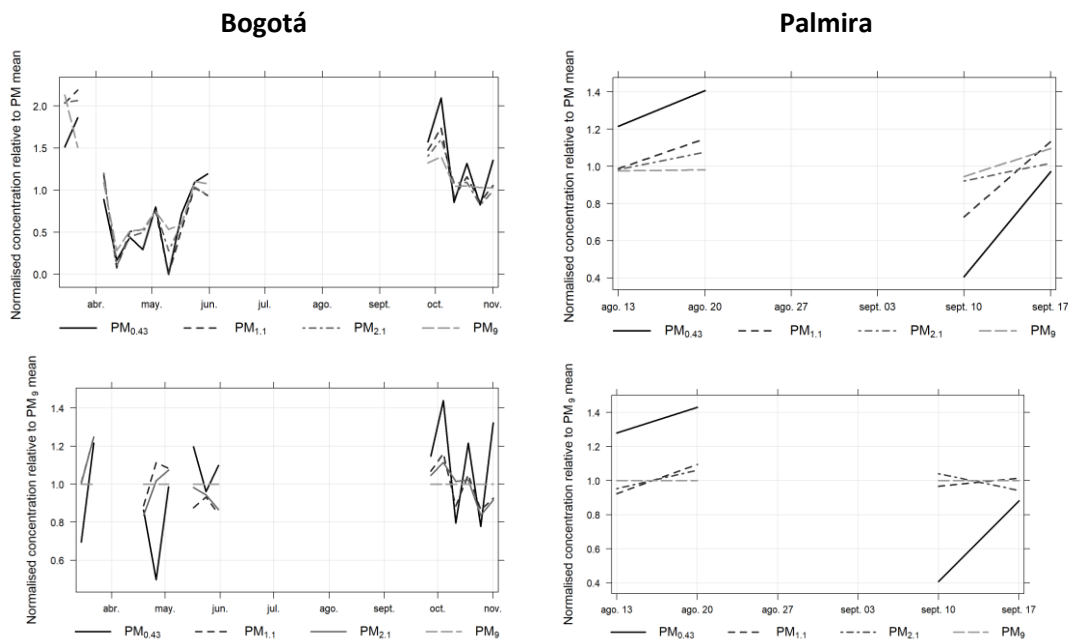
Bogotá

Palmira

Figure S3-3. Normalised meaning concentrations of PM$_9$, PM$_{2.1}$, PM$_{1.1}$ and PM$_{0.43}$ and the fractions (PM$_{0.43}$/ PM$_9$), (PM$_{1.1}$/ PM$_9$), (PM$_{2.1}$/ PM$_9$) and (PM$_9$/ PM$_9$) in Bogotá and Palmira.
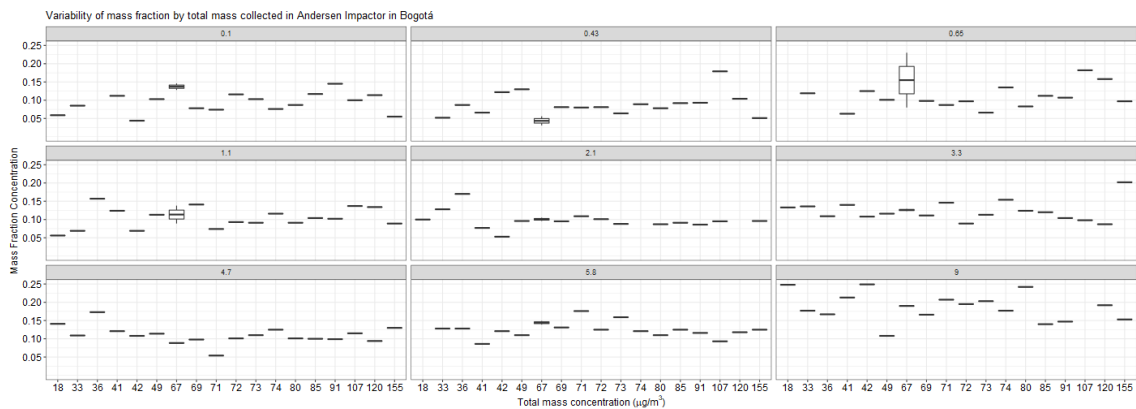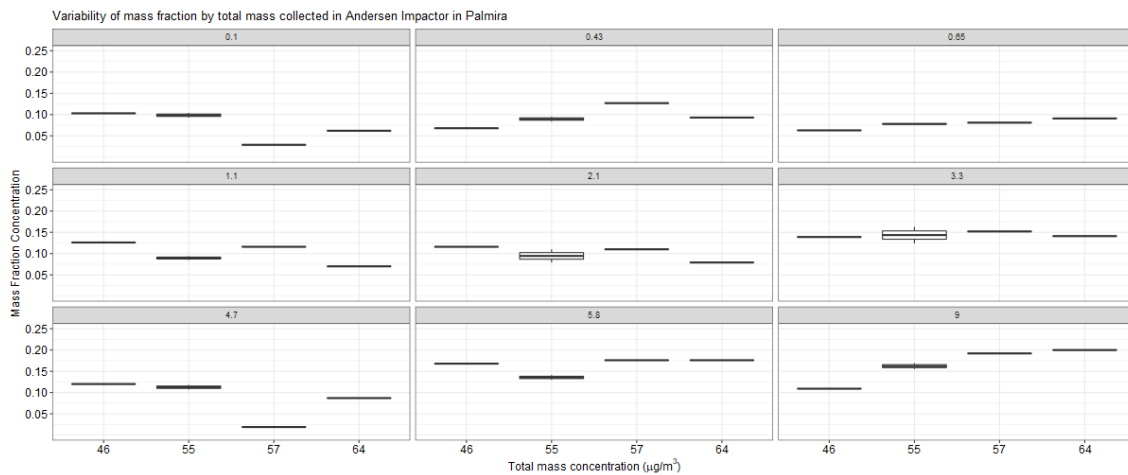
Figure S3-4. Boxplot of mass fraction collected in each stage of Andersen Impactor in observations carried out in a urban and suburban area in Colombia.
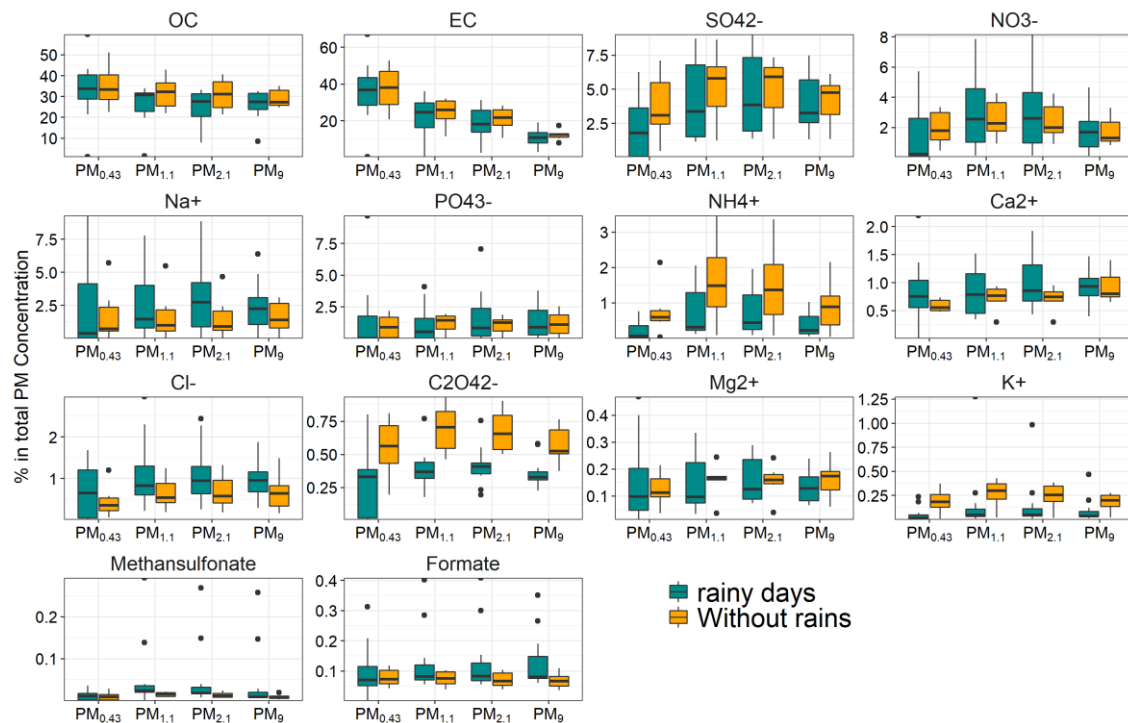
Figure S3-5. Percentage of each chemical specie over the total mass concentration of PM_9, $PM_{2.1}$, $PM_{1.1}$ and $PM_{0.43}$ for samples collected in Bogota. The green boxplots correspond to the samples collected on days when rained and the orange boxplots correspond to samples collected on days with no rain events.
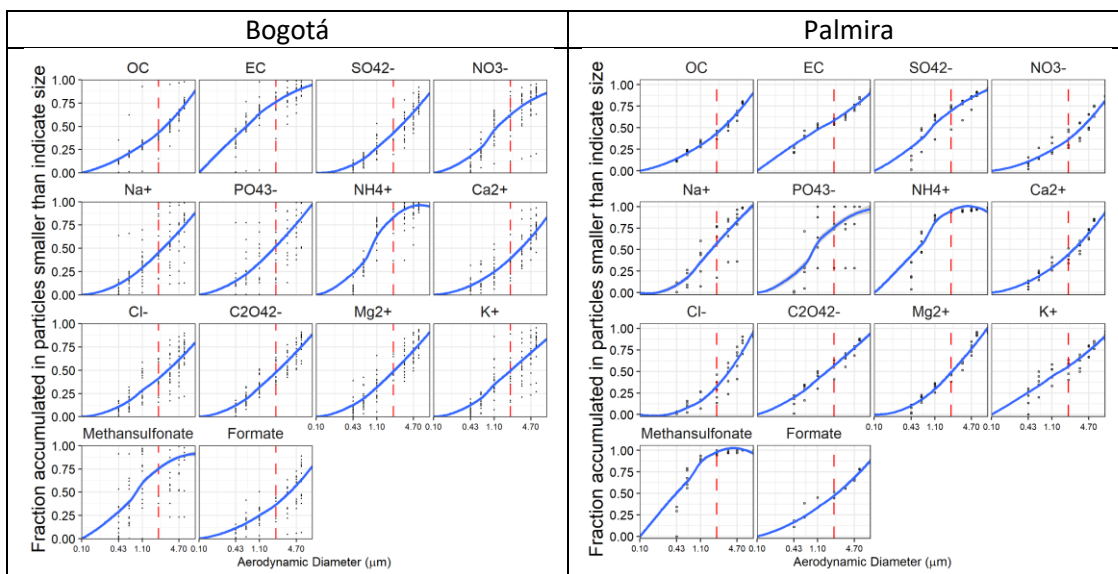
Figure S3-6. The plot of the mass fraction accumulated contained in the smaller particles than the aerodynamic diameter (μm). The red dotted line divides the fine (PM < 2.1 μm) from the coarse (PM > 2.1 μm) modes. the right side of the red dashed line corresponds to coarse mode, and the left side to fine mode. Black points show the mass fraction mass accumulated relative to each chemical species that were examined in each sample collected in the Andersen Cascade Impactor.

Table S 3-1. Median concentrations of chemical species ($\mu g/m^3$) size segregated in aerosol particles in Bogotá D.C.

Constituents	Dp <0.43 μm		0.43 – 0.65		0.65- 1.1		1.1 – 2.1		2.1-3.3		3.3-4.7		4.7 – 5.8		5.8- 9		Dp>9 μm	
	mean	sd	mean	sd	mean	sd	mean	sd	mean	sd	mean	sd	mean	sd	mean	sd	mean	sd
PM Concentration	7.161	3.577	6.407	4.092	8.919	5.236	7.601	4.021	6.541	3.051	8.921	6.012	7.569	3.981	9.043	3.895	12.535	5.714
OC	2.284	1.044	1.728	0.967	2.067	1.372	1.856	1.145	1.966	0.929	2.127	0.938	2.641	0.961	2.039	0.875	2.367	1.277
EC	2.510	1.370	1.319	0.958	1.096	0.783	0.732	0.533	0.332	0.214	0.366	0.375	0.387	0.575	0.244	0.133	0.303	0.298
SO_4^{2-}	0.205	0.227	0.305	0.294	0.590	0.558	0.433	0.351	0.263	0.185	0.284	0.225	0.324	0.286	0.243	0.137	0.402	0.516
Na^+	0.172	0.288	0.112	0.127	0.178	0.185	0.263	0.477	0.154	0.130	0.157	0.137	0.137	0.140	0.103	0.110	0.396	1.016
$NO3^-$	0.125	0.143	0.188	0.156	0.343	0.358	0.196	0.214	0.072	0.063	0.069	0.065	0.065	0.100	0.053	0.040	0.112	0.145
PO_4^{3-}	0.130	0.297	0.071	0.107	0.073	0.118	0.165	0.439	0.099	0.116	0.092	0.120	0.080	0.109	0.049	0.135	0.053	0.146
Ca^{2+}	0.053	0.062	0.041	0.033	0.073	0.058	0.086	0.101	0.067	0.035	0.081	0.055	0.080	0.046	0.080	0.060	0.149	0.176
NH_4^+	0.034	0.051	0.090	0.119	0.178	0.278	0.079	0.123	0.005	0.007	0.008	0.029	0.022	0.083	0.001	0.001	0.002	0.002
Cl^-	0.037	0.040	0.054	0.037	0.091	0.094	0.066	0.054	0.043	0.031	0.053	0.039	0.069	0.047	0.061	0.045	0.110	0.118
$C_2O_4^{2-}$	0.028	0.025	0.037	0.031	0.056	0.057	0.042	0.032	0.032	0.021	0.032	0.022	0.035	0.030	0.023	0.011	0.045	0.084
Mg^{2+}	0.010	0.013	0.009	0.009	0.016	0.016	0.015	0.017	0.011	0.009	0.012	0.010	0.011	0.009	0.008	0.007	0.014	0.022
K^+	0.007	0.010	0.012	0.018	0.031	0.054	0.010	0.013	0.004	0.004	0.006	0.008	0.008	0.019	0.005	0.005	0.026	0.078
CHO_2^-	0.007	0.005	0.007	0.005	0.007	0.003	0.006	0.003	0.006	0.001	0.009	0.009	0.008	0.005	0.013	0.014	0.043	0.123
Methansulfonate	0.001	0.001	0.002	0.004	0.003	0.004	0.002	0.003	0.001	0.003	0.001	0.003	0.002	0.004	0.001	0.002	0.001	0.002
F^-	0.000	0.000	0.001	0.001	0.001	0.002	0.001	0.001	0.001	0.002	0.002	0.003	0.002	0.003	0.001	0.002	0.003	0.009
NO_2^-	0.000	0.001	0.000	0.001	0.001	0.001	0.001	0.001	0.001	0.001	0.001	0.001	0.001	0.001	0.001	0.000	0.004	0.012
Br^-	0.000	0.000	0.000	0.002	0.001	0.002	0.000	0.002	0.000	0.000	0.000	0.000	0.000	0.000	0.000	0.000	0.000	0.000

4. Understanding aerosol composition in a tropical inter-Andean valley impacted by agro-industrial and urban emissions

The chemical characterization of PM$_{2.5}$ atmospheric particles was conducted in the municipality of Palmira, located in the Cauca River Valley Department in Colombia. The sampling campaign was carried out at the administrative building at the Palmira Campus of Universidad Nacional de Colombia, between July 25th and September 19th, 2018, with the cooperation of the research group colleagues Angela Vargas and German Rueda Saa. The chemical analysis of PM$_{2.5}$ samples was performed at Leibniz Institute for Tropospheric Research, TROPOS, with the guidance and support of Dominik van Pinxteren, Manuela van Pinxteren and Khanneh Wadinga Fomba.

The analysis results of the PM$_{2.5}$ chemical characterization was published in the manuscript titled: "*Understanding aerosol composition in a tropical inter-Andean valley impacted by agro-industrial and urban emissions*" (Mateus-Fontecha et al., 2022). The author of this dissertation set the instruments, performance of the PM2.5 sampling, carried out the sample chemical analysis, analyzed the chemical results, and prepared the draft paper, with substantial contributions from the adviser and co-adviser of this dissertation, Nestor Rojas and Rodrigo Jimenez, who led the research.

Mateus-Fontecha, Lady, Vargas-burbano, A., Jimenez, R. and Rojas, N. Y.: Understanding aerosol composition in a tropical inter-Andean valley impacted by agro-industrial and urban emissions, Atmos. Chem. Phys., 22, 8473–8495, 2022.

The paper is presented as part of this dissertation and is reproduces below:

Abstract.

Agro-industrial areas are frequently affected by various sources of atmospheric pollutants that have a negative impact on public health and ecosystems. However, air quality in these areas is infrequently monitored because of their smaller population compared to large cities, especially in developing countries. The Cauca River valley (CRV) is an agro-industrial region in southwestern Colombia, where a large fraction of the area is devoted to sugarcane and livestock production. The CRV is also affected by road traffic and industrial emissions. This

study aims to elucidate the chemical composition of particulate matter fine mode ($PM_{2.5}$) and to identify the main pollutant sources before source attribution. A sampling campaign was carried out at a representative site in the CRV region, where daily averaged mass concentrations of $PM_{2.5}$ and the concentrations of water-soluble ions, trace metals, organic and elemental carbon, and various fractions of organic compounds (carbohydrates, n alkanes, and polycyclic aromatic hydrocarbons – PAHs) were measured. The mean $PM_{2.5}$ was 14.4 ± 4.4 $\mu g\ m^{-3}$, and the most abundant constituent was organic material (52.7% ± 18.4%), followed by sulfate (12.7% ± 2.8%), and elemental carbon (7.1% ± 2.5%), which indicates the presence of secondary aerosol formation and incomplete combustion. Levoglucosan was present in all samples, with a mean concentration of (113.8 ± 147.2 $ng\ m^{-3}$), revealing biomass burning as a persistent source. Mass closure using the elemental carbon (EC) tracer method explained 88.4% of $PM_{2.5}$, whereas the organic tracer method explained 70.9% of $PM_{2.5}$. We attribute this difference to the lack of information of specific organic tracers for some sources, both primary and secondary. Organic material and inorganic ions were the dominant groups of species (79% of $PM_{2.5}$). OM_{prim} and OM_{sec} contribute 24.2% and 28.5% to $PM_{2.5}$. Inorganic ions as sulfate, nitrate and ammonia constitute 19.0%, EC 7.1%; dust 3.5%, particle-bounded water (PBW) 5.3%, and TEO, 0.9% of $PM_{2.5}$. The aerosol was acidic, with a pH of 2.5 ± 0.4, mainly because of the abundance of organic and sulfur compounds. Diagnostic ratios and tracer concentrations indicate that most $PM_{2.5}$ was emitted locally and had contributions of both pyrogenic and petrogenic sources, that biomass burning (BB) was ubiquitous during the sampling period and was the main source of PAHS, and that the relatively low $PM_{2.5}$ concentrations and mutagenic potentials are consistent with low-intensity, year-long BB and sugarcane PHB in CRV.

Keywords: agro-industry; pre-harvest burning; $PM_{2.5}$; chemical speciation; Northern South America

4.1.   Introduction

Urban and suburban locations, with moderate to high population densities, are exposed to air pollutant emissions, including of fine particulate matter (PM) from industry, road traffic, and other anthropogenic activities. Suburban areas may also be impacted by emissions from agricultural activities (Begam et al., 2016). Air quality in areas under these conditions is infrequently monitored, particularly in developing countries, despite the extensive use of highly emitting practices, including the intensive use of insecticides and pesticides, fire for

land and crop management, and diesel-based mechanization (Aneja et al., 2008, 2009). Agricultural sources emit pollutants, such as volatile organic compounds (VOCs), which are precursors of tropospheric ozone (Majra, 2011), and secondary organic aerosols (SOAs; (Majra, 2011). Most agricultural activities also emit $PM_{2.5}$ (solid and liquid particles with aerodynamic diameters smaller than 2.5 μm), which may contain black carbon (BC) and toxic and carcinogenic pollutants, e.g., polycyclic aromatic hydrocarbons (PAHs). Other agricultural activities, including mechanized land preparation, sowing and harvesting, consume significant volumes of fossil fuels, particularly diesel, and emit trace gases (including CO_2, CO, SO_2, NOx, NH_3 and VOC) that also generate O_3 and SOA, all of which affect human health and climate (Yadav and Devi, 2019). Furthermore, agricultural operations are a significant source of nitrogen-containing trace gases (NO_2, NO, NH_3 and N_2O) that are released from fertilizers, livestock waste, and farm machinery into the atmosphere (Sutton et al., 2011). Also, poultry and pig farming are high emitters of sulfur compounds, particularly H_2S.

The Cauca River valley (CRV) is an inter-Andean valley in southwester Colombia, with a flat area of 5287 km^2 (248 km long by 22 km mean width), a mean altitude of 985 m MSL (Figure 1). CRV is bounded by the Colombian Andes Western and Central Cordilleras, and is located at ~120 km from the Pacific Ocean. CRV encompasses the cities of Cali, Colombia's third-largest city with 2.2 million inhabitants (inhab), Yumbo (129 thousand inhab), an important industrial hub, and Palmira (313 thousand inhab), an important agro-industry center. Industry is also present in the other major CRV cities (Tuluá, Cartago, Jamundí, and Buga).

CRV hosts a highly efficient, resource-intensive sugarcane agro-industry with one of the highest biomass yields (up to 120 ton ha^{-1}) and the highest sugar productivities in the world (~13 ton sugar per hectare; (Asocaña, 2018, 2019). Sugarcane sowing, harvesting, and transport to mills are all mechanized and use diesel as fuel. Besides, all the sugarcane bagasse is used, to either to produce heat and electric power (cogeneration) or as feedstock to the local paper industry. Moreover, although pre-harvest burning is being phased out in the CRV, one-third of the sugarcane area in 2018 was burned prior to harvesting. CRV is also the third-largest poultry producer (351,104 ton yr^{-1}), and the first egg producer (4559 $x10^6$ million units per year) in Colombia (Min.Agricultura, 2020). In addition, CRV produces 15.1% of Colombia's pork meat (over 1 million pigs in stock) (Min.Agricultura, 2019) and 1.8% of national beef production (467,782 heads in stock) (Min.Agricultura, 2018). Poultry and livestock production are significant sources of H_2S and NH_3. Besides a long-time established energy-intensive industry, there are also a variety of smaller industries, including brick kilns. Regarding mobile

sources, there are nearly 2 million vehicles (1,951,638 vehicles) registered in CRV (RUNT, 2021). These include the standard urban categories along with off-road unregulated farming machinery. The sugarcane agroindustry uses multi-car trailers towed by diesel-powered tractors, with enough annual activity to be considered an independent source (the activity of which is proportional to the sugarcane harvested area and the distance to sugar mills). Overall, CRV mobile sources consumed 772 million L of gasoline and 590 million L of diesel in 2018 (SICOM, 2018). Moreover, the local airport, the most important in southwest Colombia, located very close to Palmira, handled 1.3 million passengers in 2019 (Aerocivil, 2019). Also, 1657 ha of sugarcane and corn were fumigated in 2020 using small aircraft (Aerocivil, 2020).

For this research, we prepared a preliminary, aggregated PM_{10} emission inventory for CRV by putting together disparate source data, including from the stationary source emission inventories of CRV's six largest cities (Cali, Tuluá, Cartago, Jamundí, Palmira, Yumbo and Buga), Cali's and other cities' mobile source emission inventories, and our estimation of sugarcane pre-harvest burning (PHB) and other point, linear and area sources (Table S4-1). Our preliminary inventory indicates that the manufacturing industry is by far the main PM_{10} emitter in CRV, with annual emissions of ~11.4 Gg PM_{10}. PM_{10} emissions from mobile sources (~1.4 Gg PM_{10} yr^{-1}) and open-field sugarcane pre-harvest burning (1.7 Gg PM_{10} yr^{-1}) are a factor ~5 smaller. The emissions of inorganic and organic secondary aerosol precursors are also significant. We estimate that 30.1 Gg of SO_2 are annually emitted in CRV (41% from sugar mills and other agro-industries, 32% from food industries, and 9% from cement, ceramic, and asphalt production). Emissions of volatile organic compounds (VOCs) are very similar (34.7 Gg yr^{-1}). Although a significant number of coal-fired boilers have been converted to natural gas, CRV's sulfur-rich coal (1.4-4% total S) is still an important industrial fuel. It must be stressed that this is a preliminary, not fully updated, regional inventory. The available information was insufficient for disaggregating the fine-mode PM emissions ($PM_{2.5}$). The multiplicity, disparity, and uncertainty of sources are indicative of the complexity of the $PM_{2.5}$ source identification, quantification, and location tasks.

The determination of the particulate matter (PM) chemical composition is instrumental for the apportionment of pollutant sources. Most field measurement-based studies have been conducted in North America, Europe, and Asia (Karagulian et al., 2015). The number of studies in Latin America and the Caribbean (LAC) is much smaller and have focused on the chemical composition of PM_{10} (Pereira et al., 2019; Vasconcellos et al., 2011), as well as the PM source apportionment in urban areas of Colombia (Ramírez et al., 2018; Vargas et al., 2012), Chile (Jorquera and Barraza, 2012, 2013; Villalobos et al., 2015), Costa Rica (Murillo et al., 2013) and

Brazil (de Andrade et al., 2010). The number of studies that involve agro-industrial sources and their impact on suburban areas is smaller. These include the Indo-Gangetic plain (Alvi et al., 2020), the Sao Paulo State in Brazil (Gonçalves et al., 2016; Urban et al., 2016), Ouagadougou in Burkina Faso (Boman et al., 2009), the Anhui Province in China (Li et al., 2014), for which the chemical composition of $PM_{2.5}$ and some of its sources have been identified. Likewise, regions in South America with sugarcane agroindustry, such as Mexico (Mugica-Alvarez et al., 2015; Mugica-Álvarez et al., 2016, 2018) and Brazil (de Andrade et al., 2010; De Assuncao et al., 2014; Lara et al., 2005; Pereira et al., 2017) have also reported on their agro-industry impact on $PM_{2.5}$ levels at nearby population centers. They are very few studies on air pollution in agro-industrial areas of Colombia. Most notably, Romero et al., (2013) measured PAHs and metals in PM_{10}. Most of the studies above identified biomass burning and fossil fuel combustion as significant PM sources, and some also identified industrial and fertilizer as relevant.

This research aimed to characterize the chemical composition of $PM_{2.5}$ at a representative location in the CRV, including EC, primary and secondary OC, ions, trace metals, and specific molecular markers, such as PAHS, n-alkanes, and carbohydrates, as well as the relationships among these components and with emission sources. Diagnostic ratios were used to identify the most important $PM_{2.5}$ components and as a tool for preliminary pollutant source attribution, including primary and secondary aerosols generated by or associated with sugarcane pre-harvest burning PHB. We believe that in the CRV case, this analysis is needed prior to source apportionment with receptor models for three reasons: 1) This is the first comprehensive investigation of PM composition in the CRV (prior studies included two types of components at most); 2) There are no suitable chemical profiles for some pollutant sources, particularly sugarcane PHB; 3) Our measurements dataset is just barely large enough for profile-free receptor modeling (positive matrix factorization). We expect that this study also motivates future research on source apportionment in the region. Our results are particularly relevant for urban communities and atmospheres impacted by large-scale intensive agriculture and industrial emissions, particularly in developing countries, especially in Latin America where PM composition information is still scarce (Liang et al., 2016).

4.2. Methods

4.2.1. Description of the sampling site

The sampling site was located on the rooftop of an 8-story administrative building at the Palmira Campus of Universidad Nacional de Colombia (3º30'44.26" N; 76º18'27.40" W, 1065 m altitude), about 27 m above the ground. The campus is located on the western outskirts of Palmira's urban area and is surrounded by short buildings on the east, and extensive sugarcane plantations, several sugar mills, and other industries elsewhere. Palmira is located at ~27 km northeast of Cali and ~22 km southeast of Yumbo, an important industrial hub. The Pacific Ocean coastline stretches at ~120 km across the Western Cordillera, as shown in Figure 3-16, where operates one of the busiest international trade seaports in Colombia (López, 2017). Most of the freight is transported by diesel-powered trucks. Road traffic is also substantial within the CRV, with Bogota and along the Pan-American highway that connects Colombia with other South American countries (Orozco et al., 2012).
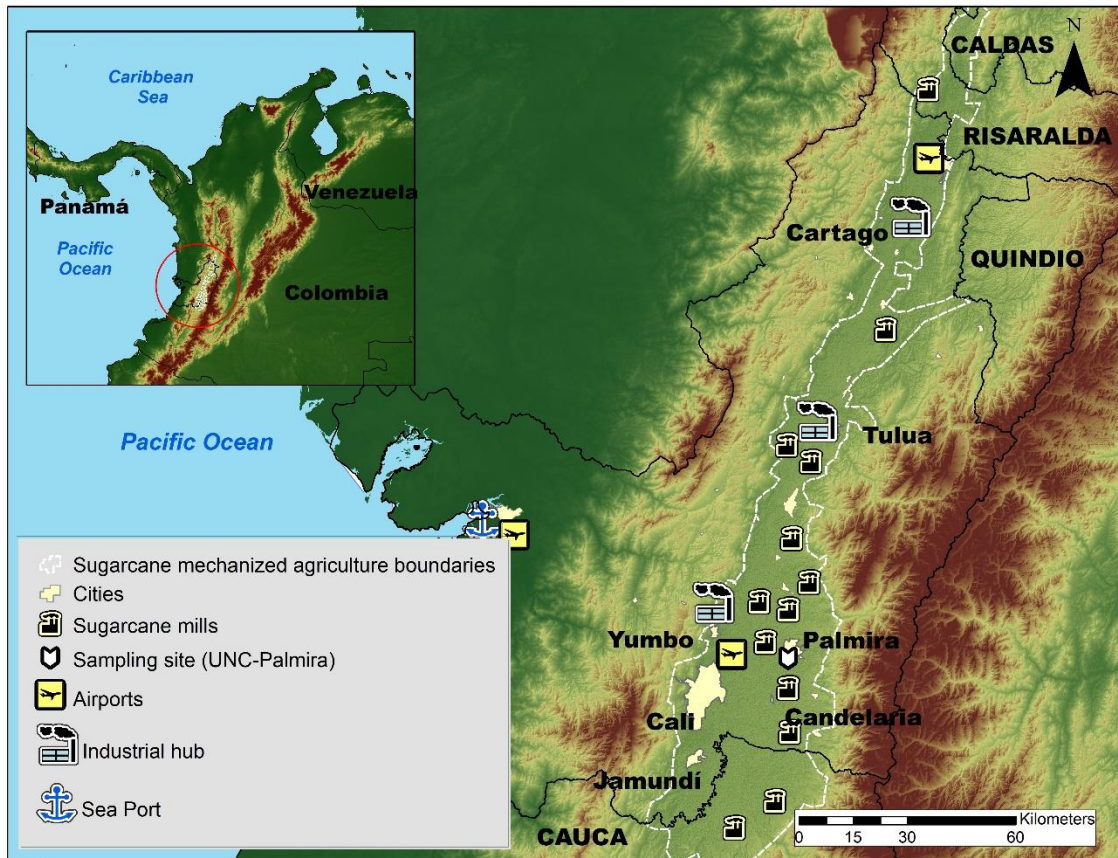
Figure 3-16. Map of the Cauca River Valley (CRV). The inset shows the location of CRV in Colombia and in Northern South America. The map shows the main cities in CRV, including Palmira (312 thousand inhabitants), our measurement site, Cali, the largest city in the southwest of Colombia, Yumbo, an industrial hub, and the main highways. Sugar mills, which produce sugar, bio-ethanol, and electric power are also shown. The dashed-line defined area is CRV's flattest (slope < 5%) bottomland, where mechanized, intensive sugarcane agriculture takes place. Significant diesel combustion emissions occur along the Buenaventura highway because it is one of the busiest ports in Colombia.

The Andes Cordillera splits into three south-to-north diverging mountain ranges (Western, Central, and Eastern Cordilleras) near the Colombia-Ecuador border (Figure 3-16). The

Western Cordillera separates the CRV from the Colombian Pacific Ocean watershed, the rainiest region on Earth (Hernández and Mesa, 2020) The elevated precipitation in this basin (Mesa and Rojo, 2020) is due to the presence of a Walker cell convergence zone at the surface, persistent under neutral and La Niña conditions. This synoptic feature is one of the most important determinants of atmospheric circulation in Colombia, with prevailing east-to-west winds in the lower troposphere along with upper troposphere return winds (Mesa and Rojo, 2020). The Andean Cordilleras are nevertheless effective barriers to the Walker circulation near the CRV surface (Lopez and Howell, 1967; Mesa S. and Rojo H., 2020). The elevated humidity in the Pacific Ocean watershed and the closeness of the two Andes branches drive a zonal regional circulation pattern, consisting ~~in~~ of west-to-east anabatic winds over the Pacific slope of the Western Cordillera during the daytime followed by rapid katabatic winds in the late afternoon (Lopez and Howell, 1967). These winds rapidly ventilate the CRV during the late afternoon – early evening period on an almost regular basis. CRV is wide (~22 km) and long (~248 km) enough to develop a valley-mountain wind circulation pattern during the daytime. Winds are very mild during this time period and expected to be highly dispersive, i.e. with high turbulence intensities (Ortiz et al., 2019). The arrival of the katabatic "tide" in the late afternoon wipes the valley-mountain wind pattern out (Lopez and Howell, 1967).

4.2.2. Sampling protocols

The sampling campaign was conducted between July 25th and September 19th, 2018. $PM_{2.5}$ aerosol particles (aerodynamic diameter < 2.5 μm) were collected on Teflon and quartz fiber filters simultaneously for 23 h (from 12:00 local time – LT – to the next day at 11:00 LT), using 2 in-tandem low-volume samplers (ChemComb speciation samplers, R&P). Each sampler used an independent pump set at a flow rate of 14 L min^{-1}. For both types of filters, three lab blank filters without exposure were analyzed. Quartz filters were pre-baked at 600 °C for 8 h before sampling to eliminate contaminant trace hydrocarbons. In total, 45 samples were collected. Prior to and after exposure, the filters were conditioned at constant humidity (36±1.5% relative humidity) and temperature (24 ± 1.2 ºC) for 24 h before being weighing on a microbalance (Sartorius, Mettler Toledo) with a 199.99 g capacity and 10 μg resolution. $PM_{2.5}$-loaded filters were saved at Petri boxes previously prepared to avoid cross-contamination of organic species. The filters were subsequently stored at –20°C until analysis to reduce the volatilization of species such as ammonium nitrate and semi-volatile organic compounds. Blank quartz filters were pre-baked and stored following an identical procedure to exposed filters to collect samples. Blank Teflon filters were treated under the same conditions of

storage, transport, and analysis as $PM_{2.5}$-loaded filters. By differential weighing, mass concentrations were determined from the Teflon filters.

Several frequent challenges can affect compound measurements in particle matter, including: 1) The absorption of some gases in the inlet's galvanic steel, which alters the gas and particle balance of the $HNO_3 \Leftrightarrow NO_3^-$ system of particles collected. During the collecting of the samples for this study, no denuders were utilized. 2) Significant temperature changes during sampling and then in the conditioning before to filter weighing can cause ammonium nitrate to volatilize. Because the samples were collected at temperatures ranging from 17 to 33 C and then conditioned to 25 C, the equilibrium of the $HNO_3 \Leftrightarrow NO_3^-$ system could be a source of ambiguity in the data reported here. The vaporization of some semi-volatile organic species throughout the sampling and storage period, as well as the absorption of organic gases over the filter material, are two additional sources of uncertainty.

It's worth mentioning that during the sampling period, 1888 sugarcane PHB episodes occurred. This register was made by the regional environmental agency (CVC, as per its acronym in Spanish), using information from sugar mills about PHB events. The vast majority of these events were intentional, controlled, size-limited (~6 ha median area), and brief (~25-minute median duration) (Fig S1).

4.2.3.   Analytical methods

The quartz-fiber filter samples were analyzed for ions, metals, elemental and organic carbon, and speciation of the carbonaceous fraction. The Teflon-membrane filter samples were analyzed for metals.

Two circular pieces with an 8 mm diameter (100.5 mm^2) were punched from each quartz and Teflon filter, following the method described by Wadinga Fomba et al., (2020), and extracted using 1 mL of ultrapure water (18 MΩ) in a shaker at 400 rpm for 120 min. The extracts were filtered through 0.45 μm syringe filters (Acrodisc Pall). An aliquot of the solution was analyzed for inorganic (K^+, Na^+, NH_4^+, Mg^{2+}, Ca^{2+}, Cl^-, NO_3^-, SO_4^{2-}, NO_2^-, PO_4^{3-}, Br^-, F^-) and some organic ions ($C_2O_4^{2-}$, $CH_3O_3S^-$, and CHO_2^-) by ion chromatography (IC690 Metrohm; ICS3000, Dionex). Another aliquot was analyzed for carbohydrates, including levoglucosan, mannosan, and galactosan, as described by Iinuma et al. (2009a). Organic and elemental carbon were determined from 90.0 mm^2 filter pieces following the EUSAAR 2 protocol (Cavalli et al., 2010), with a thermal-optical method using a Sunset Laboratory dual carbonaceous analyzer.

Seventeen metals, including K, Ca, Ti, V, Cr, Mn, Fe, Ni, Cu, As, Se, Sr, Ba, Pb, Sn, Sb, and Cu, were analyzed from Teflon (22 samples) and quartz (23 samples) filters by total reflection X-Ray Fluorescence Spectroscopy – TXRF (TXRF, PICOFOX S2, Bruker). Si was not determined as this element is part of the quartz filter substrate. Metals were analyzed from three 8-mm circular pieces punched from Teflon filters, which were digested a nitric and chloride acid solution for 180 min at 180 °C. After this, 20-µl aliquots of the digested solution were placed on the surface of polished TXRF quartz substrates along with 10 µl of Ga solution, which served as an internal standard. This solution was left to evaporate at 100°C. The samples were measured at two angles with a difference of 90° between them to ensure complete excitation of metals. More details on the analytical technique can be found in Fomba et al. (2013).

Alkanes and PAHs were determined from two circular filter punches (6 mm diameter, 56.5 mm^2), using a Curie-point pyrolyzer (JPS-350, JAI) coupled to a GC-MS (Gas Chromatography Mass Spectrometry) system (6890 N GC, 5973inert MSD, Agilent Technologies). The chemical identification and quantification of the C_{20} to C_{34} n-alkanes, as well as the following organic species were performed using the following external standards (Campro, Germany): pristane, phytane, fluorene (FLE), phenanthrene (PHEN), anthracene (ANT), fluoranthene (FLT), pyrene (PYR), retene (RET), benzo(b)naphtho(1,2-d)thiophene (BNT(2,1)), cyclopenta(c,d)pyrene (CPY), benz(a)anthracene (BaA), chrysene(+Triphenylene) (CHRY), 2,2-binaphtyl (BNT(2,2)), benzo(b)fluoranthene (BbF), benzo(k)fluoranthene (BkF), benzo(e)pyrene (BeP), benzo(a)pyrene (BaP), indeno (1,2,3-c,d)pyrene (IcdP), dibenz(a,h)anthracene (DahA), and benzo(g,h,i)perylene (BghiP), coronene (COR), 9H-Fluoreneone (FLO(9H)), 9,10-Anthracenedione (ANT (9,10)) and 1,2-Benzanthraquinone (BAQ (1,2)). Four deuterated PAHs, (acenaphthene-d10, phenanthrene-d10, chrysene-d12, and perylene-d12), and two deuterated alkanes (tetracosane-d50 and tetratriacontane-d70) were used as internal standards, following the analytical method described by (Neusüss et al., 2000). For each analyzed compound, the sample concentration was calculated by subtracting the average concentration of three blank filters from the measured concentration.

4.2.4.   Diagnostic ratios and mass closure

The main $PM_{2.5}$ components were estimated from the concentrations of EC, OC, water-soluble ions (NO_3^-, SO_4^{2-}, NH_4^+, and Na^+), and tracer metal concentrations (Ca, Ti, Fe, Ni, Cu, Zn, As, Se, Sb, Ba, and Pb) as follows: organic material (OM), EC, ammonium sulfate ((NH_4)$_2SO_4$), ammonium nitrate (NH_4NO_3), crustal material (dust), other trace elements oxides (TEOs), and particle-bounded water (PBW). $PM_{2.5}$ closure is described by Equation 4-1 (Dabek-Zlotorzynska

et al., 2011). We used the Interagency Monitoring of Protected Visual Environment (IMPROVE) equations (Chow et al., 2015) to quantify the concentrations of main compounds (Table 4-2). The aerosol particle bounded water content was estimated from the measured ionic composition, relative humidity, and temperature, following the aerosol inorganic model (AIM) described by (Clegg and Peter Brimblecombe, 1998), which is available for running online at http://www.aim.env.uea.ac.uk/aim/model2/model2a.php. The thermodynamic equilibrium of the system H^+- NH_4^+ - Na^+ - SO_4^{2-} - NO_3 - Cl^- - H_2O is described by AIM.

Equation 4-1

$$PM2.5(mass\ closure\ estimated) = OMpri + OMsec + EC + NH4SO4 + NH4NO3 + Dust + TEO + SS + PBW$$

Table 4-2. Equations used to estimate the main components of $PM_{2.5}$

Component	Equation	Reference
OM_{prim}	$= f_1\, OC_{prim}$	(Chow et al., 2015) (Turpin and Lim, 2001)
OM_{sec}	$= f_2\, OC_{sec}$	(El-Zanan et al., 2005)
SO_4	$= SO_4^{2-}$	(Chow et al., 2015)
NO_3	$= NO_3^-$	(Chow et al., 2015)
Dust	$= 1.63Ca + 1.94Ti + 2.42Fe$ (Assuming CaO, Fe_2O_3, FeO (in equal amounts) and TiO_2)	(Chow et al., 2015)
PBW	$= k\,(SO_4^{2-} + NH_4^+)$	(Clegg and Peter Brimblecombe, 1998)
TEO	$= 1.47[V] + 1.27[Ni] + 1.25[Cu] + 1.24[Zn] + 1.32[As] + 1.2[Se] + 1.07[Ag] + 1.14[Cd] + 1.2[Sb] + 1.12[Ba] + 1.23[Ce] + 1.08[Pb]$	(Snider et al., 2016)

f_1 = 1.6. This factor was estimated considering the predominant sources.

f_2 = 2.1. This factor was estimated by subtracting the non-carbon component of $PM_{2.5}$ from the measured mass.

k = 0.32 was calculated using the Aerosol Inorganic Model.

The EC tracer method was applied to estimate primary (OC_{prim}) and secondary (OC_{sec}) organic carbon (Lee et al., 2010). This method utilizes EC as a tracer for primary OC, which implies that OC_{prim} from non-combustion sources is deemed negligible. Primary and secondary OC can be estimated by defining a suitable primary OC to EC ratio ($[OC/EC]_{prim}$). See Equation 4-2 and Equation 4-3. We estimated the $[OC/EC]_{prim}$ ratio as the slope of a Deming linear fit between EC and OC measurements. The term b corresponds to the linear fit intercept, which can be interpreted as the emitted OC_{prim} that is not associated with EC emissions. This method is limited by the following assumptions: 1) $[OC/EC]_{prim}$ is deemed constant, despite the reality

that it may change throughout the day depending on factors such as wind direction and the location of the dominant emission sources. Our 23-h sampling is expected to smooth this variability source out; 2) It neglects OC_{prim} from non-combustion sources; and 3) It assumes that OC_{prim} is nonvolatile and nonreactive. Departure from these assumptions implies that the estimation of OC_{prim} and OC_{sec} might be biased, likely underestimating OC_{sec}.

Equation 4-2 $$OCprim = OC/ECmin * EC + b$$

Equation 4-3 $$OCsec = OC - OCprim$$

OC_{prim} was also estimated by using an organic tracers method from three sources significant in the CRV, namely fossil fuel combustion (OC_{FF}), biomass burning (OC_{BB}), and vegetable detritus (OC_{det}). OC_{FF}, OC_{BB} and OC_{det} were estimated using a fitted linear model (Equation 4-4) by robust regression with a M estimator with bisquare function, which were find the coefficients X, Y and Z to multiply the tracers concentrations of each source. The tracers used were the sum of the BghiP and IcdP for fossil fuel (T_{FF}); levoglucosan for biomass burning (T_{BB}); and the sum of the highest molecular weight alkanes ($C_{27} - C_{33}$) for vegetable detritus (T_{det}). The sum of each tracers multiply by X, Y and Z, respectively, Equation 4-5, corresponding to OC_{prim} attributed to known sources present in CRV. Th substration of OC_{prim} atributed to OC total is named OC_{rest}, which corresponding to another sources of OC primary and OC secondary (Equation 4-6).

Equation 4-4 $$OCprim = (TFF * X) + (TBB * Y) + (Tdet * Z)$$

Equation 4-5 $$OCprim = OCFF + OCBB + OCdet$$

Equation 4-6 $$OCrest = OC - OCprim$$

Following Table 4-2, OM was estimated from OC using conversion factors f_1 and f_2 (Chow et al., 2015), which are dependent on the OM oxidation level and the secondary organic aerosol formation and aging during transportation. Turpin and Lim (2001a) recommended an OM/OC ratio of 1.6 ± 0.2 for urban aerosols, and 2.1 ± 0.2 for non-urban aerosols, values comparable with those found by Aiken et al. (2008), of 1.71 (1.41 – 2.15), where lower values (1.6 – 1.8) are attributed to ground measurements in the morning, and higher values (1.8 – 1.9) to aircraft sample measurements. BB aerosols can have even higher f values (2.2-2.6), due to the presence of organic components with higher molecular weights, e.g., levoglucosan. However, Andreae (2019) recommends a factor of 1.6 for fresh BB aerosol, which is consistent with

Hodshire et al (2019). We believe that traffic and biomass burning are the dominant OC_{prim} sources at our site. Therefore, we used $f_1 = 1.6$ to estimate OM_{pri}. We used a factor of 2.1 to estimate OM_{sec} from the OC_{sec} fraction. This factor was chosen based on recommended ratios of 2.1±0.2 for aged aerosols (Schauer, 1998). Some of the global climate models used to estimate direct radiative forcing from organic material present in the aerosols employ OM/OC ratios without separating the sources, while others change the ratio depending on type of source using values ranging from 1.4 - 1.6 for fossil fuel and biofuel, and 2.6 for biomass burning. Other set of models use specific molecules as tracers to follow the OM, such as monoterpenes, isoprene, aromatics and alkanes. Tsigaridis et al., (2014) present a list of tracers than haven been used in various models to quantify OM in the aerosols.

Concentration ratios among distinct species were used to chemically characterize and infer the main sources of fine particle matter at Palmira. As a preliminary proxy for $PM_{2.5}$ acidity, the cation/anion equivalent ratio and the $[NH_4^+]/[SO_4^{2-}]$ molar ratio were used. The first one is based on electroneutrality and assumes that H^+ balances the excess of anions in the solution considered, and the second one ratio is an indicator of acidity attributable to those two ions, which are usually the most abundant cation and anion contained in the $PM_{2.5}$. The cation equivalent to anion equivalent ratio was calculated using Equation 3-7 and Equation 4-8 for each term.

However, these approaches to inferring the $PM_{2.5}$ acidity can result in challenging interpretations, incomplete and incorrect results due to an indirect connection to the system's acidity (Pye et al., 2020). Therefore, the E-AIM (Extended Aerosol Inorganics Model) was used to determine the equilibrium state of a system containing water and the following ions: SO_4^{2-}, NH_4^+, NO_3^-, Na^+ and Cl^-, with an atmosphere of known temperature and relative humidity, without information on gas-phase concentrations (NH_3, HNO_3 and SO_2), which were not available in this study. The H^+ mole fraction concentration from E-AIM IV (Friese and Ebel, 2010), was used to calculate pH following Equation 4-9. E-AIM requires that the input data for ionic composition be balanced on an equivalent basis, which means that the sums of the charges on the cations and anions considered in the system do balance, accordingly $[SO_4^{2-}] + [NO_3^-] + [Cl^-] = [NH_4^+] + [Na^+]$. The disadvantage of this approach is that it does not allow for the partitioning of trace gases into the vapor phase. The model is available to run on the following website: http://www.aim.env.uea.ac.uk/aim/model4/model4a.php (last access: 22 January 2022).

Equation 3-7

$AE = SO42 - 48 + NO3 - 62 + C2O42 - 44 + Cl - 35 + PO43 - 31.3 + NO2 - 46 + Br - 79.9 + F - 18.9 + CH3O3S - 95 + CHO2 - 45$

Equation 4-8 $\quad CE = Na + 23 + K + 39 + NH4 + 18 + Mg2 + 12 + Ca2 + 20$

Equation 4-9 $\quad pHx = -log10(H+)$

Parent PAH ratios are widely used to identify combustion-derived PAHS (Khedidji et al., 2020; Szabó et al., 2015; Tobiszewski and Namieśnik, 2012), although some of them are photochemically degraded in the atmosphere (Yunker et al., 2002). Additionally, n-alkanes are employed as markers of fossil fuel or vegetation contributions to PM$_{2.5}$. Carbon number maximum concentration (C$_{max}$), carbon preference index (CPI), and wax n-alkanes percentage (WNA%) were the criteria utilized to determine the n-alkane origin. Table 4-3 summarizes the diagnostic ratio equations and the expected dominating source based on the ratio value.

Table 4-3. Diagnostic ratios of organic compounds used to infer the sources of $PM_{2.5}$ in this study.

Diagnostic ratios	Equation	Value	Source	References
BeP/(BeP+BaP)		~0.5 < 0.5	Fresh particles Photolysis	(Tobiszewski and Namieśnik, 2012)
IcdP/(IcdP+BghiP)		<0.2 0.2 - 0.5 >0.5	Petrogenic Petroleum combustion Grass, wood and coal combustion	(Yunker et al., 2002) (Tobiszewski and Namieśnik, 2012)
BaP/BghiP		<0.6 >0.6	Non-traffic emissions Traffic emissions	(Tobiszewski and Namieśnik, 2012) (Szabó et al., 2015)
IcdP/BghiP		>1.25 <0.4	Brown coal* Gasoline	(Ravindra et al., 2008)
LMW/(MMW+HMW)		<1 >1	Pyrogenic Petrogenic	(Tobiszewski and Namieśnik, 2012)
C_{max}		< C_{25} C_{27} – C_{34}	Anthropogenic Vegetative detritus	(Lin et al., 2010)
CPI	$CPI = 0.5 * 1933Ci2032Ck$ $+ 1933Ci2234Ck$	CPI ~1 CPI > 1	Fossil carbon Biogenic	(Marzi et al., 1993) (Kang et al., 2018)
WNA%	$WNACn= Cn - Cn + 1 + Cn - 12$ $WNA\% = WNACnTotal\ n - alkanes$ $PNA\% = 100 - WNA\%$	WNA ~ 100 PNA ~ 100	Biogenic Anthropogenic	(Lyu et al., 2019)

*Used for residential heating and industrial operation.

As all measured variables were subject to analytical uncertainty and temporal variability, linear fitting parameters were obtained from Deming regressions as recommended for atmospheric measurements (Wu and Zhen Yu, 2018). The Spearman coefficient was selected instead of Pearson's as an indicator of statistical correlation between chemical components to reduce the effect of outliers. Derived ratios and other parameters were considered statistically significant when p-values < 0.05. The statistical analysis was conducted using R version 4.0.2, 24 including the packages corrr (0.4.2), mcr (1.2.1), cluster (2.1.0), tidyverse (1.3.0), ggplot (3.3.2), MASS (7.3-53.1) and openair (2.7-4).

4.3.   Results and discussions

4.3.1.   Meteorology

One year prior to the sampling period, we monitored the local meteorology, first at 14.5 m above the ground, a few meters over the mean canopy level, and then at 32.5 m above the ground during the sampling campaign. The box-and-whisker plot in Fig 2 shows katabatic tide winds of up to ~8 m/s at the sampling site elevation, peaking at ~17:00 LT. Wind speeds were a factor ~2-3 slower at ground level. The wind runs at the sampling height were typically above ~200 km per day (Fig S3) indicating that the samples had substantially broader spatial coverage of the CRV, much larger than it would have been at ground level. This also implies that the samples were frequently and significantly influenced by emissions coming from Yumbo's industrial hub (northwest of Palmira), and also by Palmira and Yumbo urban and highway emissions, as well as sugarcane PHB and sugarcane mill emissions. The wind rose (Fig 2a) suggests that the influence of urban emissions from Cali, CRV's largest city by far, was minor. Other meteorological variables are reported in the Supplementary Material (SM) (Fig S2). Temperature (24.2ºC on average) and relative humidity (71.6%) were very likely controlled by solar radiation (350 W m^{-2} on average). The late-afternoon katabatic tide is fast enough to temporarily reduce temperature. The daily pressure profile (~763 hPa on average) clearly showed the influence of the katabatic tide, with a ~3 hPa drop during its arrival in the late afternoon. Overall, we believe our measurements at the Palmira site are reasonably representative of the regional air quality.
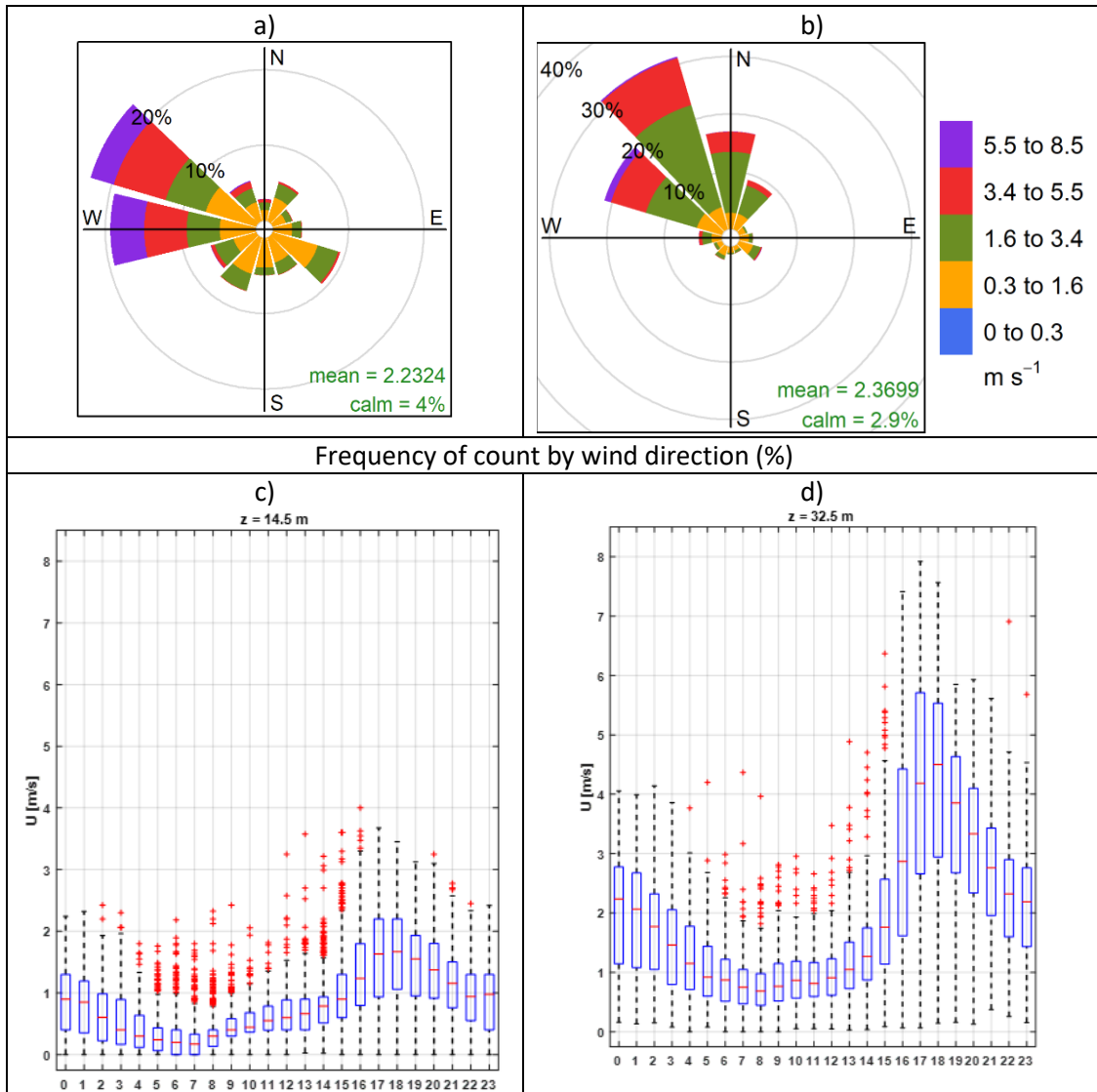
Figure 3-17. Wind pattern in the sampling location: a) predominant wind rose during the sampling period (July - September 2018), b) hourly profile of wind speed at 14.5 m above the ground (August – December 2017), and c) hourly profile of wind speed in sampling location at 32.5 m over the ground level (December 2017 – September 2018). *Red points corresponding to upper 10% outliers.

4.3.2. Bulk PM$_{2.5}$ concentration and composition

The daily PM$_{2.5}$ concentration measured in this study ranged from 6.73 to 24.45 µg m^{-3} with a campaign average of 14.38 ± 4.35 µg m^{-3} (23 h-average, ±1-sigma). Although these concentrations may appear comparatively low, it is worth stressing that samples were collected at more than 30 m height, with hourly wind speeds frequently above 4 m s^{-1}. However, most days during this study, PM$_{2.5}$ concentration exceeded the 5 µg m^{-3} annual mean and 15 µg m^{-3} 24-h mean guidelines by World Health Organization, (2021). Nevertheless, the Colombian standards are less demanding, thus observed concentrations comply with the 37 µg m^{-3} 24-h mean (MADS, 2017).

Previous studies conducted in rural areas of Brazil impacted by open field sugarcane burning reported significantly higher (mean 22.7 µg m^{-3}; Lara et al., 2005), similar (mean 18 µg m^{-3} Souza et al., 2014), and significantly lower PM$_{2.5}$ concentrations (mean 10.88 µg m^{-3}; Franzin et al., 2020). Comparable measurements in Mexico during harvest periods showed much higher concentrations, from 29.14 µg m^{-3} (Mugica-Alvarez et al., 2015) up to 51.3 µg m^{-3} (Mugica-Álvarez et al., 2016). Our PM$_{2.5}$ concentration measurements in the CRV are thus substantially lower than those usually reported in Mexico and Brazil during sugarcane burning periods. Major differences among sugarcane PHB practices in Colombia, Brazil and Mexico must be considered while comparing concentrations. First, ~1/3 of the sugarcane harvested area is burned before harvest at CRV. This fraction is much larger in Mexico and Brazil (FAO, 2020). Second, sugarcane is harvested year-round in CRV, as opposed to Brazil and Mexico, where harvest is limited to a ~6-month period (known in Spanish as *zafra*, "the harvest"). Third, the size of the individual plots burned in CRV is typically ~6 ha (median burned area; Cardozo-Valencia et al., 2019), compared to much larger plots and total areas in Brazil and Mexico (FAO, 2020).

OC was the most abundant measured PM$_{2.5}$ component with a mean daily concentration of 3.97 ± 1.31 µg m^{-3}, whereas the mean EC concentration was only 0.96 ± 0.31 µg m^{-3}. These two components contributed to 29.1 ± 8.3% and 7.2 ± 2.3% of the PM$_{2.5}$ mass, respectively (carbonaceous fractions were thus 4.93 ± 1.58 µg m^{-3}, i.e. 36.31 ± 10.41% of PM$_{2.5}$).

The most abundant water-soluble ions found in Palmira's PM$_{2.5}$ were SO$_4^{2-}$, NH$_4^+$, and NO$_3^-$, with average concentrations of 2.15 ± 1.39 µg m^{-3}, 0.67 ± 0.62 µg m^{-3}, and 0.51 ± 0.30 µg m^{-3}, respectively (12.7 ± 2.8%, 3.7 ± 1.1% and 2.6 ± 1.3% of mass concentration, respectively). Other water-soluble ions, such as Na$^+$, Ca$^+$, and C$_2$O$_4^{2-}$, had mean concentrations of around 0.1

$\mu g\ m^{-3}$, while those of K^+, PO_4^{3-}, $CH_3O_3S^-$, Mg^{2+}, and Cl^- had concentrations ranging from 10-80 $ng\ m^{-3}$ (Table 4-4).

The predominant elements were Ca (0.42 ±0.33 $\mu g\ m^{-3}$), K (0.13 ± 0.08 $\mu g\ m^{-3}$), and Fe (88 ± 65 $ng\ m^{-3}$), followed by Zn (34 ± 33 $ng\ m^{-3}$), Pb (18 ± 19 $ng\ m^{-3}$), Sn (52 ± 37 $ng\ m^{-3}$), Ti (5 ± 4 $ng\ m^{-3}$), Ba (9 ± 13 $ng\ m^{-3}$), Sr (2 ± 5 $ng\ m^{-3}$). Mn, Ni, Cr, and Se concentrations were below 2 ± 1 $ng\ m^{-3}$. Trace metals such as Ti, Cr, Mn, K, Ca, Fe, Ni, Cu, Zn Sr, Pb and Se were found in all $PM_{2.5}$ samples, while V was found only in a few samples. Other trace metals such as As and Sb were detected only at a reduced number of samples with concentrations below 20 $ng\ m^{-3}$. Table 4-4 shows the mean, standard deviation, minimum, and maximum concentration of the carbonaceous fraction, soluble ions, and metals found in the $PM_{2.5}$ samples collected in the CRV.

Table 4-4. Mean, 1 standard deviation, minimum and maximum concentrations of carbonaceous fraction, soluble ions, and metals in samples of $PM_{2.5}$ collected in Palmira.

Species	# of samples	Mean	SD	Min	Max	Units
$PM_{2.5}$	22	14.38	4.35	6.73	24.45	$\mu g\ m^{-3}$
OC	45	3.97	1.31	2.31	8.35	
EC	45	0.96	0.31	0.52	2.15	
SO_4^{-2}	45	2.15	1.39	0.98	10.27	
NH_4^+	45	0.67	0.62	0.18	4.29	
NO_3^-	45	0.51	0.30	0.11	1.45	
Na^+	19	0.21	0.16	0.02	0.45	
Ca^{+2} (Water soluble ion)	45	0.14	0.06	0.06	0.28	
$C_2O_4^{-2}$	45	0.11	0.06	0.04	0.36	
K^+ (Water soluble ion)	45	0.09	0.06	0.02	0.30	
Ca (Trace metal)	42	0.42	0.33	0.01	1.95	
K (Trace metal)	43	0.13	0.08	0.02	0.46	
Formate	13	82	88	0	217	$ng\ m^{-3}$
PO_4^{-3}	21	66	42	10	148	
Methansulfonate	45	50	36	13	256	
Cl-	30	20	19	0	75	
Mg^{+2}	45	19	10	2	52	
NO_2^-	45	3	1	1	6	
Fe	42	88	64	2	293	

Species	# of samples	Mean	SD	Min	Max	Units
Sn	23	52	37	9	137	
Zn	42	34	33	0	153	
Pb	42	18	19	0	84	
Ba	20	9	13	2	72	
Sb	19	8	5	3	22	
Cu	42	6	5	1	22	
Ti	42	5	4	0	17	
As	5	2	4	0	10	
Mn	42	2	1	0	5	
Ni	42	2	1	0	9	
Sr	42	2	5	0	28	
Cr	41	1	1	0	4	
Se	41	1	1	0	6	
V	20	0	1	0	3	

4.3.3.　　Ions

SO_4^{2-} and NH_4^+ were the most abundant anion and cation in the $PM_{2.5}$ samples. The molar ratio $[NH_4^+]/[SO_4^{2-}]$ was 1.6 ± 0.3 (min: 0.8 and max: 2.3), suggesting that $PM_{2.5}$ is acid. The pH of $PM_{2.5}$ samples was determined using the IV E-AIM thermodynamic model, which estimates the activity coefficient of these species in aqueous phase equilibrium using the H^+-NH_4^+-Na^+-SO_4^{2-}-NO_3^--Cl^--H_2O system. As a result, the pH was 2.5 ± 0.4. The correlation between the ratio $[NH_4^+]/[SO_4^{2-}]$ and the pH was strong ($r^2 = 0.96$, as plot in Figure S4-3), suggesting that the molar concentrations of those ions can significantly explain the particle acidity. Other studies have found similar $[NH_4^+]/[SO_4^{2-}]$ values for pH lower than the estimated in CRV. Xue et al., (2011), for example, shows molar ratios in ranging from 1.32 to 1.71 and pH values between -0.45 and 0.59.). Pye et al., (2020) showed that fine particles have a bimodal distribution of pH, with one mode around a pH of 1–3, and another mode around a pH of 4-5, the latter influenced by dust, sea spray, and potentially biomass burning). In this study, only one $PM_{2.5}$ sample exceed a pH value of 4. Overall, this is an indicator of the abundance of sulfate and organics compounds in samples collected in the CVR.

The pH affects the partitioning of total nitrate (NO_3^- + HNO_3) and total ammonium (NH_4^+ + NH_3) between the gas and particulate phases. Lower pH values favor the partitioning of total nitrate toward the gaseous phase (HNO_3) rather than the particulate phase (NO_3^-). In contrast,

the partitioning of total ammonium is favored toward the particulate phase, remaining as NH_4^+ in the aerosol, whereas SO_4^{2-} is a nonvolatile species that remained in the particulate phase. Acidity conditions in the samples collected in this study are consistent with concentrations of SO_4^{2-}, NH_4^+, and NO_3^- corresponding to 2.5 µg m^{-3}, 0.7 µg m^{-3}, and 0.5 µg m^{-3}, respectively. Ammoniated sulfate and ammonium nitrate are generally considered the predominant forms of nitrate and sulfate in the inorganic fraction in fine particles. In limited environmental ammonium conditions, ammonia reacts preferentially with H_2SO_4 to form ammonium sulfate ($[NH_4]_2SO_4$), letovicite ($[NH_4]_3H[SO_4]_2$) or ammonium bisulfate ($[NH_4HSO_4]$) (Lee et al., 2008). Although the correlation coefficient between SO_4^{2-} and NH_4^+ concentrations was high ($R^2 = 0.98$), the amount of ammonium contained in the samples was not high enough to neutralize sulfate completely and form $[NH_4]_2SO_4$. In environmental with limited concentrations of ammonium, is expected the formation of sulfate salts not completely neutralized, as $[NH_4]_3H[SO_4]_2$ and $[NH_4HSO_4]$ (Ianniello et al., 2011). Thus, based on the limited ammonium concentrations found in PM$_{2.5}$ of CRV, the stoichiometric molar ratio between $[NH_4^+]/[SO_4^{2-}]$ of 3:2 for letovicite and 1:1 for ammonium bisulfate, and the results of the E-AIM model, it is possible to indicate that there is a mixture of sulfate salts, such as, ammonium bisulfate, letovicite, and ammonium sulfate, which is going to form progressively, according to ammonia availability. The E-AIM model presents the saturation ratio of each solid species, which usually forms before ammonium bisulfate than letovicite and ammonium sulfate. For a molar ratio of 1.5, the aerosol phase consists almost exclusively of letovicite and to form ammonium sulfate, the ratio should be over 2.0 (Seinfeld and Pandis, 2006). As result of the $[NH_4^+]/[SO_4^{2-}]$ ratios observed in the samples collected in CRV and the pH estimated from the IV E-AIM model, there is no reason to assume that nitrate is present as ammonium nitrate in the PM$_{2.5}$.

Instead of this, NO_3^- might be bound to cations contained in sea salt and dust particles to form relative nonvolatile salts, as KNO_3, $NaNO_3$ and $Ca(NO_3)_2$. NO_3^- showed correlation with Na^+, Ca^{2+} and K^+ ($r^2 = 0.6$, 0.2 and 0.2, respectively), indicating possible formation of those salts. The correlation between Na^+ and NO_3^- could be explained by the impact of sea salt aerosol that comes from air mass origin in the Pacific Ocean. However, the amount of Na^+ is not enough to neutralize the total of NO_3^-, while Ca^{2+} showed to be enough amount to neutralize the NO_3^-. The molar ratio observed in PM$_{2.5}$ samples of CRV for $[NO_3^-]/[Ca^{2+}]$ was 2.6 ± 1.4, $[NO_3^-]/[Na^+]$ was 1.7 ± 1.3, and $[NO_3^-]/[K^+]$ was 5.0 ± 3.2, overcoming the stoichiometric molar ratio required to form $Ca(NO_3)_2$, $NaNO_3$, and KNO_3.

While, In this study, the abundance of SO_4^{2-} in $PM_{2.5}$ can be attributed to oxidation of SO_2 and SO_3 emitted by from coal fired in power plants and industrial facilities (Zíková et al., 2016), biomass burning activities (Song et al. (2006)) and the emission of H_2S in poultry production (Casey et al., 2006). The H_2S emission from poultry and pork production is estimated using the factor emission given by animal units (AU) and the time that it stays in the housing, where one AU corresponding to 500 Kg of body mass. H_2S emissions from swine and poultry housing trend to be under 5 g H_2S AU^{-1} d^{-1} Casey et al., (2006), which can reach a 3.5 Ton H_2S d^{-1} by poultry and 5 Ton H_2S d^{-1} by pork production. Ammonia emissions factors by poultry and livestock vary from 0.09 to 12.9 AU^{-1} d^{-1} which represents 9.05 Ton NH_3 d^{-1} by poultry housing and 12. Ton d^{-1} by pork production.

$PM_{2.5}$ consistently contained methansulfonate, with an average concentration of 50 ng ± 13 m-3. This ion is produced by the aqueous oxidation of dimethyl sulfide (DMS), one of the most prevalent biogenic sulfur compounds in the troposphere. DMS oxidation is a major source of non-sea salt sulfate aerosols in marine aeras (Tang et al., 2019), but also can have origin in continental origins, such as biomass burning, (Gondwe, 2004; Meinardi et al., 2003; Sorooshian et al., 2015; Stahl et al., 2020). Methanesulfonate was mainly correlated to the ions sulphate and ammonia (r^2 = 0.88) and $C_2O_4^{2-}$ (r^2 =0.66), the metals Se (r^2 = 0.74) and Fe (r^2 = 0.41) and the carbonaceous fraction EC (r^2 = 0.56) and OC (r^2 = 0.49) in this study. Knowing the origin of this ion in PM2.5 in CRV, which is not directly coastal area, prompts future studies with a higher time resolution (6-12 hours) to establish the connection with changes in the wind pattern and the impact of the katabatic circulation, especially because biomass burning, mainly from sugarcane burnt, is an activity developing during all year in CRV.

(Tang et al., 2019)(Gondwe, 2004; Meinardi et al., 2003; Sorooshian et al., 2015; Stahl et al., 2020)(Sorooshian et al., 2015)(Sorooshian et al., 2015)

The measured average ratio of $[SO_4^{2-}]/[NO_3^-]$ = 4.5 ± 2.9. This ratio is higher than the one obtained by Souza et al. (2014) at Piracicaba (3.6 ± 1.0) and Sao Paulo (1.8 ± 1.0), Brazil. The strong correlations between SO_4^{2-} and NH_4^+ (r^2 = 0.84), SO_4^{2-} and methanesulfonate ($CH_3O_3S^-$) (r^2 = 0.88), and SO_4^{2-} and oxalate dianion ($C_2O_4^{2-}$) (r^2 = 0.71) allow us to infer that inorganic secondary aerosol formation is a significant $PM_{2.5}$ source in the CRV. In addition, the presence of potassium cation (K^+) in submicron particles is recognized as a biomass burning tracer (Andreae, 1983; Ryu et al., 2004). K^+ showed a moderate correlation with nitrite anion (NO_2^-) (r^2 = 0.44) and $C_2O_4^{2-}$ (r^2=0.43) in the CRV, which suggests that biomass burning influences secondary aerosol formation. Mg^{2+} and Ca^{2+} ions, usually considered crustal metals, exhibited a moderate correlation of r^2 = 0.59 (Li et al., 2013). Also, Mg^{2+} and $C_2O_4^{2-}$ moderate correlation

(r^2 = 0.26) points to a link between crustal species and secondary aerosols. Such an association could be plausibly explained by soil erosion induced by pyro-convection during sugarcane pre-harvest burning (Wagner et al., 2018). Our study full species correlation matrix is shown in Fig 4S.

4.3.4. Metals

The measured total $PM_{2.5}$ trace metal concentration was 706 ± 462 ng m^{-3} (101.3 ng m^{-3} to 2638 ng m^{-3}). Trace metals can originate from non-exhaust and exhaust emissions. Non-exhaust emissions come from brake and tire wear, road surface abrasion, wear/corrosion of other vehicle components, and the resuspension of road surface dust (Pant and Harrison, 2013). Metals in exhaust emissions are related to fuel, lubricant combustion, catalytic converters, and engine corrosion. As shown by Kundu and Stone (2014), many of these sources share some metals in their chemical composition profile, thus an unambiguous specific source attribution is non-trivial. In this study, we found a significant correlation among Fe, Mn and Ti ($r^2 \approx 0.72$), which is typically associated with a high abundance of crustal material (Fomba et al., 2018), indicating that soil dust is a significant source in the CRV. Also, tire and brake wear tracer metals, including Zn and Cu, showed weaker but still significant correlations among them ($r^2 \approx 0.32$). Ca concentrations were quite high (405 ± 334 ng m^{-3} (1.6 ng m^{-3} to 1952 ng m^{-3}). These levels can be attributed to dust generation by agricultural practices, particularly land planning, liming and tilling, PHB pyro-convection-induced soil erosion, and traffic-induced soil resuspension on unpaved rural roads. One of the very few previous investigations into on PM composition in the CRV (Criollo and Daza, 2011) analyzed trace metals in PM_{10} at 4 CRV locations, including Palmira. They found significant enrichment of Fe and K metals at locations exposed to PHB. It must be kept in mind that PM_{10} samples included coarse mode aerosols, of which dust might have been a significant fraction. Also, environmental regulations have been successful in steadily reducing the sugarcane burned area in the CRV since 2009. The Burned area dropped from 72% in 2011 to 35.46% in 2018, our year of measurements (Cardozo-Valencia et al., 2019).

Cd, Pb, Ni, Hg and As, and other metals and metalloids are considered carcinogenic (WHO Regional Office for Europe, 2020). Measured concentrations of Pb and Ni in $PM_{2.5}$ at Palmira were 18 ng m^{-3} (+/-19) and 2 ng m^{-3} (+/-1), respectively. These mean values were below the EU target values of (0.5 μg m^{-3} and 20 ng m^{-3} respectively) (WHO, 2013a), and below the annual average limit of the Colombian national ambient air quality standard (0.5 μg m^{-3} and 0.18 μg m^{-3} respectively) (MADS, 2017). Nevertheless, these concentrations are significantly higher

than those reported for other suburban areas in Midwestern United States and remote sites in the northern tropical Atlantic (Fomba et al., 2018; Kundu and Stone, 2014). Pb concentrations are similar to those reported for Bogota and other large urban areas (SDA, 2010; Vasconcellos et al., 2007). Pb has been long banned as a fuel additive in Colombia, thus the observed levels might be associated with metallurgical industry and waste incineration. Information on ambient air hazardous metal concentrations in Latin America's urban and rural areas is still scarce.

4.3.5. Carbohydrates

Levoglucosan is a highly specific biomass burning organic tracer (Bhattarai et al., 2019). Along with K^+, OC and EC, it can be used to effectively identify the relevance of biomass burning as an aerosol source. The relative contribution of levoglucosan to the PM carbohydrate burden, and especially the levoglucosan to mannosan ratio, can be used as indicators of the type of biomass burned (Engling et al., 2009). In this study, the following carbohydrates were quantified: levoglucosan, mannosan, glucose, galactosan, fructose and arabitol. Levoglucosan was by far the most abundant (113.8 ± 147.2 ng m^{-3}), reaching values of up to 904.3 ng m^{-3}, followed by glucose (10.4 ± 6.1 ng m^{-3}), mannosan (7 ± 6.1 ng m^{-3}), and arabitol (4.1 ± 3.5 ng m^{-3}). Levoglucosan and mannosan were detected in all PM$_{2.5}$ samples, while galactosan and fructose were detected only in 9 and 11 samples, respectively. Levoglucosan was $3.5 \pm 2.3\%$ of OC and $0.96\% \pm 0.81\%$ of PM$_{2.5}$.

The levoglucosan concentration found in this study was quite similar to that reported in areas of Brazil where sugarcane production and processing are important economic activities, Figure 4-18. For instance, during the harvest (*zafra*) period in Araraquara, the levoglucosan mean concentration was 138 ± 91 ng m^{-3}, although during the non-harvest period it was unexpectedly high (73 ± 37 ng m^{-3}) (Urban et al., 2014). Likewise, the levoglucosan average concentration at Piracicaba during a reduced fire period was 66 ng m^{-3} (Souza et al., 2014). The measured mean levoglucosan/mannosan ratio in Palmira was 17.6 ± 13.0 (min: 8.1 – max: 58.1). Chemical profile studies found a levoglucosan/mannosan ratio of ~10 for sugarcane leaves burned in stoves (Hall et al., 2012; Dos Santos et al., 2002) and of ~54 for burned bagasse (Dos Santos et al., 2002). Leaves constitute the largest fraction (20.8%, Victoria et al., 2002) of pre-harvest burned sugarcane. Consistently and expectably, the levoglucosan/mannosan ratio at Palmira is much closer to the chemical profile ratio of leaves than that of bagasse. Moreover, ambient air samples in Araraquara and Piracicaba showed levoglucosan/mannosan ratios of 9 ± 5 and ~33, respectively. For comparison, the

levoglucosan/mannosan ratio in PM from rice straw and other crops burned were ~26.6 and~23.8, respectively (Engling et al., 2009). This indicates that the levoglucosan/mannosan ratio is sensitive to the type of biomass burned but also to burning conditions. The large levoglucosan/mannosan ratio in our study suggests that Palmira was impacted by sugarcane PHB most of the time, and, to a lesser extent, by bagasse combustion in sugar mills. We hypothesize that, even if these were very small, levoglucosan and mannosan combustion emissions might not be negligible as the CRV sugarcane biomass yields are very high and most of the harvested sugarcane bagasse is combusted for electric power and steam production.
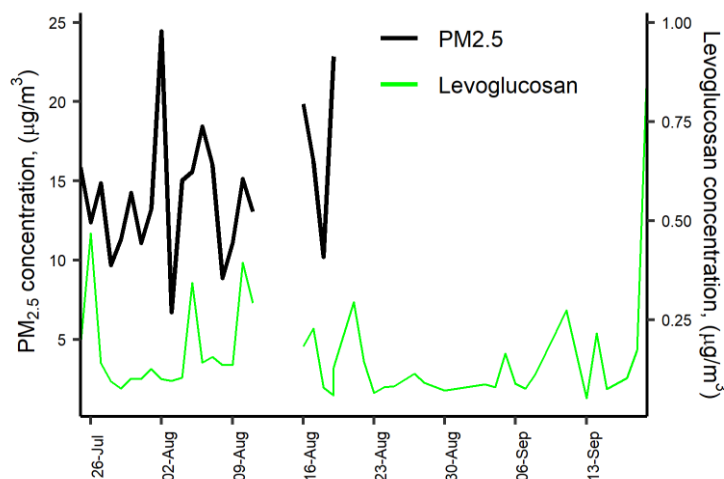
Figure 4-18. Daily variation of Levoglucosan and PM2.5 concentration at CRV.

4.3.6. Polycyclic Aromatic Hydrocarbons (PAHs)

A total of 22 PAHs were measured in each sample collected at Palmira, including the 16 PAHs listed as human health priority pollutants by WHO and US-EPA (Yan et al., 2004). The total PAHs concentration was 5.6 ± 2.9 ng m^{-3} (min: 2.3 ng m^{-3} – max: 15.8 ng m^{-3}). Figure 4-19a a shows the PAHs concentration variability during the sampling campaign (mean and standard deviation are available in Table S4-2). The most abundant PAH were FLE (44.2%±11.9% total concentration share), ANT (9,10) (10.0%±4.5%), BbF (7.4%±2.3%), BghiP (6.7%±2.4%), IcdP (6.4%±1.9%), CPY (6.0%±2.3%), FLO (9H) (5.4%±3.1%), BeP(4.6%±1.3%), and BaP(4.4%±1.6%),

which accounted for 95.1% of the total PAH concentration (Figure 4-19b). Three-ring PAHs were the most abundant (59.04% of total PAH). Put together, five- and six-ring PAHs accounted for an additional 38.44%. The less abundant PAH group was the four-ring (2.52%). A previous study in CRV, carried out on PM_{10} samples by Romero et al. (2013), showed higher FLT, PYR, and PHE concentrations in areas highly exposed to sugarcane PHB compared to other locations. In contrast, $PM_{2.5}$ FLE concentrations in this research were significantly higher than those in PM_{10} by Romero et al. (2013), while PYR and PHE levels were similar.

The carcinogenic species BaP, BbF, BkF, BaA, BghiP, FLE, CPY and BeP were identified in all the $PM_{2.5}$ samples. BaP is a reference for PAH carcinogenicity (WHO, 2013a) that is used as a PAH exposure metric, known as the BenzoaPyrene-equivalent carcinogenic potency (BaPE). We calculated BaPE using the toxic equivalent factors (TEF) proposed by Nisbet and LaGoy (1992) and (Malcolm and Dobson, 1994). PAH concentrations were multiplied by TEF and then added to estimate the carcinogenic potential of $PM_{2.5}$-bounded PAHs. The mean carcinogenicity level at Palmira, expressed as BaP-TEQ, was 0.4 ± 0.2 ng m^{-3} (min: 0.1 ng m^{-3} - max: 1.4 ng m^{-3}). Only one sample exceeded the Colombian annual limit of 1 ng m^{-3} but most of them exceeded the WHO reference level of 0.12 ng m^{-3}. The mutagenic potential of PAHs (BaP-MEQ) was estimated using the mutagenic equivalent factors (MEF) reported by Durant et al., (1996). The average BaP-MEQ was 0.5 ± 0.3 ng m^{-3} (min: 0.2 ng m^{-3} - max: 1.8 ng m^{-3}). These levels are comparable to those measured in $PM_{2.5}$ by Mugica-Álvarez et al., (2016) in Veracruz (Mexico) but during the sugarcane non-harvest period. PM_{10} BaP-MEQ levels in Araraquara (Brazil) (de Andrade et al., 2010; De Assuncao et al., 2014) were twice as high as those found in this study. This suggests that year-long sugarcane PHB in the CRV leads to lower mutagenic potentials compared to those at locations where the harvesting period (*zafra*) is shorter, thus with higher burning rates. We estimated the average BaP-TEQ and BaP-MEQ concentrations in the CRV according to their exposure to sugarcane burning products from Romero et al., (2013) data and used them as a benchmark to our measurements. PM_{10}-bound BaP-TEQ and BaP-MEQ levels for areas not directly exposed to sugarcane burning were 0.16 ng m^{-3} and =0.21 ng m^{-3}, respectively. Toxicity and mutagenicity due to PM_{10}-bound PAHs were 4 times as high as those at areas directly exposed to sugarcane burning. It is reasonable to assume that PAHs are largely bound to fine aerosol (<2.5 μm), thus that our measurements are comparable to (Romero et al., 2013). If so, our site at Palmira would be at an intermediate exposure condition, higher than areas not directly exposed to sugarcane burning but lower than directly exposed areas.

Ratios among different PAHs have been extensively used to distinguish between traffic and other PAH sources. We used the diagnostic ratios presented by Ravindra et al. (2008) and Tobiszewski and Namieśnik (2012a) to better understand the contribution of sources to PM$_{2.5}$ in the CRV. The ratio benzo(e)pyrene to the sum of benzo(e)pyrene and benzo(a) pyrene is used as an indicator of aerosol aging. Local or "fresh" aerosols have [BeP]/([BeP]+[BaP]) ratios around 0.5, while aged aerosols can have ratios as low as zero as a result of photochemical decomposition and oxidation. The [BeP]/([BeP]+[BaP]) ratio at Palmira was 0.51 ± 0.04, with a majority (84.4%, n = 38) of fresh samples a minor fraction (15.6%, n=7) of photochemically-degraded samples.

Other two diagnostic ratios were used to assess the prevalence of traffic as a PM$_{2.5}$ source. The first ratio used IcdP BghiP, two automobile emissions markers (Miguel and Pereira, 1989). Values higher than 0.5 for the ratio [IdcP]/([IdcP]+[BghiP]) indicates aged particles (Tobiszewski and Namieśnik, 2012) generated by coal, grass or wood burning (Yunker et al., 2002). The second ratio is [BaP]/[BghiP]. Ratios higher than 0.6 are indicative of traffic emissions (Tobiszewski and Namieśnik, 2012). At Palmira, the [IdcP]/([IdcP]+[BghiP]) and [BaP]/[BghiP] ratios were 0.48 ± 0.04 and 0.69 ± 0.13, which indicates that ~63% of the samples originated from combustion of oil products (n = 30), and ~36% came from non-traffic sources, like wood, grass, or coal (n = 15).

Also, the structure and size of PAHs are indicative of their sources. PAHs of low molecular weight (LMW) (two or three aromatic rings) have been reported as tracers of wood, grass, and fuel oil combustion, while those of medium molecular weight (MMW) (four rings) and high molecular height (HMW) (five and six rings) are associated with coal combustion and vehicular emissions. The ratio between LMW and the sum of MMW and HMW, LMW/(MMW+HMW), is used for source identification. Ratios lower than one are indicative of oil products combustion, while ratios larger than one are associated with coal and biomass combustion (Tobiszewski and Namieśnik, 2012). The ratio at Palmira, LMW/(MMW+HMW) = 1.43 ± 1.00, was rather variable but suggests that a large fraction of PAHs in CRV (82.2% of samples) were generated by biomass burning or combustion, as well as coal combustion in brick kilns. Just one in five samples (17.8%) had PAHs attributable to oil product combustion.

Sugarcane-burning emitted PAH are mainly LMW, especially of two (~66% of PAHs) and three rings (~27%), among which FLE, PHE and ANT are the most emitted, according to Hall et al. (2012) chemical profile. The relative abundance of 3-ring PAHs (Figure 4-19b) in CRV's PM$_{2.5}$ is likely due to open-field sugarcane PHB to a major extent, and to controlled bagasse combustion for electric power and steam production, to a lesser extent.

The highest PAH concentrations were observed on 10th August and 11th September 2018, with levels of 15.8 ng m^{-3} and 14.4 ng m^{-3}, respectively (Fig 5S). Elevated concentrations of 5 and 6 ring PAHs were observed on 10th August 2018. A change in the wind circulation pattern was observed on the previous day (Fig S2), with a wind speed reduction and a predominance of winds from the north. Later, on 11th September 2018, we observed an increase in 3-ring PAHs and winds from the NW at the average wind speed at the sampling location. This indicates that there were at least two types of sources. The abundance of HMW PAHs indicates fossil fuel combustion sources, and LMW PAHs suggest that parts of these come from non-fossil fuel combustion sources.
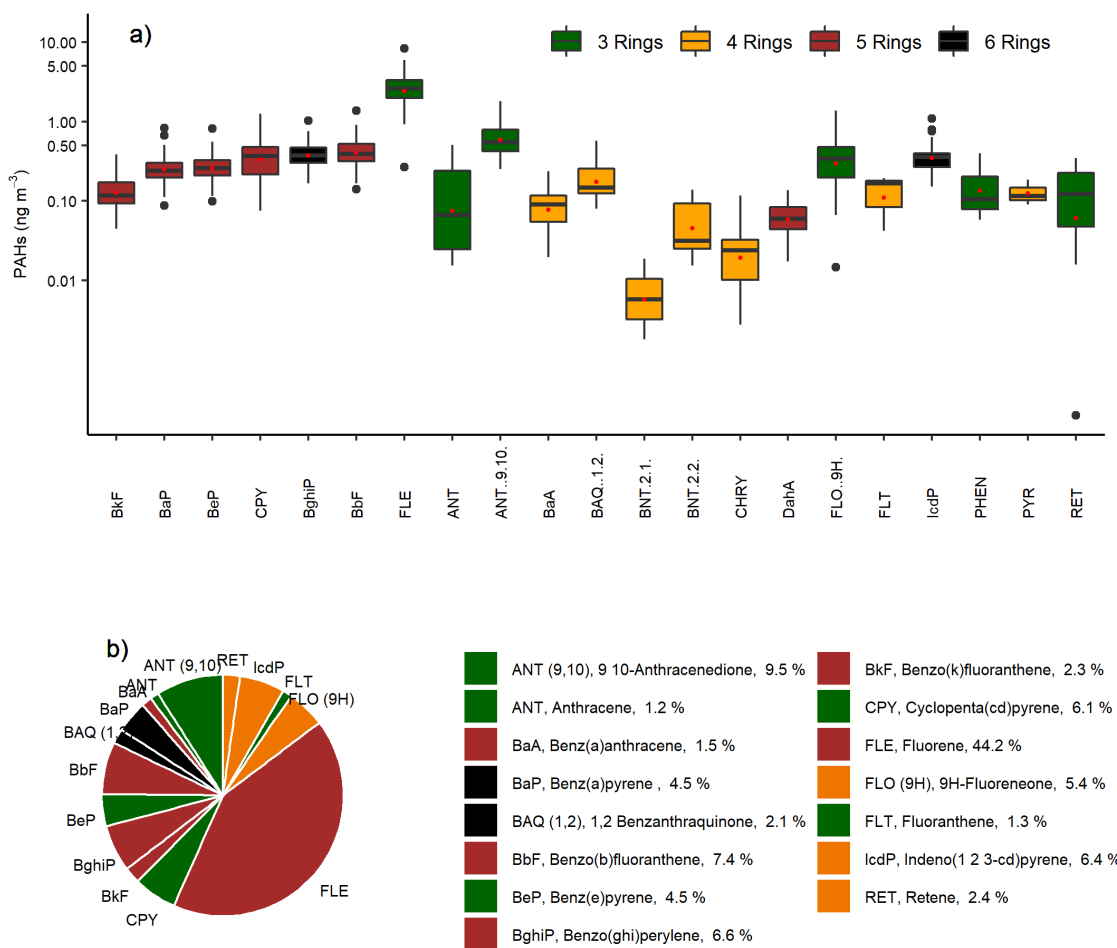
Figure 4-19. The abundance of PAHs measured in $PM_{2.5}$ samples collected in CRV, represented by colors according to the number of rings of each PAHs, green (tree rings), yellow (four rings), brown (five rings), and black (six rings). a) Boxplot of concentrations in nanogram per cubic meter (ng m^{-3}), red dots represent mean concentrations of each PAHs. b) pie-plot of the relative abundance of PAHs in $PM_{2.5}$ samples.

4.3.7.   Alkanes

A total of 16 alkanes ranging from C_{20} up to C_{34} were analyzed in this study and used to identify the presence of fossil fuel combustion and plant fragments in the $PM_{2.5}$ samples. The abundance of total n-alkanes during the whole sampling period was in the range of 13.0 to 88.45 ng m^{-3} with an average concentration of 40.36 ng m^{-3} ± 18.82 ng m^{-3}. In general, the high molecular weight n-alkanes such as C_{29} – C_{31} were the most abundant. These are characteristic of vegetative detritus corresponding to plant fragments in airborne PM (Lin et al., 2010). The most abundant n-alkanes were C_{29}, C_{30}, and C_{31} (Figure 3-20). Likewise, the carbon number maximum concentration (C_{max}) was C_{29} in 43% of samples and C_{31} in 28% of them. This result is consistent with the chemical profile of sugarcane burning reported by (Oros et al., 2006) with a C_{max} of C_{31}.

The carbon preference index (CPI) and wax n-alkanes percentage (WNA%) are parameters used to elucidate the origin of the n-alkanes and infer whether emissions come from biogenic or anthropogenic sources. The CPI represents the ratio between odd and even carbon number n-alkanes. The equation used to calculate CPI in the present study is shown in Table 4-3, following the procedure reported by (Marzi et al., 1993). Values of CPI ≤ 1 (or close to 1) indicate that n-alkanes are emitted from anthropogenic sources, while values higher than 1 indicate the influence of vegetative detritus and biomass burning in the $PM_{2.5}$ samples (Mancilla et al., 2016). In this study, the mean CPI was always greater than 1, with an average value of 1.22 ± 0.18 (min:1.02 – max:1.8) that is between the CPI for fossil fuel emissions of ~1.0 (Caumo et al., 2020) and sugarcane burning of 2.1 (Oros et al., 2006), revealing the influence of several sources over the $PM_{2.5}$ in the CRV.

Likewise, WNA% represents the preference of odd n-alkanes in the sample. The odd n-alkanes, especially of higher molecular weight, are representative of plant wax related emissions. The waxes are present on the surface of plants, especially on the leaves, and they become airborne by a direct or indirect mechanism like wind action or biomass burning (Kang et al., 2018; Simoneit, 2002). In this research, the samples analyzed showed a preference for odd

carbon on C_{27}, C_{29}, C_{31} and C_{33}, which have higher concentrations than the next higher and lower even carbon number homologs, proving the biogenic contribution over the $PM_{2.5}$ in the CRV. The WNA% was calculated using the equation shown in Table 4-3, described by Yadav et al. (2013). A larger WNA% represents the contribution from emissions of plant waxes or biomass burning. Otherwise, a smaller value represents n-alkanes from petrogenic sources, known as petrogenic n-alkanes (PNA)%. The mean WNA% calculated for the $PM_{2.5}$ samples collected from the CRV was 12.65% ± 5.21% (min: 4.71% – max: 29.92%) and can be defined as petrogenic inputs (PNA%) that were 87.35% during the sampling period. The correlation between CPI and WNA was moderate (r^2=0.53) supporting a consistent meaning between these two parameters, and they are useful for assessing the plant wax contribution to $PM_{2.5}$.

Overall, the total concentration of n-alkanes in the $PM_{2.5}$ in the CRV was lower than those reported in areas where sugarcane is often burned in Brazil (Urban et al., 2016), although the behavior of the parameters of CPI and C_{max} is similar. Compared with other urban areas in Latin America, the n-alkane concentration in the CRV was similar to that reported in the metropolitan zone of the Mexican valley (MZMV) for $PM_{2.5}$ (Amador-Muñoz et al., 2011), Bogota for PM_{10} and slightly lower than reported in Sao Paulo for PM_{10} (Vasconcellos et al., 2011). However, the CPI and WNA in these cities were smaller than in the CRV, because of the strong influence of vehicular emissions in these densely populated cities. The OC/EC ratio was moderately associated with WNA values ($r^2 = 0.41$), indicating that an increase in this ratio can be explained by the vegetative detritus contribution to $PM_{2.5}$, while the levoglucosan concentrations did not show correspondence to the CPI and WNA values; therefore, the levoglucosan levels did not explain the preference of odd carbon number homologs. These results indicated that the n-alkanes found in this study came from several sources, with a noticeable contribution from plant wax emissions. The parameters used to assess the source contribution of $PM_{2.5}$ through n-alkanes such as CPI and WNA%, were characteristic of aerosols collected in urban areas.
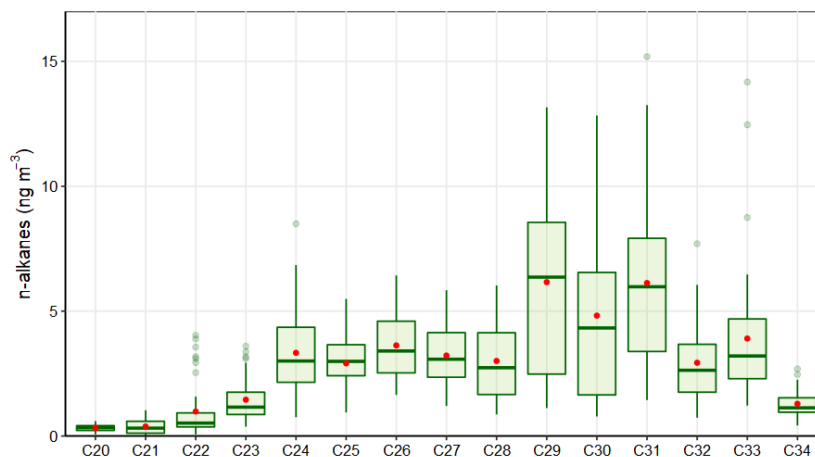
Figure 3-20. Average n-alkanes concentrations in PM$_{2.5}$ samples

4.3.8.   PM$_{2.5}$ mass closure

Mass closure (Figure 4-21) shows the crucial contribution of organic material (52.66 ± 18.44%) and inorganic fraction, represented by sulfate (12.69 ± 2.84%), ammonium (3.75 ±1.05%), nitrate (2.56±1.29%). EC constituted 7.13 ± 2.44% of PM$_{2.5}$. The mineral fraction corresponded to dust (3.51± 1.35%) and TEO (0.85 ± 0.42%). Mass closure of 88.42± 24.17% was achieved. Although PM$_{2.5}$ concentrations observed in the CRV were not so high as compared with those registered in Brazil and Mexico during the preharvest season, the EC percentage is in a similar range or slightly lower than those observed in other urban areas (Snider et al., 2016), showing the key role of incomplete combustion processes in the area.

The average (OC/EC) ratio found in CRV was 4.2 ± 0.72, from which we can infer that secondary aerosol formation had a relevant role. The segregation of OC into the primary and secondary fractions was carried out using two methods. The first was the EC tracer method applied in previous studies (Pio et al., 2011; Plaza et al., 2011), and the second was the organic tracer method, which is based on the lineal regression between OC and organic tracers from primary sources. In the EC tracer method, the (OC/EC)$_{min}$ ratio selected to differentiate OC$_{prim}$ from OC$_{sec}$ was the minimum ratio observed, equivalent to 2.12. Still, this value could induce the overestimation of OC$_{prim}$ due to the distance between the emission sources and the sampling site (27 m aboveground), and the local meteorological conditions that favor the

volatilization and oxidation of organic components into particles before being collected. As a result, OC_{prim} was estimated at 50.3% and OC_{sec} at 49.7% of the total OC, with a minimum variability of 3.8%. The estimated OM_{pri} concentration was 3.22 ± 1.09 µg m^{-3} and the OM_{sec} concentration was 4.01 ± 1.78 µg m^{-3}, which represented 24.2% and 28.5% of $PM_{2.5}$ respectively.

In the organic tracer method, the contribution of fossil fuel combustion - mainly derived from transport -, biomass burning, and vegetative detritus to OC_{prim} was estimated from a linear model by robust regression using an M estimator with bisquare function between organic tracers and OC. Resulting contributions were as follows: OC_{ff}: 16.38%, OC_{bb}: 15.19%, and OC_{det}: 1.45% of total OC measured. Overall, the use organic tracer method to estimate OC_{prim} indicates that this carbonaceous fraction represents 32.68% ± 11.02% of total OC, and it may fluctuate between 17.61% and 68.60%.

The difference between OC_{prim} from the organic tracer method and that obtained from the EC tracer method can be associated to the fact that the organic tracer method may not be representative of all sources. Industrial coal and fuel oil burning, garbage burning, cooking, charcoal production and other sources may not be accounted for by this method, since we did not have specific organic tracers for each of these activities.

The mineral fraction, quantified as the sum of the oxides present in the crustal material (dust) and other TEO contributed $3.51 \pm 1.35\%$ and $0.85 \pm 0.42\%$, respectively. Despite the non-quantification of highly abundant mineral dust elements such as Si, the concentrations of Ca, Ti, and Fe indicated the impact of soil resuspension on the $PM_{2.5}$ mass concentration.

PBW depends on the concentration of hygroscopic compounds embodied in the PM and the relative humidity of the weighing room where $PM_{2.5}$ mass collected on the filters was determined. In this study, it was assumed that (i) NH_4^+, SO_4^{2-} and NO_3^- were the main compounds responsible for absorbed water and (ii) thermodynamic equilibrium is dominated by these ions that allow calculating the H^+ molar fraction as a difference between ($SO_4^{2-}+ NO_3^-$) and NH_4^+, which is required to establish charge neutrality. Polar organic compounds and other water-soluble ions were not considered in the present study. The PBW content was estimated using the mean measured concentrations of NH_4^+, SO_4^{2-} and NO_3^- in the AIM Model, where a multiplier factor of 0.32 was found as a proportion between the concentrations of the sum of these ions and the water fraction contained in $PM_{2.5}$. As a result, PBW was 5.3% of the $PM_{2.5}$ mass concentration.
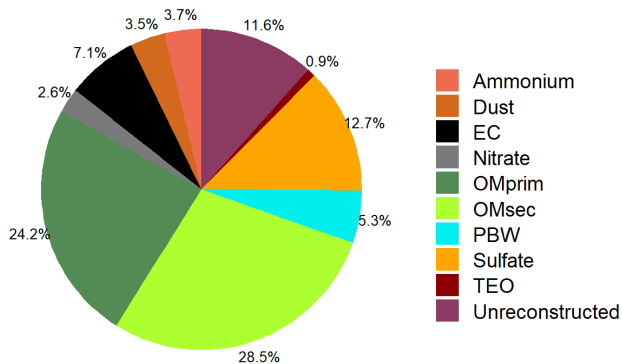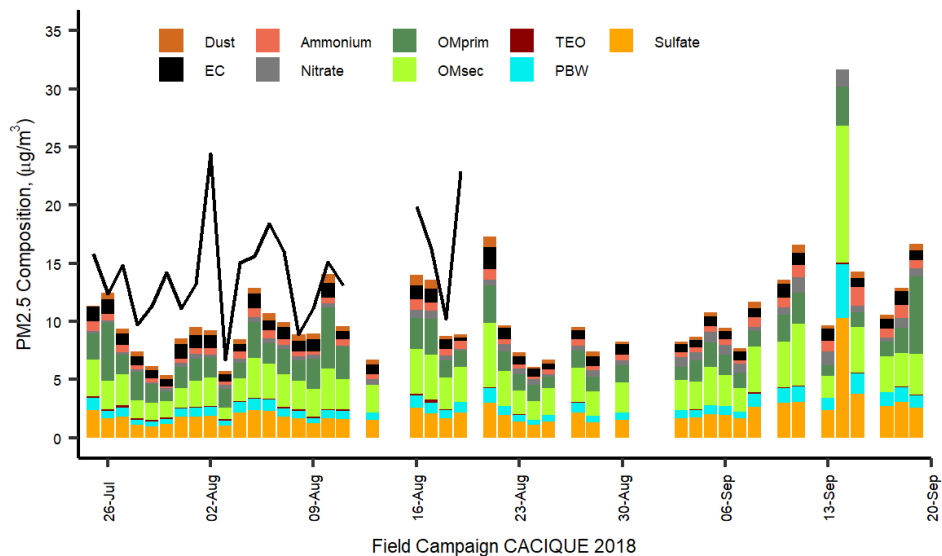
Figure 4-21. Mass reconstruction of PM$_{2.5}$ collected in CRV. Figure in upper corresponding to timeseries of PM$_{2.5}$ gravimetric mass measured and reconstructed mass from the chemical speciation in CRV during July – September 2018 and lower is the to pie plot the relative mean contributions (%) of major chemical components of gravimetric PM2.5 based on chemical speciation.

4.5.   Conclusions

$PM_{2.5}$ samples collected in the Cauca River Valley, Colombia, were analyzed to determine the main chemical components of fine aerosol particles and to qualitatively identify aerosol sources using its chemical composition and diagnostic ratios. $PM_{2.5}$ during the campaign was 14.4 ± 4.4 µg m^{-3}. Its main components were OC (4.0 ± 1.3 µg m^{-3}), sulfate (2.2 ± 1.4 µg m^{-3}), and EC (1.0 ± 0.3 µg m^{-3}), ammonium (0.7 ± 0.6 µg m^{-3}), and nitrate (0.5 ± 0.3 µg m^{-3}). OM was estimated using the EC tracer method and the organic tracer method. Mass closure using the EC tracer method explained 88.4% of $PM_{2.5}$, whereas the organic tracer method explained 70.9% of $PM_{2.5}$. We attribute this difference to the lack of information of specific organic tracers for some sources, both primary and secondary. Organic material and inorganic ions were the dominant groups of species, constituting almost 79% of $PM_{2.5}$. OM_{prim} and OM_{sec} from the EC tracer method contribute 24.2% and 28.5% to $PM_{2.5}$. Inorganic ions made up 19.0%, EC 7.1%, dust 3.5%, PBW 5.3%, and TEO 0.9% of $PM_{2.5}$.

Aerosol acidity was evaluated using three methods. The first, using the nitrate/sulfate ratio; the second using the anion/cation equivalent ratio; and the third, estimating the pH with the E-AIM thermodynamic model. All methods showed that the aerosol was acidic, with a pH of 2.5 ± 0.4, mainly because of the abundance of organic and sulfur compounds.

Diagnostic ratios applied to organic compounds indicate that most $PM_{2.5}$ was emitted locally and had contributions of both pyrogenic and petrogenic sources. In addition, levoglucosan and mannosan levels showed that biomass burning was ubiquitous during the sampling period. Fluoranthene (FLE) was the most abundant PAH, confirming the strong influence of BB associated with agro-industry. Five- and six-ring PAH associated with vehicular emissions were also abundant in $PM_{2.5}$. Our measurements point to BB as the main source of PAHs in CRV. Relatively low $PM_{2.5}$ concentrations and mutagenic potentials are consistent with low-intensity, year-long BB and sugarcane PHB in CRV, which leads to lower atmospheric pollutant burdens and mutagenic potentials compared to those at locations where the harvesting period is shorter (*zafra*) thus with higher burning rates.

Code and data availability: The data presented in this publication are depositing as related metadata in Mateus, Lady; Vargas, Angela; Jimenez, Rodrigo (2022), "Chemical composition of PM2.5 in Cauca River valley Colombia", Mendeley Data, V1, doi: 10.17632/jryhypdhy3.1

4.6.   References

Aerocivil: Estadísticas Operacionales, Operaciones aéreas totales 2000-2019 [data set], https://www.aerocivil.gov.co/atencion/estadisticas-de-las-actividades-aeronauticas/estadisticas-operacionales, 2019.

Aerocivil: Base de datos servicios fumigación aérea [data set], https://www.aerocivil.gov.co/atencion/estadisticas-de-las-actividades-aeronauticas/bases-de-datos, 2020.

Aiken, A. C., Decarlo, P. F., Kroll, J. H., Worsnop, D. R., Huffman, J. A., Docherty, K. S., Ulbrich, I. M., Mohr, C., Kimmel, J. R., Sueper, D., Sun, Y., Zhang, Q., Trimborn, A., Northway, M., Ziemann, P. J., Canagaratna, M. R., Onasch, T. B., Alfarra, M. R., Prevot, A. S. H., Dommen, J., Duplissy, J., Metzger, A., Baltensperger, U. and Jimenez, J. L.: O/C and OM/OC ratios of primary, secondary, and ambient organic aerosols with high-resolution time-of-flight aerosol mass spectrometry, Environ. Sci. Technol., 42(12), 4478–4485, https://doi.org/10.1021/es703009q, 2008.

Alvi, M. U., Kistler, M., Shahid, I., Alam, K., Chishtie, F., Mahmud, T. and Kasper-Giebl, A.: Composition and source apportionment of saccharides in aerosol particles from an agro-

industrial zone in the Indo-Gangetic Plain, Environ. Sci. Pollut. Res. 2020 2712, 27(12), 14124–14137, https://doi.org/10.1007/S11356-020-07905-2, 2020.

Amador-Muñoz, O., Villalobos-Pietrini, R., Miranda, J. and Vera-Avila, L. E.: Organic compounds of PM2.5 in Mexico Valley: Spatial and temporal patterns, behavior and sources, Sci. Total Environ., 409(8), 1453–1465, https://doi.org/10.1016/j.scitotenv.2010.11.026, 2011.

de Andrade, S. J., Cristale, J., Silva, F. S., Julião Zocolo, G. and Marchi, M. R. R.: Contribution of sugar-cane harvesting season to atmospheric contamination by polycyclic aromatic hydrocarbons (PAHs) in Araraquara city, Southeast Brazil, Atmos. Environ., 44(24), 2913–2919, https://doi.org/10.1016/j.atmosenv.2010.04.026, 2010.Andreae, M. O.: Soot Carbon and Excess Fine Potassium: Long-Range Transport of Combustion-Derived Aerosols., Science (New York, N.Y.), 10–13 pp., https://doi.org/10.1126 / science.220.4602.1148, last access: 20 May 2020, 1983.

Andreae, M. O.: Emission of trace gases and aerosols from biomass burning – An updated assessment, Atmos. Chem. Phys. Discuss., 1–27, https://doi.org/10.5194/acp-2019-303, 2019.

Aneja, V. P., Schlesinger, W. H. and Erisman, J. W.: Farming pollution, Nat. Geosci., 1(7), 409–411, https://doi.org/10.1038/ngeo236, 2008.

Aneja, V. P., Schlesinger, W. H. and Erisman, J. W.: Effects of agriculture upon the air quality and climate: Research, policy, and regulations, Environ. Sci. Technol., 43(12), 4234–4240, https://doi.org/10.1021/es8024403, 2009.

Asocaña: Aspectos Generales del Sector Agroindustrial de la Caña 2017 - 2018. Informe Anual. http://www.asocana.org/modules/documentos/15248.aspx, last access: 20 May 2020, 2018.

Asocaña: Aspectos generales del sector agroindustial de la caña Informe anual 2018-2019. https://www.asocana.org/documentos/2352019-D0CA1EED-00FF00,000A000,878787,C3C3C3,0F0F0F,B4B4B4,FF00FF,2D2D2D,A3C4B5.pdf, last access: 20 May 2020, 2019.

De Assuncao, J. V., Pesquero, C. R., Nardocci, A. C., Francisco, A. P., Soares, N. S. and Ribeiro, H.: Airborne polycyclic aromatic hydrocarbons in a medium-sized city affected by preharvest sugarcane burning and inhalation risk for human health, J. Air Waste Manag. Assoc., 64(10), 1130–1139, https://doi.org/10.1080/10962247.2014.928242, 2014.

Begam, G. R., Vachaspati, C. V., Ahammed, Y. N., Kumar, K. R., Reddy, R. R., Sharma, S. K., Saxena, M. and Mandal, T. K.: Seasonal characteristics of water-soluble inorganic ions and carbonaceous aerosols in total suspended particulate matter at a rural semi-arid site, Kadapa (India), Environ. Sci. Pollut. Res., 24(2), 1719–1734, https://doi.org/10.1007/s11356-016-7917-

1, 2016.

Bhattarai, H., Saikawa, E., Wan, X., Zhu, H., Ram, K., Gao, S., Kang, S., Zhang, Q., Zhang, Y., Wu, G., Wang, X., Kawamura, K., Fu, P. and Cong, Z.: Levoglucosan as a tracer of biomass burning: Recent progress and perspectives, Atmos. Res., 220(November 2018), 20–33, https://doi.org/10.1016/j.atmosres.2019.01.004, 2019.

Boman, J., Lindén, J., Thorsson, S., Holmer, B. and Eliasson, I.: A tentative study of urban and suburban fine particles (PM2.5) collected in Ouagadougou, Burkina Faso, X-Ray Spectrom., 38(4), 354–362, https://doi.org/10.1002/XRS.1173, 2009.

Cardozo-Valencia, A., Saa, G. R., Hernandez, A. J., Lopez, G. R. and Jimenez, R.: Distribución espaciotemporal y estimación de emisiones por quema precosecha de caña de azúcar en el Valle del Cauca, Conf. Proc. - Congr. Colomb. y Conf. Int. Calid. Aire y Salud Publica, CASAP 2019, https://doi.org/10.1109/CASAP.2019.8916696, 2019.Casey, K. D., Bicudo, J. R., Schmidt, D. R., Singh, A., Gay, S. W., Gates, R. S., Jacobson, L. D. and Hoff, S. J.: Air quality and emissions from livestock and poultry production / waste management systems, in Animal Agriculture and the Environment, National Center for Manure & Animal Waste Management White Papers, edited by: Rice, J. M., Caldwell, D. F., and Humenik, F. J., ASABE, St. Joseph, Michigan, 1–40, https://doi.org/doi:10.13031/2013.20246, 2006.

Caumo, S., Bruns, R. E. and Vasconcellos, P. C.: Variation of the distribution of atmospheric n-alkanes emitted by different fuels' combustion, Atmosphere (Basel)., 11(6), 1–19, https://doi.org/10.3390/atmos11060643, 2020.

Cavalli, F., Viana, M., Yttri, K. E., Genberg, J. and Putaud, J.: Toward a standardised thermal-optical protocol for measuring atmospheric organic and elemental carbon : the EUSAAR protocol, Atmos. Meas. Tech., 3, 79–89, https://doi.org/10.5194/amt-3-79-2010, 2010.

Chow, J. C., Lowenthal, D. H., Chen, L. W. A., Wang, X. and Watson, J. G.: Mass reconstruction methods for PM2.5: a review, Air Qual. Atmos. Heal., 8(3), 243–263, https://doi.org/10.1007/s11869-015-0338-3, 2015.

Clegg, S. L., Brimblecombe, P. and Wexler, A. S.: Thermodynamic Model of the System H+−NH4+−SO42-−NO3-−H2O at Tropospheric Temperatures, J. Phys. Chem. A, 102(12), 2137–2154, https://doi.org/10.1021/jp973042r, 1998. Last access: 20 June, 2022.

Criollo, J. and Daza, N.: Evaluación de los niveles de concentración de metales en PM 10 producto de la quema de biomasa en el valle geográfico del rio Cauca, La Salle University https://ciencia.lasalle.edu.co/ing_ambiental_sanitaria/135/ , 2011. Last access: 20 June, 2022.

Dabek-Zlotorzynska, E., Dann, T. F., Kalyani Martinelango, P., Celo, V., Brook, J. R., Mathieu, D.,

Ding, L. and Austin, C. C.: Canadian National Air Pollution Surveillance (NAPS) PM2.5 speciation program: Methodology and PM2.5 chemical composition for the years 2003-2008, Atmos. Environ., 45(3), 673–686, https://doi.org/10.1016/j.atmosenv.2010.10.024, 2011.

Durant, J. L., Busby Jr, W. F., Lafleur, A. L., Penman, B. W. and Crespi, C. L.: Human cell mutagenicity of oxygenated, nitrated and unsubstituted polycyclic aromatic hydrocarbons associated with urban aerosols, Mutat. Res. - Genet. Toxicol., 371(3–4), 123–157, https://doi.org/10.1016/S0165-1218(96)90103-2, 1996.

El-Zanan, H. S., Lowenthal, D. H., Zielinska, B., Chow, J. C. and Kumar, N.: Determination of the organic aerosol mass to organic carbon ratio in IMPROVE samples, Chemosphere, 60(4), 485–496, https://doi.org/10.1016/j.chemosphere.2005.01.005, 2005.

Engling, G., Lee, J. J., Tsai, Y.-W., Lung, S.-C. C., Chou, C. C.-K. and Chan, C.-Y.: Size-Resolved Anhydrosugar Composition in Smoke Aerosol from Controlled Field Burning of Rice Straw, Aerosol Sci. Technol., 43(7), 662–672, https://doi.org/10.1080/02786820902825113, 2009.

FAO: FAOSTAT, http://www.fao.org/faostat/en/#data/QC, last access: 21 July 2021, 2020.Fomba, K. ., Müller, K., Van Pinxteren, D. and Herrmann, H.: Aerosol size-resolved trace metal composition in remote northern tropical Atlantic marine environment: case study Cape Verde islands, Atmos. Chem. Phys., 13(9), 4801–4814, https://doi.org/10.5194/acp-13-4801-2013, 2013.

Fomba, K. W., van Pinxteren, D., Müller, K., Spindler, G. and Herrmann, H.: Assessment of trace metal levels in size-resolved particulate matter in the area of Leipzig, Atmos. Environ., 176, 60–70, https://doi.org/10.1016/j.atmosenv.2017.12.024, 2018.

Franzin, B. T., Guizellini, F. C., de Babos, D. V., Hojo, O., Pastre, I. A., Marchi, M. R. R., Fertonani, F. L. and Oliveira, C. M. R. R.: Characterization of atmospheric aerosol (PM10 and PM2.5) from a medium sized city in São Paulo state, Brazil, J. Environ. Sci. (China), 89, 238–251, https://doi.org/10.1016/j.jes.2019.09.014, 2020.Friese, E. and Ebel, A.: Temperature Dependent Thermodynamic Model of the System H^+ - NH_4^+ - Na^+ - SO_4^{2-} - NO_3^- - Cl^- - H2O., J. Phys. Chem. A, 114, 11595–11631, https://doi.org/10.1021/jp101041j, Last access: 20 June, 2022, 2010.

Gonçalves, C., Figueiredo, B. R., Alves, C. A., Cardoso, A. A. and Vicente, A. M.: Size-segregated aerosol chemical composition from an agro-industrial region of São Paulo state, Brazil, Air Qual. Atmos. Heal. 2016 104, 10(4), 483–496, https://doi.org/10.1007/S11869-016-0441-0, 2016.

Gondwe, M.: Comparison of modeled versus measured MSA : nss SO = 4 ratios : A global analysis, Global Biogeochemical Cycles, 18, 1–18, https://doi.org/10.1029/2003GB002144,

2004.

Hall, D., Wu, C. Y., Hsu, Y. M., Stormer, J., Engling, G., Capeto, K., Wang, J., Brown, S., Li, H. W. and Yu, K. M.: PAHs, carbonyls, VOCs and PM 2.5 emission factors for pre-harvest burning of Florida sugarcane, Atmos. Environ., 55, 164–172, https://doi.org/10.1016/j.atmosenv.2012.03.034, 2012.

Hernández, J. D. R. and Mesa, Ó. J.: A simple conceptual model for the heat induced circulation over Northern South America and MESO-America, Atmosphere (Basel)., 11(11), 1–14, https://doi.org/10.3390/atmos11111235, 2020.

Hodshire, A. L., Akherati, A., Alvarado, M. J., Brown-Steiner, B., Jathar, S. H., Jimenez, J. L., Kreidenweis, S. M., Lonsdale, C. R., Onasch, T. B., Ortega, A. M. and Pierce, J. R.: Aging Effects on Biomass Burning Aerosol Mass and Composition: A Critical Review of Field and Laboratory Studies, Environ. Sci. Technol., 53(17), 10007–10022, https://doi.org/10.1021/acs.est.9b02588, 2019.

Ianniello, A., Spataro, F., Esposito, G., Allegrini, I., Hu, M. and Zhu, T.: and Physics Chemical characteristics of inorganic ammonium salts in PM 2 . 5 in the atmosphere of Beijing (China), , (October), https://doi.org/10.5194/acp-11-10803-2011, 2011.

Iinuma, Y., Engling, G., Puxbaum, H. and Herrmann, H.: A highly resolved anion-exchange chromatographic method for determination of saccharidic tracers for biomass combustion and primary bio-particles in atmospheric aerosol, Atmos. Environ., 43(6), 1367–1371, 2009.

Jorquera, H. and Barraza, F.: Source apportionment of ambient PM2.5 in Santiago, Chile: 1999 and 2004 results, Sci. Total Environ., 435–436, 418–429, https://doi.org/10.1016/j.scitotenv.2012.07.049, 2012.

Jorquera, H. and Barraza, F.: Source apportionment of PM10 and PM2.5 in a desert region in northern Chile, Sci. Total Environ., 444, 327–335, https://doi.org/10.1016/j.scitotenv.2012.12.007, 2013.

Kang, M., Ren, L., Ren, H., Zhao, Y., Kawamura, K., Zhang, H., Wei, L., Sun, Y., Wang, Z. and Fu, P.: Primary biogenic and anthropogenic sources of organic aerosols in Beijing, China: Insights from saccharides and n-alkanes, Environ. Pollut., 243, 1579–1587, https://doi.org/10.1016/j.envpol.2018.09.118, 2018.

Karagulian, F., Belis, C. A., Francisco, C., Dora, C., Prüss-ustün, A. M., Bonjour, S., Adair-rohani, H. and Amann, M.: Contributions to cities ' ambient particulate matter (PM): A systematic review of local source contributions at global level, Atmos. Environ., 120, 475–483, https://doi.org/10.1016/j.atmosenv.2015.08.087, 2015.Khedidji, S., Müller, K., Rabhi, L.,

Spindler, G., Fomba, K. W., Van Pinxteren, D., Yassaa, N. and Herrmann, H.: Chemical characterization of marine aerosols in a South Mediterranean coastal area located in Bou Ismaïl, Algeria, Aerosol Air Qual. Res., 20, 2448-2473, https://doi.org/10.4209/aaqr.2019.09.0458, 2020.

Kundu, S. and Stone, E. A.: Composition and sources of fine particulate matter across urban and rural sites in the Midwestern United States, Environ. Sci. Process. Impacts, 16(6), 1360–1370, https://doi.org/10.1039/c3em00719g, 2014.

Lara, L. L., Artaxo, P., Martinelli, L. A., Camargo, P. B., Victoria, R. L. and Ferraz, E. S. B.: Properties of aerosols from sugar-cane burning emissions in Southeastern Brazil, Atmos. Environ., 39(26), 4627–4637, https://doi.org/10.1016/j.atmosenv.2005.04.026, 2005.

Lee, S., Wang, Y. and Russell, A. G.: Assessment of secondary organic carbon in the southeastern United States: A review, J. Air Waste Manag. Assoc., 60(11), 1282–1292, https://doi.org/10.3155/1047-3289.60.11.1282, 2010.Lee, T., Yu, X., Kreidenweis, S. M., Malm, W. C. and Collett, J. L.: Semi-continuous measurement of PM 2.5 ionic composition at several rural locations in the United States, Atmos. Environ., 42, 6655–6669, https://doi.org/10.1016/j.atmosenv.2008.04.023, 2008.

Li, J., Song, Y., Mao, Y., Mao, Z., Wu, Y., Li, M., Huang, X., He, Q. and Hu, M.: Chemical characteristics and source apportionment of PM2.5 during the harvest season in eastern China's agricultural regions, Atmos. Environ., 92, 442–448, https://doi.org/10.1016/J.ATMOSENV.2014.04.058, 2014.

Li, X., Wang, L., Ji, D., Wen, T., Pan, Y., Sun, Y. and Wang, Y.: Characterization of the size-segregated water-soluble inorganic ions in the Jing-Jin-Ji urban agglomeration: Spatial/temporal variability, size distribution and sources, Atmos. Environ., 77, 250–259, https://doi.org/10.1016/j.atmosenv.2013.03.042, 2013.Liang, C. S., Duan, F. K., He, K. B., and Ma, Y. L.: Review on recent progress in observations, source identifications and countermeasures of PM2.5, Environ. Int., 86, 150–170, https://doi.org/10.1016/j.envint.2015.10.016, 2016.

Lin, L., Lee, M. L. and Eatough, D. J.: Review of recent advances in detection of organic markers in fine particulate matter and their use for source apportionment, J. Air Waste Manag. Assoc., 60(1), 3–25, https://doi.org/10.3155/1047-3289.60.1.3, 2010.

López Larada, J.: |Zona portuaria de Buenaventura: y su importancia en Colombia, Univ. San Buenaventura, 1–14 http://bibliotecadigital.usbcali.edu.co/bitstream/10819/7099/1/Zona_Portuaria_Buenaventura_Lopez_2017.pdf, last access: 23 February 2022, 2017.

Lopez, M. and Howell, W.: Katabatic Winds in the equatorial Andes, J. Atmos. Sci., 24(1), 29–35, 1967.

Lyu, R., Shi, Z., Alam, M. S., Wu, X., Liu, D., Vu, T. V., Stark, C., Xu, R., Fu, P., Feng, Y. and Harrison, R. M.: Alkanes and aliphatic carbonyl compounds in wintertime PM2.5 in Beijing, China, Atmos. Environ., 202(November 2018), 244–255, https://doi.org/10.1016/j.atmosenv.2019.01.023, 2019.

MADS: Res. No 2254, Ministerio de Ambiente y Desarrollo Sostenible, Colombia., http://www.ideam.gov.co/documents/51310/527391/2.+Resoluci%C3%B3n+2254+de+2017+-+Niveles+Calidad+del+Aire..pdf/c22a285e-058e-42b6-aa88-2745fafad39f , 2017.

Majra, J. P.: Air Quality in Rural Areas, in Chemistry, Emission Control, Radioactive Pollution and Indoor Air Quality, https://doi.org/10.5772/16890, , 2011.

Malcolm, H. M., and Dobson, S.: The calculation of an Environmental Assessment Level (EAL) for atmospheric PAHs using relative potencies, Department of the Environment, London. 1994.

Mancilla, Y., Mendoza, A., Fraser, M. P. and Herckes, P.: Organic composition and source apportionment of fine aerosol at Monterrey, Mexico, based on organic markers, Atmos. Chem. Phys., 16(2), 953–970, https://doi.org/10.5194/acp-16-953-2016, 2016.

Marzi, R., Torkelson, B. E. and Olson, R. K.: A revised carbon preference index, Org. Geochem., 20(8), 1303–1306, https://doi.org/10.1016/0146-6380(93)90016-5, 1993.Meinardi, S., Simpson, I. J., Blake, N. J., Blake, D. R. and Rowland, F. S.: Dimethyl disulfide (DMDS) and dimethyl sulfide (DMS) emissions from biomass burning in Australia, Geophys. Res. Lett., 30(9), https://doi.org/10.1029/2003GL016967, 2003.

Mesa S., Ó. J. and Rojo H., J. D.: On the general circulation of the atmosphere around Colombia, Rev. la Acad. Colomb. Ciencias Exactas, Fis. y Nat., 44(172), 857–875, https://doi.org/10.18257/RACCEFYN.899, 2020.

Miguel, A. H. and Pereira, P. A. P.: Benzo(k)fluoranthene, benzo(ghi)perylene, and indeno(1, 2, 3-cd)pyrene: New tracers of automotive emissions in receptor modeling, Aerosol Sci. Technol., 10(2), 292–295, https://doi.org/10.1080/02786828908959265, 1989.

Min.Agricultura: Cadenas cárnicas bovina - bufalina, Bogotá D.C. https://sioc.minagricultura.gov.co/Bovina/Documentos/2018-12-30 Cifras Sectoriales.pdf, last access: 20 June 2022, 2018.

Min.Agricultura: Cadena Carnica Porcina, Bogotá D.C. https://sioc.minagricultura.gov.co/Porcina/Documentos/2019-12-30 Cifras sectoriales.pdf, last

access: 20 June 2022, 2019.

Min.Agricultura: Cadena Avícola, segundo trimestre 2020, Bogotá D.C.https://sioc.minagricultura.gov.co/Avicola/Documentos/2020-06-30%20Cifras%20Sectoriales.pdf, last access: 20 June 2022, 2020.

Mugica-Álvarez, V., Santiago-de la Rosa, N., Figueroa-Lara, J., Flores-Rodríguez, J., Torres-Rodríguez, M. and Magaña-Reyes, M.: Emissions of PAHs derived from sugarcane burning and processing in Chiapas and Morelos México, Sci. Total Environ., 527–528, 474–482, https://doi.org/10.1016/j.scitotenv.2015.04.089, 2015.

Mugica-Álvarez, V., Ramos-Guízar, S., Rosa, N. S. la, Torres-Rodríguez, M. and Noreña-Franco, L.: Black Carbon and Particulate Organic Toxics Emitted by Sugarcane Burning in Veracruz, México, Int. J. Environ. Sci. Dev., 7(4), 290–294, https://doi.org/10.7763/ijesd.2016.v7.786, 2016.

Mugica-Álvarez, V., Hernández-Rosas, F., Magaña-Reyes, M., Herrera-Murillo, J., Santiago-De La Rosa, N., Gutiérrez-Arzaluz, M., de Jesús Figueroa-Lara, J. and González-Cardoso, G.: Sugarcane burning emissions: Characterization and emission factors, Atmos. Environ., 193, 262–272, https://doi.org/10.1016/j.atmosenv.2018.09.013, 2018.

Murillo, J. H., Roman, S. R., Felix, J., Marin, R., Ramos, A. C., Jimenez, S. B., Gonzalez, B. C. and Baumgardner, D. G.: Chemical characterization and source apportionment of PM10 and PM2.5 in the metropolitan area of Costa Rica, Central America Jorge, Atmos. Pollut. Res., 4(2), 181–190, https://doi.org/10.5094/APR.2013.018, 2013.

Neusüss, C., Pelzing, M., Plewka, A. and Herrmann, H.: A new analytical approach for size-resolved speciation of organic compounds in atmospheric aerosol particles: Methods and first results, J. Geophys. Res. Atmos., 105(D4), 4513–4527, https://doi.org/10.1029/1999JD901038, 2000.

Nisbet, I. C. T. and LaGoy, P. K.: Toxic equivalency factors (TEFs) for polycyclic aromatic hydrocarbons (PAHs), Regul. Toxicol. Pharmacol., 16(3), 290–300, https://doi.org/10.1016/0273-2300(92)90009-X, 1992.

Oros, D. R., Abas, M. R. bin, Omar, N. Y. M. J., Rahman, N. A. and Simoneit, B. R. T.: Identification and emission factors of molecular tracers in organic aerosols from biomass burning: Part 3. Grasses, Appl. Geochemistry, 21(6), 919–940, https://doi.org/10.1016/j.apgeochem.2006.01.008, 2006.

Orozco, C., Sanandres, E. and Molinares, I.: Colombia, Panamá y la Ruta Panamericana: Encuentros y Desencuentros, Memorias Rev. Digit. Hist. y Arqueol. desde el Caribe, 16(ISSN

1794-8886) http://www.scielo.org.co/scielo.php?script=sci_arttext&pid=S1794-88862012000100005, last access: 23 February 2022, 2012.

Ortiz, E. Y., Jimenez, R., Fochesatto, G. J. and Morales-Rincon, L. A.: Caracterización de la turbulencia atmosférica en una gran zona verde de una megaciudad andina tropical, Rev. la Acad. Colomb. Ciencias Exactas, Físicas y Nat., 43(166), 133, https://doi.org/10.18257/raccefyn.697, 2019.

Pant, P. and Harrison, R. M.: Estimation of the contribution of road traffic emissions to particulate matter concentrations from field measurements: A review, Atmos. Environ., 77, 78–97, https://doi.org/10.1016/j.atmosenv.2013.04.028, 2013.

Pereira, G. M., Teinilä, K., Custódio, D., Gomes Santos, A., Xian, H., Hillamo, R., Alves, C. A., Bittencourt de Andrade, J., Olímpio da Rocha, G., Kumar, P., Balasubramanian, R., Andrade, M. de F. and de Castro Vasconcellos, P.: Particulate pollutants in the Brazilian city of São Paulo: 1-year investigation for the chemical composition and source apportionment, Atmos. Chem. Phys., 17(19), 11943–11969, https://doi.org/10.5194/acp-17-11943-2017, 2017.

Pereira, G. M., Oraggio, B., Teinilä, K., Custódio, D., Huang, X., Hillamo, R., Alves, C. A., Balasubramanian, R., Rojas, N. Y. and Sanchez-Ccoyllo, O.: A comparative chemical study of PM 10 in three Latin American cities : Lima, Medellín, ans São Paulo, Air Qual. Atmos. Heal., 12, 1141–1152, https://doi.org/10.1007/s11869-019-00735-3, 2019.

Pio, C., Cerqueira, M., Harrison, R. M., Nunes, T., Mirante, F., Alves, C., Oliveira, C., Sanchez de la Campa, A., Artíñano, B. and Matos, M.: OC/EC ratio observations in Europe: Re-thinking the approach for apportionment between primary and secondary organic carbon, Atmos. Environ., 45(34), 6121–6132, https://doi.org/10.1016/j.atmosenv.2011.08.045, 2011.

Plaza, J., Artíñano, B., Salvador, P., Gómez-Moreno, F. J., Pujadas, M. and Pio, C. A.: Short-term secondary organic carbon estimations with a modified OC/EC primary ratio method at a suburban site in Madrid (Spain), Atmos. Environ., 45(15), 2496–2506, https://doi.org/10.1016/j.atmosenv.2011.02.037, 2011.Pye, H. O. T., Nenes, A., Alexander, B., Ault, A. P., Barth, M. C., Clegg, S. L., Collett, J. L., Fahey, K. M., Hennigan, C. J., Herrmann, H., Kanakidou, M., Kelly, J. T., Ku, I. T., Faye McNeill, V., Riemer, N., Schaefer, T., Shi, G., Tilgner, A., Walker, J. T., Wang, T., Weber, R., Xing, J., Zaveri, R. A. and Zuend, A.: The acidity of atmospheric particles and clouds, Atmospheric chemistry and physics, 20 (8), 4809-4888, https://doi.org/10.5194/acp-20-4809-2020, last access: 20 June 2022, 2020.

Ramírez, O., Sánchez de la Campa, A. M., Amato, F., Catacolí, R. A., Rojas, N. Y. and de la Rosa, J.: Chemical composition and source apportionment of PM10 at an urban background site in a high–altitude Latin American megacity (Bogota, Colombia), Environ. Pollut., 233, 142–155,

https://doi.org/10.1016/j.envpol.2017.10.045, 2018.

Ravindra, K., Sokhi, R. and Van Grieken, R.: Atmospheric polycyclic aromatic hydrocarbons: Source attribution, emission factors and regulation, Atmos. Environ., 42(13), 2895–2921, https://doi.org/10.1016/j.atmosenv.2007.12.010, 2008.

Romero, D., Sarmiento, H. and Pachón, J. E.: Estimación de hidrocarburos aromáticos policíclicos y metales pesados asociados con la quema de caña de azúcar en el valle geográfico del río Cauca , Colombia, Rev. Épsilon, 21(2013), 57–82, 2013.

RUNT. (2021). [Vehicles fleet dataset Cauca Valley Department] [Unpublished raw data]. Registro Unico del Transito.

Ryu, S. Y., Kim, J. E., Zhuanshi, H., Kim, Y. J. and Kang, G. U.: Chemical composition of post-harvest biomass burning aerosols in gwangju, Korea, J. Air Waste Manag. Assoc., 54(9), 1124–1137, https://doi.org/10.1080/10473289.2004.10471018, 2004.

Dos Santos, C. Y. M., Azevedo, D. de A. and De Aquino Neto, F. R.: Selected organic compounds from biomass burning found in the atmospheric particulate matter over sugarcane plantation areas, Atmos. Environ., 36(18), 3009–3019, https://doi.org/10.1016/S1352-2310(02)00249-2, 2002.

Schauer, J. J.: Sources contributions to atmospheric organic compound concentrations: Emissions measurments and model predictions, Ph.D. thesis, California Institute Technology, doi:10.7907/3FPH-HY50, last access: 20 June 2022, 1998.

SDA: Plan decenal de descontaminación del aire de Bogotá, Bogotá D.C. https://uniandes.edu.co/sites/default/files/asset/document/parte-A-PDDB.pdf, last access: 20 June 2022, 2010.Seinfeld, J. H. and Pandis, S. N.: Atmospheric Chemistry and Physics: From Air Pollution to Climate Change,2nd ed., Wiley, Hoboken, 2006.

SICOM: Boletín estadístico, Boletín Estad. EDS automotriz y Fluv. https://www.sicom.gov.co/index.php/boletin-estadistico, last access: 15 February 2022, 2018.

Simoneit, B. R. T.: Biomass burning - A review of organic tracers for smoke from incomplete combustion, Appl. Geochemistry, 17(3), 129–162, https://doi.org/10.1016/S0883-2927(01)00061-0, 2002.

Snider, G., Weagle, C. L., Murdymootoo, K. K., Ring, A., Ritchie, Y., Stone, E., Walsh, A., Akoshile, C., Anh, N. X., Balasubramanian, R., Brook, J., Qonitan, F. D., Dong, J., Griffith, D., He, K., Holben, B. N., Kahn, R., Lagrosas, N., Lestari, P., Ma, Z., Misra, A., Norford, L. K., Quel, E. J., Salam, A., Schichtel, B., Segev, L., Tripathi, S., Wang, C., Yu, C., Zhang, Q., Zhang, Y., Brauer, M.,

Cohen, A., Gibson, M. D., Liu, Y., Martins, J. V., Rudich, Y. and Martin, R. V.: Variation in global chemical composition of PM2.5: emerging results from SPARTAN, Atmos. Chem. Phys., 16(15), 9629–9653, https://doi.org/10.5194/acp-16-9629-2016, 2016.

Sorooshian, A., Crosbie, E., Maudlin, L. C., Youn, J., Wang, Z., Shingler, T., Ortega, A. M., Hersey, S., and Woods, R. K.: Surface and airborne measurements of organosulfur and methanesulfonate over the western United States and coastal areas, J. Geophys. Res. Atmos., 120, 8535–8548, https://doi.org/10.1002/2015JD023822, 2015.

Souza, D. Z., Vasconcellos, P. C., Lee, H., Aurela, M., Saarnio, K., Teinilä, K. and Hillamo, R.: Composition of PM2.5 and PM10 collected at Urban Sites in Brazil, Aerosol Air Qual. Res., 14(1), 168–176, https://doi.org/10.4209/aaqr.2013.03.0071, 2014.

Stahl, C., Cruz, M. T., Bañaga, P. A., Betito, G., Braun, R. A., Aghdam, M. A., Cambaliza, M. O., Lorenzo, G. R., Macdonald, A. B., Hilario, M. R. A., Pabroa, P. C., Yee, J. R., and Simpas, J. B.: Sources and characteristics of size-resolved particulate organic acids and methanesulfonate in a coastal megacity : Manila , Philippines, Atmos. Chem. Phys., 20, 15907–15935, last access: 20 June 2022, 2020.

Sutton, M. A., Billen, G., Bleeker, A., Erisman, J. W., Grennfelt, P., Grinsven, H. Van, Grizzetti, B., Howard, C. M. and Leip, A.: Technical summary Part I Nitrogen in Europe : the present position, Eur. Nitrogen Assess. Sources, Eff. Policy Perspect., (December 2015), Xxxv–Lii, https://doi.org/10.1017 / CBO9780511976988.003, 2011.

Szabó, J., Szabó Nagy, A. and Erdős, J.: Ambient concentrations of PM10, PM10-bound polycyclic aromatic hydrocarbons and heavy metals in an urban site of Győr, Hungary, Air Qual. Atmos. Heal., 8(2), 229–241, https://doi.org/10.1007/s11869-015-0318-7, 2015.

Tang, M., Guo, L., Bai, Y., Huang, R., Wu, Z. and Wang, Z.: Impacts of methanesulfonate on the cloud condensation nucleation activity of sea salt aerosol, Atmos. Environ., 201(October 2018), 13–17, https://doi.org/10.1016/j.atmosenv.2018.12.034, 2019.

Tobiszewski, M. and Namieśnik, J.: PAH diagnostic ratios for the identification of pollution emission sources, Environ. Pollut., 162(November 2018), 110–119, https://doi.org/10.1016/j.envpol.2011.10.025, 2012.

Tsigaridis, K., Daskalakis, N., Kanakidou, M., Adams, P. J., Artaxo, P., Bahadur, R., Balkanski, Y., Bauer, S. E., Bellouin, N., Benedetti, A., Bergman, T., Berntsen, T. K., Beukes, J. P., Bian, H., Carslaw, K. S., Chin, M., Curci, G., Diehl, T., Easter, R. C., Ghan, S. J., Gong, S. L., Hodzic, A., Hoyle, C. R., Iversen, T., Jathar, S., Jimenez, J. L., Kaiser, J. W., Kirkeväg, A., Koch, D., Kokkola, H., H Lee, Y., Lin, G., Liu, X., Luo, G., Ma, X., Mann, G. W., Mihalopoulos, N., Morcrette, J. J., Müller, J. F., Myhre, G., Myriokefalitakis, S., Ng, N. L., O'donnell, D., Penner, J. E., Pozzoli, L., Pringle, K.

J., Russell, L. M., Schulz, M., Sciare, J., Seland, Shindell, D. T., Sillman, S., Skeie, R. B., Spracklen, D., Stavrakou, T., Steenrod, S. D., Takemura, T., Tiitta, P., Tilmes, S., Tost, H., Van Noije, T., Van Zyl, P. G., Von Salzen, K., Yu, F., Wang, Z., Wang, Z., Zaveri, R. A., Zhang, H., Zhang, K., Zhang, Q. and Zhang, X.: The AeroCom evaluation and intercomparison of organic aerosol in global models, Atmos. Chem. Phys., 14(19), 10845–10895, https://doi.org/10.5194/acp-14-10845-2014, 2014.

Turpin, B. J. and Lim, H.: Species Contributions to PM2.5 Mass Concentrations: Revisiting Common Assumptions for Estimating Organic Mass, Aerosol Sci. Technol., 35:1(September 2014), 37–41, https://doi.org/http://dx.doi.org/10.1080/02786820119445, 2010.

Urban, R. C., Alves, C. A., Allen, A. G., Cardoso, A. A., Queiroz, M. E. C. and Campos, M. L. A. M.: Sugar markers in aerosol particles from an agro-industrial region in Brazil, Atmos. Environ., 90(2014), 106–112, https://doi.org/10.1016/j.atmosenv.2014.03.034, 2014.

Urban, R. C., Alves, C. A., Allen, A. G., Cardoso, A. A. and Campos, M. L. A. M.: Organic aerosols in a Brazilian agro-industrial area: Speciation and impact of biomass burning, Atmos. Res., 169, 271–279, https://doi.org/10.1016/j.atmosres.2015.10.008, 2016.

Vargas, F. A., Rojas, N. Y., Pachon, J. E. and Russell, A. G.: PM10 characterization and source apportionment at two residential areas in Bogota, Atmos. Pollut. Res., 3(1), 72–80, https://doi.org/10.5094/APR.2012.006, 2012.

Vasconcellos, P. C., Balasubramanian, R., Bruns, R. E., Sanchez-Ccoyllo, O., Andrade, M. F. and Flues, M.: Water-soluble ions and trace metals in airborne particles over urban areas of the state of São Paulo, Brazil: Influences of local sources and long range transport, Water. Air. Soil Pollut., 186(1–4), 63–73, https://doi.org/10.1007/s11270-007-9465-2, 2007.

Vasconcellos, P. C., Souza, D. Z., Ávila, S. G., Araújo, M. P., Naoto, E., Nascimento, K. H., Cavalcante, F. S., Dos, M., Smichowski, P. and Behrentz, E.: Comparative study of the atmospheric chemical composition of three South American cities, Atmos. Environ., 45(32), 5770–5777, https://doi.org/10.1016/j.atmosenv.2011.07.018, 2011.

Victoria, J. I., Amaya, A., Rangel, H., Viveros, C., Cassalett, C., Carbonell, J., Quintero, R., Cruz, R., Isaacs, C., Larrahondo, J., Moreno, C. A., Palma, A., Posada, C., Villegas, F. T., and Gomez, L. A.: Características agronómicas y de productividad de la variedad Cenicaña Colombia (CC) 85-92, Cenicaña, Cali, 90 pp., https://www.cenicana.org/pdf_privado/serie_tecnica/st_30/st_30.pdf, last access: 21 June 2022, 2002.

Villalobos, A. M., Barraza, F., Jorquera, H. and Schauer, J. J.: Chemical speciation and source apportionment of fine particulate matter in Santiago, Chile, 2013, Sci. Total Environ., 512–513,

133–142, https://doi.org/10.1016/j.scitotenv.2015.01.006, 2015.

Wadinga Fomba, K., Deabji, N., El Islam Barcha, S., Ouchen, I., Mehdi Elbaramoussi, E., Cherkaoui El Moursli, R., Harnafi, M., El Hajjaji, S., Mellouki, A. and Herrmann, H.: Application of TXRF in monitoring trace metals in particulate matter and cloud water, Atmos. Meas. Tech., 13(9), 4773–4790, https://doi.org/10.5194/amt-13-4773-2020, 2020.

Wagner, R., Jähn, M. and Schepanski, K.: Wildfires as a source of airborne mineral dust - Revisiting a conceptual model using large-eddy simulation (LES), Atmos. Chem. Phys., 18(16), 11863–11884, https://doi.org/10.5194/acp-18-11863-2018, 2018.WHO Regional Office for Europe: Air quality guidelines for Europe, pp. 457–465, World Health Organization, Copenhagen, Denmark, https://doi.org/10.1525/9780520948068-070, 2020.

World Health Organization: Review of evidence on health aspects of air pollution - REVIHAAP Project. http://www.euro.who.int/pubrequest%0Ahttp://www.euro.who.int/__data/assets/pdf_file/0004/193108/REVIHAAP-Final-technical-report-final-version.pdf., last access: 20 June 2022, 2013.

World Health Organization: WHO global air quality guidelines: particulate matter (PM2.5 and PM10), ozone, nitrogen dioxide, sulfur dioxide and carbon monoxide, World Health Organization. https://www.who.int/publications/i/item/9789240034228, last access: 22 February 2022, 2021.

Wu, C. and Zhen Yu, J.: Evaluation of linear regression techniques for atmospheric applications: The importance of appropriate weighting, Atmos. Meas. Tech., 11(2), 1233–1250, https://doi.org/10.5194/amt-11-1233-2018, 2018.

Xue, J., Lau, A. K. H. and Yu, J. Z.: A study of acidity on PM2.5 in Hong Kong using online ionic chemical composition measurements, Atmos. Environ., 45(39), 7081–7088, https://doi.org/10.1016/j.atmosenv.2011.09.040, 2011.

Yadav, I. C. and Devi, N. L.: Biomass burning, regional air quality, and climate change, in: Earth Systems and Environmental Sciences, edited by: Nriagu, J., Elsevier Inc., Waltham, 386–391, https://doi.org/10.1016/B978-0-12-409548-9.11022-X, 2019.

Yadav, S., Tandon, A. and Attri, A. K.: Monthly and seasonal variations in aerosol associated n-alkane profiles in relation to meteorological parameters in New Delhi, India, Aerosol Air Qual. Res., 13(1), 287–300, https://doi.org/10.4209/aaqr.2012.01.0004, 2013.

Yan, J., Wang, L., Fu, P. P. and Yu, H.: Photomutagenicity of 16 polycyclic aromatic hydrocarbons from the US EPA priority pollutant list, Mutat. Res. - Genet. Toxicol. Environ.

Mutagen., 557(1), 99–108, https://doi.org/10.1016/j.mrgentox.2003.10.004, 2004.

Yunker, M. B., Macdonald, R. W., Vingarzan, R., Mitchell, H., Goyette, D. and Sylvestre, S.: PAHs in the Fraser River basin: a critical appraisal of PAH ratios as indicators of PAH source and composition, Org. Geochem., 33, 489–515, https://doi.org/doi.org/10.1016/S0146-6380(02)00002-5, 2002.

Zíková, N., Wang, Y., Yang, F., Li, X., Tian, M., and Hopke, P. K.: On the source contribution to Beijing PM2.5 concentrations, 134, 84–95, https://doi.org/10.1016/j.atmosenv.2016.03.047, 2016

4.7. Supplementary information

Table S4-1. Preliminary PM$_{10}$ emission estimate in CRV region reported in Ton year.

Sector	Source Emission	Year	Emission (Ton PM10 year^{-1})	Reference
Manufacturing processes	Food and beverage industry	2017	6853.81	(CVC and Fulecol, 2018; CVC and K2, 2018b, 2018c, 2018d, 2018a;CVC, 2012)
Mobile	Traffic	2017	3425.36	(CVC and Fulecol, 2018; CVC and K2, 2018b, 2018c, 2018d, 2018a)
Manufacturing processes	Paper and printing industry	2017	2766.9	(CVC and Fulecol, 2018; CVC and K2, 2018a; CVC, 2012)
Sugarcane burning	Sugarcane burning	2018	1740.31	(Cardozo et al., 2019)
Manufacturing processes	Power generation, incinerators, and other services	2017	608.39	(CVC and Fulecol, 2018; CVC and K2, 2018c, 2018d, 2018a; CVC, 2012)
Manufacturing processes	Production of cement, asphalt, and tiles	2017	585.07	(CVC, 2012)
Manufacturing processes	Metallurgical industry	2017	260.13	(CVC and Fulecol, 2018; CVC and K2, 2018c)
Manufacturing processes	Luminaire and battery industry	2012	27.37	(CVC, 2012)
Manufacturing processes	Chemistry Industry	2012	27.71	(CVC, 2012)
Manufacturing processes	Leather and textile industry	2012	18.27	(CVC, 2012)
Other	Other	2018	21.27	

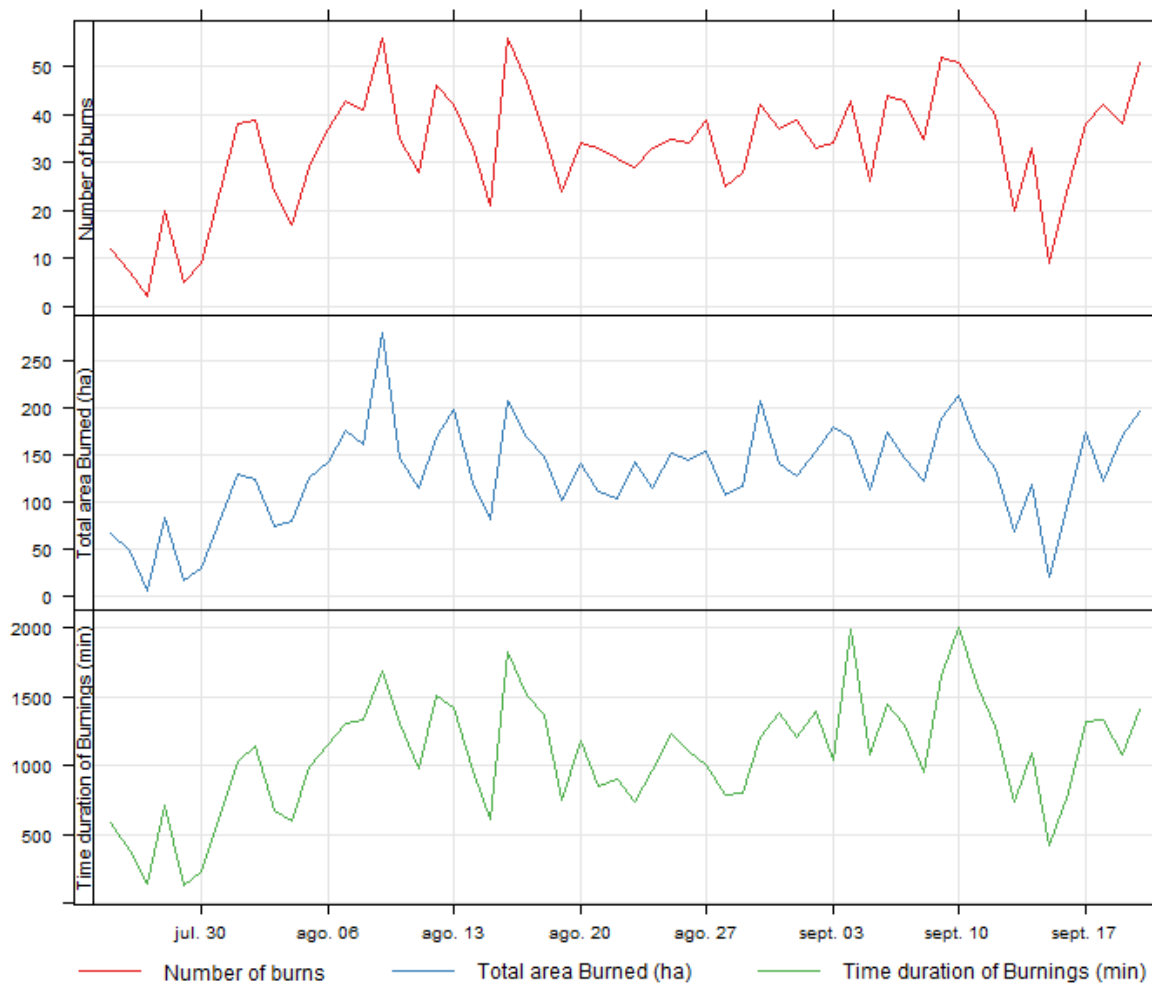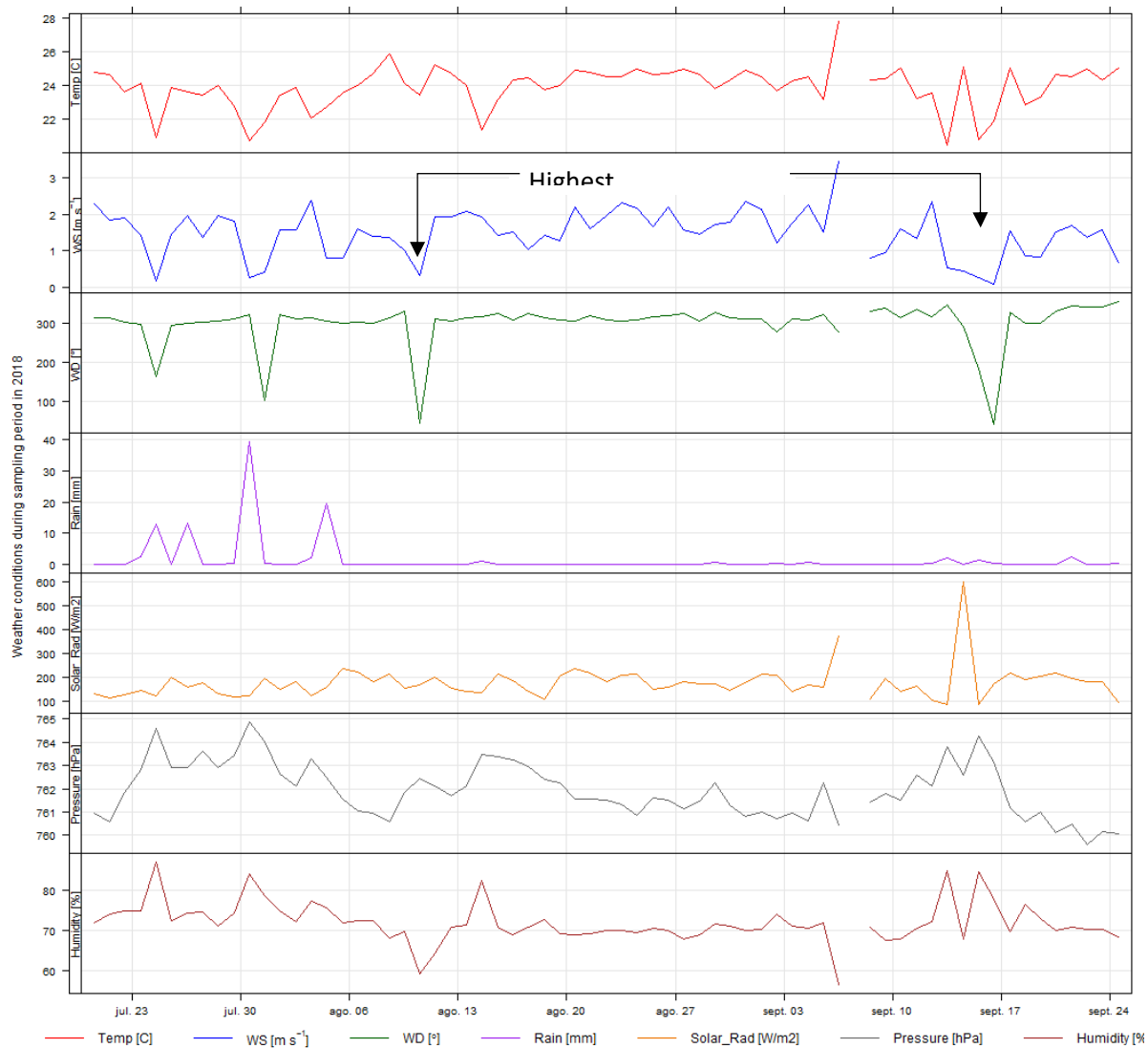Figure S4-1.Number of preharvest sugarcane burnings registered during this study, area burned and time of those burnings.

Figure S4-2. Weather conditions during the samdpling period in Palmira.
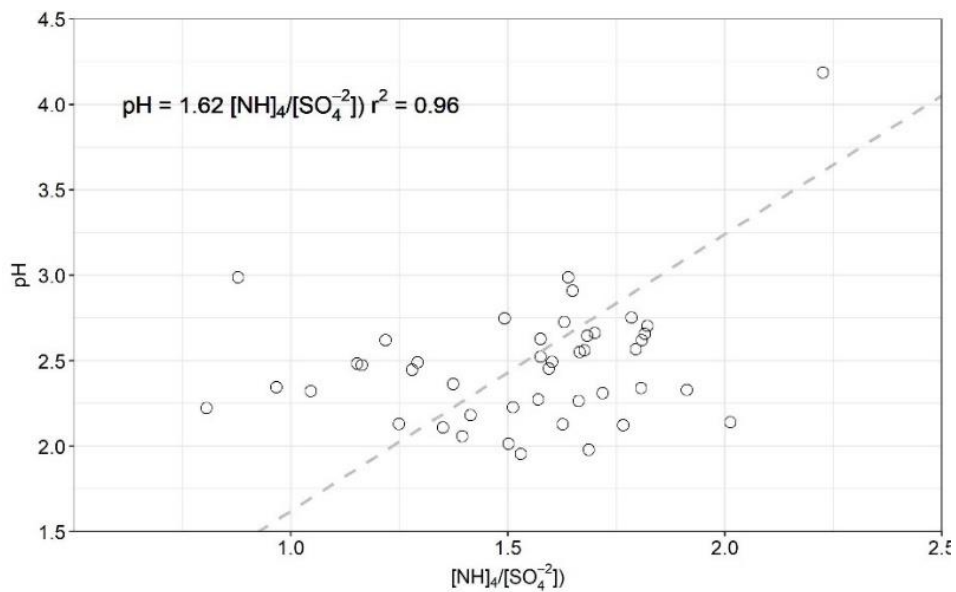
Figure S4-3. Scatter plot of $[NH_4^+]/[SO_4^{2-}]$ ratio and pH for $PM_{2.5}$ samples collected in CRV.
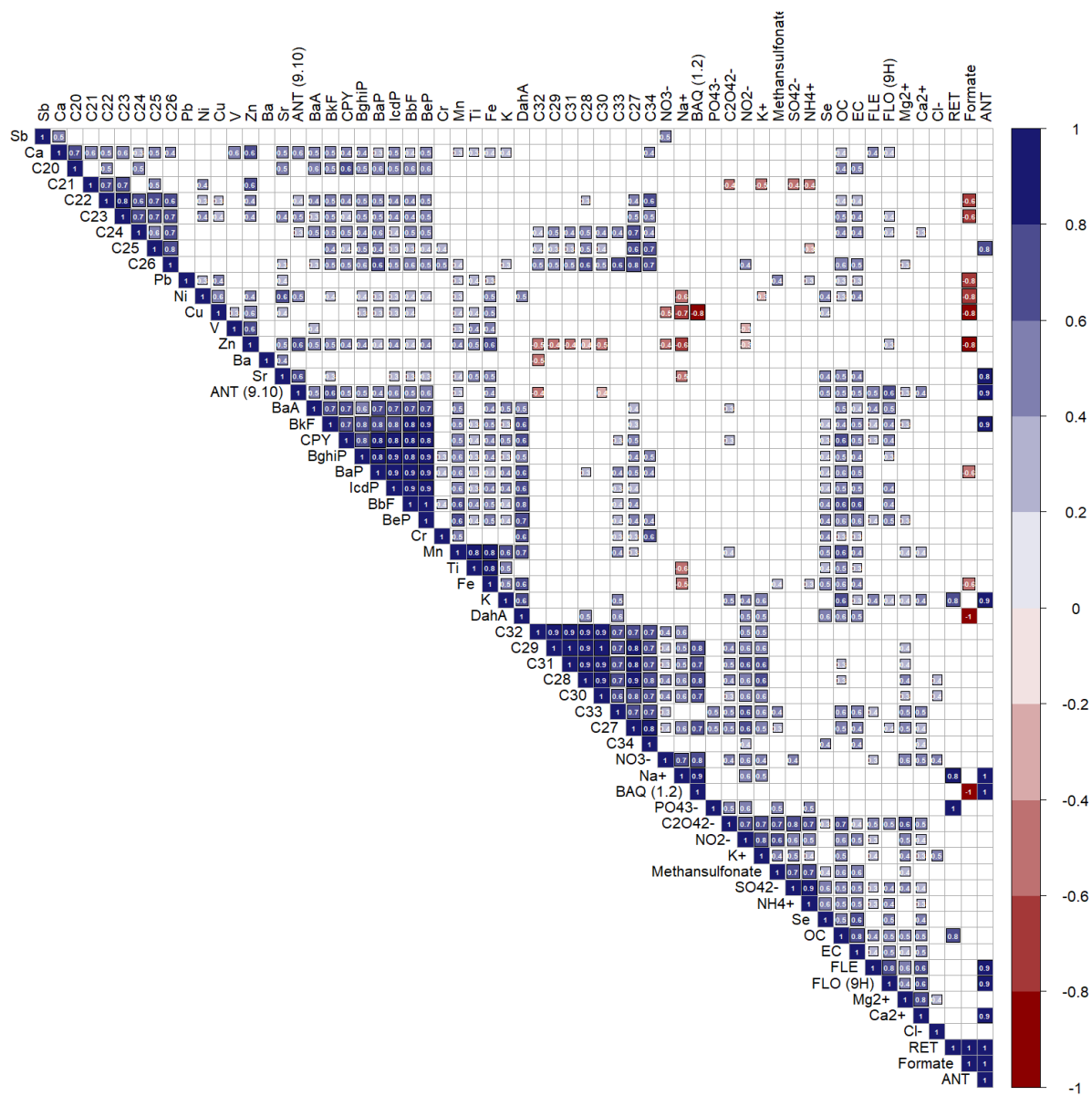
Figure S4-4. Correlation matrix of chemical compounds. White areas corresponding to correlation with p value > 0.05
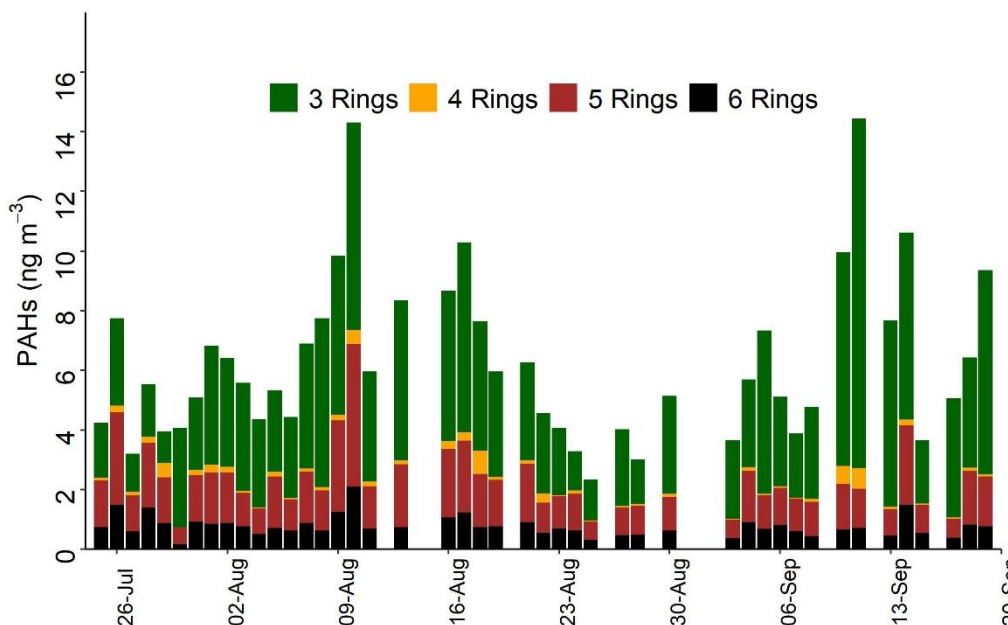
Figure S4-5. Time series of PAHs in PM$_{2.5}$ samples collected in CRV during 2018.

Table S4-2. Mean and one standard deviation concentrations of PAHs measured in the samples of PM$_{2.5}$ collected in CRV region, concentrations reported in ng m^{-3}.

PAHs	Abbreviation	Rings	Mean	sd
Fluorene	FLE	3 rings	2.82	1.52
9 10-Anthracenedione	ANT (9,10)	3 rings	0.67	0.33
Benzo(b)fluoranthene	BbF	5 rings	0.44	0.22
9H-Fluoreneone	FLO (9H)	3 rings	0.41	0.34
Benzo(ghi)perylene	BghiP	6 rings	0.40	0.17
Cyclopenta(cd)pyrene	CPY	5 rings	0.38	0.21
Indeno(1 2 3-cd)pyrene	IcdP	6 rings	0.38	0.18
Benz(e)pyrene	BeP	5 rings	0.28	0.13
Benz(a)pyrene	BaP	5 rings	0.27	0.14
1,2 Benzanthraquinone	BAQ (1,2)	4 rings	0.21	0.15
Phenanthrene	PHEN	3 rings	0.19	0.18
Anthracene	ANT	3 rings	0.08	0.18

Benzo(k)fluoranthene	BkF	5 rings	0.14	0.08
Retene	RET	3 rings	0.14	0.11
Fluoranthene	FLT	4 rings	0.13	0.08
Pyrene	PYR	4 rings	0.12	0.05
Benz(a)anthracene	BaA	4 rings	0.09	0.05
Dibenz(ah)Anthracene	DahA	5 rings	0.06	0.03
2, 2-Binaphthyl	BNT (2.2)	4 rings	0.03	0.05
Chrysene(+Triphenylene)	CHRY	4 rings	0.02	0.03
Benzo(b)naphtho(1 2)thiophene	BNT (2,1)	4 rings	0.01	0.01
BaP TEQ			0.38	0.23
BaP MEQ			0.54	0.29
∑ PAH 3 Rings (LMW)			3.3	2.09
∑ PAH 4 Rings (MMW)			0.12	0.18
∑ PAH 5 Rings (HMW)			1.48	0.77
∑ PAH 6 Rings (HMW)			0.72	0.35
BeP/(BeP+BaP)			0.51	0.04
IcdP/(IcdP+BghiP)			0.48	0.04
BaP/BghiP			0.69	0.13
IcdP/BghiP			0.93	0.14
LMW/(MMW+HMW)			1.43	1.00

Table S4-3. Median concentrations and 1 standard deviation of n-alkanes analyzed in $PM_{2.5}$ samples collected in CRV (ng/m^3).

n-Alkane	Mean	sd
C20	0.34	0.17
C21	0.30	0.29
C22	0.51	1.08
C23	1.14	0.83
C24	3.03	1.68
C25	2.96	1.08
C26	3.40	1.30
C27	3.06	1.15
C28	2.68	1.41
C29	6.35	3.41
C30	4.22	3.31
C31	5.87	3.37
C32	2.53	1.58
C33	3.15	2.64
C34	1.10	0.61
$\sum$n-alkanes	40.36	18.82
CPI	1.22	0.18
WAX (%)	12.65	5.21

5. Conclusions and Perspective

5.1. Conclusions

The focus of this chapter is to compile the key findings from the previous four chapters and to provide a broad overview of the findings. This dissertation provide knowledge about particle size distribution of aerosols in urban areas of Colombia, identifying the Particle Number Concentration, and size distribution of number, volume, and mass of airborne aerosols. In addition, this research contributes in expand our understanding of the chemical composition of urban aerosols in Colombia using two approaches: sized segregated for PM_{10} in nine stages simulating the parts of the human respiratory system, and the second approach way was through samples of bulk $PM_{2.5}$.

The most relevant findings in this research are present below:

The Particle Number Concentration and Number Particle Size Distribution was assess using the ELPI$^+$, which is a cascade impactor that classifies particles through inertial impaction and then counts them using the electrical charge provide individually to each particle in order to be sensed with the electrometers installed in each stage of the impactor. The ELPI$^+$ showed an acceptable in terms of particles number concentration accuracy in size range from 17 nm and 10 μm.

Despite the two stations of the Bogota Air Quality Network used to determine the Particle Number Concentration had similar hourly $PM_{2.5}$ concentrations, the Particle Number concentration was higher in the urban background station of San Cristobal (3.8×10^3 #/cm^3) than the traffic station of Las Ferias (2.8×10^3 #/cm^3). In both stations, around 80% of the particles are nanoparticles, meaning they are smaller than 100 nm, similar to what has been reported in other urban areas.

Particle number concentrations varied more hourly in the Las Ferias station than in the San Cristobal site. The maximum value of particle number concentrations was reached at 7:00 H with concentrations of 8.2×10^3 #/cm^3 in San Cristobal and 5.8×10^3 #/cm^3 in Las Ferias. In comparison, the minimum concentration was observed at midnight, which almost four times lower than the maximum.

In terms of the weekly variability, the changes experimented on Bogotá's dynamics during the weekend represent a further reduction of particle number concentration in Las Ferias than in San Cristobal. Hence, the reduction of the traffic rate during the weekend near Las Ferias station means a reduction of a third part of the particle number concentration. But the changes that happened during the weekend in San Cristobal, just contribute to a reduction of fifty percent of particles in this station.

The measurement of the Number Particle Size Distributions with ELPI$^+$ showed similar diameters values compere with a reference instrument. However, a smaller mode observed in accumulation range size (~120 nm) was not perceivable with the ELPI$^+$, as in the reference instrument. The maximum number of particles finding in the diameter mode of the measurement's performance with ELPI$^+$ was twice that reported by the reference instrument.

The Number Particles Size Distribution found in Las Feria's station was unimodal centered in 120 nm, without variability during the diurnal pattern. On the other hand, in San Cristobal was evidenced a bimodal distribution, especially notorious in the traffic rush hours, with a second mode centered in 30 nm, which is the size range with more uncertainty in the performance of ELPI$^+$.

The Lung Deposition Surface Area concentration reveled a higher potential for particles in the urban background stations of San Cristobal than in the traffic station of Las Ferias. The average Lung Deposition Surface Area concentration in San Cristobal was 48.1 $\mu m^2/cm^3$, whereas in Las Ferias was 34.2 $\mu m^2/cm^3$, which were higher than reported in other studies conducted in urban areas, even though with significant influence of traffic emissions.

Another significant conclusion of this research was that the hourly patterns of PM$_{2.5}$ concentrations and lung deposition surface area did not line up. The maximum PM$_{2.5}$ concentrations were recorded at 19:00 H, while the maximum LDSA concentration occurred in the morning at 7:00 H.

This study determined that vehicle emissions are the primary source of ultrafine particles in two urban environments assessed in Bogotá. Further, this research identifies a background concentration of particles in the range of 500 $\#/cm^3$ associated with higher-speed easterly winds. Higher concentrations were detected mainly in the hours of greatest vehicular traffic.

The relative humidity wasn't associated with the PNC in both stations because this meteorological condition did not show a correlation between the concentration of Aitken particles and ultrafine particles.

As result of this study was determined the concentration of particulate matter that can reach the alveolar region in the human respiratory system, which correspond to submicrometric particles of PM_1. In Bogota was 20.8 $\mu g/m^3$ and in Palmira was 13.8 $\mu g/m^3$. The fraction of submicrometric particles ($PM_{1.1}$) contained in the coarse particles of PM_9 did not show a substantial deviation, even in rainy patterns.

The mass size distribution has a bimodal distribution centered in 0.43 – 1.1 μm and 4.7 – 9.0 μm in Bogotá and Palmira. In term of chemical composition, elemental carbon was mainly accumulated in $PM_{2.1}$, in such a way that 57% of the elemental carbon was this size fraction for the samples collected in Palmira and 72 % for samples collected in Bogota. On the other hand, organic carbon was more evenly distributed in fine and coarse fraction. 42% of organic carbon is contained in $PM_{2.1}$. The sulfate ion was one of the most abundant water-soluble ions in two sites. This ion shows the largest size distribution differences, while in Palmira was mainly accumulated in fine mode, in Bogota was dispersed across the two-size fraction.

The aerosol acidity was evaluated using the anion/cation equivalent ratio, revealing an acidic tendency of $PM_{1.1}$ and $PM_{2.1}$, which promotes the solubility of tracer metals in the aqueous phase of the particles.

The percentage of ambient particulate matter breathily that can enter, deposit, and be retained in the nasal cilia, tracheobronchial tree, bronchioles, and alveoli was 16.3%± 6.3%, 23.3%±2.3%, 31.7%±4.4% and 28.7% ± 6.5%, respectively.

Percentage of ambient particulate matter that can enter, deposit, and be retained in the tracheobronchial tree, bronchioles, and alveoli was, respectively, 16.3%±6.3%, 23.3%± 2.3%, 31.7%±4.4%, and 28.7%±6.5%.

As the result of this research, now it is possible to recognize that $PM_{2.5}$ concentrations are not correlated with the concentration of ultrafine particles. This means the exposure to lower concentrations of $PM_{2.5}$ does not indicate that the number of particles that could penetrate lungs were lower to reported in other areas. Besides, there is new information of PM in urban areas in Colombia, showing the chemical composition of sub-micrometer particles related to their size. Moreover, this study provides a methodology to do sources apportionment from measurement online of particles number size distribution, which offers faster and cheaper results than the previous source apportionment made from the chemical composition of PM_{10} or $PM_{2.5}$ in Colombia.

The $PM_{2.5}$ chemical characterization of samples collected in Cauca River Valley (CRV) reveled the abundance of secondary organic and inorganic components in the particles present in this region. The chemical characterization of $PM_{2.5}$ from samples collected in the Cauca River Valley (CRV) indicated the high concentration of secondary organic and inorganic components in the particles found there. Particularly, the abundance of Organic Carbon (OC) and the ions sulfate and ammonia reveling the relevant influence of agro-industrial emissions on the air quality of CRV. In addition, levoglucosan and mannosan levels showed that biomass burning was ubiquitous during the sampling period. Fluoranthene (FLE) was the most abundant PAH, confirming the strong influence of BB associated with agro-industry. Five- and six-ring PAH associated with vehicular emissions were also abundant in $PM_{2.5}$.

The outcomes of this study will contribute to understanding the effects of long-term exposure to aerosols on human health at both locations, inferring the major sources of aerosol emissions, and establishing effective methods to lessen the impact on population.

5.2.   Perspectives

As part of future work, it is recommended to determine the bulk particle density through simultaneous measurements of PVSD and particle mass size distribution. In addition, assessing the impact of ambient particle's morphology and shape factor (χ) on the equivalence of aerodynamic and mobility diameter would be a significant contribution.

Regard, the filter stage measurements in the size range of 6 to 17 nm could not be considered reliable in this study, therefore the nucleation mode was not clearly established in the urban areas studied in Colombia. As part of future studies, could be considered other instruments with higher number of bins in this size range with the goal of establishing the differences between particles formed by nucleation and traffic emissions.

The fact that the device utilized to count ELPI$^+$ particles did not have a better breakdown by particle size in the range from 6 to 400 nm, where most of the particles discovered in urban environments were, is one of the limitations of this study. Therefore, it is recommended in further studies to use instruments with larger size range resolution in order to segregate gasoline and diesel emissions.

The results of this research show that the concentration of PAH exceeds the limit set by resolution 2254 of 2017, therefore should be priories research to determine the spatial and temporal variability of PAH in Bogotá.